POST FAILURE ENERGY ABSORBING MECHANISMS OF FILAMENT WOUND COMPOSITE TUBES

R KEAL

Thesis submitted in accordance with the requirements of the University of Liverpool for the degree of Doctor in Philosophy by Robert Keal.

September 1983

Department of Metallurgy
and Materials Science,
University of Liverpool.

ABSTRACT

Composites have many attractive specific properties when compared to conventional materials. This makes them attractive for use in automobile structures where weight saving is important. Their ability to absorb energy in uncontrolled impacts is, however, generally poor. The aim of this work was to investigate and identify the mechanisms of energy absorption during the axial crushing of filament wound composites.

The specific energy absorption of crushed tubes was determined for varying fibre orientations, resin properties and test speeds. All tubes were pre-triggered with a bevel cut into one end of the tube wall. This ensured that, in nearly all cases, crushing was progressive. The reinforcement was 'E' glass fibres with either a polyester or epoxy matrix. The resins were modified by additives designed to control the properties of fracture toughness and tensile modulus. Test speeds from 2.33×10^{-3} ms^{-1} to 13.8 ms^{-1} were used.

It was found that for $0^{o}/90^{o}$ tubes the specific energy absorption was dependent on both test speed and resin properties. Resin properties of tensile modulus, fracture toughness and tensile strength were important in controlling the specific energy absorption of tubes. Polyester $0^{o}/ 90^{o}$ tubes showed a decreasing energy absorption with increasing test speed. The opposite was found for epoxy $0^{o}/90^{o}$ tubes. This was attributed to the different effects of test speed on the fracture toughness of epoxy and polyester resins. The specific energy absorption of helically wound tubes was found to be dependent on the winding angle which controlled the failure mechanism.

The crushing mechanisms of polyester $0^{o}/90^{o}$ tubes were studied by optical and scanning electron microscopy. These were found to be complex with many fracture processes occurring

simultaneously. Individual fracture mechanisms were isolated and identified by comparison with known fracture surfaces produced from unidirectional composites. The energy absorption of each fracture mechanism was determined using appropriate fracture toughness data. Discrepancies were found between the derived values and empirical results for energy absorption.

The main conclusion was that the specific energy absorption of filament wound tubes during axial crushing could be superior to that of conventional materials such as mild steel.

ACKNOWLEDGEMENTS

The author would like to thank Professors B.L.Eyre and D.Hull for the use of departmental facilities.Special thanks are due to Professor Hull as research supervisor for many stimulating discussions and assistance during the production of this thesis.

Thanks are also due to the other members of the Energy Absorbing Composites Group for assistance with experimental work and informal discussions and all other members of the department,in particular Mr C.H.Gatward,who donated their time,energy,knowledge and friendship.

A Science and Engineering Research Council grant is gratefully acknowledged for the first two years of the project.Acknowledgements are also due to the sponsors of the EAC project.These were the Ford Motor Company,Pilkington Brothers,British Petroleum and SERC polymer engineering directorate who provided financial and material support throughout the project along with many useful discussions.

The author would like to thank Mrs K.Darcy for typing this thesis.Finally thanks are due to my wife for support and encouragement without which this thesis would probably not have completed.

CONTENTS

LIST OF FIGURES

Page No.

Chapter 4

Chapter 5

LIST OF TABLES

CHAPTER 1 - INTRODUCTION

1.1 Composite Materials

1.1.1 History and background

The combination of two or more dissimilar materials to give improved properties is not new. Wood is a composite of cellulose fibres, whilst bone and teeth are naturally occurring multiphase materials. Early man soon became aware of the benefits that could be obtained by using unlike materials to produce the required article. An early example was the ancient Egyptians use of straw as reinforcement for mud bricks.

Other examples include the Mongolian Bow constructed from animal tendons, wood and horn, the use of animal hair in plaster and Damascus gun barrels.

It was not until the early 1920s that there was a demand for a glass fibre that could be used in electrical insulation tape. This became known as Electrical or 'E' glass. During the same era, polyester resins were synthesised and it was discovered that fibres of 'E' glass combined with the resin produced a strong lightweight material which soon became known as glass reinforced plastic (GRP). Developments were rapid and by the end of World War II, GRP was being used in aircraft radomes. The post-war space programmes and the production of new fibres and matrix materials gave an additional impetus to composite research and development. Today, composites are common and widely used structural materials.

Reinforced plastics have many advantages over conventional structural materials: high strength to weight ratios, the ability to be easily processed into complex shapes, good thermal properties, excellent resistance to corrosion under normal conditions and strength that can be designed to meet specific requirements. However, rein-

forced plastics have several disadvantages: the properties of many composites are highly anistropic, they require complicated jointing procedures and cannot easily be welded, the compressive properties can be poor and they generally do not deform plastically to any great extent. The advantageous properties have made reinforced plastics viable in automotive, aeronautical and marine applications where strength to weight ratios are important. In the aeronautical industry, for example, where weight-saving is a prime concern in order to increase payload capacity, reinforced plastics now account for 10% of the structural weight of the 'F 18' fighter plane. Up to a few years ago, automotive applications were more limited as weight savings were not so important. With the recent increases in fuel costs, however, the weight factor has become more critical, resulting in an increased interest in reinforced plastics.

1.1.2 Reinforcing phase

In composites, the reinforcing fibres act to strengthen the comparatively weak matrix. These fibres can be formed from many materials, such as carbon, glass, boron and aramids. Fibres are used because of the improvement in strength that can be obtained over the bulk material. For example, bulk glass has a tensile strengh of the order of 170 MPa, whilst 10μ diameter fibres have a strength of 3 GPa, which is 20 times greater. This has been explained by the inherent defects in the surface and structure of the bulk material, which act as stress raisers, whilst drawn fibres, on the other hand, have fewer, smaller surface flaws and a more perfect internal structure (1).

Some properties of the common reinforcing fibres are shown in Table 1, together with those of a quenched and tempered low-alloy steel. It is the high specific values of the fibres which give the composite its attractive properties.

Table 1 - Comparative Properties of Reinforcing Fibres

Fibre	Specific gravity	Modulus, GPa	Specific Modulus, GPa	Tensile Strength, GPa	Specific Strength, GPa
'E' glass	2.54	76	30	1.75	0.7
Boron	2.50	420	168	2.5	1.0
Carbon	1.75	224	128	2.3	1.3
Aramid	1.45	126	90	2.3	1.6
Steel(Bulk)	7.9	200	25	1.5	0.2

1.1.3 Matrix Phase

The properties of the matrix and the reinforcing agent are dissimilar. This is apparent from a comparison between Tables 1 and 2. The matrix is not normally employed to provide strength and stiffness to the composite. It does, however, have several important functions: it acts as a bridge keeping the fibres in place and maintaining structural integrity; it protects the fibres from mechanical damage, abrasion and chemical attack; and it also transmits stresses to the fibres, which is particularly important in off-axis and compressive loading.

Both epoxies and polyesters are widely used in composite materials. Epoxies are generally preferred for advanced composites because of their higher strengths, greater temperature resistance, excellent adhesion and lower shrinkage on curing. Polyesters have advantages in that they are easily handled and lubricated, give good "wet out" of the fibres due to lower viscosity and tend to be cheaper. Typical properties of both resins are shown in Table 2.

Table 2 - Typical properties of thermosetting resins

Resin	Specific Gravity	Modulus, GPa	Specific Modulus, GPa	Tensile Strength, GPa	Specific Strength, GPa
Epoxy	1.2	4.5	3.75	0.08	0.07
Polyester	1.2	3.0	2.5	0.06	0.05

1.1.4 Comparison with conventional materials

The attractive properties of the reinforcing fibres are modified by the diluting effect of the matrix. A comparison between the properties of conventional materials and several composites is shown in Table 3. Fibre reinforced composite materials do not have a clear advantage on the basis of strength and stiffness. The major advantages over conventional materials appear when the modulus per unit weight (specific modulus) and the strength per unit weight (specific strength) are considered. The higher values of specific properties means that the overall weight of a component can be reduced. These parameters are of importance in applications where weight savings result in greater efficiency in energy usage.

Unidirectional composites are anisotropic; this can be a serious limitation. For example, the tensile strength of unidirectional carbon fibre-epoxy falls from 1400 MPa to 38 MPa when tested parallel and perpendicular to the fibres. This property can be an advantage, as it allows the stiffness and strength of the composite to be used in the parts of the component where the properties are actually required. An element of flexibility can be introduced into the design, but at the cost of increased complexity in that design.

Table 3 - Typical properties of composite and conventional materials

Material	Specific gravity	Modulus, GPa	Specific Modulus, GPa	Tensile strength, GPa	Sp. tensile Strength, GPa
Aluminium Alloy	2.80	72	25.7	0.50	0.18
Steel	7.90	200	25.3	1.50	0.19
Carbon fibre-epoxy (Unidirectional)	1.60	220	138	1.40	0.88
Glass fibre-polyester (Unidirectional)	1.90	38	20	0.75	0.39
Glass fibre-polyester (Random fibres)	1.50	8.5	5.7	0.11	0.07

1.2 Filament Winding

Historically, the technique of strengthening structures by circumferentially wrapping with a strong fibre was used in mediaeval times, when gun barrels and wooden water pipes were wrapped with metal wire. This process has developed into winding continuous fibres around a suitably shaped mandrel. The windings usually consist of many individual continuous fibres which, in the case of glass, are often termed rovings. These fibres are impregnated with resin immediately before being wound onto the mandrel. After the resin has cured, the mandrel is removed to give the finished article.

Filament winding has advantages over other manufacturing processes in that continuous fibres can be very accurately aligned to produce the final article. Continuous fibres are more efficient as a reinforcement than short lengths and accurate alignment gives the most efficient use of the strength and stiffness of the fibres. Reviews of filament winding can be found in several publications (2, 3, 4, 5).

1.3 Composites in Automobiles

1.3.1 Present usage

Composite materials have been used in automobiles for a considerable time. It is difficult to ascertain the first use, but the trend is towards increased usage of plastic, both reinforced and unreinforced.

For example, the amount of all types of plastics that is used has increased from under 1 kg per car in 1940 to 100 kg in 1980 (6). This trend is expected to continue. Approximately 50% of the plastics used in automobiles can be considered to be composite materials. Specific examples are numerous: headlamp shells in Dough Moulding Compound (polyester resin reinforced with short glass fibres), cover plates, bumpers and body panels in Sheet Moulding Compounds (similar composition to D.M.C.), filament-wound drive shafts in continuous fibres and epoxy resin, body parts and interior trim in polyurethanes reinforced with short fibres, leaf springs in carbon fibres and epoxy resin, truck and bus body panels made from either chopped strand glass mat with polyester resin or S.M.C., complete body shells made from chopped strand glass and polyester resin.

Several cumulative factors were responsible for this increasing use of composite materials. Large increases in fuel costs occurred in the 1970's These resulted in the need to improve fuel consumption. One way of accomplishing this was to use lightweight materials in order to reduce total vehicle weight. These reductions can be effective because the mass of an automobile is the major factor in the energy required to increase momentum from zero to normal operating speed, i.e. to produce the kinetic energy of the automobile. It has been shown (7) that a reduction in weight of a car by 30% results in an improvement in

fuel consumption of up to 6 m.p.g.

Manufacturing techniques for composites were improved, allowing production economies. Legislation also was a factor in increasing the amount of research and development into reinforced plastics. This was due to the mandatory fuel consumption figures which had to be met by manufacturers in the U.S.A. Legal requirements were also introduced to cover the protection of passengers during 15 Km/h impacts. These legal requirements caused a reappraisal of the properties of conventional materials, an example being the requirement of a "soft" front end to minimise slow-speed impact injuries.

1.3.2 The problem

A knowledge of the properties of a material during uncontrolled impacts, e.g. vehicle crash, is essential when considering automobile structures. Legislation is most specific about this and requires that passengers be protected by a strong compartment with the kinetic energy of the moving vehicle being absorbed in a controlled manner by the frontal structure (in the case of a frontal impact). This control of the kinetic energy depends on the design of the vehicle and the properties of the materials being used. Metals, particularly steel, have desirable properties from the point of view of absorbing energy during a continual crushing process. The frontal structural steel members of a vehicle, which absorb most of the kinetic energy, do so by buckling and crumpling in a predictable manner.

Work (8, 9) has shown that steel automobile structures tend to fail in a ductile manner. This occurs progressively, without an appreciable sharp yield drop,with large scale plastic folding taking place, continually absorbing energy via a buckling process.

The ideal material from an energy absorption viewpoint would be characterised by a load-displacement graph as shown in Fig. 1.1. The absence of a high yield point reduces the initial shock transmitted to the passenger compartment, whilst a constant load allows the kinetic energy of the vehicle to be absorbed in a controlled manner. Reinforced plastics generally do not fail in a ductile manner; hence problems arise when the kinetic energy of the vehicle has to be dissipated in a controlled manner. This poor response of composite materials in the area of crashworthiness is a major factor preventing the wider usage of those materials in automobile structure. Little is understood of the post-failure behaviour of structures made with composite materials, particularly in the manner in which energy is absorbed during crushing.

1.4 Objectives and methods of approach of the present work

The aim of this work was to study the mechanisms of energy absorption of filament wound tubes subjected to axial crushing. Tubes provide simple structures that are relatively easy to construct and enable material and constructional variables to be made.

To obtain a concept of the failure mechanisms, an investigation was made on crushed specimens, both in the final state and also during sequential crushing, using metallographic techniques. These included macro-, micro- and scanning electron microscopy.

The next stage was to evaluate and quantify, where possible, the relative contribution of each of the many mechanisms to the overall energy absorption. This was to be carried out using current published data and in some instances the results of standard mechanical tests to provide the required information.

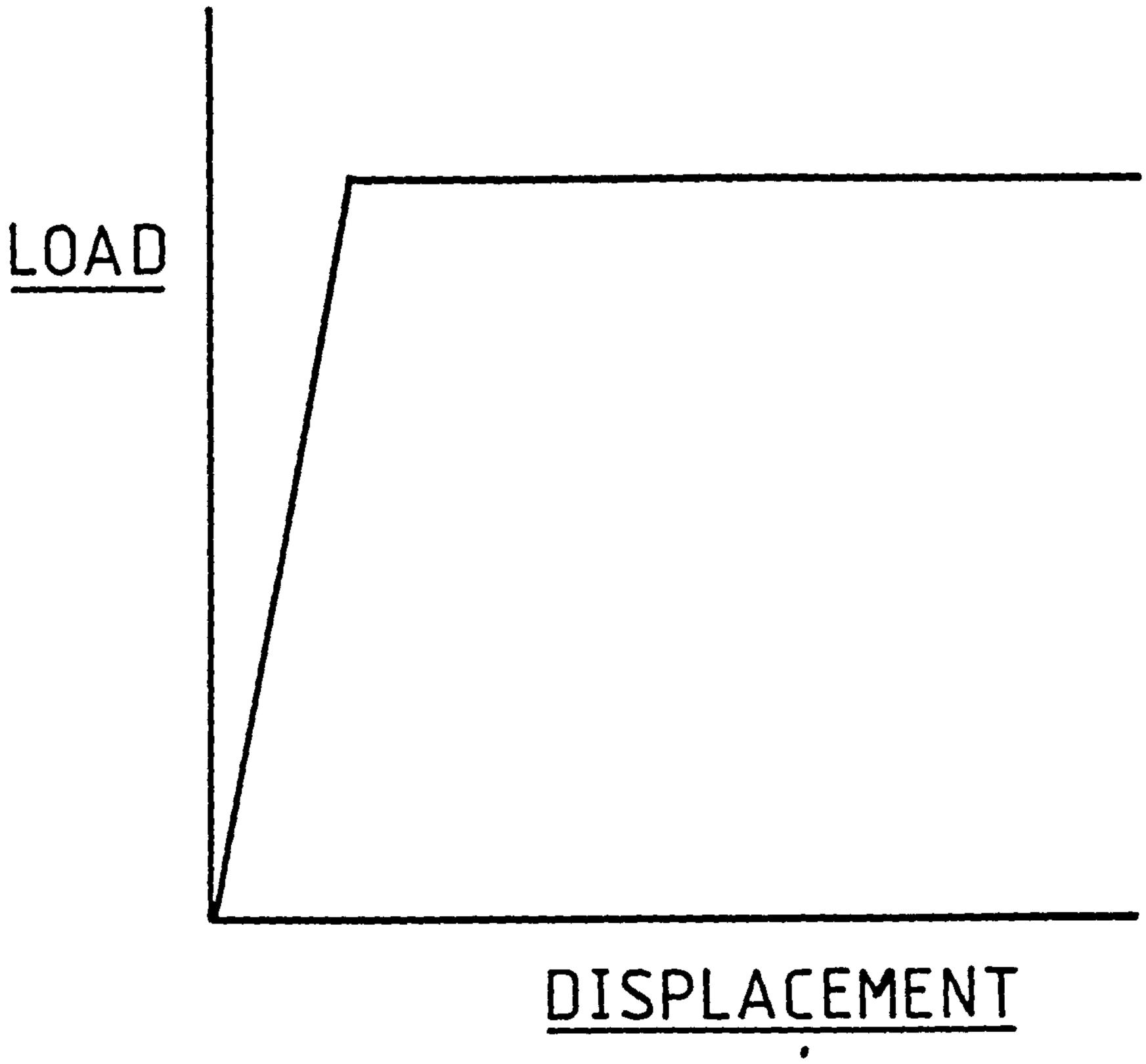

Fig. 1.1. Ideal load-displacement trace for an energy absorbing material.

Once the basic concepts of an energy absorption mechanism had been established, the effects of material and testing variables on the failure process were determined. These included the following;

a) Changes in the rate of testing to establish the effect of cross-head speed.

b) Variations in the orientation of the fibres with respect to the load axis.

c) Changes in matrix properties with emphasis on fracture properties, modulus and tensile strength.

It is hoped that this work will provide a greater understanding of the mechanisms of energy absorption of filament wound structures and assist in applications where energy absorption is an important property of the composite structure.

CHAPTER 2 - LITERATURE REVIEW

2.1 Failure Mechanisms of Composite Materials

2.1.1 Introduction

In this section the failure mechanisms and energy absorption process for composites under specific loading conditions are discussed. Values of energy absorption for individual mechanisms are important in the quantitative assessment of the energy absorbed during the crushing of tubes.

Composites, unlike metals, fail in many different ways, depending on the relationship between the loading axis and the fibre orientation. Generally accepted loading situations are as follows:

(a) tensile forces applied parallel to the fibres, with failure occurring normal to the fibres ($\sigma_{\parallel T}$);

(b) compressive forces applied parallel to the fibres, for which several failure modes have been proposed ($\sigma_{\parallel c}$);

(c) tensile forces applied normal to the fibre direction, with failure parallel to the fibre ($\sigma_{\perp T}$);

(d) compressive forces applied normal to the fibres, with failure taking place via a shear mechanism ($\sigma_{\perp C}$);

(e) forces applied parallel to the fibres giving a shear mechanism, with failure parallel to the fibre direction (τ).

Different failure mechanisms give dissimilar values of failure stress owing mainly to the anisotropic and non-homogeneous nature of composite materials. Table 4 shows representative values for a glass-polyester composite.

Table 4 - Typical values of strength for a unidirectional composite.

Glass-polyester $V_f \sim 0.50$ (10)

Tensile-parallel, σ_{11T}	Compression-parallel, σ_{11c}	Tensile-normal, σ_{1c}	Compression-normal, σ_{1c}	Shear, τ
700 MPa	950 MPa	25 MPa	110 MPa	57 MPa

The various failure mechanisms are discussed in greater detail below.

2.1.2 Longitudinal tensile failure

Several mechanisms can occur concurrently during the failure of a unidirectional composite under tension applied parallel to the fibres. Whilst the mathematical analysis describing each individual process varies slightly between authors, the actual failure of a brittle fibrous composite is generally accepted (11, 12, 13, 14) as being due to: (a) matrix and fibre elastic strain energy leading to crack propagation, in which the energy absorbed is small as both components are brittle; (b) debonding of the fibres from the resin; (c) pull-out of the broken fibres from their sockets in the resin; and (d) in some analyses (15), redistribution of the stress as the strain energy from the fibre is given to the matrix after a filament breaks.

All the analyses demonstrate the complex relationship between factors such as the interfacial bond strength, the failure strength of the fibres and the matrix, the volume fraction and diameter of the fibres and the modulus of the fibres and matrix.

The values of fracture toughness can be very high for a composite (of the order of $10^4 - 10^5$ Jm^{-2}), which is much higher

than can be accounted for by adding the contributions from the fibres and the matrix (of the order of 100-200 Jm^{-2} for the matrix and $6Jm^{-2}$ for glass). The interaction between the two materials is responsible for the improved toughness.

Debonding, first proposed by Outwater and Murphy (16), is observed in glass-polyester composites by areas turning milky white. This mechanism gives values of energy of the interface shear strength times the failure strain of the resin and is usually in the region of 500 Jm^{-2}(14). After debonding, major energy absorbing processes of pull-out and fibre fracture occur. All the processes contribute to the overall energy absorption during tensile failure and thus control the failure mechanisms.

2.1.3 Longitudinal compressive failure

Several mechanisms have been proposed for the compressive failure of unidirectional composites: none completely predict the failure stress. The compressive strength is dependent on many factors, including fibre and resin properties, interface strength and void content. It would appear that the failure mode is very sensitive to the fibre volume fraction and resin properties. This has been shown by several workers who have identified three major failure mechanisms.

Rosen (17) introduced the idea of microbuckling in an elastic manner. This followed, in detail, a treatment by Timoshenko (18) for the buckling of a column by an end load when laterally supported by elastic members uniformly spaced along its length. For a composite this lateral support is taken to represent the matrix. Hence the elastic properties of the matrix are important. This mode only applies if the fibres buckle out of phase, and was found to be applicable at low volume fractions.

At higher volume fractions an inphase mode of buckling was predicted. The proposed theory over-estimated the strength of the composite, and other workers (19), using boron/epoxy composites, improved the earlier results by using a factor applied to the results. For the inphase mode, this over-estimation was due to localised fracture of the fibres and fibre-resin interface.

Shear failure of resin and fibres has been demonstrated by several workers (21, 22, 23) and many micro-photographs have been produced to support the view that failure was due to a shear-initiated mechanism in which a kink band progresses across the specimen. The shear failure mode predicts higher values of compressive strength than those obtained experimentally and would appear to be an upper bound for the compressive strength of a composite. The reasons for this have been investigated. Misalignment of the fibres in relationship to the loading axis has been observed (24). Micro-structural inhomogeneities such as voids and buckling of the fibres, have been proposed as another cause of lower-than-predicted compressive strength (25). This work also identified the energy absorbing mechanisms as matrix shear and interfacial failure but did not describe the process quantitatively.

It is obvious that at present no single satisfactory account of compressive failure and energy absorption is available. These mechanisms are affected by many factors including those discussed above.

2.1.4 Compressive failure normal to fibres

During compression the maximum shear stress operates on all planes at 45^{o} to the compression axis (26). The orientation of the fibres in the plane of maximum stress is important in determining the shear strength. In Fig. 2.1, shear at 45^{o} can

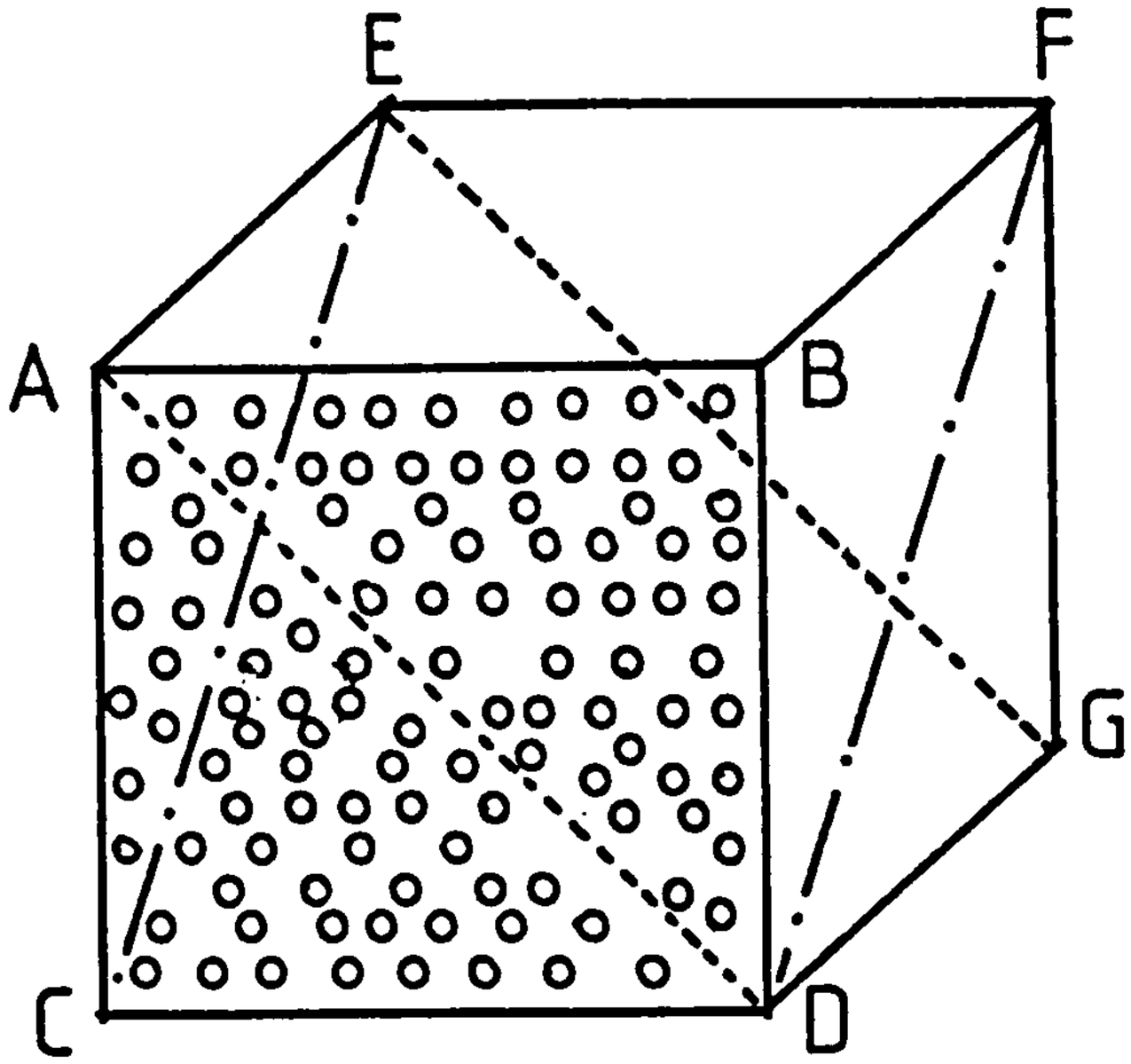

Fig. 2.1. Diagram showing the possible shear planes available during compressive loading of a unidirectional composite.

occur on planes AEGD and EFCD. With the former, shear can take place without fibre fracture, even though under the action of the compressive force, sliding of the two surfaces over each other is inhibited by friction. Shear on EFCD is even more difficult as fibre fracture is involved in addition to matrix failure and friction.

In both cases the shear strength is much higher than the in-plane or intralaminar shear strength similar to failure on AEDG, i.e. no fibre fracture and no compressive stress acting.

2.1.5 Transverse tensile failure

In this mode the fibres are orientated normal to the applied load, with the crack travelling parallel to the fibres. The transverse strength and failure mechanism are governed by several factors (26). These are the matrix, fibres, interface bond, presence and distribution of voids, and internal stress and strain distributions due to interactions between fibres, voids and inhomogeneities within the matrix. A full analysis is outside the scope of this work but several comments are applicable. The transverse strength is usually less than the strength of the matrix. When interface bonding between the fibres and matrix is negligible, the transverse strength is determined by the strength of the resin around the "holes" of the fibres which contribute nothing to the strength. The matrix strength is reduced by stress concentrations around the holes, and if plastic flow does not occur to relieve stress as with a brittle resin, this reduction in strength is significant.

If the fibres and matrix are strongly bonded, transverse strength is dependent on the bond strength and matrix properties. With a high bond strength there tends to be a stress magnification in the resin and this is at a maximum between the fibres. The

Poissons ratio of the resin and the volume fraction of the fibres are important in this context. Any stress concentration results in a reduction in the strength of the composite.

The effect of voids on the resin matrix is marked (27). This effect is magnified as the voids tend to cause debonding of fibres in addition to that caused by stress concentration effects.

Values of fracture energy for transverse failure are quoted as 60 - 80 Jm^{-2} (see Table in Section 2.3.4). This compares with bulk resin values of 50 - 300 Jm^{-2}.

Several methods have been proposed whereby improvements in the transverse properties could be obtained. Rubber toughening of the matrix which improves the fracture toughness of the resin without reducing the strength or stiffness is likely to be of use with low volume fraction composites (26). The use of an intermediate layer at the fibre-matrix interface in order to reduce the stress magnification effect is also proposed (28).

Even though the mechanism of crack propagation in transverse tension is one of matrix cracking and debonding at the fibre-matrix interface, in actual composites, where fibres are never perfectly aligned, a certain amount of fibre pull-out occurs (29, 30). Despite the fact that the number of fibres involved in the pull-out/debonding is low, the contribution is a significant part of the total fracture energy. This could account for the superiority of woven materials such as fabrics over unidirectional fibres in respect of transverse tensile strength.

2.1.6 Shear Failure

The shear strength of a composite depends initially on the direction of the applied forces relative to the fibre orientation.

The lowest shear strength occurs with a shear stress applied parallel to the fibres. This strength is dominated by the matrix properties as crack propagation can occur though the matrix without disturbing or breaking the fibres. The fracture energy in a direction parallel to the fibre is approximately the same as for the bulk resin,for example a DGEBA epoxide, gives G_{1C} values of 150 - 200 Jm^{-2}. These are only slightly lower than for a unidirectional glass fibre-epoxy composite (31).

The shear strength of a composite is also affected by the strength of the interfacial bond, and the stress concentration effects associated with the presence of fibres and voids (32). Voids are often formed when air is trapped between the filaments during the resin-impregnation process. These can be viewed as small cracks and a relationship has been defined between void content and shear strength (33).

The effect of fibre volume fraction on the stress concentration factor is minimal below about 0.6 volume fraction, after which the concentration factor increases rapidly. At high fibre volume fractions, the stress concentration effects produce a value of the shear stress of the laminate which is lower than that of the pure resin. The possibility of fibre bunching also aggravates the problem, as does the use of brittle resins (34).

The effect of the interfacial bond strength on the intralaminar shear stress (ILSS) of carbon fibre-epoxy composites has been demonstrated (35). Fibres which had been treated with a chemical surface agent designed to facilitate the bonding between fibres and resin increased the ILSS. Whilst there is, however, a general trend of increasing ILSS with increasing fracture toughness of the bulk resin, the effect is not always consistent. Composites of unidirectional carbon fibres in epoxy tested by a double cantilever beam method showed a slight reduction in ILSS

as the fracture toughness of the resin increased from 160 to 3200 Jm^{-2}. The fracture toughness of the comparable composite with cracks parallel to the fibre direction only increased from 240 to 490 Jm^{-2}. This was attributed to a suppression of the rubber toughening effect in the thin films that oocurred in the composites. The work demonstrated that the fracture energy of the resin, composite and ILSS were dependent on the resin cure systems. These effects were also shown (36) by determining the ILSS of various composites made with the same resin but using different curing cycles. The fully cured resin gave consistently higher ILSS values.

Theoretically, inter- and intralaminar shear are considered to take place without disturbing the fibres. In fact,during intralaminar shear some misaligned fibres still tend to hold the crack together, and this causes an increase in the fracture toughness. With interlaminar shear, however, where cracks can propagate entirely through the resin between the laminae, a tied zone does not normally occur.

Representative values of ILSS are shown in Table 5, together with a brief note of the test method and type of composite. As can be seen, the ILSS values are generally within the range 40 - 70 MPa.

Table 5 - Intralaminar shear strength of composite materials

Ref.	Composite	Test method	ILSS, MPa
36	1. Unidirectional carbon in epoxy V_f = 0.67 (a) Full curve (b) No post curve 2. Unidirectional glass in polyester 3. Woven glass in polyester	Grooved tensile	1a. 74.5 1b. 38.5 2. 22.8 3. 13.9
35	Unidirectional carbon in epoxy: V_f = 0.4, untreated fibres V_f = 0.4, surface-treated fibres V_f = 0.6, untreated fibres V_f = 0.6, surface-treated fibres Unidirectional glass in epoxy V_f = 0.4 V_f = 0.6	Short beam shear	 50 70 55 80 52 54
31	Unidirectional carbon in epoxy: cured by MNA ; BDA cured by Piperidine + 3.2% C.T.B.N. } rubber + 6.2% C.T.B.N. } toughening + 9.0% C.T.B.N. } agent	Short beam shear	 67 71 72 65 68
37	Unidirectional graphite in polyesters V_f = 0.33 (N.B. high number of V_f = 0.50 voids)	Short beam shear	 21 26
10	Unidirectional glass in various polyester resins with 'E' glass	Torsion of a filament-wound tube	48.3-59.6

2.2 Failure Mechanisms and Energy Absorption of Tubular Structures During Axial Compression

2.2.1 Introduction

Failure mechanisms and energy-absorbing processes during axial compression of tubes can be divided into ductile and brittle modes. Most metallic and thermoplastic materials fail in a ductile, plastic manner whilst most composite structures and certain thermoplastics fail in a brittle manner. These two failure modes are discussed below.

2.2.2 Ductile-plastic failure

A review of the failure modes of metals and related energy absorbing parameters is available (38). The main energy absorbing process is that of plastic deformation forming hinges in the tube wall which undergo large amounts of plastic deformation. The mechanism is one of slip and dislocation movement; hence strain hardening, alloying and heat treatment all affect the mechanical response of the metal to large amounts of deformation.

The collapse modes of metallic tubes are also dependent on structural variables. Axisymetric buckling of a tube wall is promoted (39) by a low ratio of wall thickness (t) to tube diameter (D). In contrast, a higher value of t/D promotes a diamond folding mode of collapse (40). It has been shown (41) that for aluminium and steel tubes, tested under axial compression, the energy absorbed divided by specific tensile stress is a constant which depends on t/D.

Thermoplastic tubes such as PVC also exhibit ductile folding during axial crush (42). It has been noted that a transition from ductile diamond folding to a brittle failure mode with negligible energy absorption occurs at cross-head speeds of the order of 1 ms^{-1}. This is due to the compressive yield stress increasing with strain rate until

nucleation of fracture occurs and brittle failure takes place.

2.2.3 Brittle failure

In contrast to ductile materials such as steel with a strain to failure of the order of 20 - 50%, composite materials using glass, carbon or kevlar with a thermosetting resin matrix have a tensile strain to failure of 1 - 3%. These materials are generally considered to be brittle. Yield processes of slip and dislocation motion are not available. During loading, the composite deforms elastically then fractures. This process is controlled by the properties of the materials in the composite, the interface between the materials and the amount, distribution and arrangement of the reinforcing fibres.

The amount of published work connected with post-failure mechanisms and energy absorption of composite tubes is limited. One of the first references briefly compared structures made from glass and carbon fibre reinforced plastics with metallic structures (43). Failure mechanisms were not discussed, but it was concluded that high values of specific energy absorption could be obtained with fibre-reinforced plastics. A comparison was made between various materials by using the concept of specific energy absorption, which is a measure of the amount of energy absorbed per unit weight of tube crushed during axial compression. This was obtained by dividing the energy absorbed during the test by the compression distance to give the average collapse force during the test. The average collapse force was then divided by the weight per unit length of the tube to give the specific energy absorbed (SEA).

This method of comparison has disadvantages in that any deformation in advance of the cross-head, which progresses at a rate different from that of the cross-head is ignored in the

calculation. It cannot,therefore,be applied to plastically deforming tubes, where the front of the deformed zone moves at a speed different from that of the cross-head. Hence the above definition slightly over-estimates the specific energy absorbed as the crush distance is taken as the cross-head displacement. With composite materials, the frontof the crush zone moves at the same speed as the cross-head and the width of the crush zone is constant throughout the deformation process (44).

A study by Jahnle (45) showed that structures made from glass-reinforced plastics could have significant energy absorption capacities during axial compression. Little mention was made of the failure modes, but triggering of the structures was used in order to promote progressive collapse. This triggering involved machining a 45^{o} bevel around the top of the tube so that failure was initiated at that end.

The first systematic approach to the evaluation of composite materials from an energy absorption viewpoint was carried out in 1979 (46). This used a variety of materials in both cloth, tape and pultruded form with epoxy and polyester matrices to manufacture tubes. A trigger mechanism similar to that used by Jahnle was used to initiate collapse, which was found to progress in a stable manner. As with earlier work by Thornton (41) on metal tubes, the specific energy absorption was defined as the energy absorbed per unit weight of collapsed tube, as derived from the area under the load-compression curve. The reinforcement was mainly of a $0^{o}/90^{o}$ cloth or tape made up into circular or square cross-sectional structures. Testing was carried out over a range of cross-head speeds from 0.085 mm s^{-1} up to 8.5 ms^{-1}. Temperature was also varied.

The experimental results indicated that carbon and glass-epoxy structures exhibited little rate dependence. This could

not be said for the glass-polyester tubes which were not tested at different cross-head speeds because of machine limitations. The load-compression curves were noted as being more erratic and jagged at the higher cross-head speeds. Specific energy values for $0^{o}/90^{o}$ cloth-epoxy tubes were 60-80 Jg^{-1} The variation in values was due to different specific relative densities of the tubes used. This was defined as the ratio of the solid volume of the tube to the volume of a solid of the same external dimensions. For cylinders this was equal to 4t/D. Increasing relative density caused an increase in the specific energy absorbed according to a relationship given as: $E = a\phi+b$ where a and b were empirical constants, ϕ the specific relative density and E the SEA. The comparable relationship for metal tubes was given as:

$$E = A\phi^{m}$$

where A and m were experimental constants. A large degree of experimental scatter was observed with all materials, but it was found that glass and Kevlar cloths had a lower specific energy absorption than carbon for similar structures i.e. 52, 60 and 75 Jg^{-1} for glass, Kevlar and carbon, respectively, ($0^{o}/90^{o}$ cloths with an epoxy matrix).

The temperature dependence of energy absorption was also investigated. Temperatures from $-200^{o}C$ to $150^{o}C$ had little effect on the SEA for carbon cloth-epoxy, but over $150^{o}C$ the energy value fell dramatically. Glass cloth-epoxy was found to show a similar response although the decrease in energy value was noted at $100^{o}C$. Glass cloth-polyester tubes were found to give a rapidly decreasing SEA at $150^{o}C$ to $200^{o}C$.

Similar collapse characteristics were observed for many of the specimens. This was described as one of disintegration via

interlaminar shear and fibre fracture. Carbon composites were found to give smaller fragments that glass composites, which tended to retain some cohesion with the remaining uncrushed base material. Strain rate and temperature were not found to have much effect on the collapse characteristics except that at high temperatures the specimens tended to remain intact and not to disintegrate into small fragments.

At a more detailed level, the failure mechanism of interlaminar cracking was observed to have cracks propagating 0.5 cm ahead of the collapsed zone. The main crack propagation path was along the interface adjacent to a 0^{o} layer. Cracks that travelled between the 90^{o} layer had a much shorter and more irregular path.

The variables of structural size, material properties and SEA were quantified via simple equations. The structural effectiveness, n, was related to the specific energy absorption divided by the specific interlaminar shear strength (τ^{s}). This was based on earlier work by the same author with metal tubes in which the structural effectiveness was the SEA divided by the specific ultimate tensile stress. For composite tubes this was given as:

$$n = \frac{SEA}{\tau^{s}}$$

The relative density, ϕ, of a composite tube was related empirically to the structural effectiveness by:

$$n = 5.09\phi^{0.688}$$

This was found to hold, within experimental error, for all circular tubes. The importance lies in the use of the interlaminar shear stress as a material parameter. Unfortunately, the ILSS for the materials used in the investigation could not be determined experimentally and nominal values were used to determine the value of the structural effectiveness.

A mathematical model of collapse for composite tubes was also proposed. This did not use the ILSS of the material previously shown to be important, but utilised a buckling criterion for the axially orientated fibres. An equation was derived based on the Euler Buckling load of the axial fibres. This gave a predicted crushing load to within a factor of 2. The equation was as follows:

$$P_{CR} = n\ N\ P_E$$

where P_{CR} was the total crushing load,

n was the number of longitudinal bundles of fibres per unit length per layer,

N was the number of layers in the composite wall,

P_E was the Euler Buckling load given by

$$P_E = \frac{\pi^2\ EI}{4l^2}$$

where E was the modulus of the composite,

I the second moment of area for a fibre bundle,

l the crack length.

This equation ignored any contribution to the load by the hoop (90^{o}) fibres. It was assumed that most of the load-bearing support arose from the 0^{o} fibres, as the hoop fibres had become separated from the body of the tube wall in the region of the collapse interface. Euler Buckling is, however, only applicable to long thin beams. A generally accepted criterion is that the length to thickness ratio should be above 5-10 for buckling to apply. Below this ratio, failure is by a crushing mechanism (47). Rough calculations based on the examples given by Thornton indicate that the bundle of fibres had the dimensions of 0.45 mm width, 0.25 mm depth and a height of 1 mm giving a ratio of between 2 and 4.

The equation also included the stiffness of the material via the modulus of the Euler Buckling load, but the ILSS was not included. This equation would thus not cover variations in the interface bond between the resin and the fibres. For maximum energy absorption a composite tube would, according to the equation, require little hoop reinforcement, a very high modulus, and a high resistance to crack propagation, i.e. a small value of 1. Resin properties would only become apparent via the modulus term.

The relatively small effect of testing speed on glass-polyester structures was noted by Kirsh and Jahnle (48). Glass with 2 in long fibres and glass woven fabric with a 50/50 hoop to axial ratio were used with polyester resin to construct a variety of structures of circular, rectangular and square sections. Testing speeds from 2 $in\,min^{-1}$ up to 30 miles h^{-1} were used. All structures had bevelled ends and progressive failure was reported in all cases. The same authors also used sheet moulding compound and found that the SEA increased with glass content, but that testing speed effects were negligible.

In a recent paper (44) the mechanisms of collapse of composite tubes were shown to be dependent on many variables. These were said to include the fibre and matrix type, the fibre aligrment in short-fibre materials and the lay-up structure in laminated structures. Many different types of composite materials were examined and variations in the failure processes and energy absorption mechanisms were noted.

A major difference was observed between the crushing mechanism of the centre failure of end-reinforced tubes and the progressive end crushing of bevelled-end tubes. End-reinforced tubes constructed from glass cloth-epoxy, SMC and $\pm 55^{o}$ glass-polyester helically wound tubes gave a sharp drop in load after initial failure. The post-failure crushing mechanism was deemed to give low energy absorption values because of the small volume of material actually involved in the crushing process. In contrast, bevelled-end tubes made from all composite materials investigated were found to undergo progressive crush with a high SEA value. Several types of progressive crush were identified. These were fibre splaying and bending, fibre splaying and axial tearing, and micro-fragmentation. Fibre splaying and bending were found to occur with filament wound glass tubes with laminate orientations of $\pm 55^{o}$ and $90^{o}/0^{o}/0^{o}/90^{o}$. Fibre splaying and axial tearing were noted with mica-shellac and paper-phenolic tubes made by a tube rolling process. Many layers of paper and mica were used. Delamination of the layers, regular axial tearing and splaying inwards and outwards were observed. Micro-fragmentation was found to be involved to a greater or lesser extent in all examples.

Testing speeds from 4×10^{-3} ms^{-1} to 4 ms^{-1} were employed. The results, as tabulated, indicated that the failure modes did not change drastically with testing speed, but some variation in SEA was apparent with continuous glass-polyester and glass cloth-polyester

tubes. Glass-polyester appeared to give a reducing energy absorbing value, whilst the opposite was true for glass cloth-epoxy. This phenomenon was not explained.

The paper concluded that numerous failure mechanisms were operating. These were itemised as fibre pull-out, compressive buckling, compressive shear, transverse cracking and various unspecified resin fracture processes. The relative contribution of each of these mechanisms was not evaluated, but the possibility was suggested that energy could also be absorbed in friction between the crushed tube and the compression platens.

2.3 Fracture energy of composites

2.3.1 Introduction

To obtain reliable estimates of the energy absorbed in the crushing of tubes, two pieces of information are required. The first is an accurate assessment of the failure mechanisms in a given tube. The second is a measure of the energy required to cause the mode of fracture under investigation. In this work, it was found that progressive crushing of filament wound tubes involved many different fracture processes. In this section, data relevant to fracture toughness in different failure modes is reviewed.

2.3.2 Derivation of fracture toughness values

The derivation of values to quantify the energy absorbed is generally based on fracture toughness measurements. The resistance of a material to crack propagation is often called the fracture toughness and is measured by the fracture surface energy. This is defined empirically as the minimum amount of energy required to create unit area of fracture surface. An increased fracture surface energy, by inhibiting crack propagation, causes increased resistance to fracture under both static and shock loading.

Much of the earlier work on fracture mechanics is based on the work of Griffiths (1). Methods soon become more refined, however, and now techniques have been developed for application to the fracture of thermosetting polymers and composites. These developments resulted in linear elastic fracture mechanics (LEFM). The theory behind LEFM is well documented (49, 50). The normal practice is to determine values of the critical stress intensity factor K_c, which is defined by;

$$K_c^2 = Y\sigma_f^2 a$$

where Y is a geometrical factor, a is the half crack length and σ_f of the tensile fracture stress. For plane stress, K_c is related to fracture toughness by;

$$K_c^2 = EG_c$$

where E is the modulus and G_c is the strain energy release rate, often termed the fracture toughness value. G_c is normally measured in terms of energy per unit area (Jm^{-2}) and hence is a very useful parameter in determining total energy absorption in the failure process. K_c is normally quoted in $Nm^{-3/2}$, and is the more common value used in LEFM.

For isotropic materials, simple relationships have been derived relating K_c and G_c for conditions of plane stress and strain (51, 52, 53). The relationship for plane stress has been given above. The equivalent for plane strain is:

$$G_c = \frac{(1 - \nu^2)}{E} K_c^2$$

where ν is Poissons ratio. Plane strain conditions are applicable to the experimental techniques used to determine the resin fracture toughness in this work (50). However, with the complex fracture situations encountered in a tube during compression, it is unlikely that a total plane strain or stress situation is applicable.

The mode of fracture can vary depending on the manner in which the crack is loaded (49). Referring to Fig. 2.2, three main modes are normally studied: Mode I , opening or tensile; Mode II, sliding or in-plane; and Mode III, tearing or out of plane shear. With most fracture toughness work Mode I is the more common and much data are available for values for epoxies, polyesters and composites in various testing conditions. From observations of the fracture mechanisms in composite tubes reported in the published literature (44, 46), shear would appear to be the major deformation process. Hence Mode II would be the more applicable failure mode.

For an isotropic material, the relationship between the stress intensity factor and the strain energy release rate for Mode II failure in plane strain is given (51, 52) as:

$$G_{IIC} = \frac{K_{IIC}^2(1 - \nu^2)}{E}$$

However problems arise when a non-isotropic material is considered. In order to apply fracture mechanics to composite materials, several extra factors have to be taken into account. Elastic anisotropy must be considered in the derivation of expressions for the elastic strain energy released as the crack advances. The resistance of the material to crack propagation (i.e. the G value) will differ for different directions of crack path, depending on the fibre

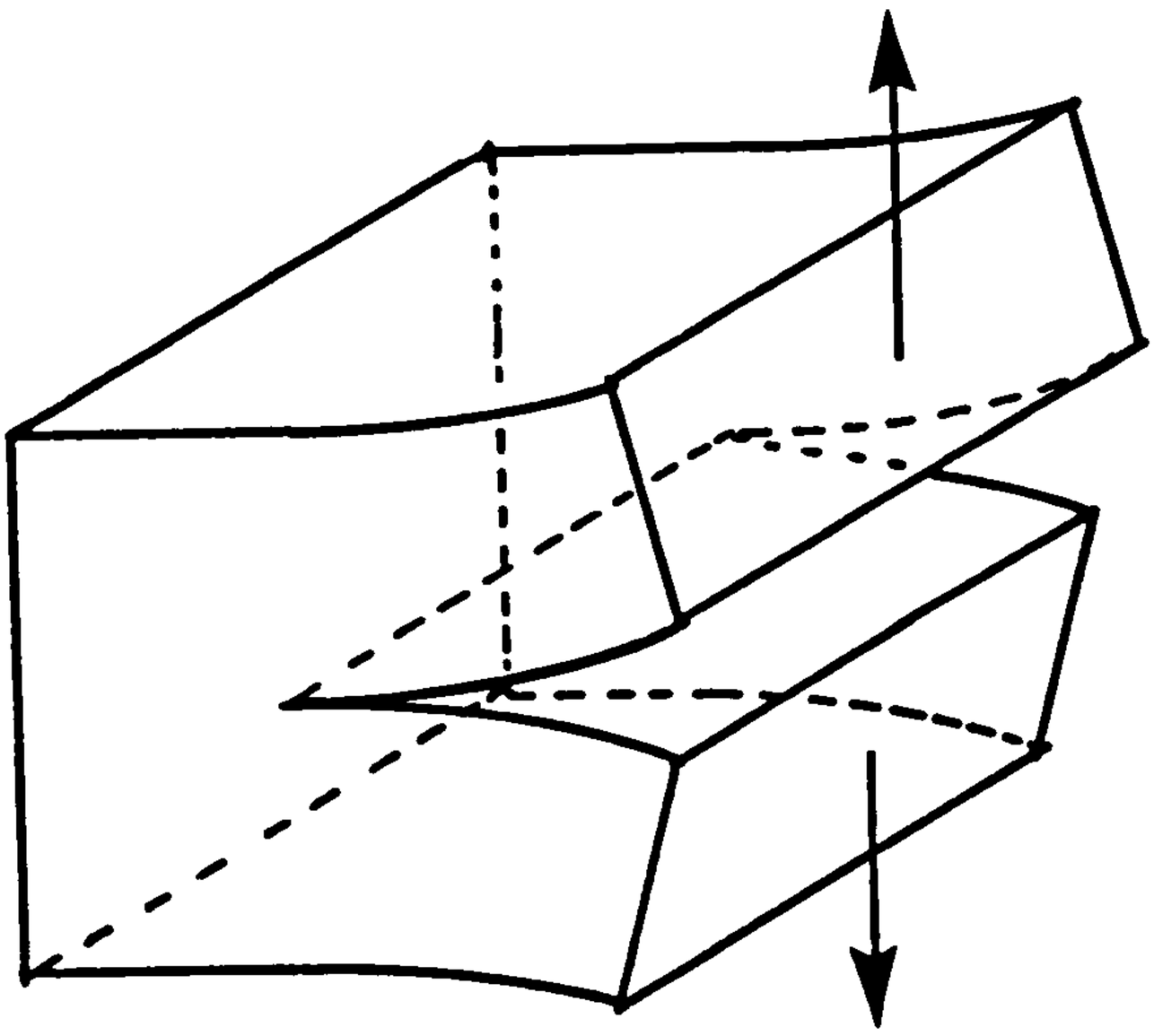

MODE 1

Opening.

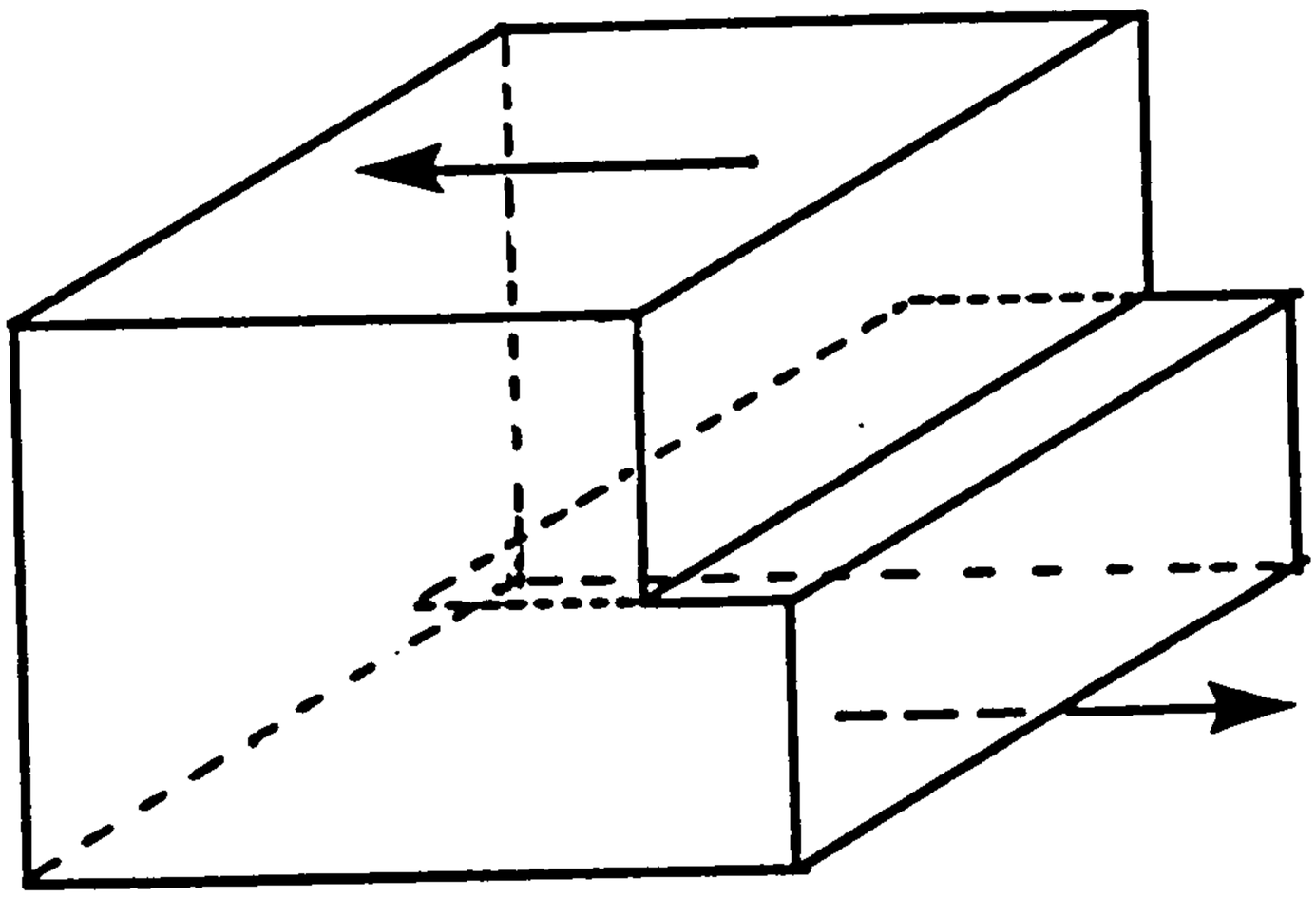

MODE 2

Forward shear.

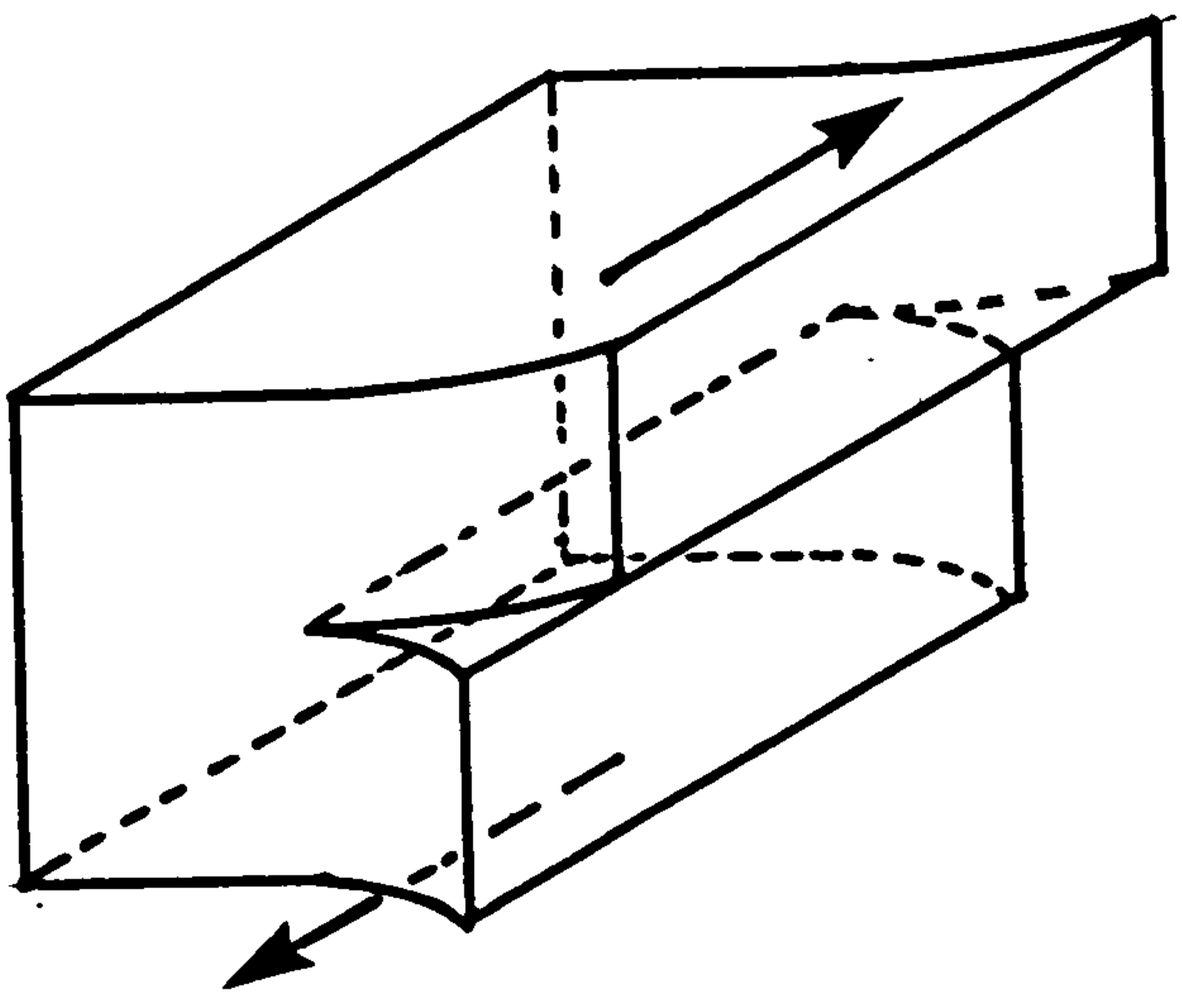

MODE 3

Parallel shear.

Fig.2.2. Schematic of crack propagation modes generally used in LEFM.

orientation and mode of failure. Finally, interactions between the materials which contribute to the value of G must be considered. Thus in moving from an isotropic to an orthotropic material such as a unidirectional composite, a complex situation arises. The relationships have been deduced (51, 52, 54) for plane strain as:

$$\text{Mode I: } G_{1C} = K_{1C}^2 \left(\frac{S_{11}\, S_{22}}{2}\right)^{\frac{1}{2}} \left[\left(\frac{S_{22}}{S_{11}}\right)^{\frac{1}{2}} + \frac{2S_{12} + S_{66}}{2S_{11}}\right]^{\frac{1}{2}}$$

$$\text{Mode II: } G_{11C} = K_{11C}^2 \left(\frac{S_{11}}{\sqrt{2}}\right)\left[\left(\frac{S_{22}}{S_{11}}\right)^{\frac{1}{2}} + \frac{2S_{12} + S_{66}}{2S_{11}}\right]^{\frac{1}{2}}$$

In these equations the term $\left(\frac{1 - \nu^2}{E}\right)$ for isotropic material is replaced by terms relating the elastic compliances (S_{ij}) of the body in question. These equations are for cracks travelling parallel to the fibres, i.e. with no fibre breakage. The immediate point is that the values of Mode I and Mode II strain energy release rates will be different. Experimental data obtained from the literature are shown in Section 2.3.4 and indicate that in the case of fibrous materials, Mode II gives much higher values of both K_C and G_C. This implies that care must be taken in selection of the correct value of strain energy release rate, not only for the material under study, but also for the type of failure or crack propagation mode.

The relationship between the crack direction and the fibre orientation is critical with respect to the fracture toughness of the material. Thus the value of G_C for a tensile opening mode will depend on whether the crack runs parallel or normal to the fibres. For example, taking a glass-epoxy system, G_{1C} for a

crack parallel to the fibres can be as low as 0.1 Jm^{-2}, whereas a crack normal to the fibres gives a value of 10^5 Jm^{-2}(49). Actual values of G_{1C}, taken from experimental work (55), for cracks travelling parallel and normal to the fibres are given as 900 Jm^{-2} and 133 x $10^3 Jm^{-2}$ respectively. The difference between the two values was attributed to fibre pull-out, debonding of fibres and deformation of the matrix, all occurring with cracks progressing normal to the fibres. For a crack travelling parallel to the fibres without fibre fracture, the major energy absorbing mechanisms lie in the resin and resin-fibre interface.

In summary, the fracture energy of a composite is dependent on the orientations of the crack and the reinforcing fibres, and the direction of the applied stress. Mode I values of crack opening are lower than those for Mode II forward shear cracking. Crack propagation normal to the fibres gives a higher value than propagation parallel to the fibres. It is possible to calculate strain energy release rates from stress intensity factors for isotropic and special orthotropic materials provided the elastic properties of the material are known.

2.3.3 Fracture toughness testing

Although the ultimate properties of a reinforced composite are normally dominated by the fibres, especially for tension parallel to the fibres, the performance with respect to other loading conditions is controlled by matrix properties, particularly in the propagation of cracks within the matrix.

The most convenient way of studying the crack propagation of thermosetting resins is through linear elastic fracture mechanics. For this to apply to a material, the stress-strain curve must be linear to fracture, any plastic deformation being confined to regions close

to the crack tip. In general,polyesters and epoxies are brittle materials, showing limited plastic deformation and meeting the requirements of LEFM (56).

Many testing arrangements are available to determine the fracture toughness of a resin. These are reviewed by Young (50). A useful requirement of a test specimen is that the stress intensity factor should be independent of crack length (57). Two such specimen configurations are the double torsion and tapered double cantilever beam. Both have been widely used for the study of crack propagation in thermosets (58, 59).

With these test pieces a constant cross-head speed leads to crack propagation at a fixed load, or stress intensity factor, for a specimen undergoing continuous crack propagation. For specimens which undergo stick-slip rather than progress crack growth, the load displacement trace has a characteristic saw-tooth shape. Propagation takes place at the peak load and ceases at the minimum load. Many material variables have been shown to affect the stability of crack propagation and the stress levels at which it occurs in thermosetting resins. These include the type of resin and curing agent (50, 60-64); the amount of curing agent and curing conditions (58, 59, 62, 65); testing speed (66, 67); test temperature (50, 60, 68); and the effects of additives to the resin (65, 69, 70).

By the use of LEFM techniques, values for the stress intensity factor and the fracture energy can be obtained for most thermosetting resins such as polyesters and epoxies. The situation is not simple when dealing with composite materials. The fracture energy of a composite material may be measured by several methods which are different in principle. Two such methods are work of fracture and linear elastic fracture mechanics. The work of fracture method (71) breaks a specimen in a controlled manner such that all the

stored elastic energy in the specimen-machine system is absorbed in the creation of the fracture surface. The fracture surface energy obtained in this way is given by the area under the load-deflection curve divided by twice the specimen cross-section. This is called the work of fracture. LEFM techniques based on the Griffith criterion are similar to those used for resins. The fracture surface energy is obtained from the load at failure, via analytical solutions which relate G_C or K_C to the load, crack length, specimen geometry and material elastic constants. Care must be exercised, however, as often different specimen geometries and different test methods give different results (72).

2.3.4 Fracture toughness values for composites and resins

Representative values, taken from current literature, for the fracture toughness of resins and composites are shown in Tables 6 and 7. In some instances both K_C and G_C values have been quoted; in others one value has been quoted with sufficient data to allow the other to be calculated. The test method has been shown.

For resins, the results show that fracture toughness values for epoxies are generally in the region of 100 to 200 Jm^{-2}, with modifiers giving improvements up to 600 Jm^{-2}. Values for polyesters would appear to be slightly lower, with G_{1C} around 100 Jm^{-2}. Flexibilisers give significant improvements up to 3300 Jm^{-2}. The application of LEFM to a highly flexibilised resin with high strains to failure is, however, rather questionable.

Composites with cracks travelling parallel to the fibres give fracture toughness values similar to those of pure resin. Cracks normal to the fibres give values much higher, up to 1×10^5 J m^{-2}. Limited results comparing Mode I and II crack propagation show fracture toughness values for Mode II to be much higher.

Table 6 - Fracture toughness values for thermosetting resins

Ref.	Material	Test method	K_{1C}, MNm^{-2}	G_{1C}, Jm^{-2}	Comments
64	Polyester orthophthalate	SEN TDCB SDCB		40-50	
50	Epoxy DGEBA + various hardeners	Various		86-575	Value depended on type and amount of hardener
59	DGEBA epoxy with DDM hardener	TDCB	0.9- 0.73	200- 174	Lower values of K and G taken at higher crosshead speeds
31	Epoxy DGEBA + modifier	TDCB		160- 320	Modifier was CTBN, gave increase in G_{1C}
35	Epoxy DGEBA	DCB		1000- 2000	Values appear to be very high
73	Epoxy DGEBA + various hardeners and modifiers	CT (round and rectangular) DCB		136-181 154-187 352-478	With HHPA with Piperidine with 15% CTBN
74	Polyester orthophthalate + flexibiliser (PMA)	CNT	0.72 2.16	130 3300	Resin only + 50% flexibiliser

Key SEN - single edge notch
TDCB - tapered double cantilever beam
SDCB - simple double cantilever beam
DCB - double cantilever beam
CT - compact tension
CNT - compact notched tension

Table 7 - Fracture toughness values for composite materials

Ref.	Material	Test method and crack path	K_C, MN $m^{-3/2}$	G_C, Jm^{-2}	Comments
75	Parallel glass in epoxy (Scotch ply 1002)	CB and tensile/ compressive shear. Cracks parallel to fibres	K_1 = 1.1 K_{11} = 4.0	G_1 = 57 G_{11} = 1498	G values calculated from K values
76	Parallel graphite in epoxy (PRD279)	Cracks parallel to fibres	K_1 = 1.75 K_{11} = 10.95	G_1 = 65 G_{11} = 6834.	G values calculated from K values
55	Woven glass with 5:4 warp:weft. Polyester resin V_f =0.5	DCB test. Crack travelling parallel to fibres		G_I values 900 $133x10^3$	Parallel to fibre Normal to fibre
77	Parallel carbon in epoxy	Work of fracture measurement. Cracks normal to fibres		G_1 = $2.3x10^4$	
29	Parallel carbon in epoxy	DCB cracks parallel to fibres		G_1 = 300	
78	Parallel glass in polyester	DCB cracks normal to fibres	K_1 = 0.7	G_1 = 180	V_f very low ~0.0009 Resin G_1 = 80
79	Parallel glass in polyester (Crystic 272)	Simple cantilever beam. Crack parallel to fibres		G_1= 120 G_{11}= 3230 G_{111}= 2500	$V_f \approx 0.55$

Key CB - cantilever beam
DCB - double cantilever beam

2.4 Influence of testing speed and temperature on the mechanical properties of composite materials

2.4.1 Introduction

The effects of testing speed and temperature on common materials such as metals are well known (80). This is not the case for composite materials whose response to testing rate and temperature are complicated by the dissimilar responses of their component parts. For example, the tensile modulus of a unidirectional composite is dependent on the fibre properties, and hence the response of the fibres to the test conditions are more important than those of the matrix. However, the shear properties of the composite are more dependent on the fibre-matrix interface and the matrix; hence the effects of test variables on these components are more important.

The section below discusses the effects of temperature and cross-head speed on the matrix, fibres and composite material.

2.4.2 Glass fibres

The effects of strain rate on the modulus, ultimate strength and strain to failure of glass fibres have been reported by Armenàkas et al (81). The modulus of 'S' glass increased by 56% on a linear basis with log strain rate from $0.00044s^{-1}$ to $500s^{-1}$. The ultimate tensile strength and strain to failure were found to be constant for strain rates from $0.002\ s^{-1}$ up to $0.17s^{-1}$ in tests carried out at room temperature.

Cameron (82), using 'E' glass noted an increase in the tensile strength that was linearly related to log strain rate up to $0.008s^{-1}$. Above this strain rate, a slowing of the increase was followed by an eventual decrease in strength with increasing strain rate.

'E' glass fibres show a slightly decreasing modulus with increase in temperature. A decrease of 5-10% over a range of -20°C to 650°C was noted by Otto (83). However, over a more limited range of -20°C to 100°C it would be difficult to detect any variation in modulus. The tensile strength behaviour was also found to be similar (84, 85) but at high temperatures, in the region of 600°C, yielding was found to occur.

2.4.3 Polyester/epoxy resins

The deformation behaviour of thermosetting resins is time and temperature dependent. Most of the work has been carried out with bulk resin samples and has tended to be combined with fracture toughness testing.

For a DGEBA epoxy resin cured with TETA the modulus was found to increase slightly with increasing cross-head speeds from 0.05 to 5 mm min^{-1} (68). Increase in temperature caused the modulus of the resin to decrease slowly until at temperatures approaching the Tg of the resin, the modulus decreased rapidly. The yield strength was found to increase slightly with testing speed, but decrease significantly with temperature. A similar effect was noted with the shear stress at failure. The failure mechanism during fracture toughness testing was found to be dependent on temperature. Below 0°C, continuous crack growth took place, whilst above 0°C, stick-slip occurred. The form of the curve depended on the amount of hardener and the cure cycle of the resin, but it was found that K_{1C} for arrest during stick-slip remained constant. The authors concluded that at the higher temperatures, stick-slip was caused by a crack blunting mechanism.

The increase in modulus with testing speed has also been noted by other workers (59). A similar epoxy resin was used

with a different curing system and cross-head speeds of 0.1 to 10 mm min^{-1} were employed. Fracture toughness values showed a slight decrease with increasing test speed. This strain rate effect on the fracture toughness was noted by Bascom et al (70) using strain rates from 0.01 to $10^3 s^{-1}$. Epoxy resins cured with diphenol were employed. The addition of a toughening agent to the resin increased the fracture toughness but resulted in an increasing sensitivity to strain rate, i.e. as the strain rate increased, the fracture toughness reduced significantly.

The amount of literature on polyester as opposed to epoxy resins is limited. In general the effects of strain rate and temperature are similar, but polyesters have a much lower heat distortion temperature. For epoxies, the HDT is in the region of 300°C whilst for polyesters it is not normally over 110°C (86). This results in a greater sensitivity to temperature effects. However, it would appear that the response of modulus, failure strength and fracture toughness to strain rate and temperature tend to be variable depending on the resin used, the chemical curing system and the cure cycle.

2.4.4 Composite materials

When two homogeneous isotropic materials such as glass and resin are combined into an anisotropic composite, strain rate and temperature effects often become complex.

Harding and Parry (87), using woven glass in polyester resin, carried out compression tests over a wide range of strain rates (10^{-3} to 10^3 s^{-1}) corresponding to a cross-head speed of 1.27 mm min^{-1} up to 15 ms^{-1}. Three orientations of fibre with respect to the loading axis were used. In type I, the compression

axis was in the plane of reinforcement and parallel to one axis of the fibres. In type II, the compression axis was inclined at 45^{o} to the plane of the plate containing the woven reinforcement. In type III, the compression axis was perpendicular to the plane of reinforcement. For type I and type III, little variation with strain rate was noted in the ultimate compressive strength and strain to failure. For type II, however, a large increase in compressive strength occurred as the strain rate increased. The modulus was also found to increase rapidly at strain rates over $500s^{-1}$, but below this value it appeared to be constant.

The authors explained the differences between the various types as being due to matrix and interface effects. These were deemed to be more important in controlling the properties with type II than with the other two types. In an earlier work by the same author (88) using punch tests on woven roving glass-polyester, the shear load to cause failure increased by 250% as strain rate increased.from 10^{-4} to $10^{4}s^{-1}$. Similar results were found by other workers using continuous glass in polyester (89). Strain rates from 10^{-3} up to 10^{3} s^{-1} were used in both longitudinal and off-axis compression tests on roving and cloth-reinforced specimens. The compressive strength increased with strain rate. Little fibre breakage in the roving specimens occurred, but oblique cracks and a large amount of fibre breakage were found to take place in the cloth specimens. The strain rate effect was attributed by the authors to the matrix material.

Daniel et al (90) carried out tensile tests on unidirectional graphite in epoxy at strain rates up to $500s^{-1}$. They concluded that for 0^{o} specimens the modulus increased by 20% when compared with the static values. The ultimate strength and

strain at failure were unchanged. The transverse modulus and strength increased by between 2 to 4 times the static values, whilst the shear modulus increased by 30%. These results were attributed to matrix, interface and surprisingly to the strain rate effect on fibres. This work was an extension of an earlier paper (91) covering strain rates up to $27s^{-1}$ on unidirectional boron, graphite, polyester and kevlar with epoxy matrices. Here 0^{o} properties were governed by fibres with little increase in mechanical properties. Kevlar-reinforced composites were the exception and showed an increase in modulus and strength with strain rate. Shear and transverse properties for all materials were found to increase by 15% over the static properties. This effect was attributed to resin strain rate sensitivity.

Other authors (92, 93) using varying materials and strain rates have also reported similar results to those indicated above. Composite materials showing strain-rate dependancy were more sensitive to properties that were resin or interface dependent.

Barker et.al (94) carried out tests on carbon fibre-epoxy composites at varying temperatures. They found that interlaminar shear strength, tensile strength, modulus and impact strength of unidirectional composites showed a variation with temperatures from $-80^{o}C$ to $120^{o}C$. The major influence of temperature was on the modulus of the matrix and on the interfacial strength of the fibres. Changes in the matrix, via temperature were found to control fracture modes, particularly during impact tests. The response of each composite was found to be sensitive to the epoxy resin used and also the carbon fibres. The optimum values were obtained with an epoxy resin of high HDT combined with surface-treated carbon fibres. In general, the composite properties were drastically reduced as the

HDT of the resin matrix was approached.

As temperature has been shown to be a factor affecting the mechanical properties of resins, a reference concerning the temperature rise during compression testing is interesting (95). Four hard thermoplastics were tested in compression at strain rates from 10^{-4} to $10^{3}s^{-1}$. It was found that for total amounts of strain below 6-8%, temperature rise in the specimens tested at strain rates of $760s^{-1}$ was minimal. Friction was minimised by lubricating the ends of the specimens and keeping the cross-sectioned area small. Above strain values of 8%, temperature rises were found to be appreciable, in the region of 11-20°C.

CHAPTER 3 - EXPERIMENTAL METHODS AND MATERIALS

3.1 Introduction

Preliminary experimental work on tubes with various end constraint systems indicated that bevelled-end tubes crushed progressively and gave consistent results. The materials used and tube manufacturing techniques are described below. 'E' glass was selected as the reinforcing agent, with commercially available polyester and epoxy resins as the matrix. Crush speed, fibre orientation and matrix properties were investigated individually and in combination as the major experimental variables. The fracture mechanisms involved were studied by standard micrographical techniques which are described below.

3.2 Materials

3.2.1 Reinforcement

The 'E' glass reinforcement in most of this work was produced by Pilkington Fibreglass plc under the name Equerove 23/47 FGRE. This was supplied as internally unwinding cheeses of 2400 tex rovings. The fibres had been treated with a general purpose size compatible with polyester and epoxy resins. Fibre diameters were measured by micrography as being approximately 15 μm.

The principle mechanical properties are shown in Table 8.

Table 8 - Properties of 'E' glass fibres (96)

Property	Value
Specific gravity	2.56
Single fibre tensile strength	3.6 GPa
Youngs modulus	76 GPa
Failure strain	4.8%
Softening point	850°C

3.2.2 Matrix

3.2.2.1 Polyester resin

The standard polyester used was an isophthalic resin supplied by Scott Bader Ltd under the name Crystic 272. This is an unsaturated resin designed for high-performance applications, giving excellent "wet out" when used with continuous rovings in filament winding. The curing system was 0.5 pph cobalt octoate (Scott Bader 'E') and 1 pph methyl ethyl ketone peroxide catalyst (Scott Bader 'M'). These were added separately to the resin before winding commenced. These proportions were found to give a resin gel time sufficient for the construction of a tube. The properties of unfilled cast resin are shown in Table 9.

3.2.2.2 Epoxy resin

The epoxy resin used was commercially available system marketed under the name Araldite MY750 by Ciba-Geigy Ltd. MY750 is an unmodified liquid resin, which is solvent free and designed for laminating and filament winding. The hardener used was Ciba-Geigy HY917, a methyltetra hydrophthalic anhydride, used in the proportion of 90 pph of HY917 to MY750. An accelerator, Ciba-Geigy DY070 was added to the hardener, prior to mixing, in the proportion of

1.5 pph of DY070 to HY917. In order to facilitate mixing and improve winding properties, both resin and hardener were heated to 40°C prior to, and during, mixing and winding. This aided both processes and reduced voids in the finished tube to a minimum. The properties of the unfilled cast resin are shown in Table 9.

Table 9 - Properties of polyester and epoxy resin (97,98)

Property	Polyester 272	Epoxy MY750
Specific gravity	1.20	1.21
Tensile strength	75 MPa	75 - 90 MPa
Tensile modulus	3.5 GPa	2.5 - 3.5 MPa
Strain to failure	3.8%	3 - 5%
Head deflection temperature under load (HDT)	75°C	~ 130°C
Shrinkage on cure	8.3%	Not available

3.2.2.3 Resin additives

Resin additives were used to control and modify the basic resin properties. A flexibiliser, Crystic 586, was used in varying proportions with Crystic 272. The effect of this flexibiliser is to increase toughness and resilience whilst at the same time reducing the brittleness of the standard resin. The addition of Crystic 586 has, however, an adverse effect on other mechanical and chemical properties (99).

A resin modifier was also used with Crystic 272. This was an experimental reactive liquid rubber which is compatible with polyester resins. The compound, named CRC 1080, was manufactured by Scott Bader. Proportions up to 30 pph were used with the basic resin.

Araldite CY208, a flexibiliser, was used with MY750 to provide a degree of control of the resin properties. The proportions used were 50/50 with the basic resin. Araldite CY208 is a fully reactive liquid epoxy resin designed to improve toughness and impact strength. It has the disadvantage, however, of reducing the heat deflection temperature (100).

3.3 Experimental methods

3.3.1 Filament winding

All tubes were manufactured using a filament winding machine. The machine was a bench-top model, of a lathe type, designed by ICI and built in conjunction with Unimatic Engineers Ltd. (see Fig. 3.1). It consisted of a machined metal mandrel driven by a water-cooled stepping motor and an accurately machined lead screw with its long axis parallel to the mandrel driven by another stepping motor. A feed bath (Fig. 3.2) was mounted on this lead screw which could traverse parallel to the mandrel as the screw was rotated. Fibre tension was controlled by the position of the guide pins in the resin bath, which also removed excess resin from the impregnated glass fibres.

The relative speed and direction of the two motors controlled the fibre angle of the tube being wound. The angle was variable from $\theta=35^{o}$ up to $\theta=89^{o}$ where θ is the angle between the fibres and the long axis of the mandrel. The low-angle limitation during winding was found to be 35^{o}. Any angle below 35^{o} resulted in a large degree of fibre slippage.

With angle-ply tubes alternate fibre rovings were laid down in the helical winding process giving rise to an open basket-weave structure. Each fibre laid down at $+\theta^{o}$ had a complementary fibre interwoven at $-\theta^{o}$. In covering the mandrel

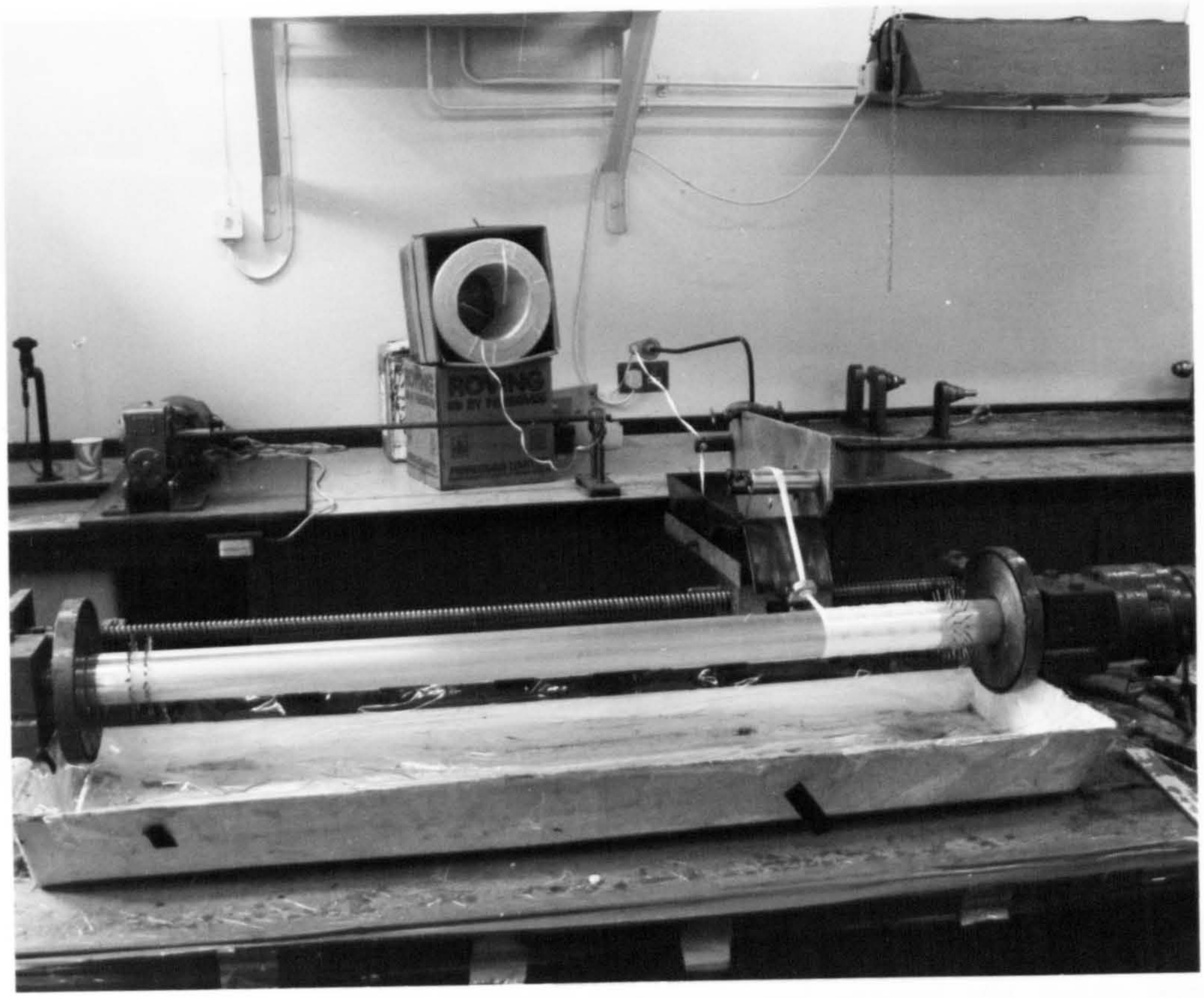

Fig. 3.1. General view of the construction of a 0/90 tube on the filament winding machine (resin omitted for clarity).

Fig.3.2. Resin bath on the filament winding machine.Note the glass fibres passing through the bath and around the guide pins. Resin omitted to improve clarity.

once, two interwoven laminae were laid down at $+\theta^{o}$ and $-\theta^{o}$. Figure 3.3 shows the build-up of a complete cover. Each angle pipe was made from two such complete covers i.e. the lamination being $+\theta^{o}$ $-\theta^{o}$ + θ^{o} $-\theta^{o}$.

For hoop-wound tubes (θ=90^{o}), the construction was slightly different. Winding commenced from one end of the mandrel, with one complete pass being made along the mandrel at slow speed so that a complete cover was laid down. This was reversed and another complete cover of fibres laid down over the top of the first layer. Thus, interweaving of the fibres did not occur. Further details of filament winding can be found in Legg (101) and Jones (102).

As filament winding below 35^{o} was impractical, the production of tubes with axial (0^{o}) fibres necessitated modifications to the mandrel. A system of fixed pins was incorporated into the ends of the mandrel which enabled the impregnated fibres to be wound sequentially around the pins at each end. The pins were positioned at 10^{o} intervals giving, for a 50 mm diameter mandrel, a spacing between pins of 4.4 mm. This distance was chosen as experience had shown that impregnated fibres when laid down were approximately 5 mm in width. Thus a complete cover of axial fibres could be laid down on the modified mandrel which is shown in Figure 3.4.

0^{o}/90^{o} tubes were manufactured by initially winding one complete layer of hoop fibres and then manually laying down a layer of axial fibres, with the winding machine acting only as a support for the mandrel and bath. The excess resin was removed from the axial fibres and the whole allowed to rotate slowly until gelling of the resin took place. After this, a second layer of axial fibres

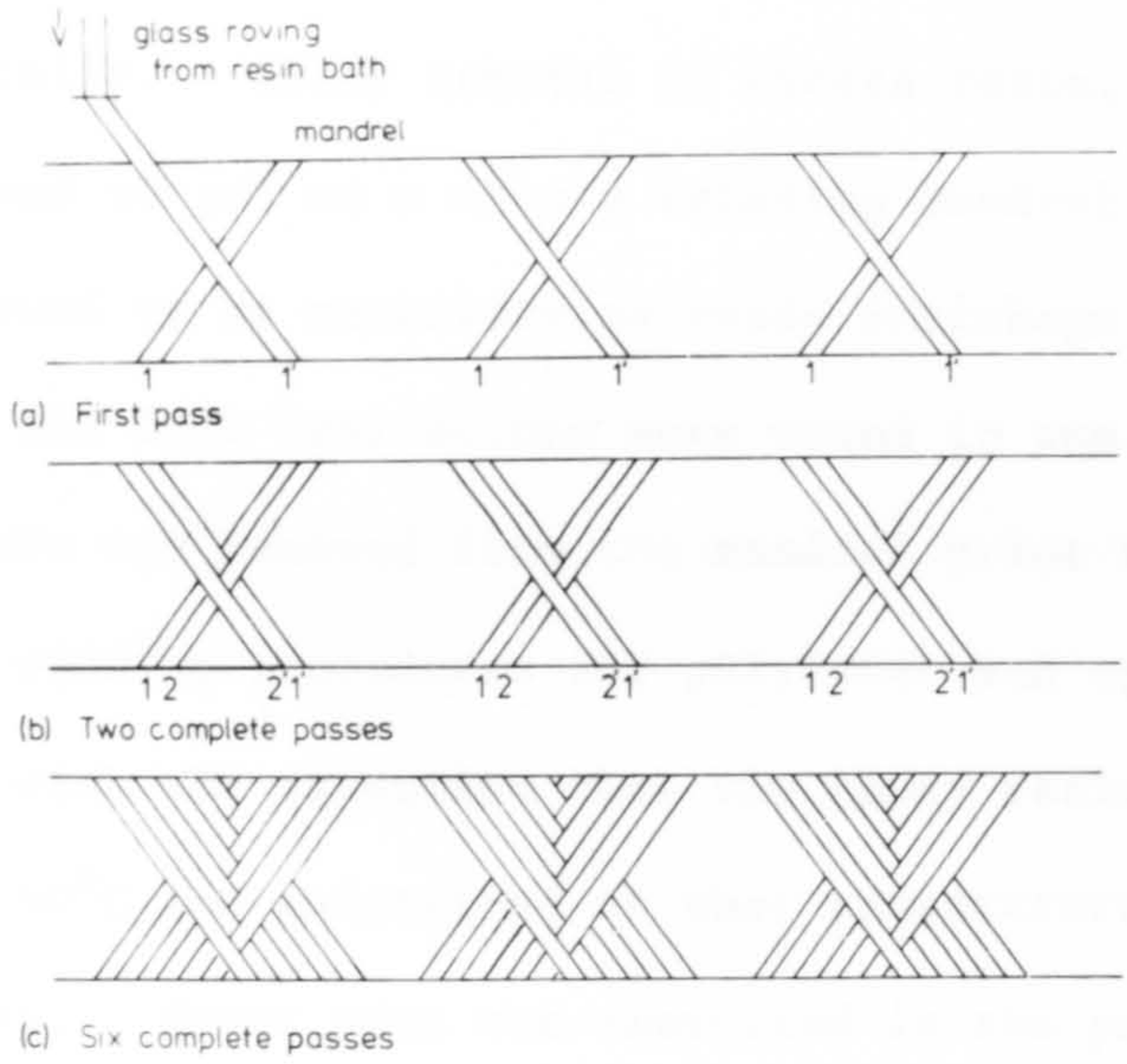

Fig. 3.3. Diagram of the build-up of a complete cover during angle-ply winding showing cross-over points.

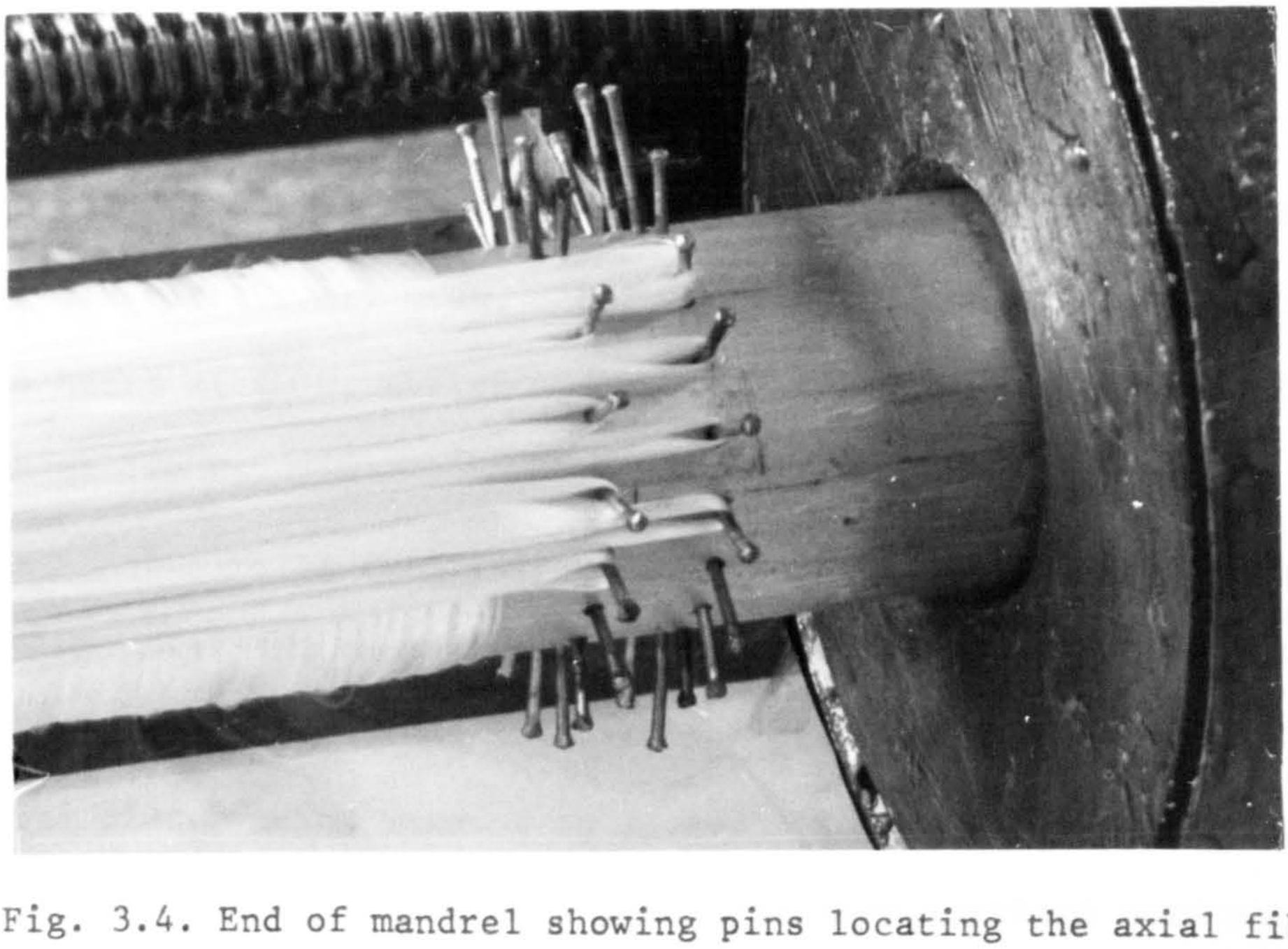

Fig. 3.4. End of mandrel showing pins locating the axial fibres.

Resin omitted for clarity.

was laid down by hand, followed immediately by a layer of hoop fibres wound mechanically. After removal of excess resin, the completed tube was allowed to gel on a slowly rotating mandrel. The delay in winding was found to be necessary as resin shrinkage was difficult to control if all four laminations were wound in one session. After gelling the tube was removed from the mandrel prior to post-curing.

The winding procedures for polyester and epoxy resins were similar, with the exception that the epoxy resin had to be pre-heated to 40°C and maintained at that temperature during the winding process. Great care was exercised in the preparation of the mandrel prior to winding in order to facilitate its extraction from the tube. The most reliable method was to lightly abrade the mandrel with 1200 grade wet and dry paper, coat with a non-silicone wax, polish off and then coat with a proprietary mould release agent based on polyvinyl alcohol.

3.3.2 Preparation of tubular specimens

After extraction from the mandrel, all tubes were post-cured in an air circulatory oven. Polyester-based tubes were post-cured for 4 hours at 80°C, whilst epoxy-based tubes were post-cured for 4 hours at 120°C.

Following post-cure, the tubes were cut into specimen lengths, ensuring that the ends of the tube were at right angles to the long axis. The internal and external diameter were measured in several places using vernier calipers. The tubes were weighed and the length noted. A 45° bevel was then machined onto one end of the tube. Initially, this was carried out on a lathe to ensure an accurate bevel. However, experience showed that reliable results could be obtained by hand-machining a bevel onto the tube with a linishing belt. This method was adopted as being fast and

effective.

3.3.3 Flat composite plates

Micrographical studies on fracture surfaces required the production of flat unidirectional composites for 3-point bend, transverse and off-axis tensile testing. These were manufactured on the filament winding machine using a modified mandrel. Details of the technique are given by Gatward (103).

3.3.4 Flat resin sheets

Resin sheets were produced from Crystic 272, epoxy MY750 and epoxy MY750/CY208. The resin was poured between two thick, parallel, vertical steel plates clamped together onto steel shims of a specific thickness. The steel plates were sealed around the edge with a rubber strip. The resins were pre-mixed (accelerated and catalysed) at least 30 minutes before casting in order to allow entrapped air to escape from the resin. After cure, the steel mould was carefully split, the resin plate was removed and post-cured between two glass plates for the same time and temperature as the filament-wound tubes. The sheets were then cut to size for either fracture toughness or tensile testing depending on the sheet thickness. Fracture toughness specimens for double torsion testing were cut to a nominal size of 80 x 250 mm. The thickness of the sheet was 6 mm. A single groove 0.152 mm wide and 1 mm deep was cut down the length of the specimen using a slitting wheel. This groove was cut to the full depth of the specimen for 1 cm from the edge. This aided crack initiation. The groove was flat bottomed and, prior to testing, was notched with a sharp razor blade.

For tensile testing, flat sheets 3.2 mm thick were cast. Specimen sizes to ASTM D638 Type 1 were machined between templates,

the edges being ground and polished by hand to 1 μm.

3.4 Mechanical testing

3.4.1 Tubes

Testing of tubes to determine the crushing load under axial compression was carried out on one of three machines depending on the required cross-head speed. For speeds below 4×10^{-3} m s^{-1} a conventional hydraulic Instron machine (Model no. 1273) was used. For speeds from 4×10^{-3} to 4 m s^{-1}, a unique servo-hydraulic testing machine was used. This was designed and built to Liverpool University specifications by Cranfield Institute of Technology. This machine had a load capacity of 170 kN and was equipped with two load cells of either 250 or 120 kN capacity. Operating under displacement control, constant cross-head speed could be maintained over virtually all of the stroke of 500 mm. Data were stored digitally via a Bryan Southern 512A transient data store, and subsequently output to a Bryan Southern 50,000, x-y recorder.

Higher speeds over 4 m s^{-1} were available on a catapult impact machine with a maximum speed at impact of 15 m s^{-1} (35 miles h^{-1}). This machine was designed by Liverpool University and built by Mand Testing Machines Ltd. The machine consisted of a sled measuring 700 mm x 810 mm and weighing 290 kg upon which the specimens were mounted. The sled was driven along an 8 metre track by parallel bungee cords at an initial acceleration of 3g. The track was mounted in a rigid box frame carried on six axles and terminated at the impact end by a thick steel target plate. All forces were contained within the framework so that floor reactions were negligible during acceleration and impact. On-board accelerometers were used to measure the deceleration produced by the specimen and a track mounted steel wire was used to determine the position of the sled

with respect to the frame. Impact forces were measured by four load cells which supported the target plate. Data were stored digitally and processed via an Apple II computer to produce acceleration and velocity profiles and energy absorbed versus crush distance diagrams. A line diagram and photograph of the crash rig are shown in Figs. 3.5 and 3.6.

The main difference, apart from speed, between the crash machine and conventional testing machines lies in the control of the cross-head platen during testing. With conventional machines, displacement is at a constant rate. With the crash machine, the velocity of the specimen and sled was at a maximum at the point of impact. The velocity then decreased at a rate governed by the energy absorbing characteristics of the specimen. Hence, with specimens exhibiting progressive deformation, the speed of the deformation zone travelling down the specimen varied from impact speed to rest.

3.4.2 Double torsion testing

The equipment for double tension testing is shown in Figs 3.7 and 3.8. It was designed to be compatible with the Cranfield testing machine and consisted of two 15.7 mm diameter touching steel balls fixed directly to a bar connected to the load cell. Two parallel steel bars 64 mm apart on which the specimen rested were bolted to the moving cross-head. The resin specimen was positioned with the notched end central under the two loading balls with the goove downwards. The resin sheet was held onto the steel bars by light pressure supplied by two elastic bands.

During testing, not all specimens failed with the crack staying in the groove. In some instances the crack travelled in the

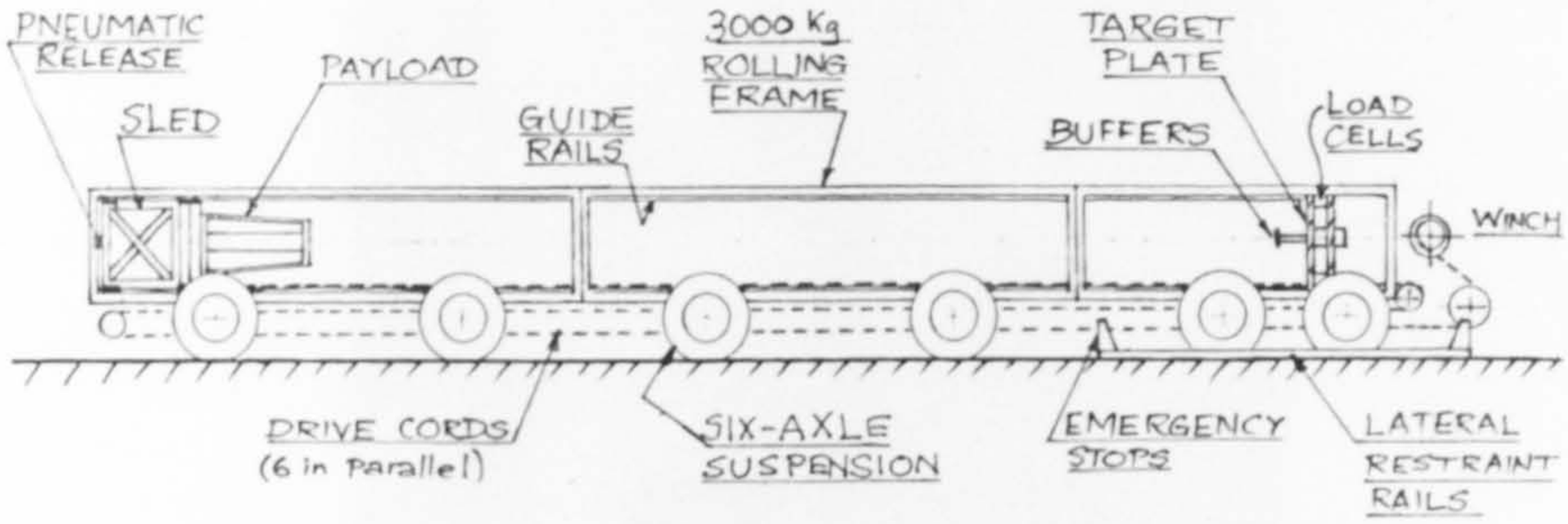

Fig.3.5. Diagram of the crash rig(courtesy Mr.J.Blears).

Fig.3.6. Photograph of the crash rig.Target plate is at the far end.

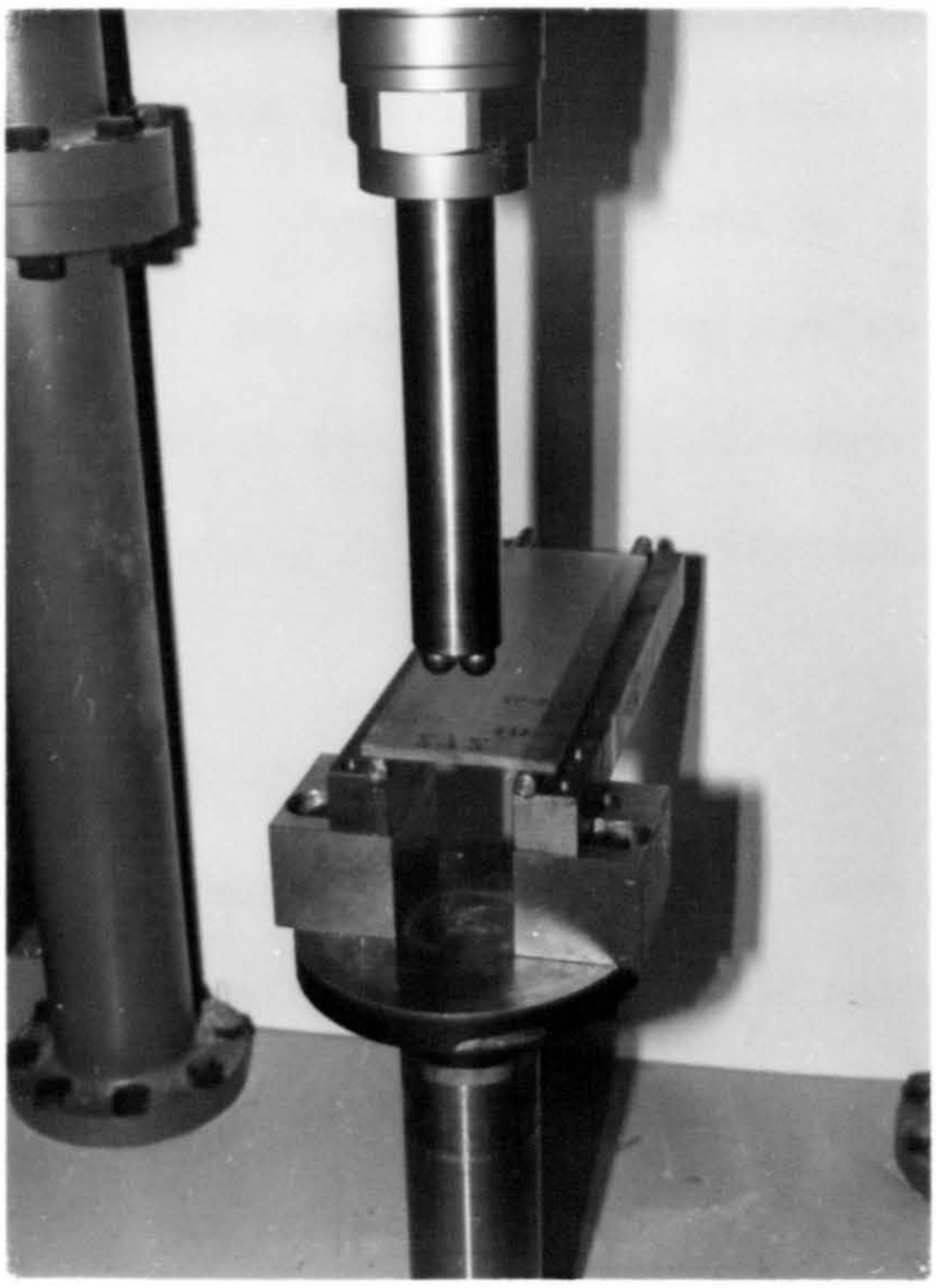

Fig. 3.7. Equipment for double-torsion testing.

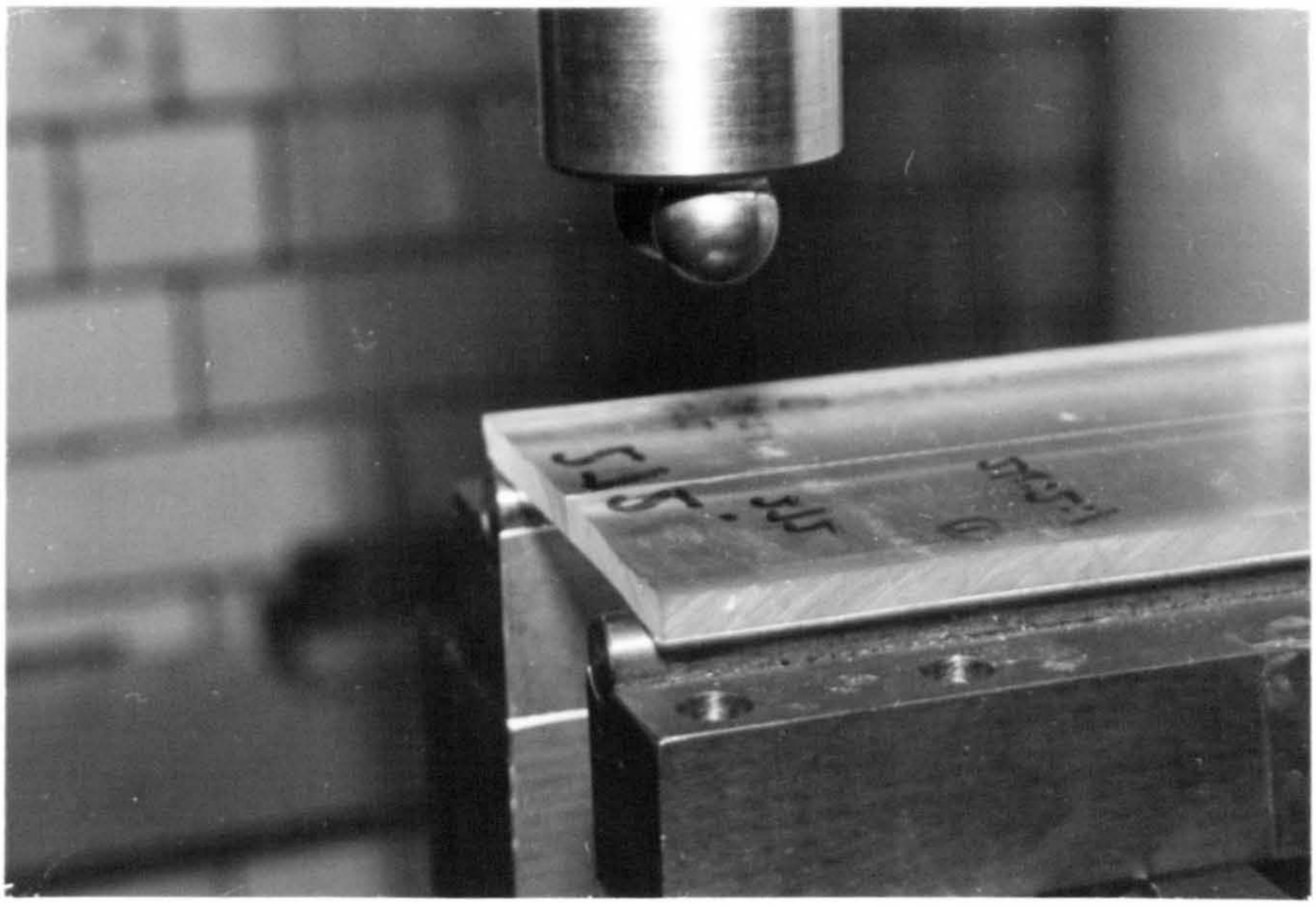

Fig. 3.8. Close up of loading situation during double-torsion testing of resin plates.

groove long enough to give a valid result. In other instances the crack progressed away from the cut groove almost immediately, making the test invalid. Cross-head speeds up to 1 m s^{-1} were used. At speeds above 1 m s^{-1} the ability of the equipment to accurately monitor the load was poor, owing to the low loads and the rapid fluctuations of load values as the crack progressed along the specimen.

3.4.3 Tensile testing

Tensile testing was carried out on pure resin specimens using standard grips on an Instron screw feed machine (Model 1185). Load measurement was by load cell and strain measurement by a clip gauge attached to the test piece, reading on to a chart recorder. Cross-head speed was constant at 10 mm min^{-1}. Strain and load were constantly recorded during the test so that modulus, failure strain and ultimate stress could be determined.

As an aid to micrographical studies, tensile testing was carried out on specimens cut from unidirectional plates constructed from 'E' glass-polyester '272' resin. Specimens were cut from flat unidirectional sheets so that the fibre orientation was either perpendicular or at 10^{o} to the loading axis. Specimens with fibres perpendicular to the axis were designed to fail in a transverse tensile manner, whilst those tested at 10^{o} failed generally in a shear mode. The dependence of the failure modes on orientation is discussed by Hull (26). As these specimens were for micrographical studies, no measurements were taken of load or displacement.

3.4.4 Three-point bend testing

In order to provide shear fracture surfaces for

micrographical examination, three-point bend tests were carried out on unidirectional 'E' glass-'272' polyester resin specimens. Short samples were cut from thick plates manufactured on the filament winder. Testing was carried out using a three-point bend fixture on an Instron screw machine at 10 mm min^{-1}. A span-to-depth ratio of 5 was used in order to promote intralaminar shear on the centre plane (104). No direct measurements of load or displacement were taken.

3.4.5 Volume fraction determination

A limited number of fibre volume fractions were determined according to standard methods (105). This involved the ignition of the resin from a small sample taken from the tube wall.

3.5 Micrographical examination

Examination of specimens at magnifications up to x25 was carried out on a Wild M8 binocular microscope equipped with photographic facilities. Sections were taken through the crush zone using a small fret-saw with a sharp, fine blade. These sections were required to simulate conditions during crush and so were placed in rubber test tube clamps which were tightened until further crush occurred. They were then polished, still under load, using standard metallographic techniques, finishing with 6μ diamond paste. The specimens were then examined on the microscope using reflected light.

Medium magnification optical studies were carried out on a Reichert Zetopan microscope equipped with photographic facilities using reflected light. Specimens were prepared by taking a small section from the crush zone using a fret-saw. The specimen was then mounted in Scandi-Plast cold setting compound. Polishing

was carried out using standard metallographic techniques, finishing with 1μ diamond paste. An etchant was used to increase contrast between the fibres and the resin. This was 48% hydrofluoric acid which was diluted 50% by volume with distilled water. The polished specimen was immersed for 5 to 10 seconds, thoroughly washed in distilled water, then immersed for 30 minutes in a solution of sodium bicarbonate in water. The latter was to ensure that no trace of hydrofluoric acid remained that could damage the microscope lens. After drying the samples were mounted on a glass slide and examined on the microscope.

Fracture surfaces were examined by scanning electron microscopy, using segments taken from the crush zone. These were mounted on small metal stubs designed to fit into the microscope, cleaned in an ultrasonic cleaner with distilled water and dried. The surfaces were then coated with a thin layer of gold in an Edwards S150 sputter coater, and the coated specimens examined in a Phillips 501 scanning electron microscope.

CHAPTER 4 - EXPERIMENTAL RESULTS AND INITIAL DISCUSSION OF COMPRESSION TESTING AND FRACTURE TOUGHNESS

4.1 Introduction

The results of the experimental work are presented in this and the subsequent chapter. Chapter 4 contains the specific energy absorbed results for the axial crushing of tubes under various conditions. The results of fracture toughness tests and a limited number of tensile modulus tests on bulk resin are also included. Chapter 5 contains the results of the micrographical studies.

The preliminary work was mainly concerned with angle-ply filament-wound glass-polyester tubes. Initially, end reinforcements were wound onto the tubes prior to testing. This always resulted in a centre failure mode, as discussed by Hull (106). Consequently, in later work, bevelled rather than reinforced ends were used. This resulted in an increase in the energy absorbed and provided a reliable trigger mechanism for progressive failure during axial crushing. Further development work on filament winding techniques provided tubes with continuous fibres in the axial (0^{o}) direction. Tubes could then be produced consistently with an orientation to the tube axis of one layer of fibres at 90^{o}, two layers at 0^{o} and one layer at 90^{o}. This configuration was used in the majority of the experimental work with variables of matrix properties and test-rate. The tubes were examined micrographically in order to determine the major failure mechanisms that were taking place during crushing. These results are presented in Chapter 5. Limited work was carried out on bevelled-end angle-ply tubes to investigate the effects of winding angle on energy absorption and failure mechanism.

Owing to a lack of published data, a certain amount of back-

ground work on fracture toughness and modulus was found to be necessary, in order to provide data on resin properties. Micrographical studies were also carried out on unidirectional specimens that had been fractured in a controlled manner, in order to provide reference fracture surfaces for comparison with the fracture surfaces of crushed tubes.

4.2 Axial crushing of tubes

4.2.1 Determination of specific energy absorption.

The results from the axial crushing of tubes are given as average crushing load and specific energy absorption (SEA). The average crushing load, P, was determined directly from the load-displacement trace. Two methods of determination were used depending on the shape of the load trace. The load traces from the crushing of the majority of the tubes were serrated, with a constant average load. Other tubes, such as those made with epoxy resin, gave a slightly decreasing load trace which then levelled out to a constant value as crushing continued. The energy absorption, Ea, was determined in these cases from measurement of the area under the load-displacement trace. Both methods of calculation are shown in Fig. 4.1. The SEA was then calculated from either the average crush load, P, or the total energy absorbed, Ea, in conjunction with the specimen length and weight before bevelling, in accordance with the equations given in Fig. 4.1.

These equations apply to all tubes where the dimensions of the crush zone are approximately constant throughout the crushing process, with reference to the face of the cross-head platen. For polyester $0^{o}/90^{o}$ tubes, the crush zone was found to be 10-15 mm wide (see Section 6.7) and to be independent of crush distance over the displacements used. The crush zone varied with fibre orientation

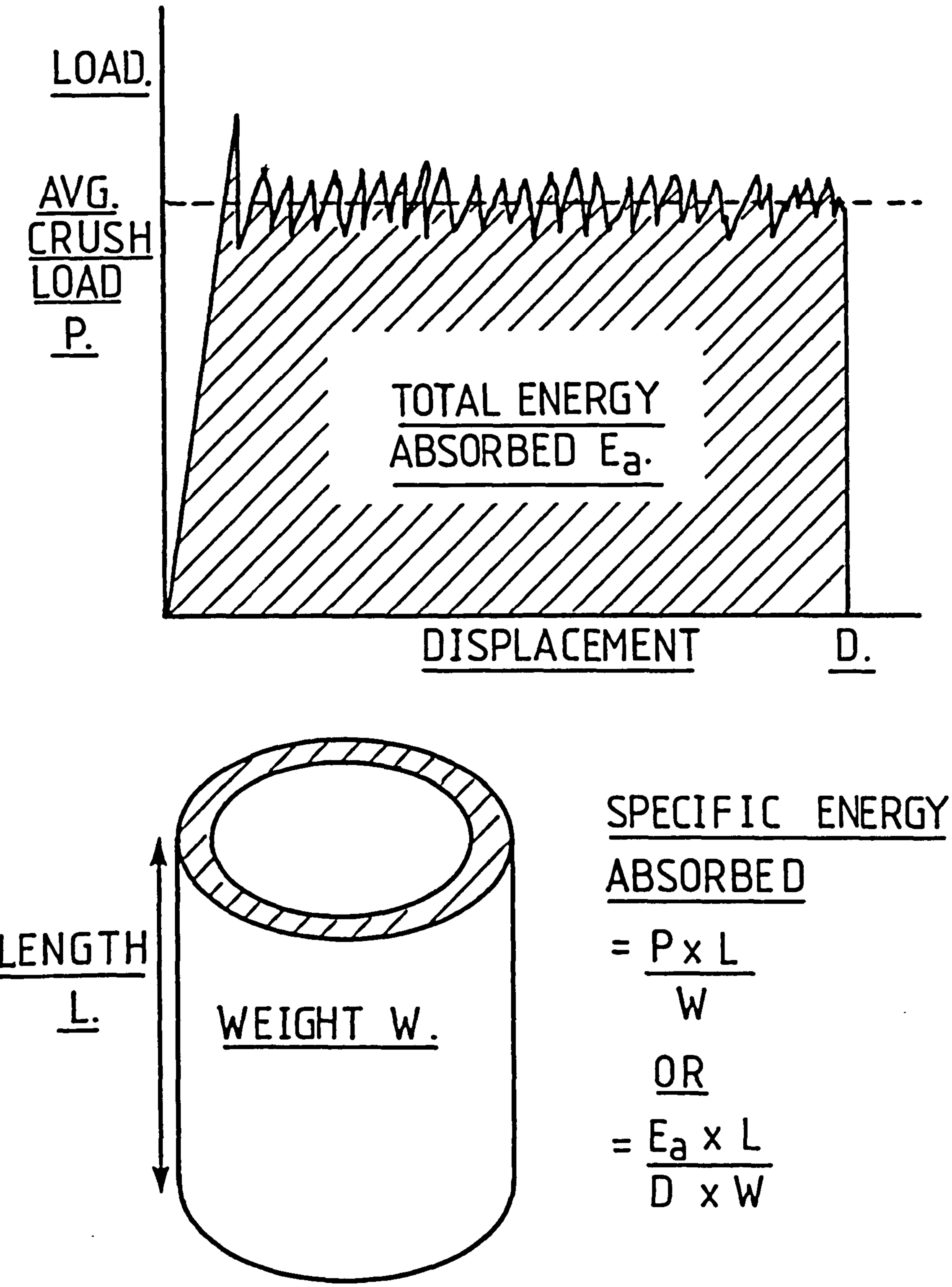

Fig. 4.1. Schematic load-displacement trace for the crush of a bevelled tube and the method for determination of specific energy.

and material properties, but remained approximately constant during each crush.

Unless stated, testing was carried out at ambient temperature ($20^{o}C \pm 3^{o}C$). The glass volume fraction is also quoted for each tube in conjunction with values of energy.

4.2.2 Effect of cross-head speed

The results for axial compression of polyester $0^{o}/90^{o}$ tubes are shown in Table 10. All tubes were tested with a 45^{o} bevel machined onto one end. Failure was by progressive crushing from the bevelled end. Using the Instron or Cranfield machines, constant cross-head speeds of between 0.33×10^{-3} and $4.4\ ms^{-1}$ could be obtained. Higher speeds of up to $13.8\ m\ s^{-1}$ were produced on the crash rig using a variable cross-head speed.

For tubes tested on the Instron or Cranfield machine (average tube length approx. 200 mm) strain rates were of the order of 1.6×10^{-3} to $20\ s^{-1}$. It is important to note that only a small proportion of the tube is directly involved in the crushing process; hence the traditional concept of strain-rate is not entirely valid for these materials and deformation modes. The higher speeds on the crash rig were all carried out with longer tubes, giving a conventionally calculated strain rate of $17.2\ s^{-1}$.

The results are shown in Fig. 4.2. Average values of SEA for each test speed have been used to determine the trend with respect to speed. The graph shows energy absorption decreasing with increasing speed. The results obtained at very high speed on the crash rig were much lower than expected, probably because of the different loading conditions, i.e. the variable displacement rate.

Table 10 - Specific energy absorption values for $0^{o}/90^{o}$ tubes : effect of cross-head speed

Resin : Crystic 272

Fibre orientation : $90^{o}/0^{o}/0^{o}/90^{o}$

Cross-head speed m s^{-1}	Tube dimensions				Glass volume fraction	Average crush load KN	Specific energy absorbed J g^{-1}
	ID, mm	OD, mm	Length, mm	Weight, g			
0.33×10^{-3}	49.96	57.99	73	86	0.40	93.7	79.5
0.33×10^{-3}	49.99	57.94	59	69	0.40	87.5	74.3
4.0×10^{-3}	50.00	57.58	188	216	0.36	86.0	74.9
4.2×10^{-3}	49.97	57.05	168	183	0.42	73.8	67.6
4.2×10^{-3}	50.00	57.31	164	183	0.42	69.8	62.4
4.3×10^{-3}	49.99	57.29	217	241	0.47	81.0	73.0
4.3×10^{-3}	49.94	57.42	210	242	0.44	79.7	69.0
4.3×10^{-3}	49.92	57.51	227	267	0.43	69.7	59.4
4.4×10^{-3}	49.94	57.90	167	203	0.42	89.4	73.5
4.4×10^{-3}	49.98	58.14	158	196	0.43	90.4	72.9
34.2×10^{-3}	49.97	57.58	227	257	0.44	78.9	69.6
34.2×10^{-3}	49.98	57.51	213	242	0.47	73.8	64.8
1.7	49.95	57.54	216	246	0.44	69.7	60.9
1.7	49.99	57.31	222	247	0.47	68.7	61.9
1.7	49.94	57.65	213	247	0.43	66.6	57.3
1.9	49.96	56.56	166	182	0.42	62.3	56.8
1.9	49.99	57.51	168	193	0.42	64.1	55.8
3.6	49.96	57.70	216	255	0.43	65.0	54.2
3.9	49.99	57.72	163	196	0.42	70.0	58.2
3.9	49.97	58.15	158	197	0.43	73.4	58.9
10.8(Var.)	49.97	56.83	633	688	0.46	57.0	54.1
13.8(Var.)	50.07	57.18	758	882	0.44	49.2	40.4
13.8(Var.)	50.00	57.58	188	216	0.36	86.0	41.7

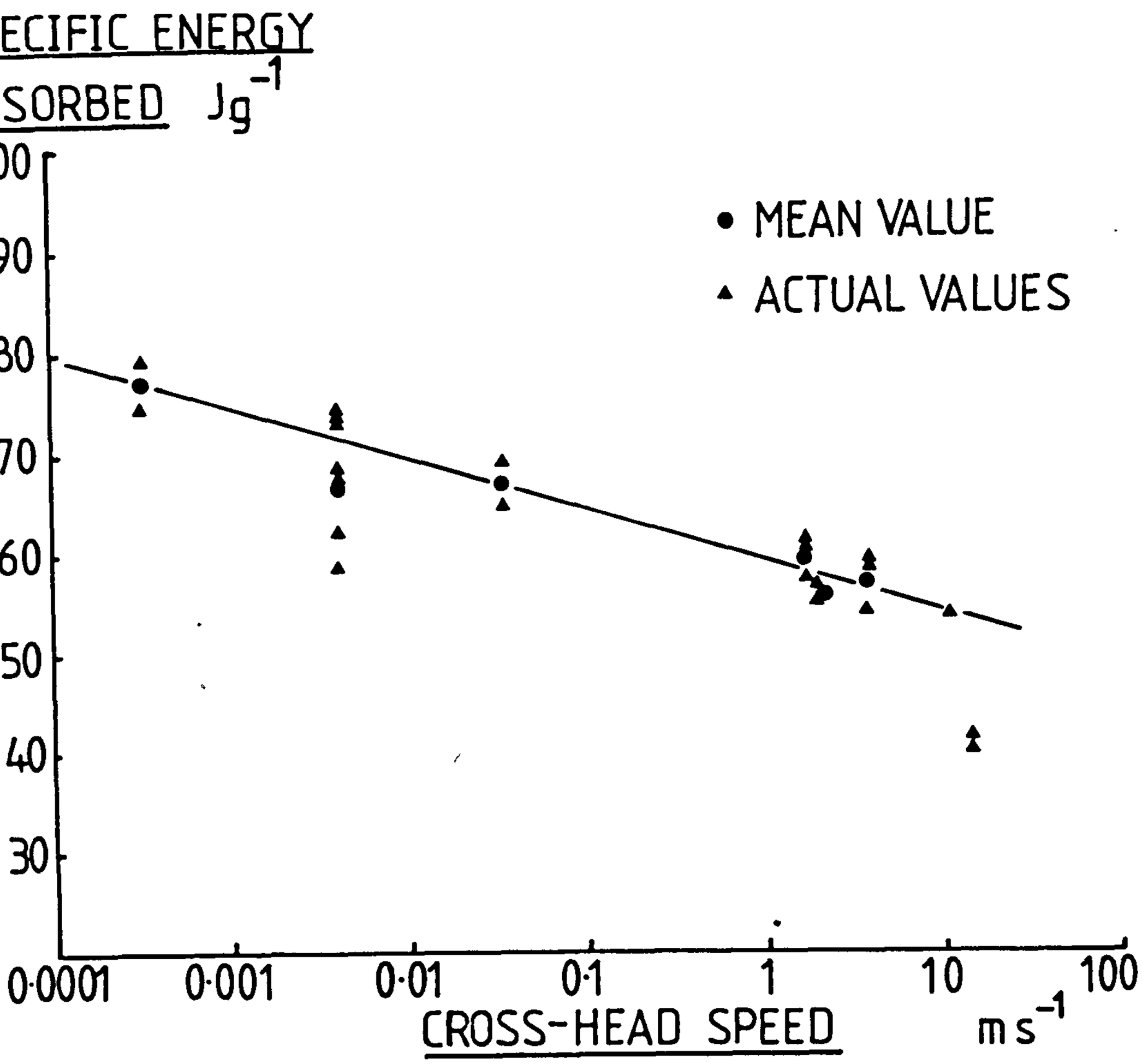

Fig. 4.2. Variation of specific energy absorption during crushing of polyester 0/90 degree tubes with cross-head speed.

The load-displacement traces were generally constant with variations about a mean. Typical load-displacement traces are shown in Figs.4.3 to 4.6 for four different speeds. All traces show random variations about a mean value, with the magnitude of the serrations increasing as the cross-head speed increased.

With the variable deformation rate of the crash rig, it would be expected that the crushing load would increase as the rate of crush becomes progressively slower. This is predicted from the rate sensitivity of polyester tubes, which give a higher crushing load at slower speeds. This anomalous situation may be due to the effect of friction during crushing, which gives rapid increases in temperature in the region of the crush zone. The temperature increase may affect the properties of the tube.

The scatter of results in Fig. 4.2 is due to several factors. Some variations in the construction of each tube were inevitable because of the method of hand lay-up of the axial fibres. Variations in the tension of the fibre tows were difficult to avoid especially during winding around the locating pins. This was further aggravated by the removal of excess resin from the axial fibres of the inner axial lamina, which tended to cause long thin voids between the fibre tows. These voids did not, unfortunately, become visible until the other laminations were wound on the tube and curing had been completed.

Different batches of resin were used during the experimental work, and there may have been some variation in consistancy between batches. This problem has also been encountered by other workers using epoxy resins (60). The problem of batch to batch resin variation is particularly noticeable with tubes tested at 4×10^{-3} $m\,s^{-1}$.

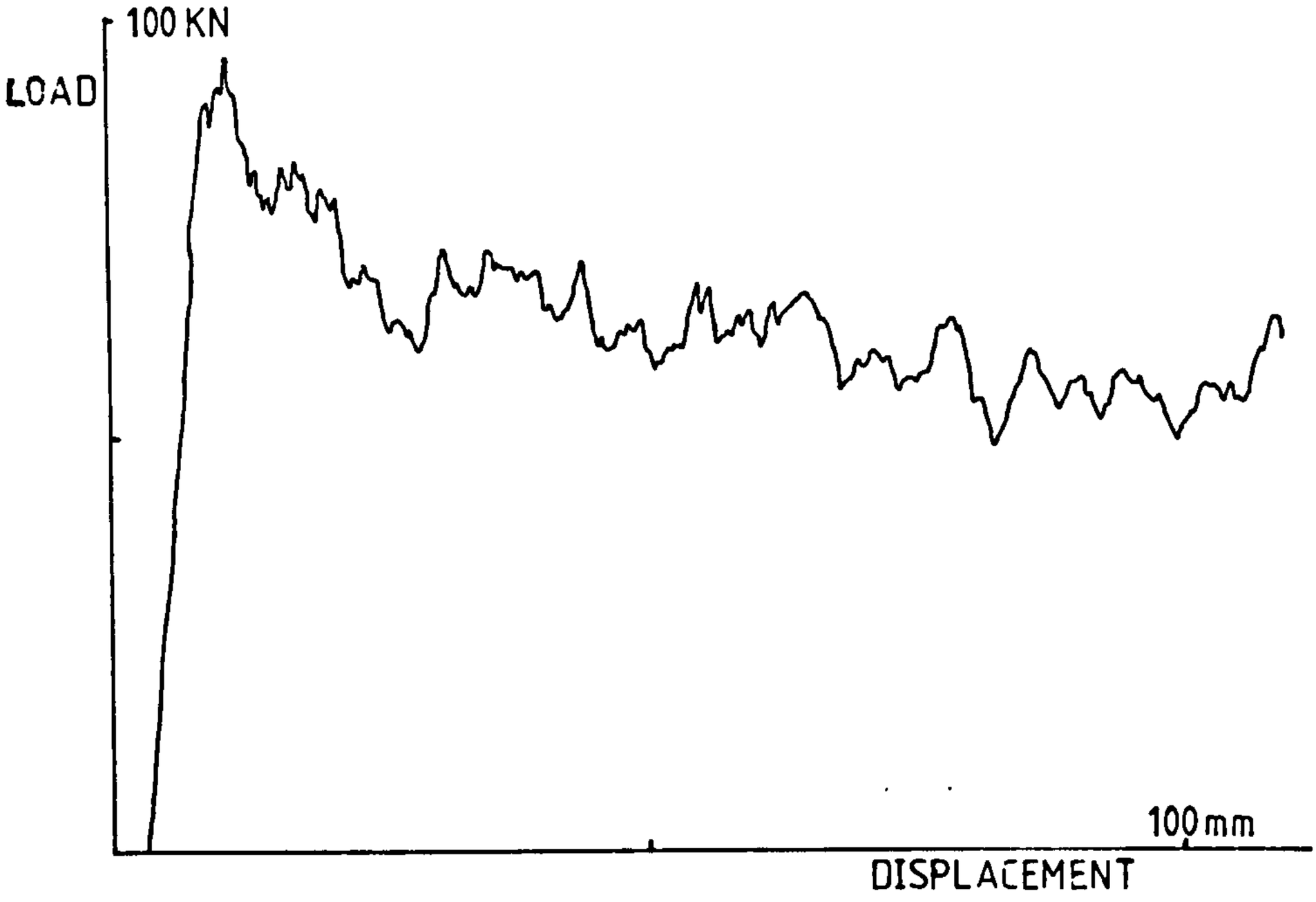

Fig. 4.3. Typical load-displacement trace for a 0/90 degree tube, Crystic 272 resin, tested at 4 mm s^{-1}.

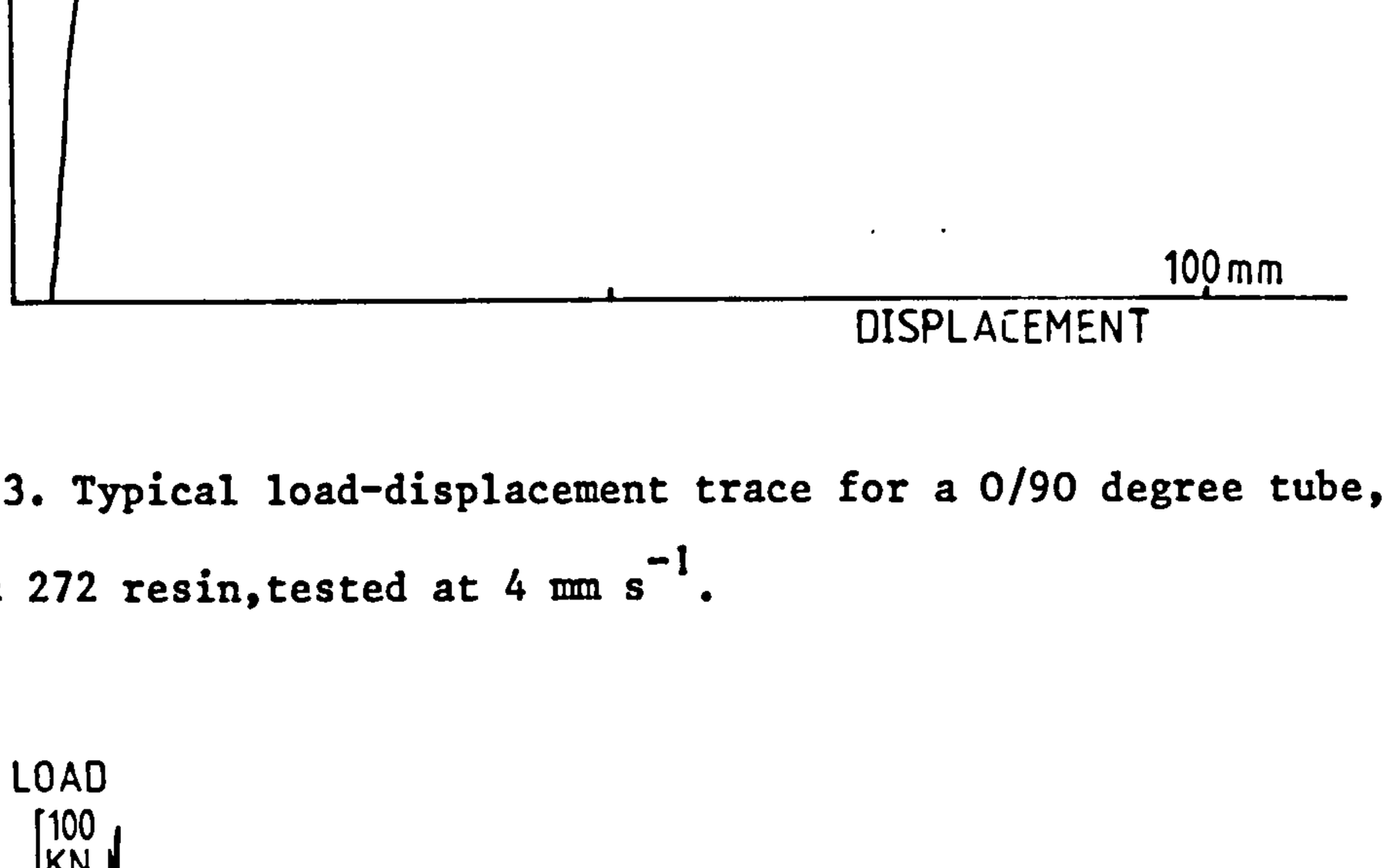

Fig. 4.4. As above but tested at 1.74 ms^{-1}.

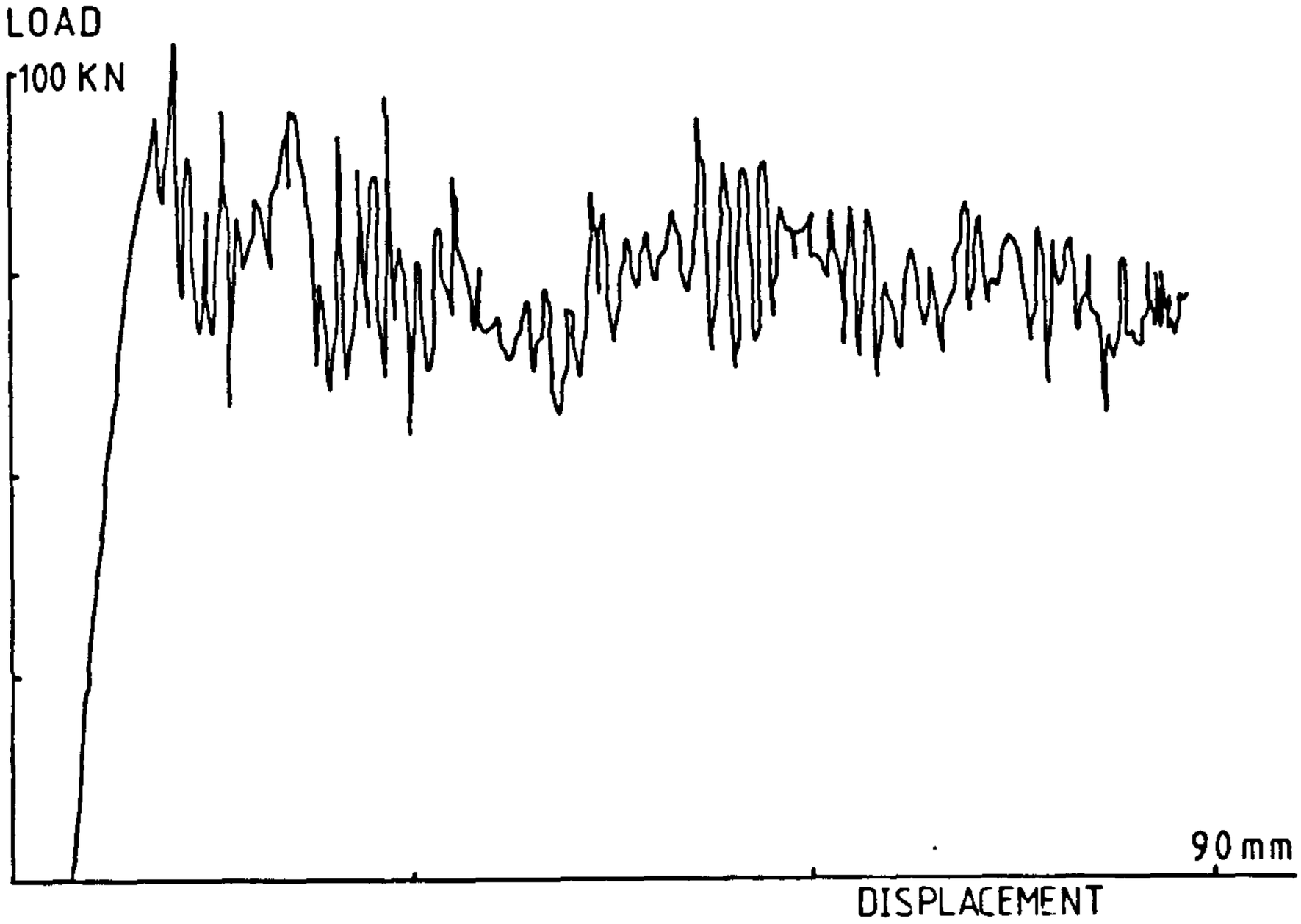

Fig. 4.5. Typical load-displacement trace for a 0/90 degree tube, Crystic 272 resin, tested at 4 ms^{-1}.

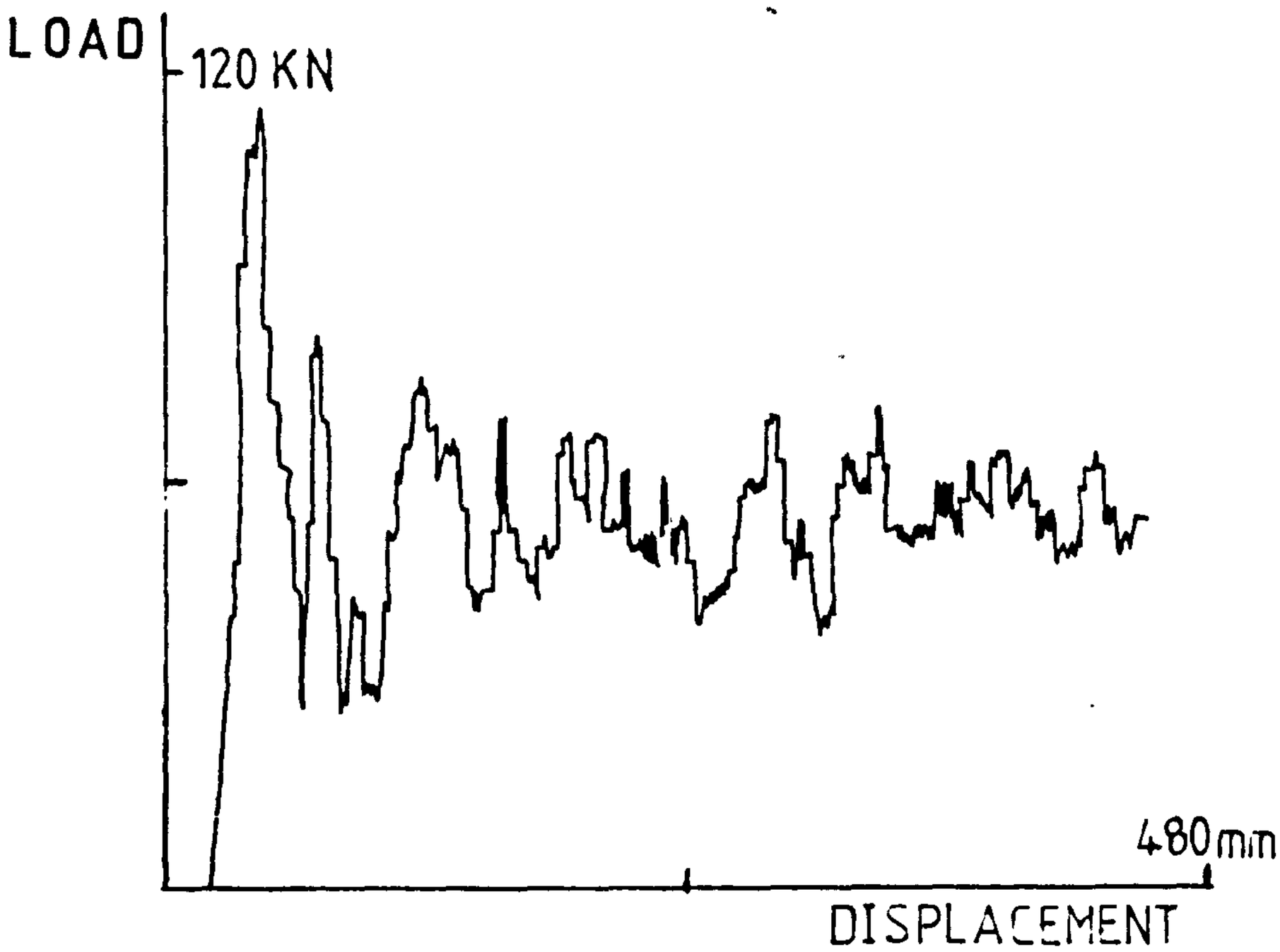

Fig.4.6. As above but tested at 13.8 ms^{-1}.

These tubes were made from several batches, whilst tubes tested at other speeds tended to be made from a single batch of resin.

Variations in tube fibre volume fraction were inevitable. The glass volume fractions are indicated in Table 10. Even though such variations would be expected to affect the specific energy absorption, the results do not show any definite relationship. High volume fractions were associated with both high and low values of energy absorption.

4.2.3 Effect of resin modification and cross-head speed

Two types of modification were carried out on the basic Crystic 272 resins. The first modifier was a polyester resin, Crystic 586, which was a flexibiliser having a low modulus. The second was a reactive liquid rubber, CRC 1080. The aim of these modifications was to improve the fracture toughness of the resin without greatly affecting the other mechanical properties.

The results are shown in Tables 11-14 for test speeds of 4.3×10^{-3} and 4 m s^{-1}, and are displayed graphically in Figs.4.7 and 4.8. In all cases, a $0^{o}/90^{o}$ winding configuration was used. All tubes were bevelled and in every case failure was progressive from the bevelled end. Results for unmodified resin were taken from average values in section 4.2.2.

At the low speeds, there was an increase in the SEA with increasing CRC 1080 content, reaching a maximum value at 10-15% by volume. Further additions resulted in a reduction in SEA. At the high speed, this effect was not noticed, with additions of CRC 1080 giving only slight increases in SEA. With 30% by volume CRC 1080 the SEA at high and low test speeds were similar. Little variation could be attributed to the effects of glass volume fraction, as this was in the range 0.42 to 0.45 for all tubes tested.

Table 11 - Specific energy absorption of $0^{o}/90^{o}$ tubes : effect of CRC 1080 resin modifier in Crystic 272. Test speed 4.3×10^{-3} ms^{-1}

CRC 1080 in Crystic 272 vol %	Tube dimensions				Glass volume fraction	Average Crush load, kN	Specific energy absorbed, Jg^{-1}
	ID, mm	OD, mm	Length, mm	Weight, g			
5	49.98	57.62	161	182	0.44	82.2	72.5
5	50.02	57.52	155	176	0.44	99.6	78.4
10	49.99	57.74	154	177	0.43	97.1	84.4
10	49.98	57.46	164	184	0.43	89.8	80.0
15	49.93	58.38	158	197	0.38	99.0	79.4
15	49.99	59.02	165	214	0.38	106.9	82.5
20	49.97	58.09	153	183	0.41	94.2	78.8
20	49.99	58.07	151	179	0.41	94.4	79.9
30	50.05	57.91	154	178	0.39	77.0	66.4
30	49.94	58.37	167	200	0.39	83.6	69.9

Table 12 - Specific energy absorption of $0^{o}/90^{o}$ tubes : effect of CRC 1080 resin modifier in Crystic 272. Test speed 4 m s^{-1}

CRC 1080 in Crystic 272, vol %	Tube dimensions				Glass volume fraction	Average crush load, kN	Specific energy absorbed, Jg^{-1}
	ID, mm	OD, mm	Length, mm	Weight, g			
5	49.96	57.78	154	175	0.44	66.6	58.6
5	49.97	57.95	160	189	0.44	70.4	59.6
10	49.97	57.59	157	178	0.43	70.0	61.6
10	50.01	57.57	185	209	0.43	70.2	62.3
15	49.97	58.52	156	192	0.38	64.5	52.0
15	49.90	58.70	156	199	0.38	77.4	60.4
20	50.00	58.20	166	196	0.41	72.6	61.6
20	49.98	57.70	165	191	0.41	73.7	62.4
30	49.97	58.45	104	196	0.39	73.2	61.3
30	50.00	58.55	173	208	0.39	78.2	65.0

Table 13 - Specific energy absorption of $0^{o}/90^{o}$ tubes : effect of Crystic 586 modifier in Crystic 272 Testing Speed 4.3×10^{-3} m s^{-1}

Crystic 586 in Crystic 272, vol %	Tube dimensions				Glass volume fraction	Average crush load, KN	Specific energy absorbed, J g^{-1}
	ID mm	OD mm	Length, mm	Weight, g			
15	49.96	57.79	169	198	0.43	73.2	62.7
15	49.99	57.40	165	191	0.43	81.8	70.9
30	49.96	57.73	168	192	0.42	82.5	72.1
30	49.95	57.74	171	199	0.42	87.8	75.1
40	50.03	57.74	169	190	0.44	80.0	71.4
40	49.96	57.43	155	171	0.44	78.5	70.9
50	49.98	57.18	148	164	0.45	65.5	59.3
50	50.00	57.12	159	176	0.45	80.0	71.4

Table 14 - Specific energy absorption of $0^{o}/90^{o}$ tubes : effects of Crystic 586 modifier in Crystic 272 Testing Speed 4 m s^{-1}

Crystic 586 in Crystic 272, vol %	Tube dimensions				Glass volume fraction	Average crush load, KN	Specific energy absorbed, J g^{-1}
	ID mm	OD mm	Length, mm	Weight, g			
15	49.94	56.82	161	165	0.45	62.5	61.0
15	50.00	57.06	168	178	0.45	55.3	52.5
30	49.98	57.57	152	179	0.42	66.9	56.6
30	49.98	57.70	154	178	0.42	70.7	60.8
40	49.96	57.14	165	182	0.44	61.2	55.4
40	50.03	57.55	182	208	0.44	70.0	61.2
50	49.91	57.30	152	168	0.45	56.7	51.5
50	50.02	57.14	189	209	0.45	64.1	58.0

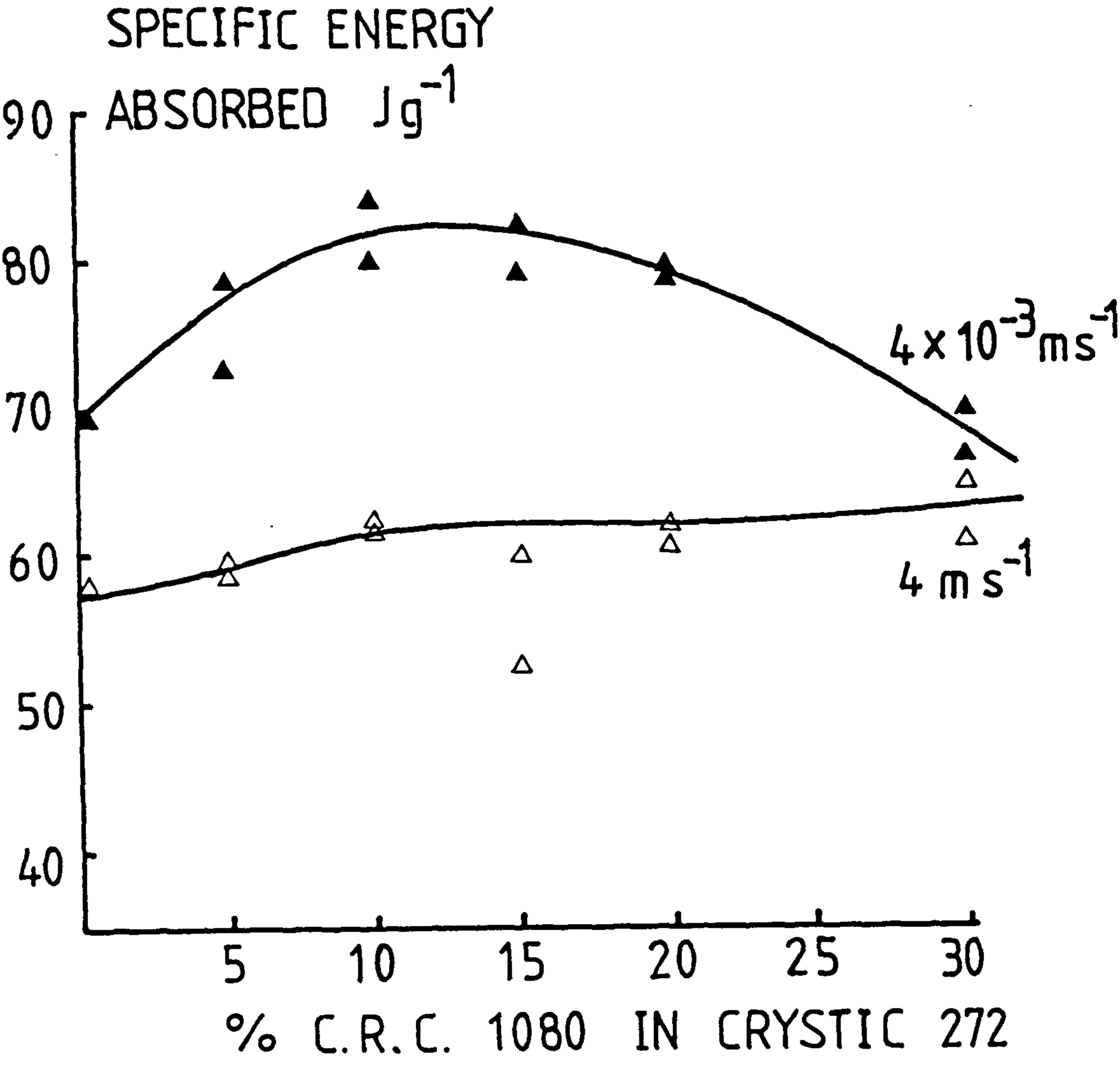

Fig. 4.7. Effect of resin modification by CRC1080 on the energy absorption of polyestar 0/90 tubes crushed at $4x10^{-3}$ and 4 ms^{-1}.

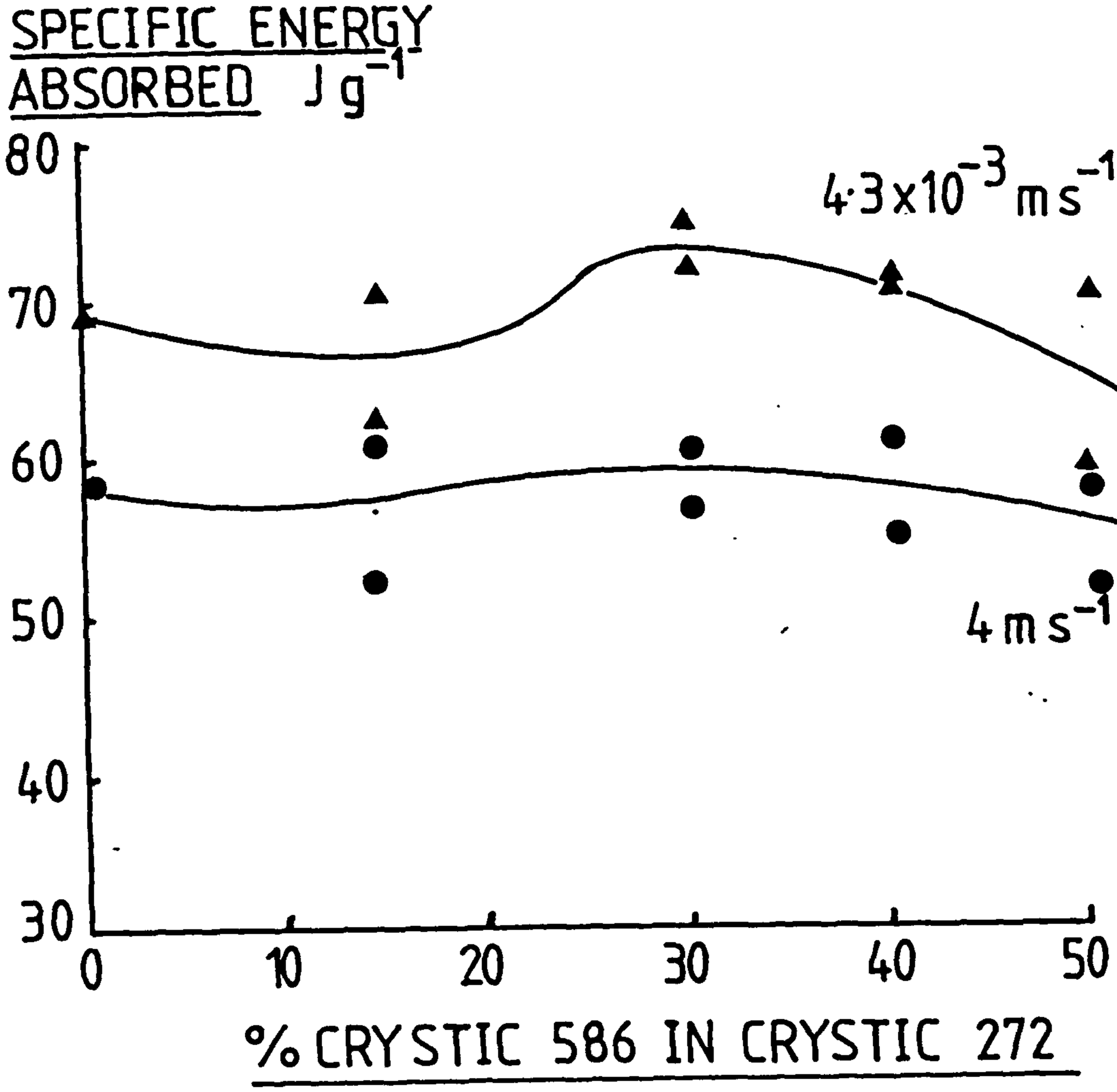

Fig.4.8. Effect of resin modification by Crystic 586 on the energy absorption of polyester 0/90 degree tubes crushed at $4x10^{-3}$ and $4ms^{-1}$.

Typical load-displacement traces are shown in Figs. 4.9 and 4.10 for a tube with 30% by volume CRC 1080 tested at high and low speeds. These traces are similar to those obtained with tubes made with Crystic 272, (Figs.4.3 and 4.4), with the exception that the traces for tubes with addition were slightly less serrated. more pronounced at the low speed of 4.3×10^{-3} m s^{-1}.

Fig. 4.8 shows the effects of adding a flexibiliser, Crystic 586, to the basic resin. Only minor variations were apparent at both low and high test speed. For additions in excess of 40% by volume, the energy absorption decreased. Load-displacement traces for tubes with varying amounts of Crystic 586, were similar to those shown in Figs. 4.3 and 4.4

The effects of modification and flexibilisation are discussed further in Chapter 6.

4.2.4 Effect of testing speed on epoxy tubes

The results for tubes tested at varying speeds are presented in Tables 15 and 16. These tubes were manufactured using Epoxy MY 750 as the matrix. In all cases, the standard $0^{o}/90^{o}$ winding configuration was used. All tubes were bevelled and in every instance failure was progressive from the triggered end. Several tubes were manufactured with a modified epoxy resin matrix, produced using the flexibiliser Araldite CY208. Its effect on the basic resin was similar to that of Crystic 586 on Crystic 272. These results are shown in Table 16.

The results (Fig. 4.11) show that the SEA increases with test speed. The limited number of tests carried out with modified epoxy resin also exhibit this trend, but at uniformly higher value of energy absorption. This effect of test speed on energy absorption was opposite to that with polyester tubes. The results from the

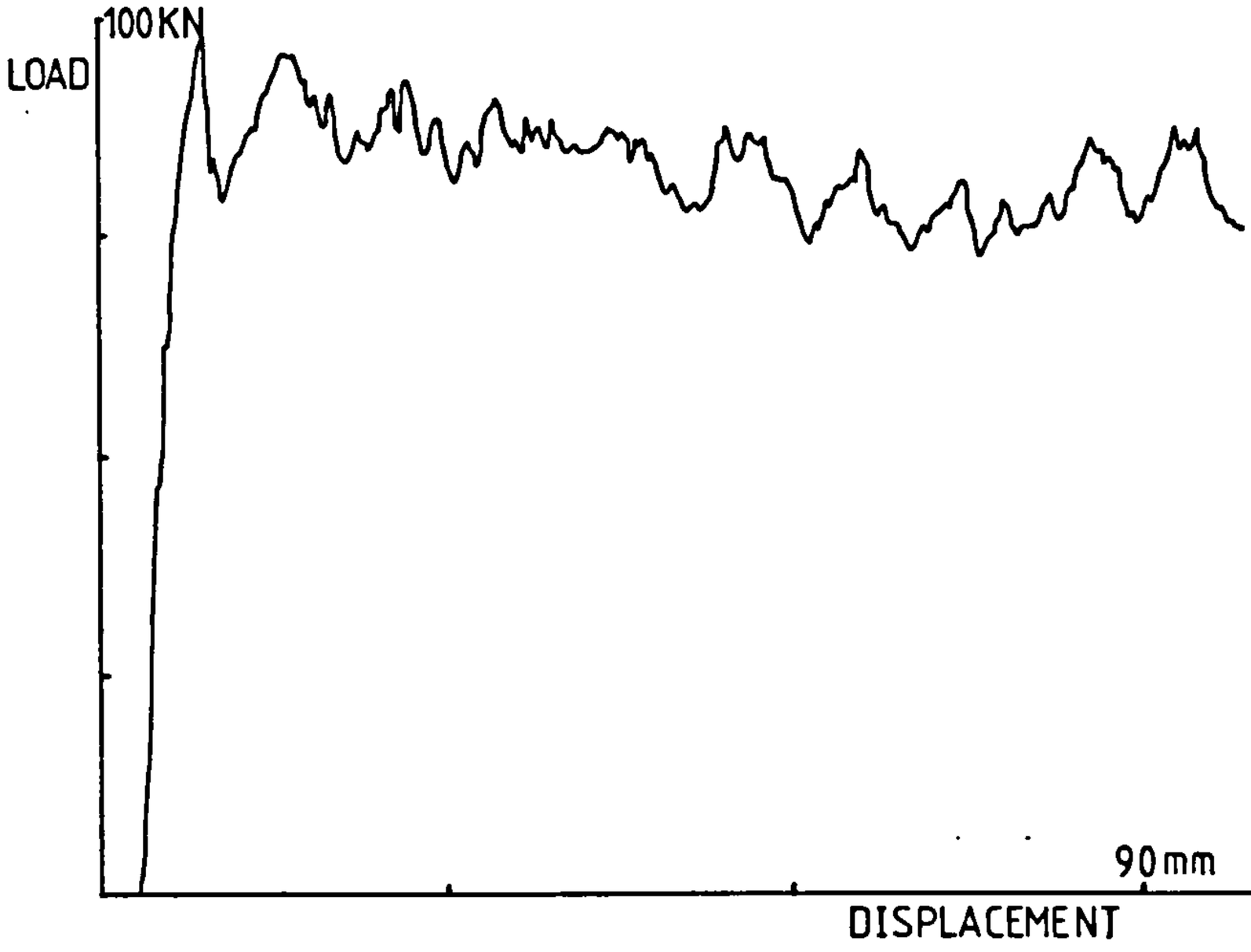

Fig. 4.9. Typical load-displacement trace for a 0/90 degree tube, Crystic 272 + 30% CRC 1080, tested at 4 mms^{-1}.

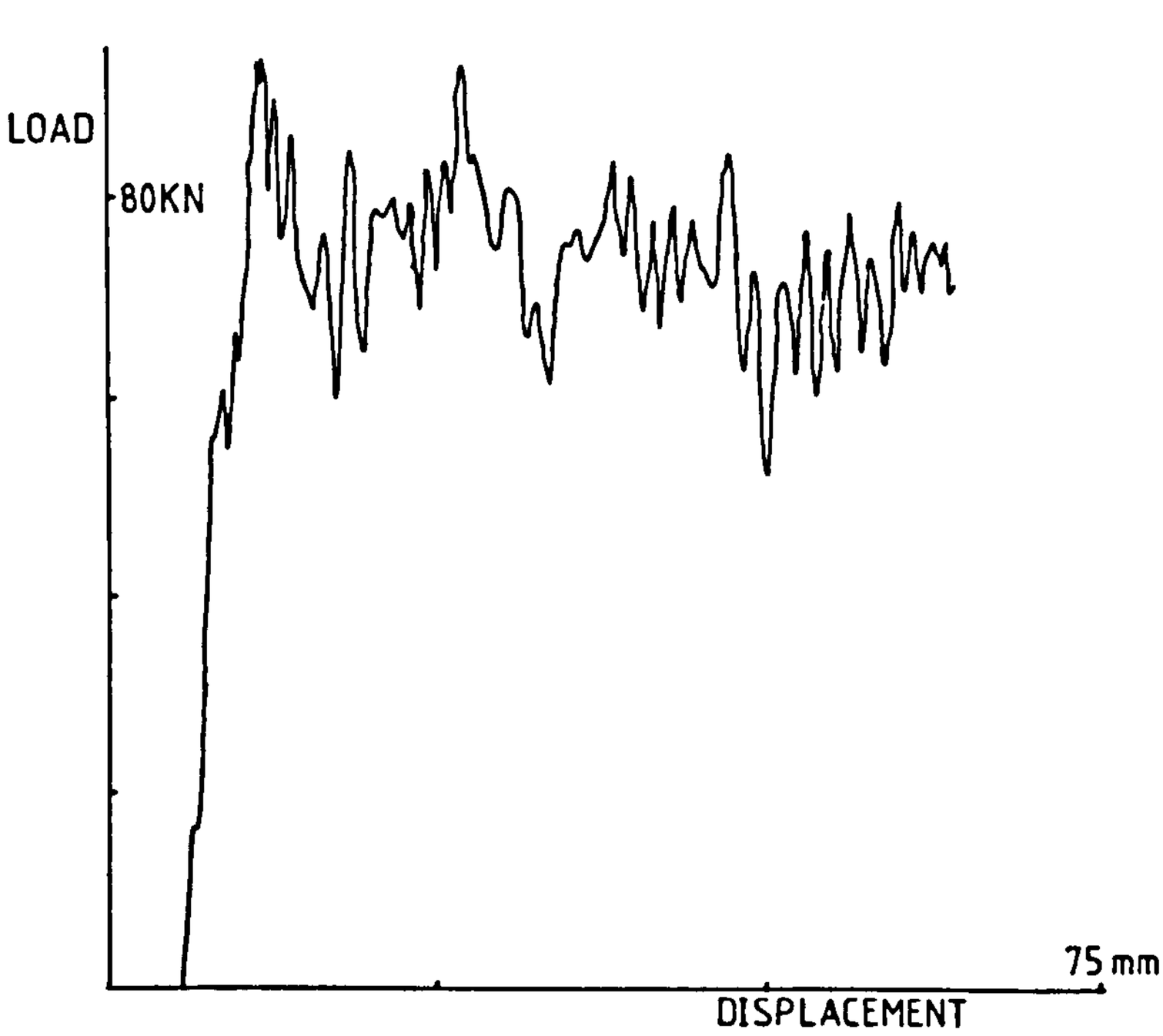

Fig. 4.10. As above but tested at 4 ms^{-1}.

Table 15 - Specific energy absorption values for $0^{o}/90^{o}$ tubes with epoxy matrices : effect of cross-head speed

Resin : Ciba-Geigy Araldite MY 750/HY 917/DY 070

Cross-head speed, $m\ s^{-1}$	Tube dimensions				Glass volume fraction	Average crush load, kN	Specific energy absorbed, Jg^{-1}
	ID, mm	OD, mm	Length, mm	Weight g			
2.0×10^{-3}	49.94	57.39	182	208	0.44	50.5	44.2
2.0×10^{-3}	50.07	56.87	186	200	0.44	58.0	53.9
4.0×10^{-3}	50.04	57.46	182	209	0.44	56.6	49.3
4.0×10^{-3}	49.99	58.03	189	224	0.44	63.5	53.4
4.4×10^{-3}	50.03	56.81	178	185	0.44	61.9	59.6
1.92	50.05	57.07	176	188	0.44	69.0	64.2
1.92	49.97	57.29	184	213	0.44	71.5	61.8
3.96	50.01	56.77	186	192	0.40	60.5	58.6
3.96	49.97	57.18	191	213	0.40	67.5	60.5
4.06	50.05	57.70	181	211	0.40	67.4	57.8
4.06	50.03	57.57	167	192	0.45	72.5	63.1
11.4(var.)	49.98	56.20	635	645	0.45	58.0	57.0
13.8(var.)	49.98	56.97	768	806	0.43	62.4	59.5

Table 16 Specific energy absorption values for $0^{o}/90$ tubes with epoxy matrices : effect of cross-head speed

Resin : MY 750 Flexibilised with CY 208

Cross-head speed, ms^{-1}	Tube dimensions				Glass volume fraction	Average crush load, KN	Specific energy absorbed, Jg^{-1}
	ID, mm	OD, mm	Length, mm	Weight, g			
4.0×10^{-3}	50.03	56.16	158	155	0.45	64.8	66.0
4.0×10^{-3}	50.03	56.38	191	188	0.45	61.0	62.0
4.0	50.02	56.28	181	179	0.47	69.0	69.8
4.0	50.06	56.17	191	190	0.47	71.0	71.4

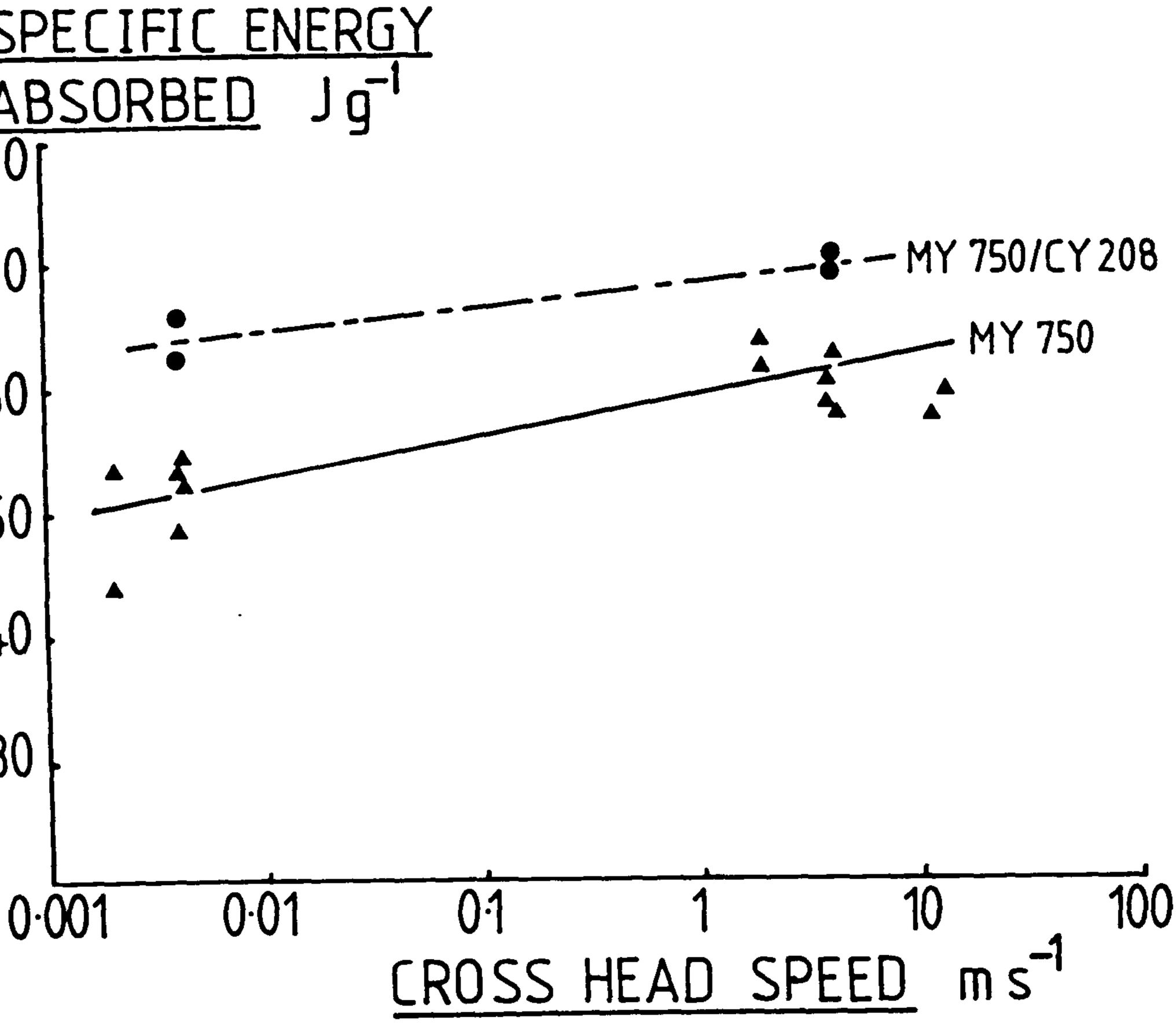

Fig. 4.11. Effect of cross-head speed on the specific energy absorption of crushed 0/90 degree epoxy tubes.

crash rig were lower than expected, this being similar to the results obtained with polyester tubes.

The effects of flexibiliser additions on epoxy and polyester tubes are dissimilar. The addition of flexibiliser at the 50% level to epoxy MY 750 gave an improvement in energy absorption, whilst additions of Crystic 586 to Crystic 272 had little effect up to 40%, when a decrease in energy values occurred.

Typical load-displacement traces for epoxy tubes tested at 4.0×10^{-3} and 4 m s^{-1} are shown in Figs. 4.12 and 4.13. Both traces are serrated in a similar manner to those from crushed polyester tubes, although the serrations are less pronounced, especially at the lower test speed. Epoxy tubes tested at this speed showed a decreasing load trace before becoming constant. This was not noted with any other resin/speed combination, and similar epoxy resin tubes tested at 4 m s^{-1} gave a level trace. Observation of the tubes tested at 4.4×10^{-3} m s^{-1} showed that the axial fibres tended to remain in contact with the cross-head platen for a greater period of time than normally noted with all other resin/speed combinations. This partially explains the unique form of the trace. Crushing mechanisms are discussed in Chapters 5 and 6.

As with polyester tubes, no relationship between the glass volume fraction and the SEA of epoxy tubes could be detected.

4.2.5 Effect of fibre orientation

The fibre orientation in a composite with reference to the loading axis is a major factor in determining the response of that composite to an applied force. The effect of fibre orientation on the SEA of tubes during axial compression was assessed by a series of tests on tubes with winding angles varying from hoop (90^{o}) to almost all axial (0^{o}).

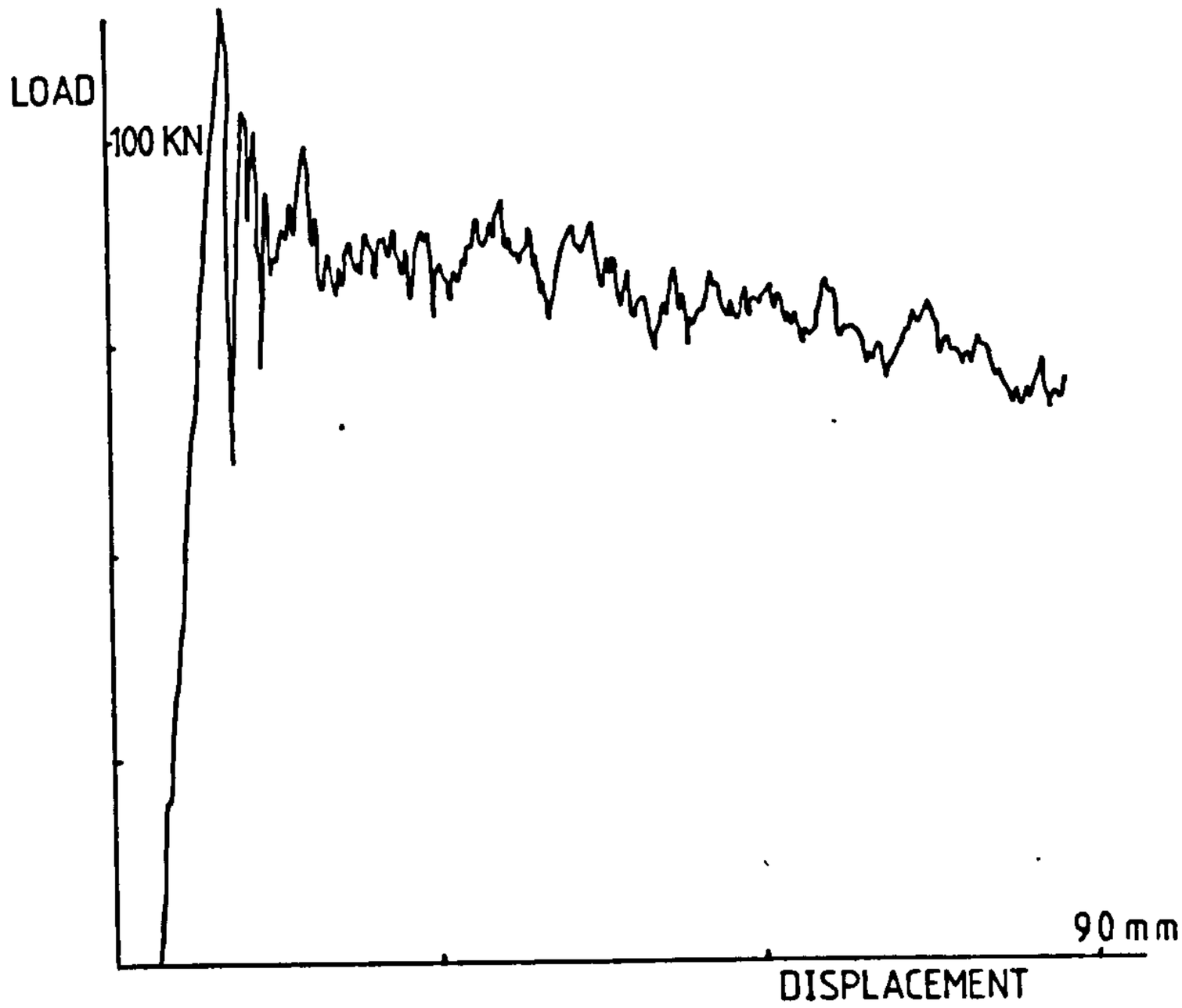

Fig. 4.12. Typical load-displacement trace for a 0/90 degree tube, Epoxy MY750 resin, tested at 4 mms^{-1}.

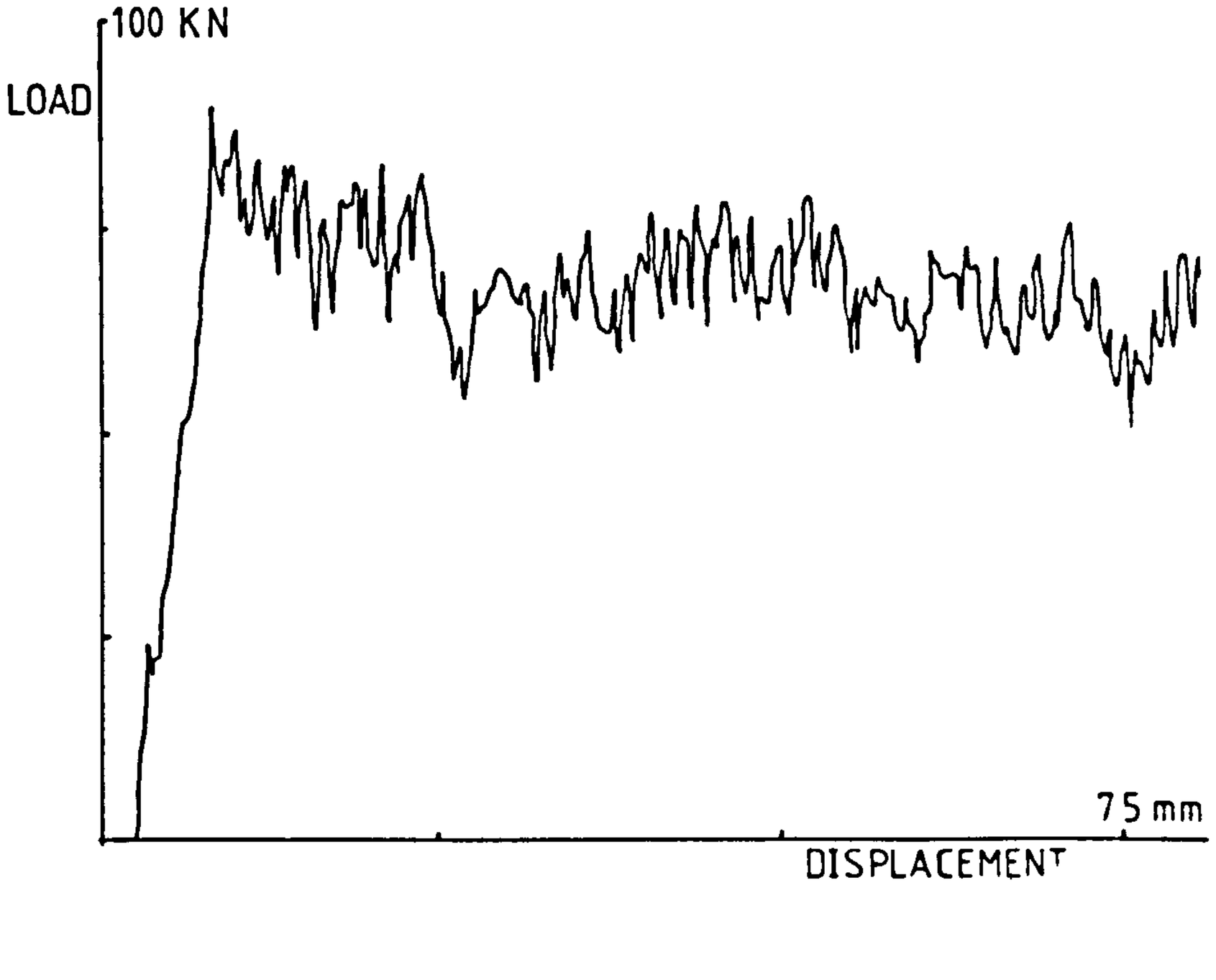

Fig. 4.13. As above but tested at $4ms^{-1}$.

The results are shown in Table 17. A constant test speed of 0.16×10^{-3} m s^{-1} was employed. Polyester Crystic 272 resin and Equerove 'E' glass were used to manufacture the tubes. The angle-ply tubes all consisted of 2 separate laminations with orientations of $\pm\theta^{o}$, where θ is the angle to the tube axis. The hoop-wound tubes (90^{o}) consisted of 2 complete laminations wound on top of each other. The axial-wound tubes were manufactured using a layer of veil cloth on the inside and outside of two layers of axially orientated fibres. This was necessary in order to hold the axial fibres in place during cure. The physical restraintprovided by the veil cloth after cure was small, as the results show.

The results are plotted in Fig. 4.14 and show a maximum value of SEA at a winding angle of approximately 65^{o}. The SEA decreased gradually, at greater and smaller angles reaching a value under 30 Jg^{-1} at 35^{o}. Tubes constructed from axial fibres only gave low results, in the region of 10-15 Jg^{-1}. The failure mechanism for these tubes, which will be described later, differed most dramatically from that for the other tubes. Unfortunately, because of production methods on the filament winder, angles between 0^{o} and 35^{o} could not be achieved.

The volume fractions of angle-wound tubes varied to a greater extent than with $0^{o}/90^{o}$ tubes. The major variation from the average was with axial tubes which had a glass volume fraction of 0.27. This was due to the production method employed, tension on the axials being very low, with little compaction due to overwinding. The variation of SEA for a given winding angle was less than for $0^{o}/90^{o}$ tubes, owing to the replacement of the manual element in axial winding with machine-controlled, constant-tension, angle-ply winding.

Table 17 - Specific energy absorption of tubes with different winding angles

Orientation and lay-up sequence, degrees	Tube dimensions				Glass volume fraction	Average crush load, kN	Specific energy absorbed, Jg^{-1}
	ID mm	OD mm	Length, mm	Weight g			
2 x 90°	50.86	54.66	165	94	0.42	20.8	36.8
2 x 90°	50.88	54.61	165	92	0.42	22.7	40.9
2 x 90°	50.49	54.88	171	96	0.42	21.4	38.2
±/± 85°	50.89	55.96	191	92	0.53	18.0	37.2
±/± 85°	50.89	53.99	159	76	0.53	13.4	28.0
±/± 85°	50.89	53.94	177	86	0.53	19.6	40.7
±/± 75°	50.91	54.57	170	97	0.45	23.9	42.2
±/± 75°	50.91	54.57	166	94	0.45	26.2	46.4
±/± 75°	50.90	54.57	168	96	0.45	21.1	47.5
±/± 65°	50.62	54.12	174	93	0.49	25.6	48.1
±/± 65°	50.64	54.01	168	89	0.49	24.6	46.3
±/± 65°	50.64	54.18	156	83	0.49	27.1	50.6
±/± 55°	51.03	54.03	172	85	0.49	21.9	44.3
±/± 55°	50.99	54.44	150	77	0.49	21.6	41.9
±/± 55°	50.85	54.39	150	77	0.43	22.7	44.0
±/± 55°	50.89	54.64	155	83	0.43	23.0	42.8
±/± 55°	50.79	54.40	147	77	0.43	22.2	42.8
±/± 55°	50.87	54.35	151	78	0.43	21.4	41.5
±/± 45°	50.92	54.44	147	79	0.48	18.5	34.5
±/± 45°	50.93	54.24	163	83	0.48	18.9	37.1
±/± 35°	50.61	54.33	120	80	0.46	18.8	28.2
±/± 35°	50.74	54.30	164	92	0.47	15.7	27.9
±/± 35°	50.75	54.34	168	89	0.47	15.9	30.0
2 x 0°*	49.93	56.92	168	150	0.27	7.5	8.4
2 x 0°*	49.90	56.21	81	66	0.27	13.0	15.9

* plus 2 layers of veil cloth

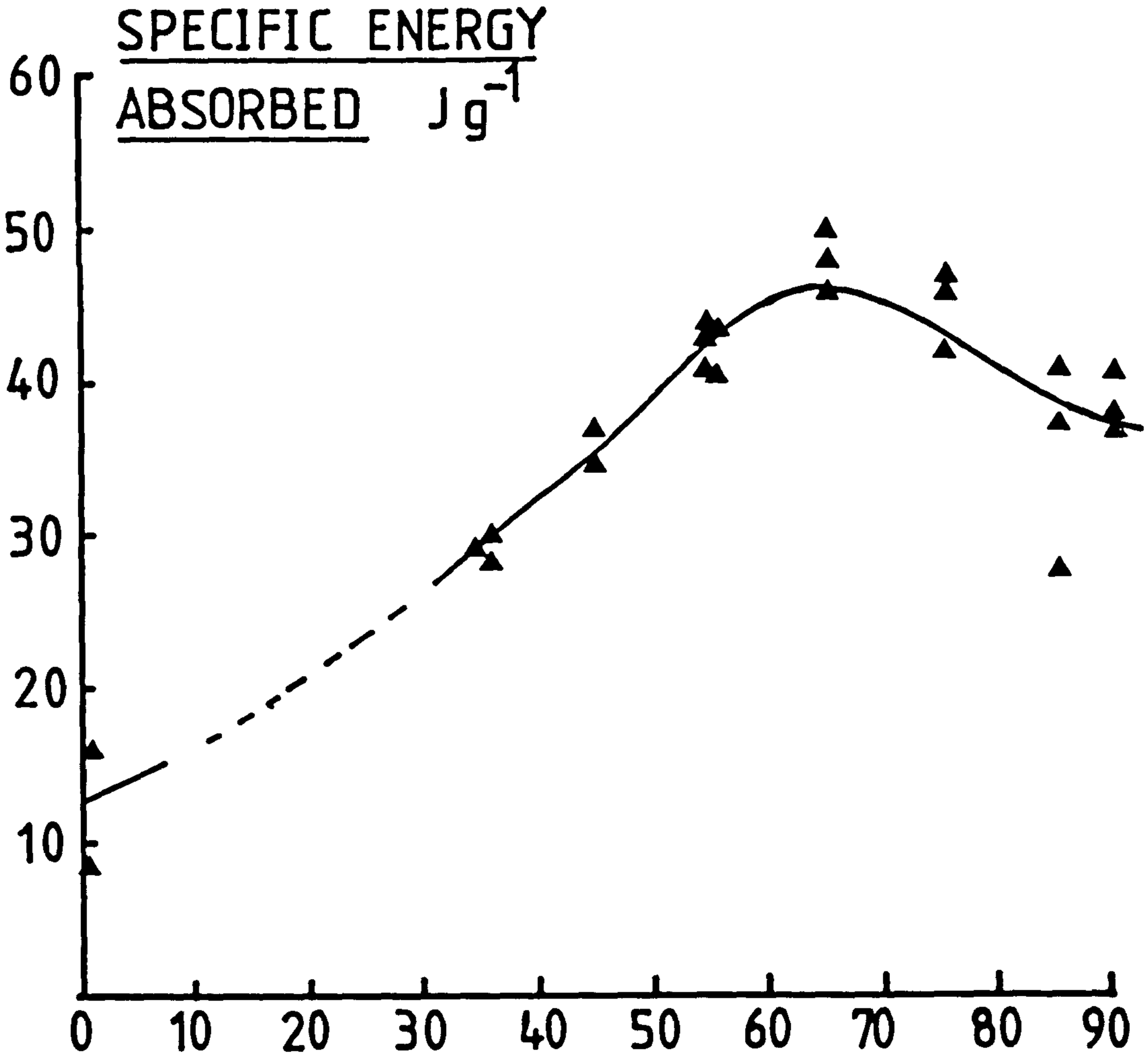

Fig, 4.14. Effect of fibre orientation on the specific energy absorption of polyester tubes crushed at 0.16×10^{-3} ms^{-1}.

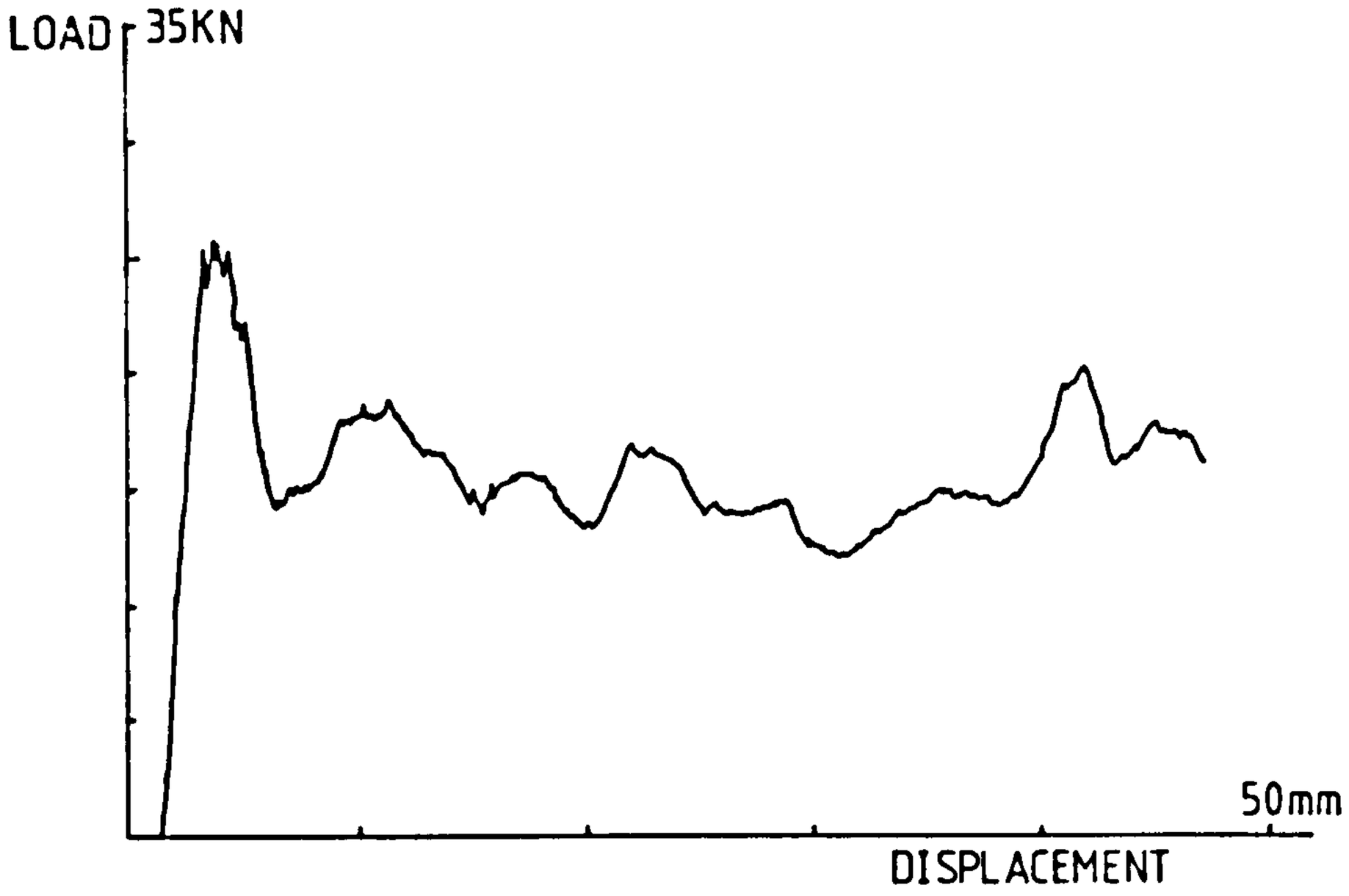

Fig. 4.15. Typical load-displacement trace for a 35 degree angle tube.

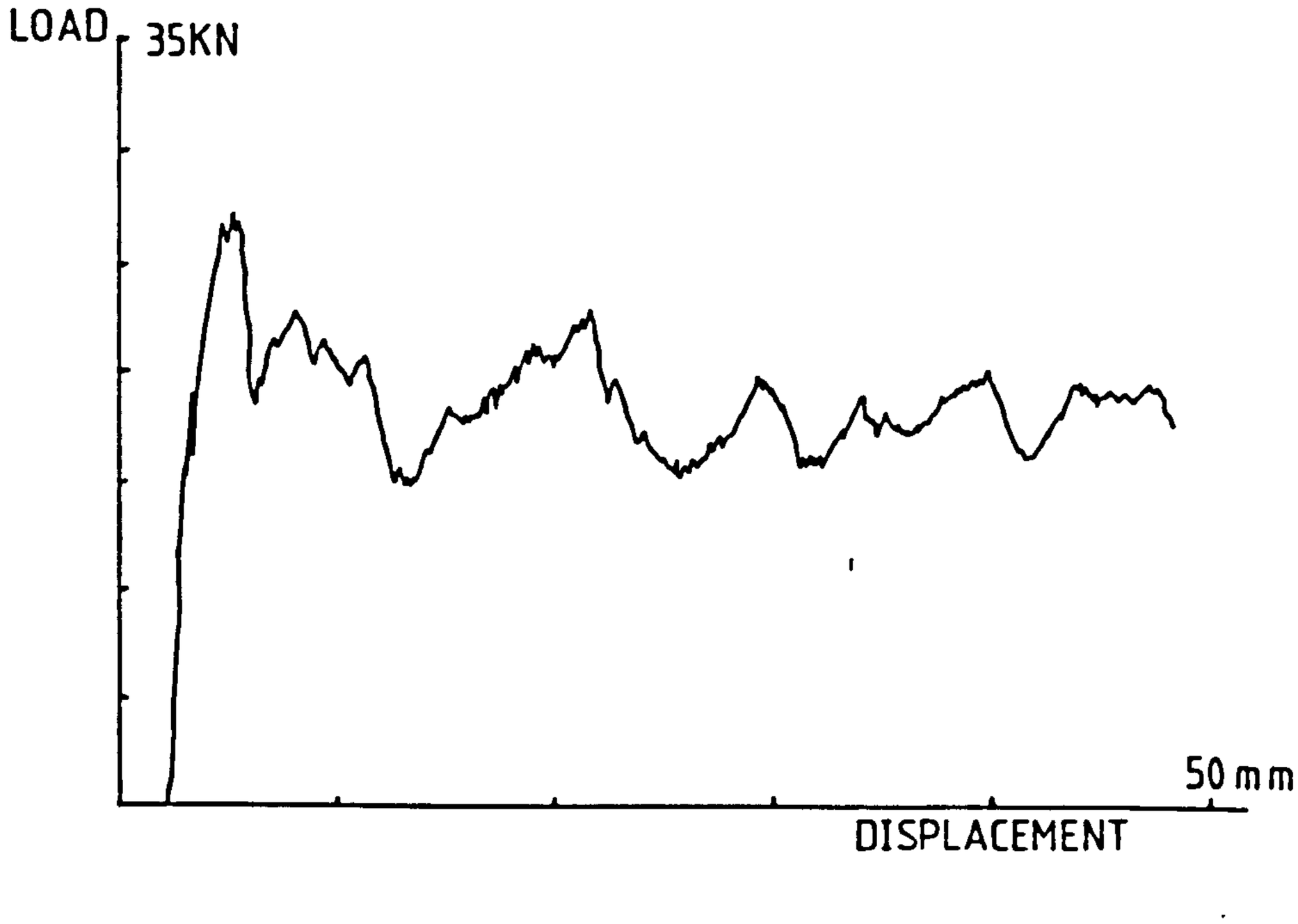

Fig. 4.16. Typical load-displacement trace for a 45 degree angle tube.

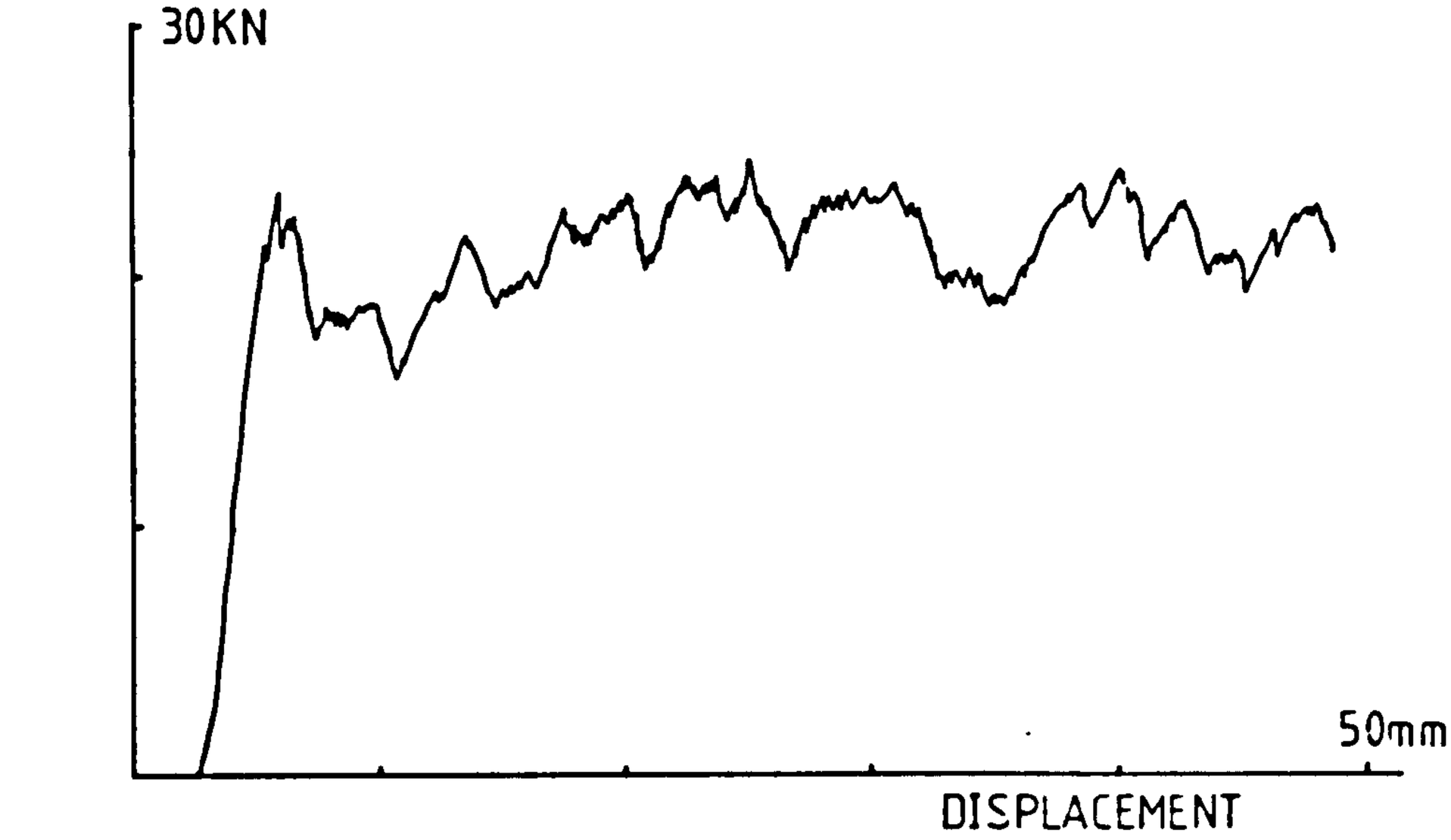

Fig. 4.17. Typical load-displacement trace for a 55 degree angle tube.

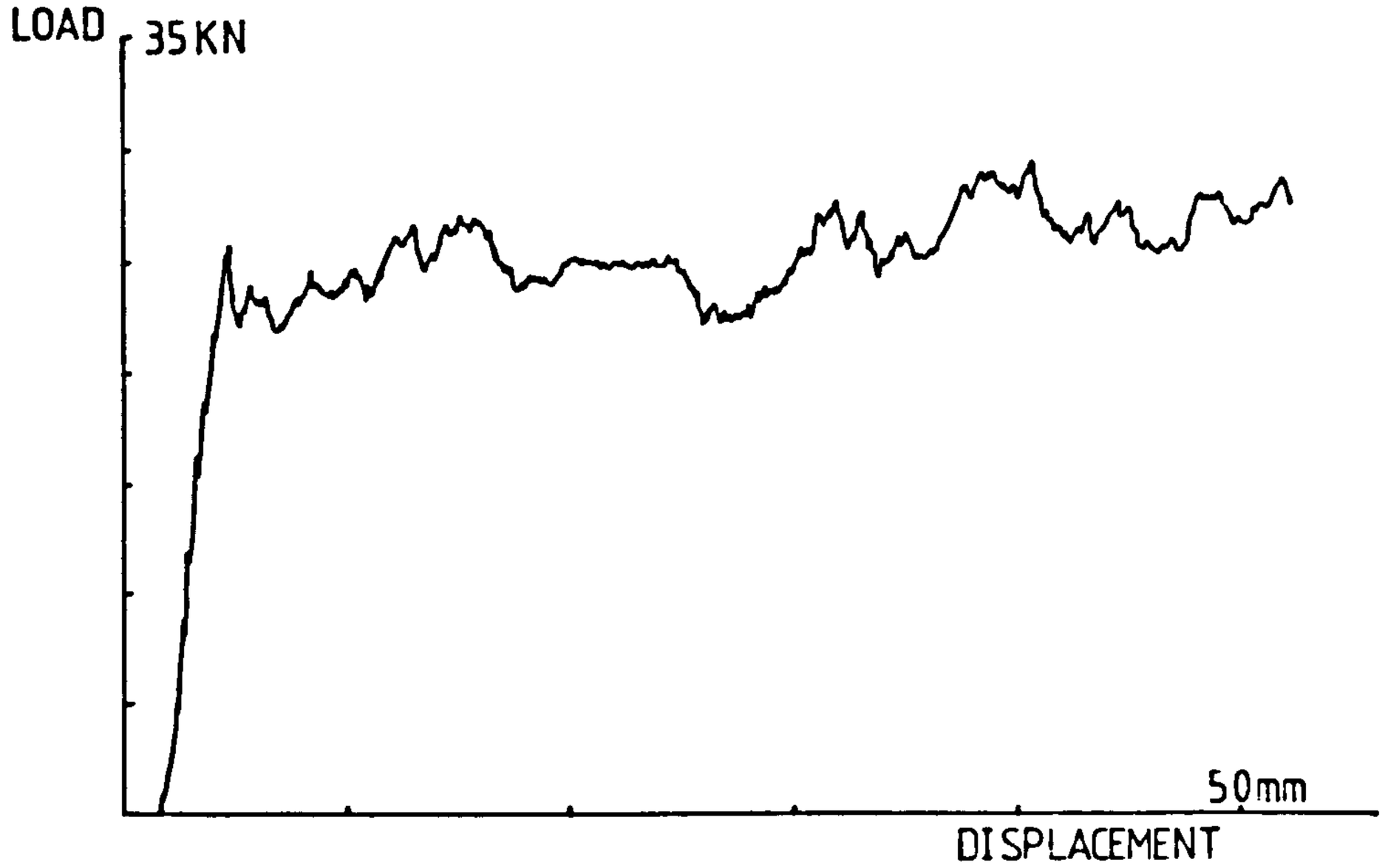

Fig. 4.18. Typical load-displacement trace for a 65 degree angle tube.

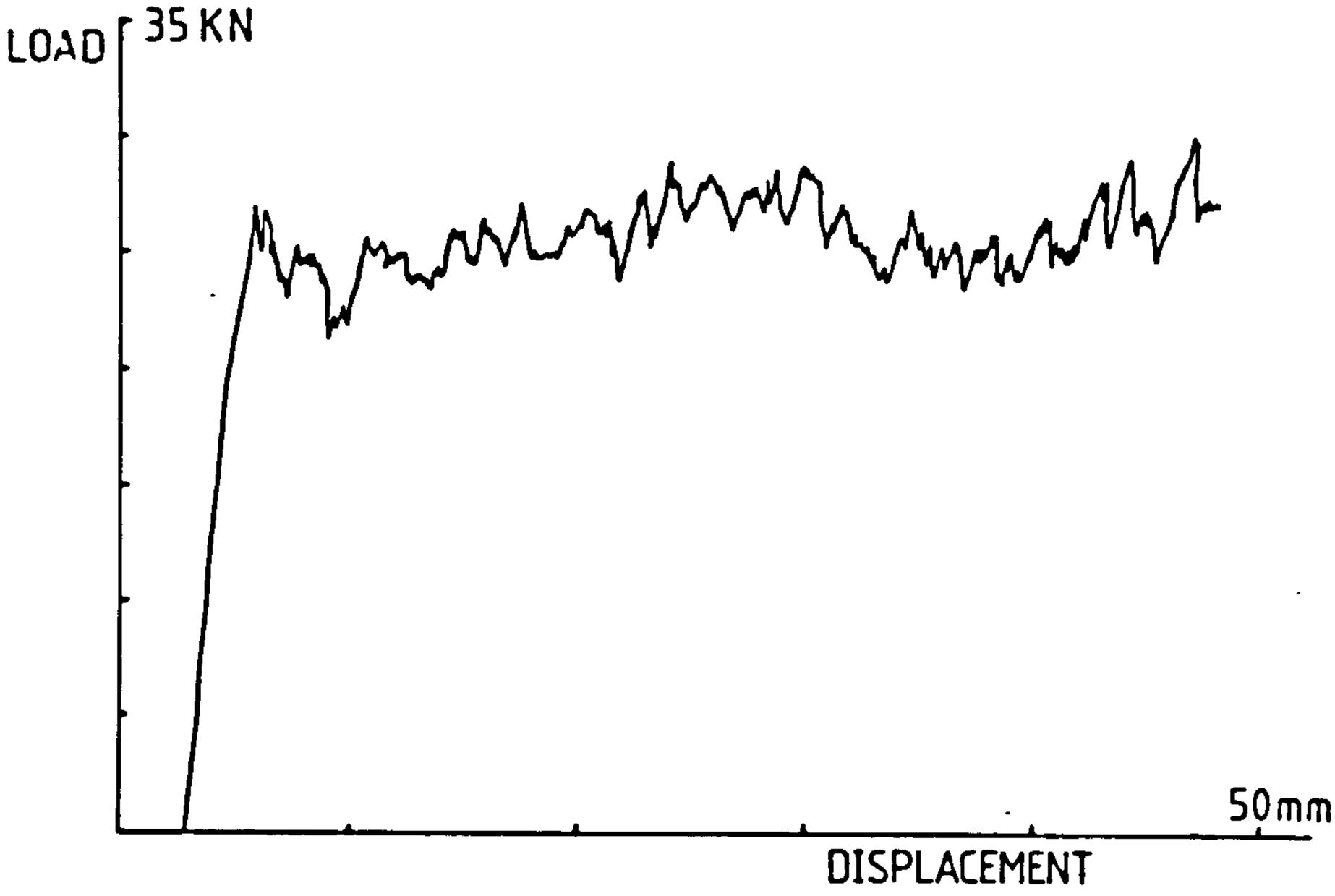

Fig. 4.19. Typical load-displacement trace for a 75 degree angle tube.

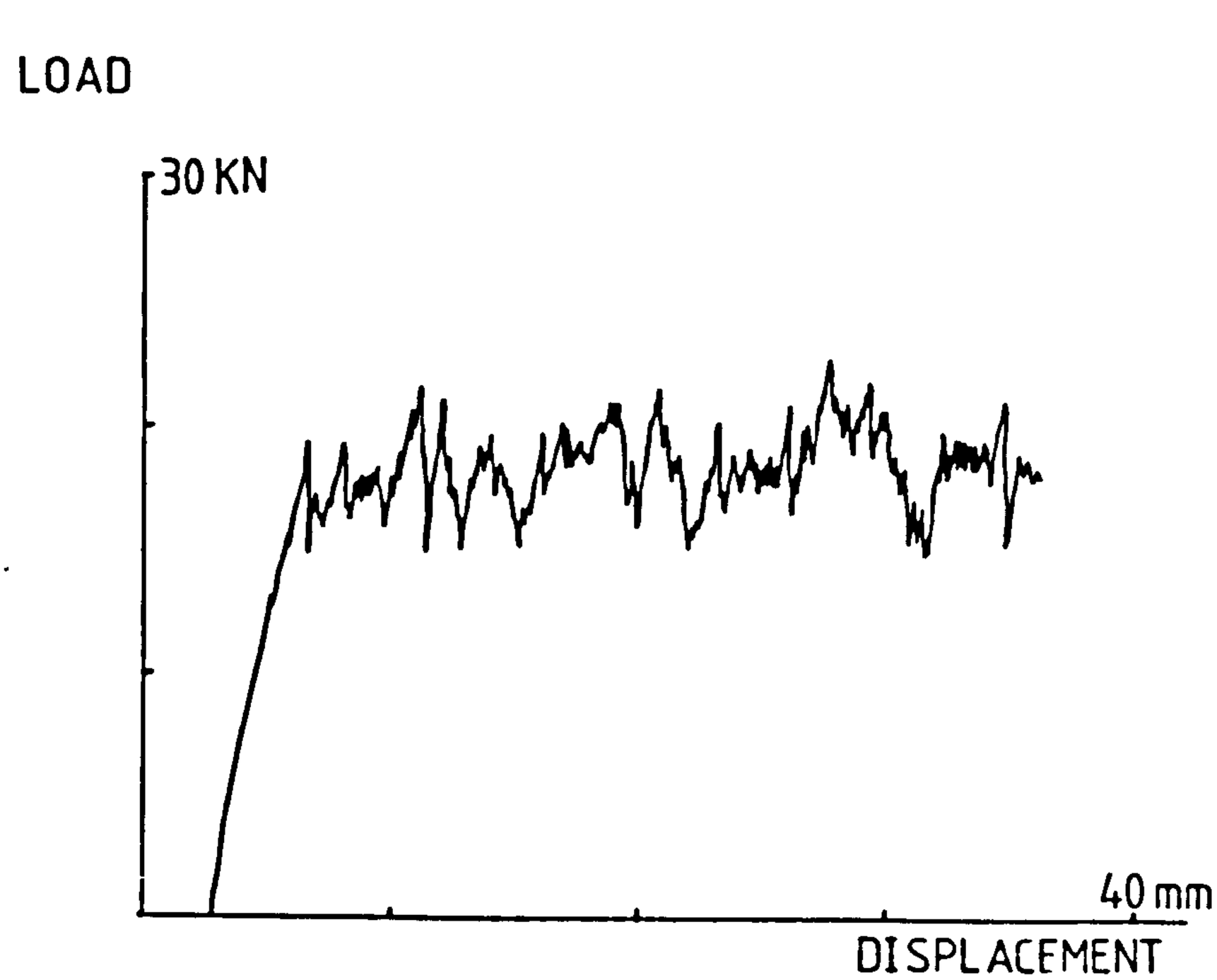

Fig.4.20. Typical load-displacement trace for a 85 degree angle tube.

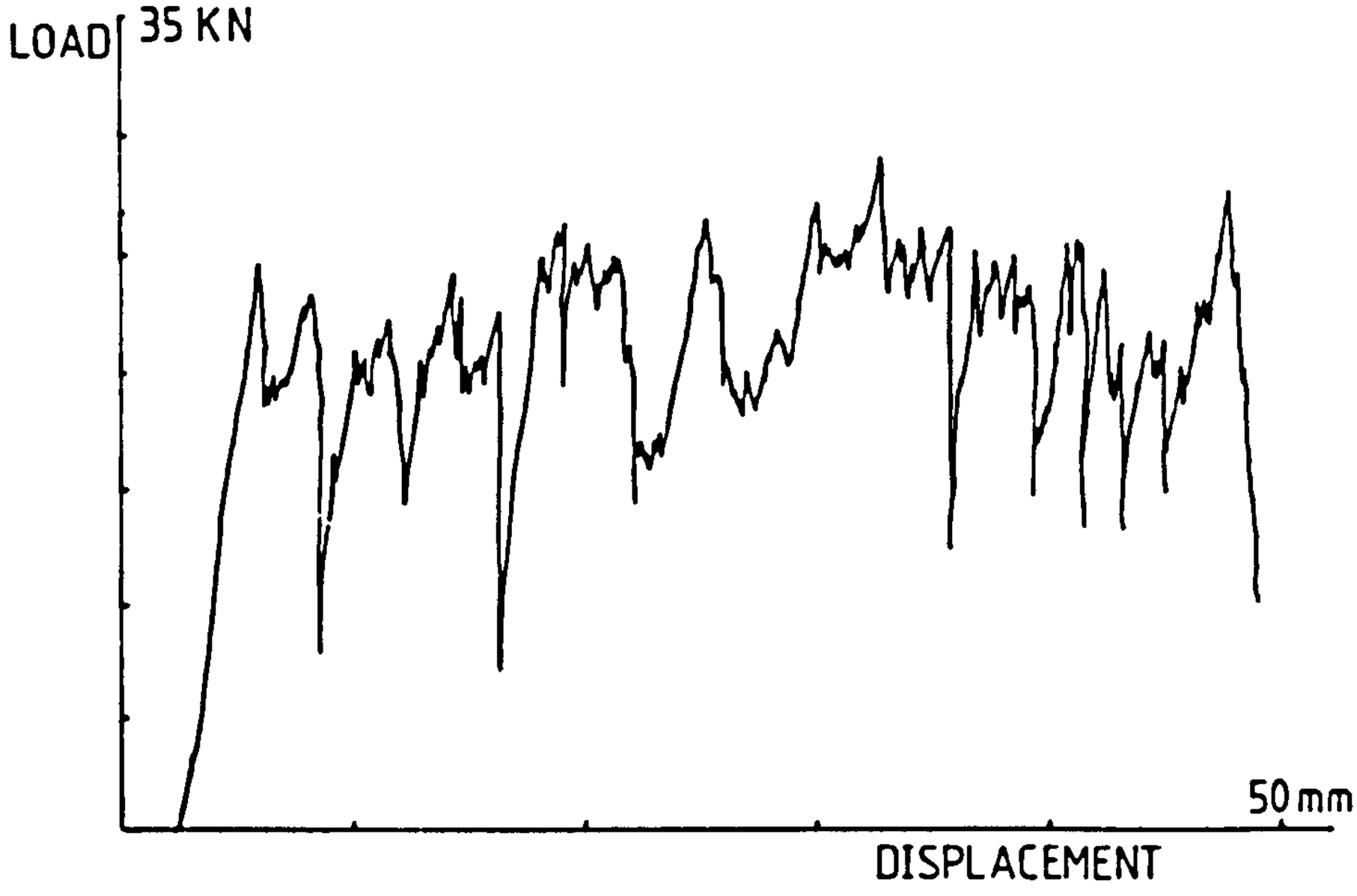

Fig. 4.21. Typical load-displacement trace for a 90 degree (hoop) angle tube.

Typical load-displacement traces are shown for each angle in Figs.4.15 - 4.21. The traces for the hoop-wound tubes were highly serrated when compared with traces from tubes wound at other angles. In general, the magnitude of serrations increased with winding angle.

4.3 Resin fracture toughness

The fracture toughness results from double torsion testing are shown in Tables18 and 19 for polyester and epoxy resins respectively. Test speeds were from 0.5×10^{-3} to 1 m s^{-1}. Stick-slip, as opposed to continuous crack growth, was more prevalent at lower speeds for polyester resins. Epoxy resins failed with continuous crack propagation at all testing speeds. K_{IC} values were determined from the load values. Stick-slip K_{IC} values for initiation, growth and average are presented. G_{IC} was calculated from K_{IC} using modulus (E) and Poisson ratio (ν). The relationship used was:

$$G_{IC} = K_{IC}^2 \frac{(1 - \nu^2)}{E}$$

Fracture toughness versus cross-head speed is shown for polyester and epoxy resins in Fig. 4.22. For Crystic 272, G_{IC} appears to change little at speeds of up to 1 m s^{-1}. At this speed, a slight increase was noted. However, epoxy MY 750 showed a steady increase over the range of speeds. Values of G_{IC} were calculated from modulus values obtained at a test speed of 0.08×10^{-3} m s^{-1}. Data were not available for modulus values at higher strain rates and hence these single-speed values were used throughout. Published work (68, 59), discussed in Chapter 2, indicates that the modulus of epoxy resins is only slightly sensitive to strain rate, although only a limited range of test speeds was reported. If it is

Table 18 - Fracture toughness of epoxy resin at different speeds

Double torsion testing

MY 750 : Poisson ratio 0.38, modulus 2.7 GPa

MY 750/CY 208 : Poisson ratio 0.38, modulus 2.1 GPa

Cross-head speed m s^{-1}	Resin	K_{IC} (mean), MN $m^{-3/2}$	Average K_{IC}, Mn $m^{-3/2}$	Calculated G_{IC} J m^{-1}
0.5×10^{-3}	MY 750	0.41 0.47 0.43 0.45	0.44	61
4.0×10^{-3}	MY 750	0.54 0.63 0.70 0.72	0.65	134
4.0×10^{-3}	MY 750/ CY 208	0.61 0.76 0.78	0.72	211
500×10^{-3}	MY 750	0.77 0.79	0.78	193
1.0	MY 750	0.87 0.93 0.90 0.98	0.92	268
1.0	MY 750/ CY 208	0.89 0.82	0.85	294

Table 19 - Fracture toughness of polyester resin at different speeds

Double torsion testing

Crystic 272 : Poisson ratio 0.35, modulus 3.7 GPa

Cross-head speed, m s^{-1}	K_{IC}, MN $m^{-3/2}$			Average K_{IC}, MN $m^{-3/2}$	Calculated C_{IC}, J m^{-1}
	Initiation	Arrest	Average		
0.5×10^{-3}	0.57	0.48	0.52	0.60	85
	0.68	0.60	0.63		
	-	-	0.66		
4.0×10^{-3}	-	-	0.57	0.59	83
	-	-	0.61		
	0.68	0.53	0.61		
	0.65	0.55	0.59		
	0.61	0.59	0.57		
	-	-	0.57		
	-	-	0.62		
	0.71	0.58	0.65		
	-	-	0.58		
	0.67	0.55	0.61		
3.5×10^{-3}	-	-	0.60	0.61	88
	0.74	0.62	0.68		
	0.63	0.55	0.58		
			0.59		
500×10^{-3}	-	-	0.64	0.63	94
	-	-	0.61		
	-	-	0.67		
	-	-	0.63		
	-	-	0.60		
1.0	-	-	0.77	0.76	137
	-	-	0.76		
	-	-	0.80		
	-	-	0.70		

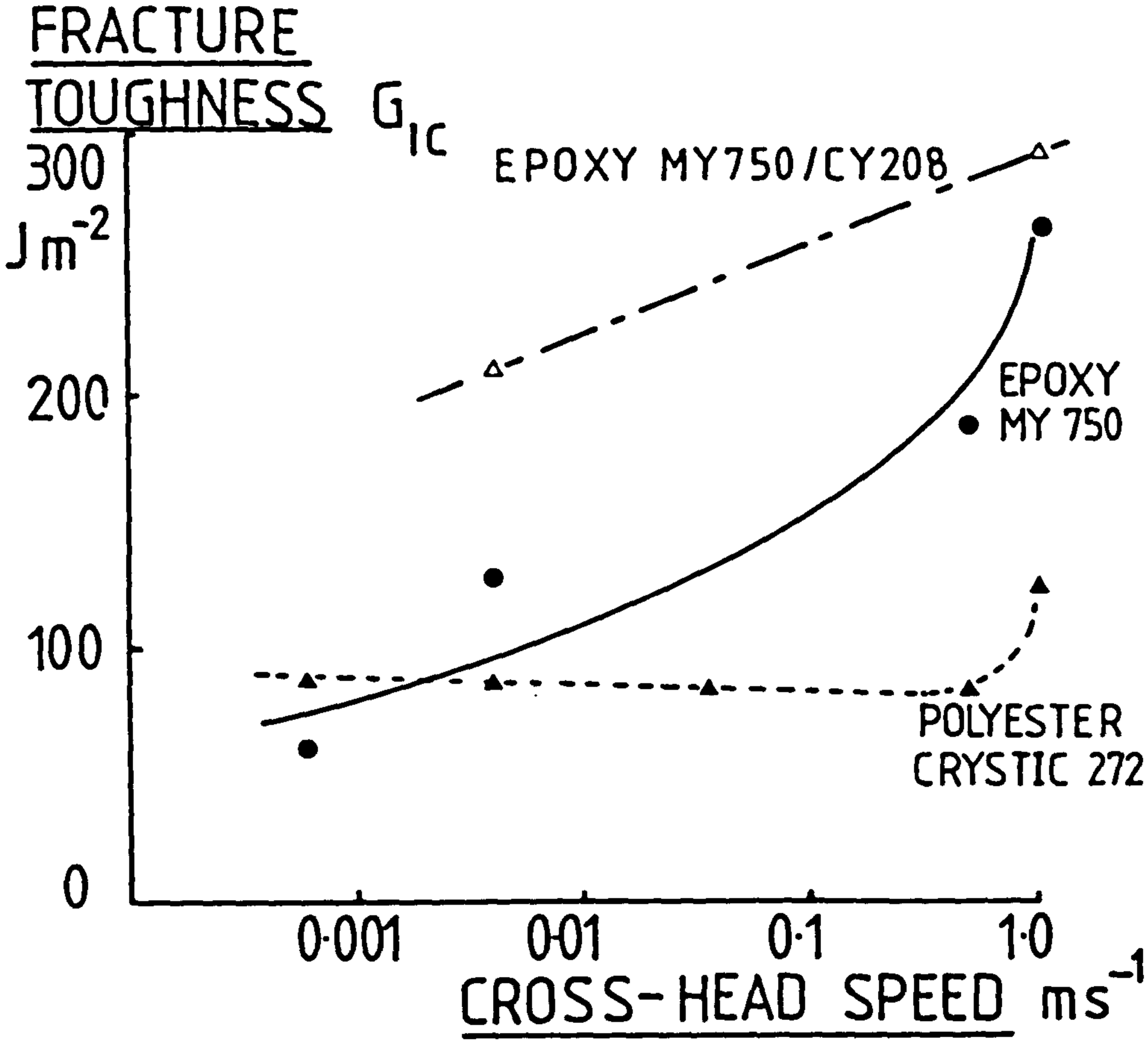

Fig. 4.22. Effect of cross-head speed on the fracture toughness of epoxy and polyester resins.

assumed that the modulus increases slowly with strain rate, then the calculated values of G_{IC} at the higher rates would be slightly high. However, the main purpose of the fracture toughness work was to permit comparison between epoxy and polyester resins, and any errors would probably be the same for both materials.

The comparison between the two resin types shows that, because the fracture toughness of epoxy resin increases rapidly with strain rate, at 1 m s^{-1} epoxy is twice as tough as polyester. The experimental results for epoxy showing an increase in fracture toughness are not in general agreement with published results (58, 59, 70), which were obtained using a limited range of testing rates, i.e. 0.0017×10^{-3} to 0.17×10^{-3} m s^{-1}. Comparisons between this and other work using different resins is difficult, as every resin appears to have unique properties, with the cure cycles and the level and type of curing agent all affecting the response to test variables.

The flexibilised epoxy resin MY 750/CY 208 also exhibited an increase in fracture toughness as speed increased. In general, the G_{IC} values were higher than those for the unflexibilised resin over the whole range of speeds.

The different fracture toughness behaviour of epoxy MY 750 and polyester Crystic 272 with testing rate gives a partial insight into the effect of testing rate on the SEA of tubes made with these resins. As previously noted, the SEA of polyester tubes decreases with increasing speed whilst the opposite is true for epoxy MY 750. The fracture toughness of epoxy increases by four times over a speed range from 0.5×10^{-3} to 1 m s^{-1}, whilst over a similar range, the fracture toughness of Crystic 272 increases by just over one and half times. Obviously many other factors are

contributing to the testing rate effect on the SEA, but resin properties, particularly fracture toughness, would appear to be important.

4.4 Resin mechanical properties

Details of tensile tests on bulk resin specimens are shown in Table 20. The results are from various sources, as indicated. The effect of modifiers on the modulus, tensile strength and fracture toughness of the resin is shown. Unless otherwise stated, testing was carried out at 0.08×10^{-3} m s^{-1}.

For a given deterioration in modulus, a greater toughening effect is obtained with CRC 1080 than with Crystic 586. From the table, a modulus of 3.0 GPa corresponds to a fracture toughness of 880 Jm^{-2} for Crystic 272 modified with CRC 1080. An equivalent modulus corresponds to a fracture toughness of 200 J m^{-2} for Crystic 272 modified with Crystic 586. This may explain some aspects of the increase in the SEA of tubes made with polyester resin modified with CRC 1080, particularly in comparison with the lack of improvement, found with Crystic 586. This is discussed further in Chapter 6.

Table 20 - Resin properties

Test Speed : 0.08×10^{-3} m s^{-1} except where stated

Additions are as volume percentage

Resin	Tensile strength, MPa	Youngs modulus, GPa	Fracture toughness		Source
			K_C, MN m^{-2}	G_C, J m^{-2}	
Crystic 272 only	62.9	3.7	0.62	96	(10)
272 + 10% 586	57.9	3.5	0.69	118	(28)
272 + 20% 586	70.2	3.5	0.73	132	(28)
272 + 30% 586	71.8	3.5	0.77	146	(28)
272 + 40% 586	56.4 (a)	2.7	1.09	374	(28)
272 + 50% 586	48.8 (a)	2.8	1.55	721	(28)
272 + 10% CRC	80.9 (a)	3.3	1.34	470	(28)
272 + 20% CRC	69.5 (a)	3.0	1.76	883	(28)
272 + 30% CRC	56.6 (a)	2.7	1.92	1147	(28)
Epoxy MY 750	59.5	2.7	0.65 (b)	134 (b)	This work
Epoxy MY 750/ CY 208	63.1 (a)	2.1	0.72 (b)	211 (b)	This work

(a) At yield

(b) Test speed 4×10^{-3} m s^{-1}

CHAPTER 5 - EXPERIMENTAL RESULTS AND INITIAL DISCUSSION OF VISUAL AND MICROGRAPHICAL EXAMINATION OF CRUSHED TUBES

5.1 Introduction

The results of visual and micrographical studies on crushed tubes are described in this chapter. Preliminary work was necessary to identify those specific failure mechanisms caused by shear and transverse tension in a glass-polyester system identical to that used in polyester tubes. This was carried out on flat unidirectional specimens. The more common failure mechanisms were found to be already well documented (26).

Visual examination of crushed tubes was used to establish the general nature of the failure mechanism of both $0^{o}/90^{o}$ and angle-wound tubes. This is described in Section 5.3. The failure mechanisms of a standard $0^{o}/90^{o}$ tube subjected to incremental crushing and studied by normal metallographic techniques are described in Section 5.3.

In section 5.5 results are given of scanning electron microscopic studies of the individual failure mechanisms contributing to the overall crushing process. Section 5.6 contains the results of measurements made on sections from the crush zone under load.

5.2 Fracture of unidirectional laminae

The fracture surfaces of unidirectional glass-polyester composite were examined by SEM. Shear and transverse tensile fracture surfaces were obtained from short beam shear tests, transverse and 10^{o} off-axis tensile tests. These tests were carried out on flat unidirectional specimens. In this way the characteristics of the fracture surfaces in these failure modes could be used to evaluate the failure mechanisms during the crush

of $0^{o}/90^{o}$ polyester tubes.

Representative micrographs of shear fracture surfaces from off-axis and short beam shear are shown in Figs. 5.1 and 5.2. In both cases the crack direction was parallel to the fibre direction. The fracture surfaces from both testing methods were characterised by clean fibres without adhering resin, indicating that the crack propagated along the interface between the fibre and the resin.

The resin between the fibre showed a characteristic jagged torn surface with "chunks" of resin which appeared to have been torn and raised from between the fibres. The 10^{o} off-axis fracture surface showed that, for the resin-glass system studied, the matrix was torn into a narrow flake-like structure between the fibres.

Typical fracture surfaces obtained from transverse tensile testing are shown in Fig. 5.3. The difference between this and shear fracture surfaces is immediately obvious. Resin appears to adhere to the fibre surfaces, failing in a planar manner, both around the fibres and through the matrix. Superimposed on the resin fracture mechanism are a large number of small, shallow, irregular indentations, totally dissimilar from the jagged torn surface associated with shear fracture.

5.3 General mechanisms of progressive crushing

5.3.1 $0^{o}/90^{o}$ polyester tubes

A general view of a $0^{o}/90^{o}$ tube subjected to axial crushing at 4×10^{-3} m s^{-1} is shown in Fig. 5.4. A close-up view of the crush zone is shown in Fig. 5.4(b). The progressive nature is apparent with crushing commencing at the bevelled end. The outer axial fibres were bent outwards with limited fibre breakage.

(a) Fracture surface showing clean fibres with jagged torn resin.

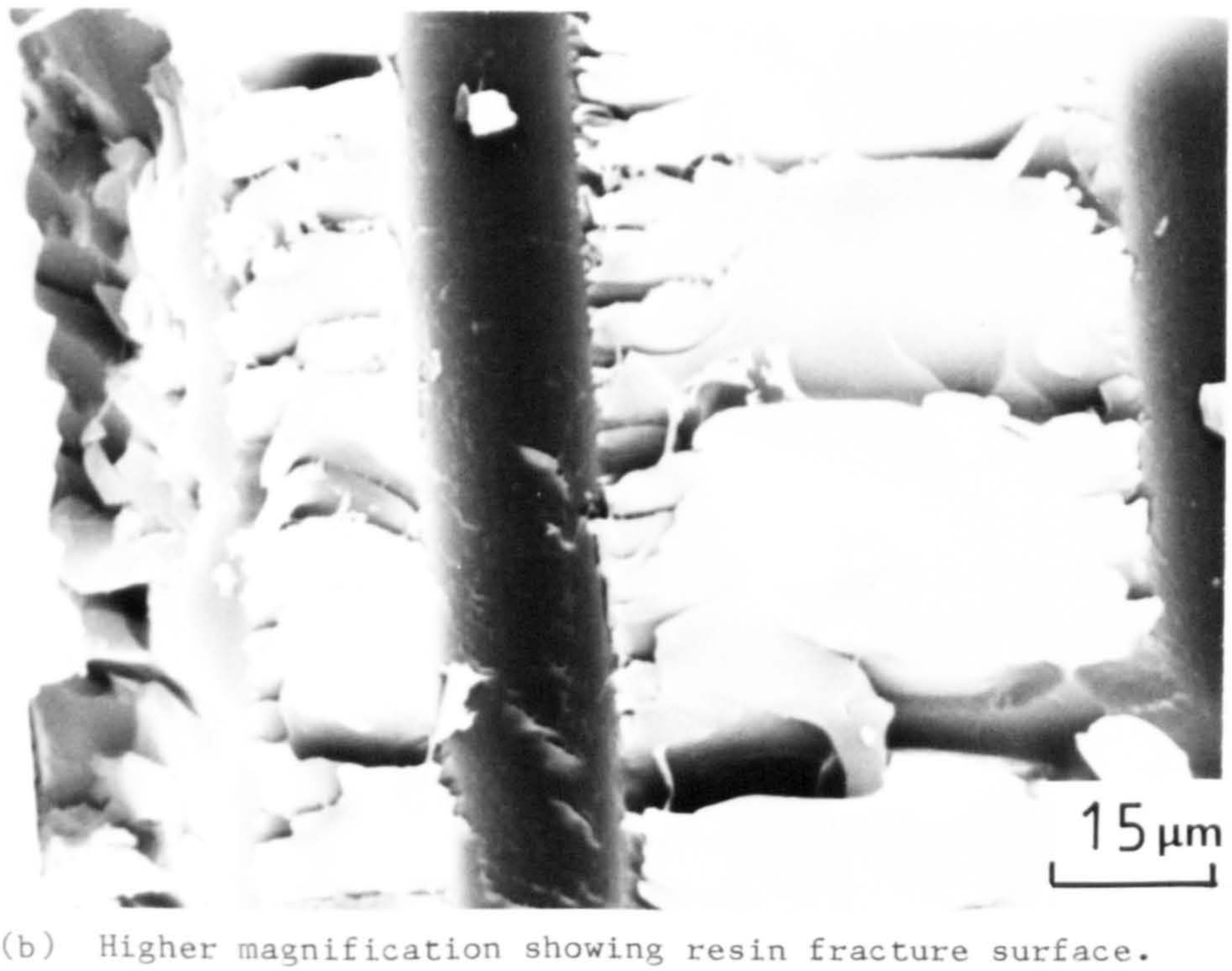

(b) Higher magnification showing resin fracture surface.

Fig.5.1. SEM photomicrograph of the fracture surface from a 10° off-axis tensile test of a unidirectional glass-polyester specimen.

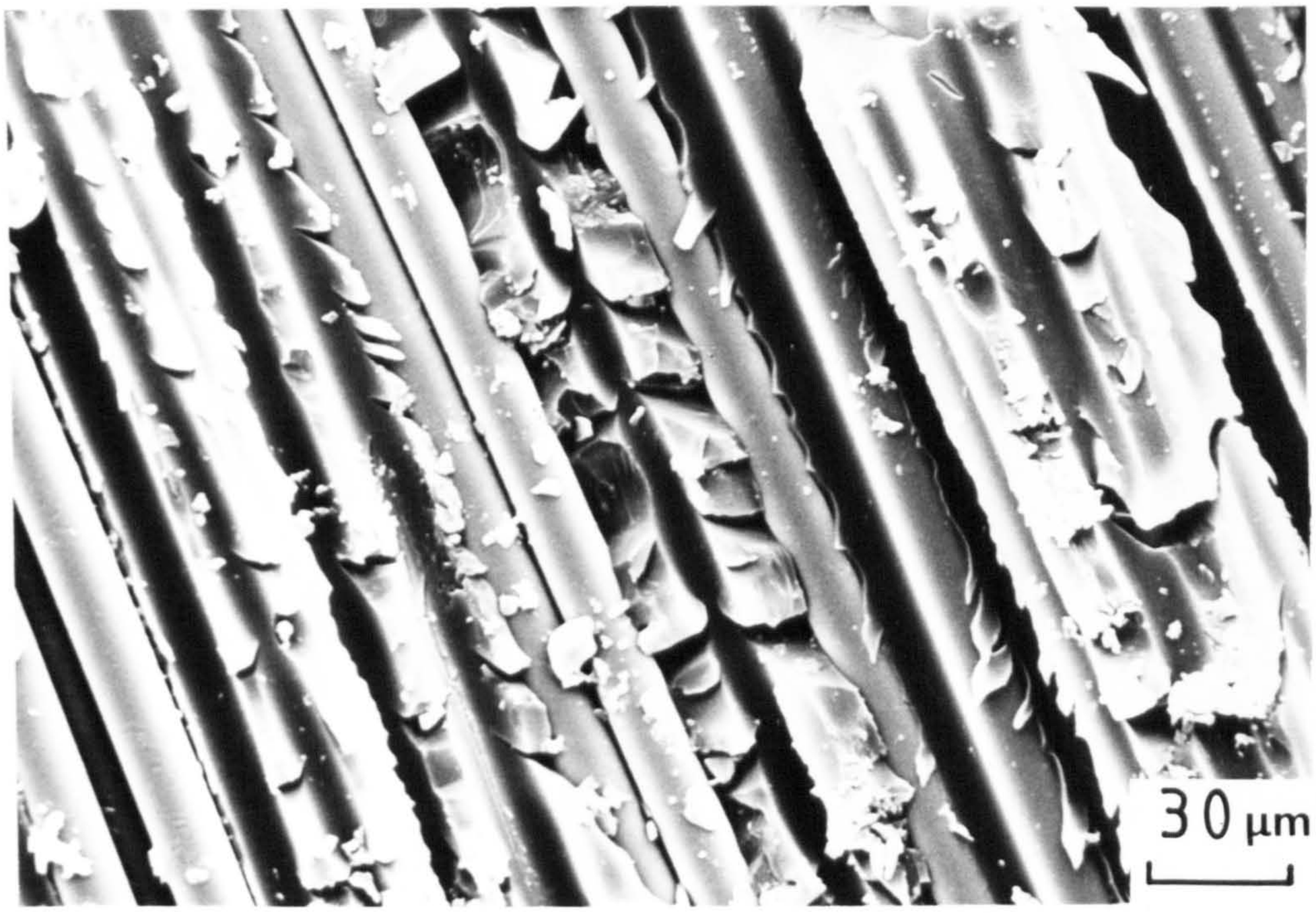

(a) Fracture surface showing torn jagged resin with clean fibres.

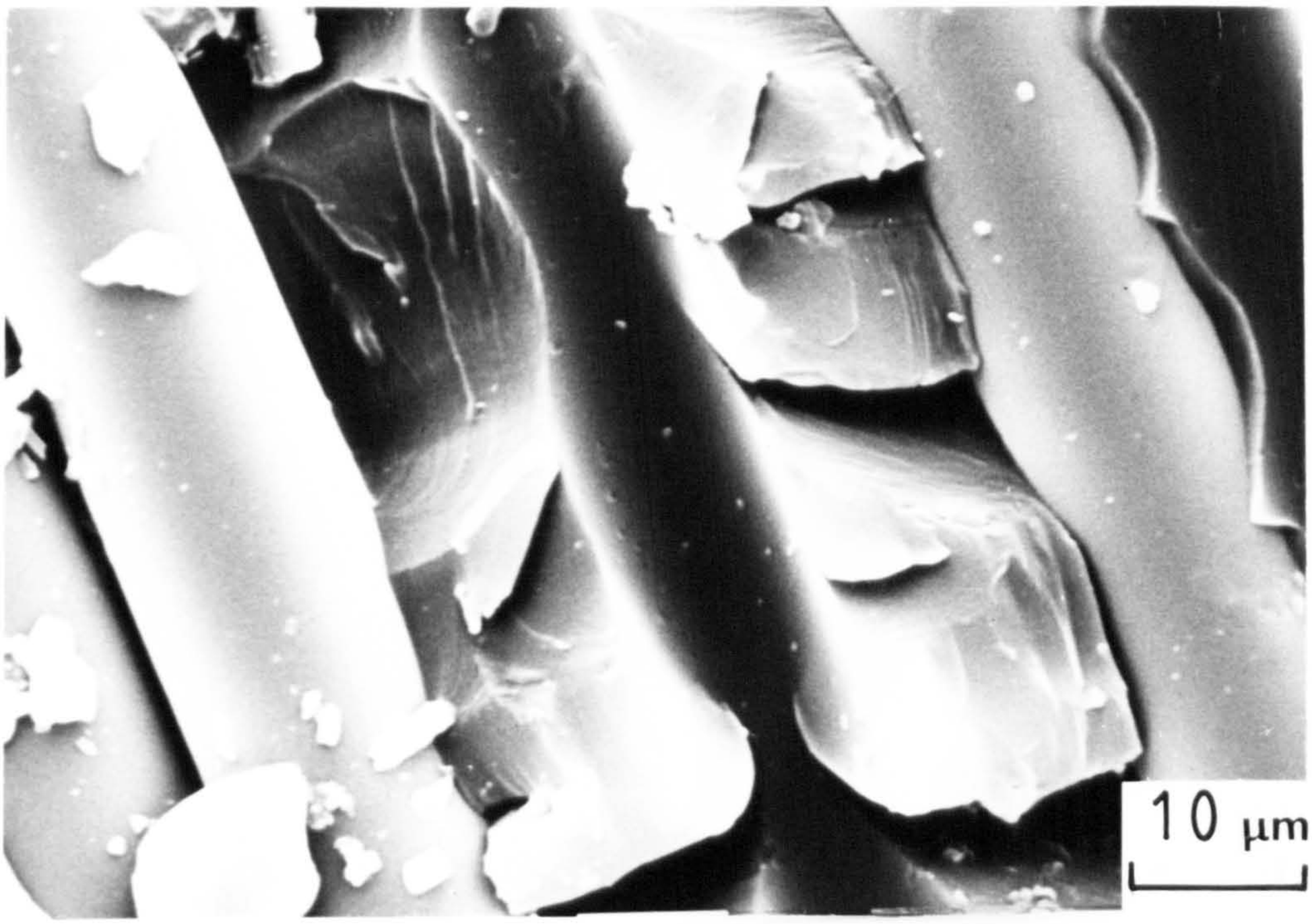

(b) Higher magnification showing torn resin surface.

Fig.5.2. SEM photomicrograph of the fracture surface from a short beam shear test of a unidirectional glass-polyester specimen.

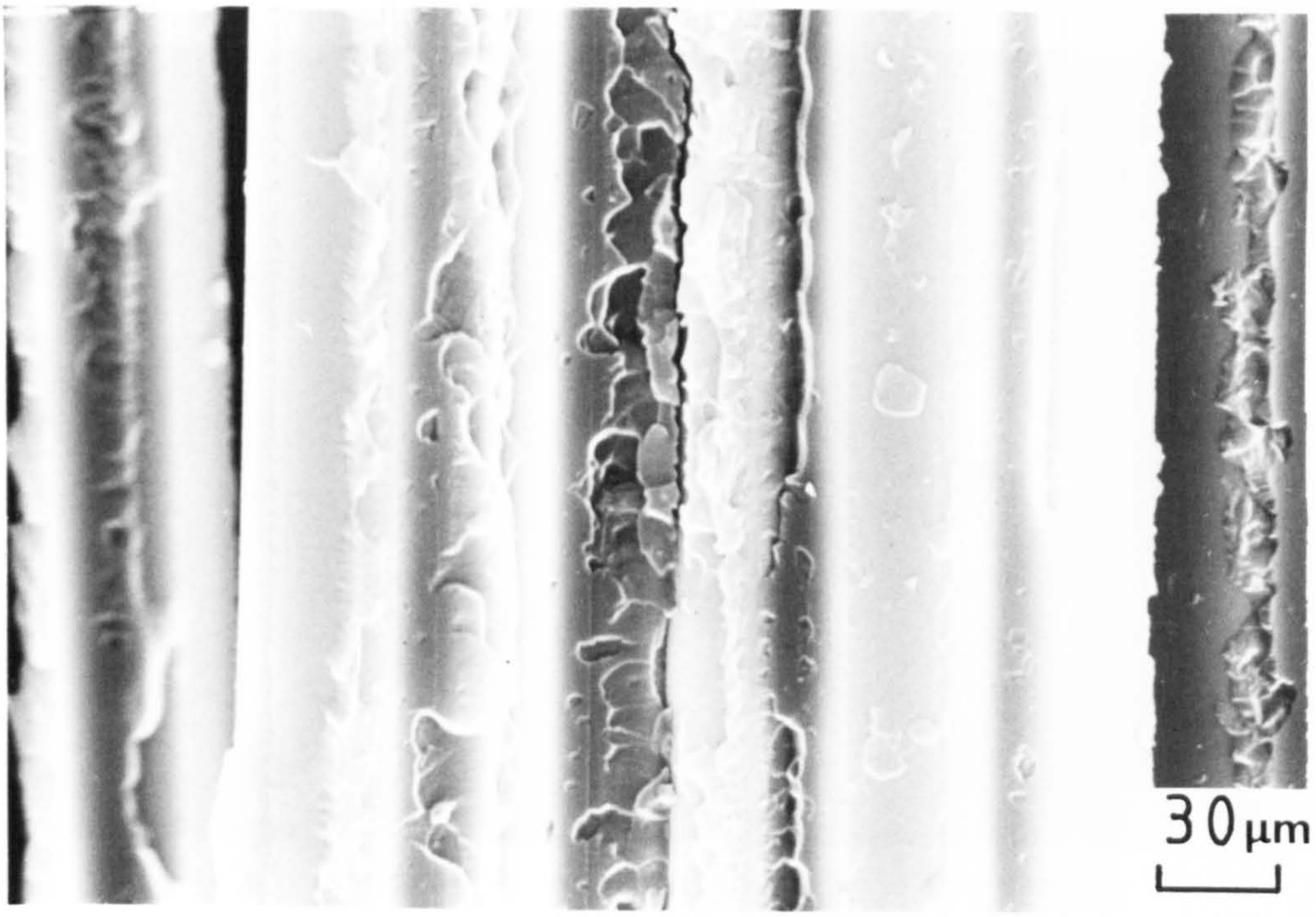

(a) Fracture surface showing flat pitted resin surface with resin adhering to the fibres.

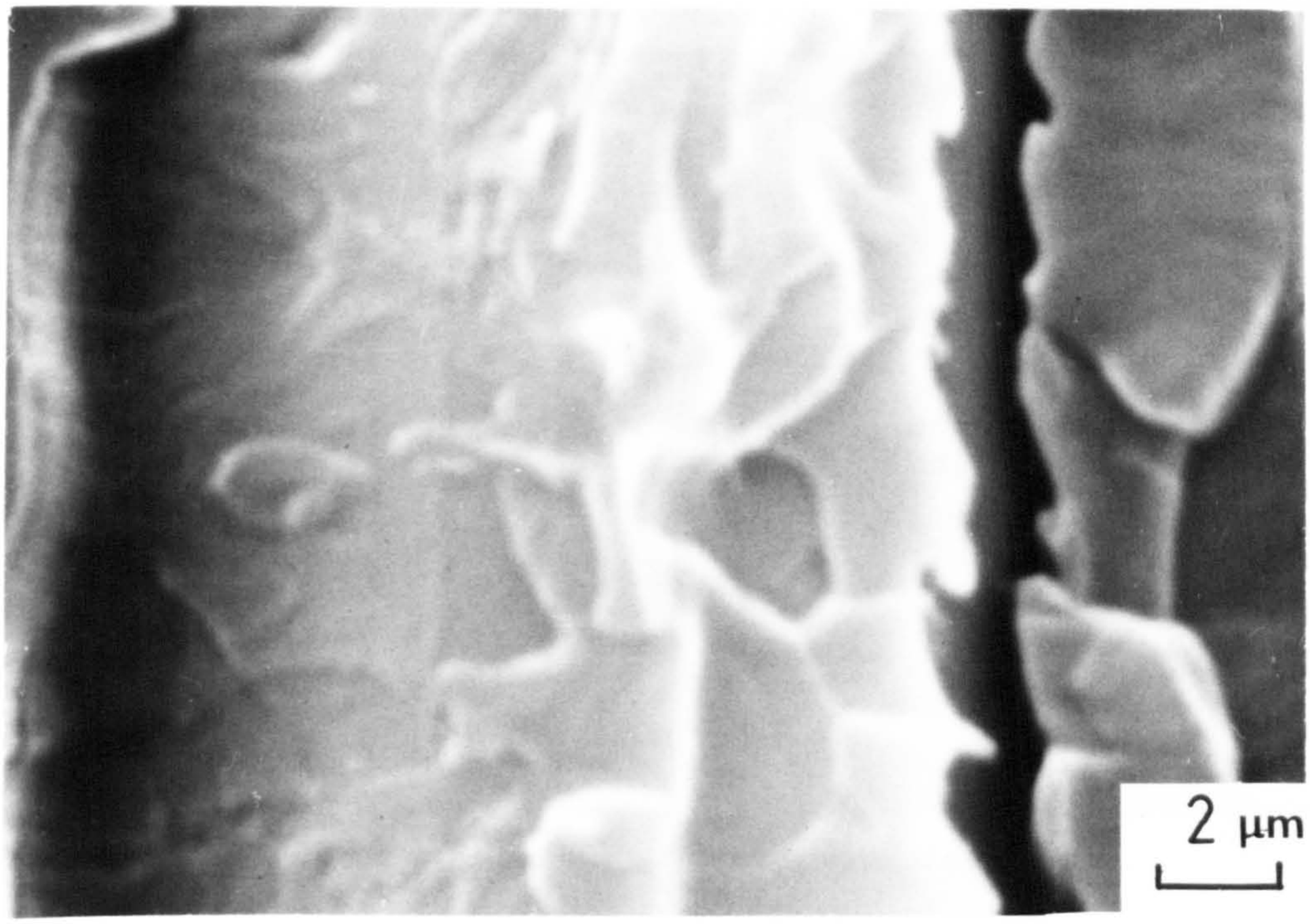

(b) Higher magnification showing pitted resin surface.

Fig.5.3. SEM photomicrograph of the fracture surface from a transverse tensile test of a unidirectional glass-polyester specimen.

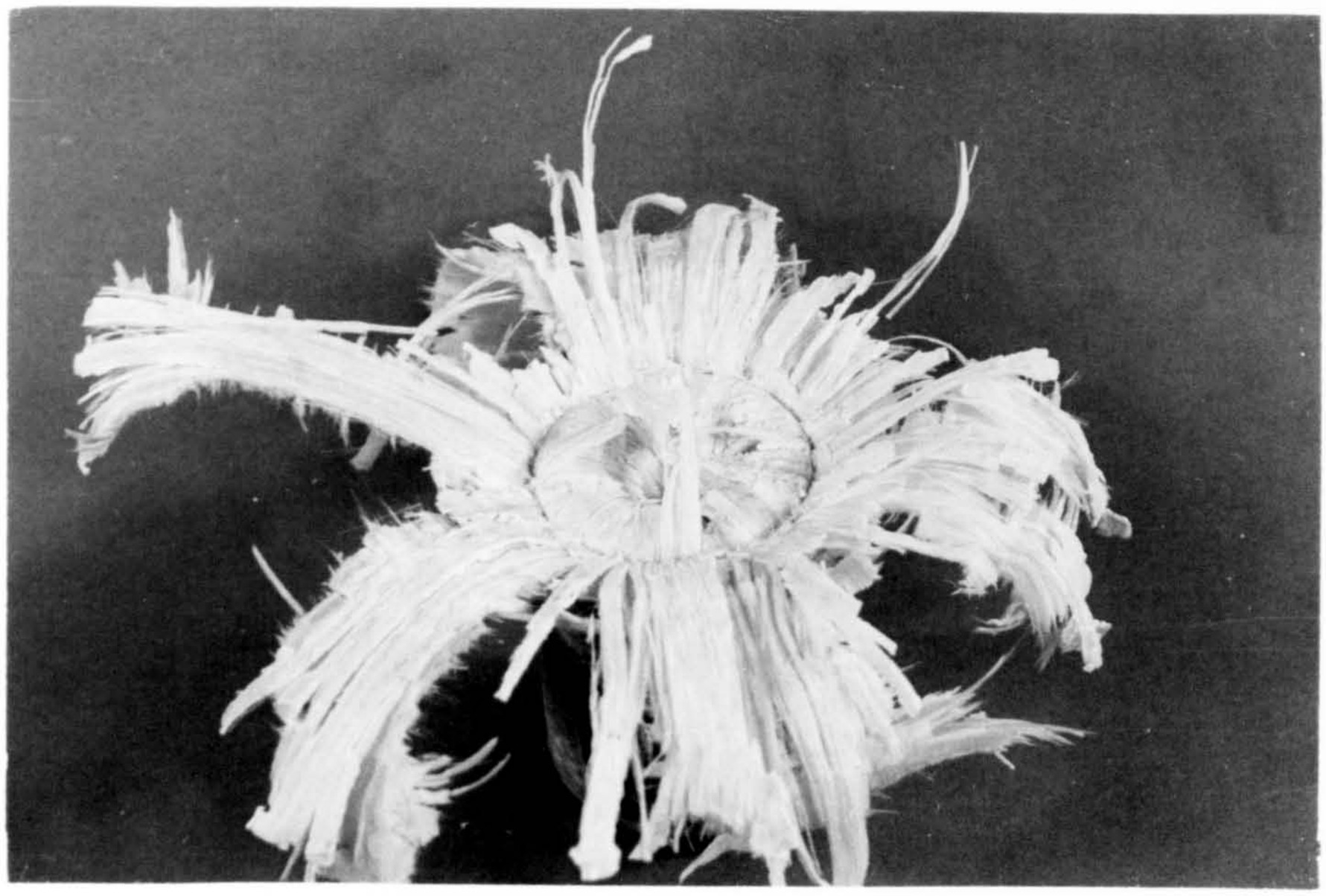

(a) General view of crush zone. The axial fibres are bent and fractured.

(b) Close-up of crush zone showing fractured fibres.

Fig.5.4. Crushed polyester 0°/90° tube tested at 4×10^{-3} m s^{-1}.

The inner axial fibres were also bent and compressed into the tube centre, undergoing a certain amount of fracture. Some springback and relaxation took place when the tubes were removed from the test machine so that the actual crush front differs somewhat from the photograph.

The outer axial fibres were split into bundles of various widths by axial cracking. The outer hoop windings either fractured into long thin fibre bundles which became separated from the tube wall, or into shorter plate-like bundles which still maintained partial integrity with the axial fibres. These plate-like bundles had the same length as the width of the axial fibre bundles. A region of tightly packed crushed material formed in the centre of the tube wall between the inner and outer axial fibres. This can be clearly seen in Figs. 5.4(b) and 5.8(b). This is termed a bundle wedge and will be described later.

The inner axials were completely inverted into the tube cavity, being subjected to a complex fracture process. Owing to the limited volume available inside the tube, the axial fibres were bent and fractured by impingement with other fracture material following the effective reduction in circumference. This also applied to the inner hoop fibres which fractured by a complicated bending and interpenetrating process.

Fig. 5.5 shows a typical $0^{o}/90^{o}$ tube tested at 4 m s^{-1}. The general appearance is similar to that of the tube tested at 4×10^{-3} m s^{-1} (Fig. 5.4), except that the axial fibres are not fractured to such an extent and the fibre bundle width is less. The region of compressed material in the centre of the tube wall is clearly visible.

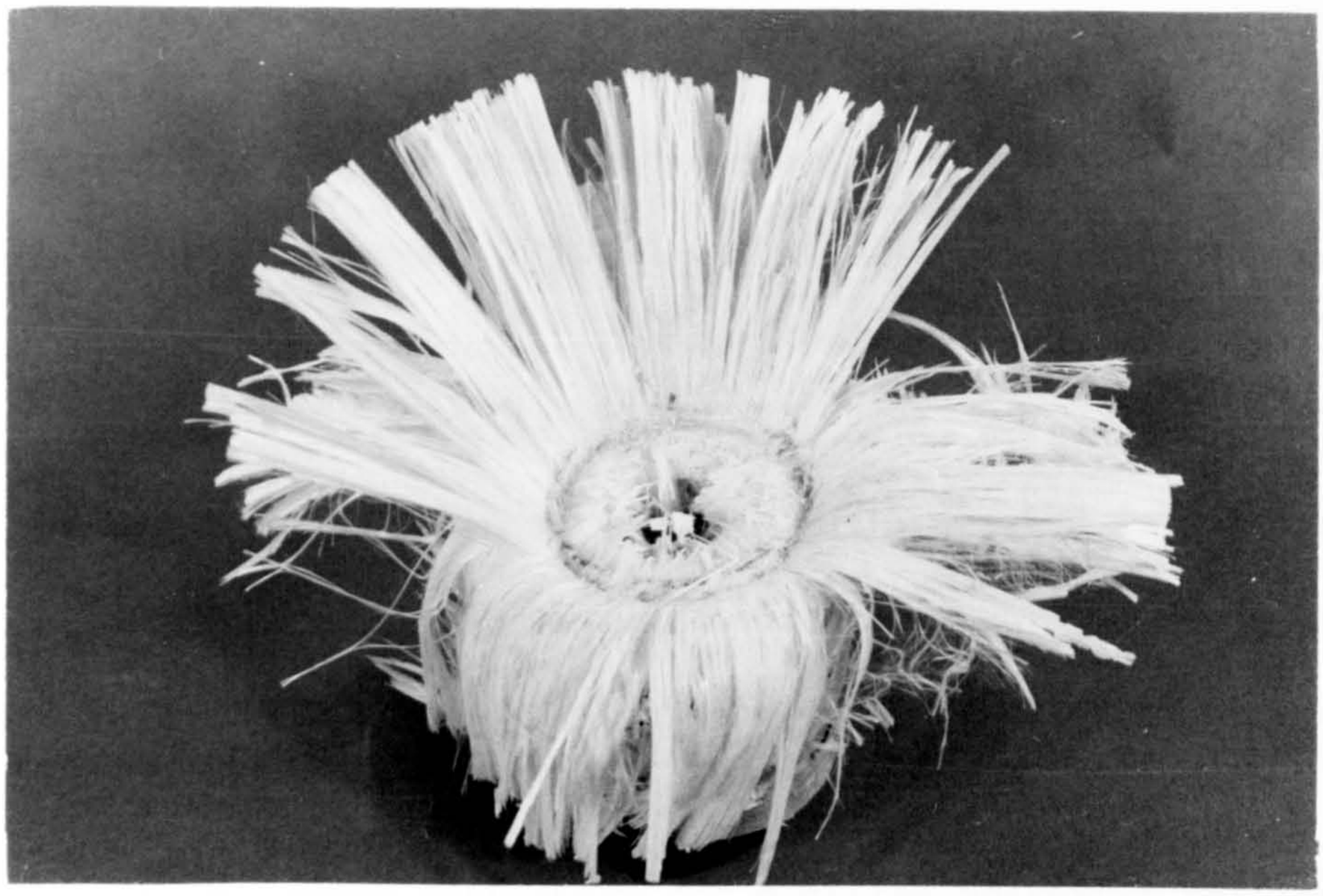

(a) General view of crush zone. The axial fibres are generally unbroken.

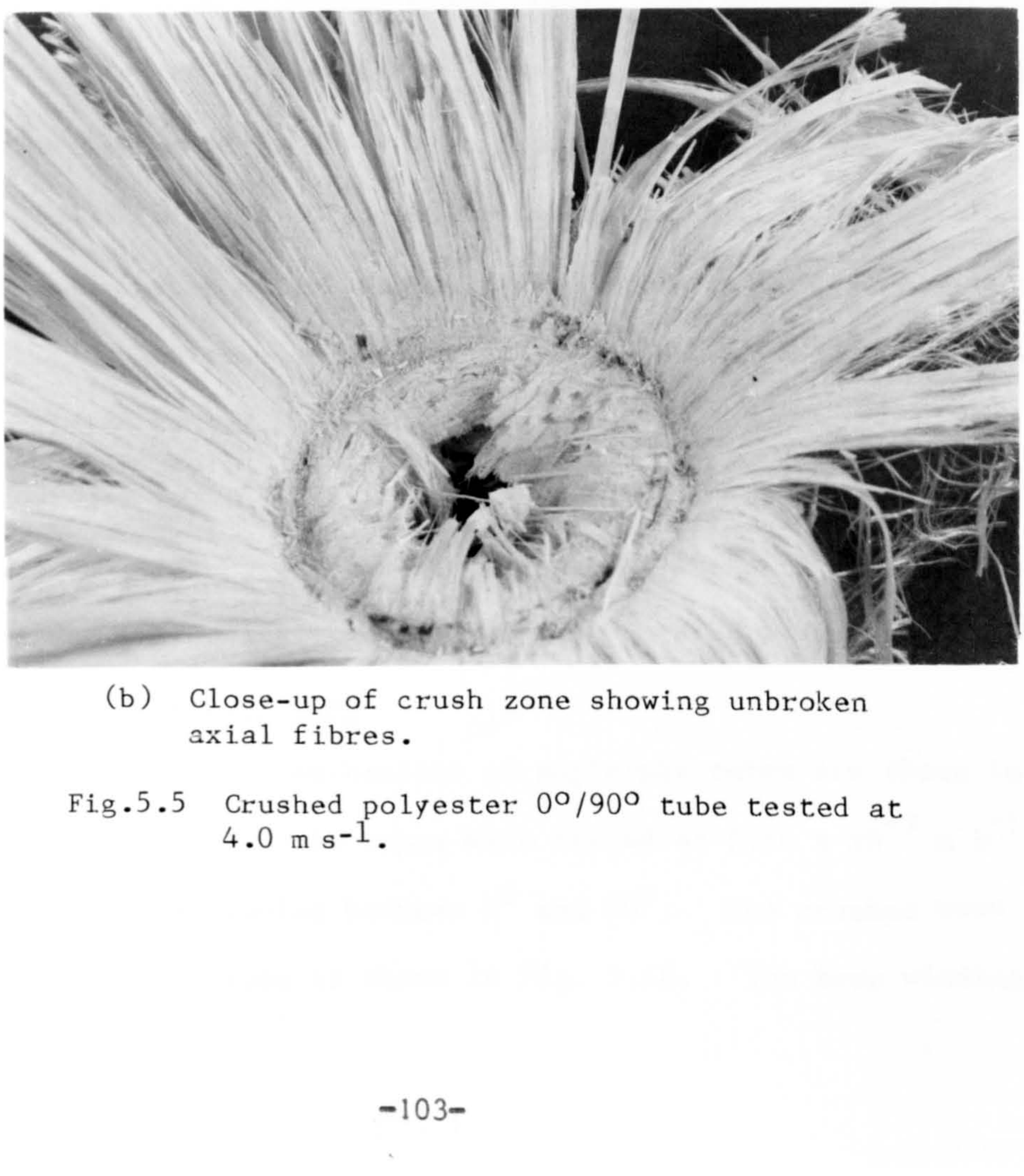

(b) Close-up of crush zone showing unbroken axial fibres.

Fig.5.5 Crushed polyester 0°/90° tube tested at 4.0 m s^{-1}.

A general view of a crushed $0^{o}/90^{o}$ tube tested at an intermediate speed of 1.7 m s^{-1} is shown in Fig. 5.6(a). The crushed axial laminae were similar to those in tubes tested at 4 m s^{-1} (Fig. 5.5), with little fibre breakage. The amount of axial splitting was less, giving a greater bundle width. A $0^{o}/90^{o}$ tube tested at 13.8 m s^{-1} using the crash rig is shown in Fig. 5.6(b). The original tube length was 850 mm,with 500 mm of the tube being crushed in a progressive manner. The outer axial fibres were unbroken. This can be clearly seen in Fig. 5.6(b). The inner hoop and axial fibres were completely inverted into the tube centre.

5.3.2 $0^{o}/90^{o}$ tubes with epoxy and modified polyester matrices

Typical appearances of a $0^{o}/90^{o}$ epoxy (MY 750) tube crushed at 4 x 10^{-3} and 4 m s^{-1} are shown in Figs 5.7 and 5.8. The crush process was similar to that for tubes with polyester (Crystic 272) matrices. As with polyester $0^{o}/90^{o}$ tubes, the amount of axial fibre fracture was less at 4 m s^{-1} than at 4 x 10^{-3} m s^{-1}. A well-defined bundle wedge formed in the centre of the tube wall.

Modification of the polyester matrix by Crystic 586 or CRC 1080 had little effect on the crush mechanism. Fig. 5.9 shows the typical appearance of the crushed zone from a $0^{o}/90^{o}$ tube with resin modified by the addition of 30% by volume of CRC 1080. The appearance was similar to that of a crushed $0^{o}/90^{o}$ polyester tube (Figs 5.4 and 5.5). The differences in the amount of axial fibre fracture due to testing speed can be seen in Figs 5.9(a) and 5.9(b).

5.3.3 Angle-ply tubes

The crushing mechanisms of angle-ply tubes are shown in Figs. 5.10 to 5.17. All tubes were tested at 0.16 x 10^{-3} m s^{-1}. The winding angles varied between 0^{o} and 90^{o}. The crushed zone of a hoop-wound (90^{o}) tube is shown in Fig. 5.10. The hoop windings

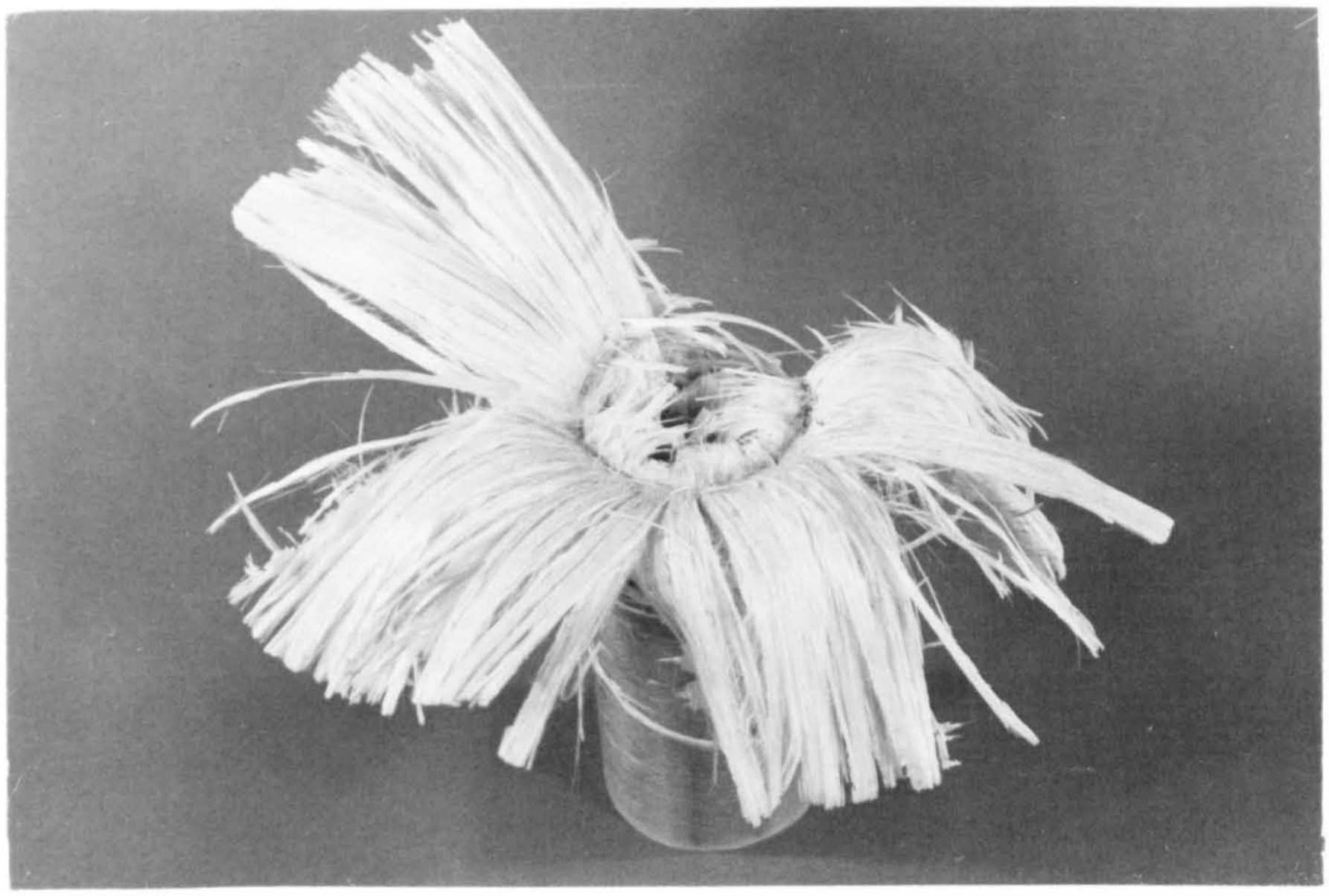

(a) General view of crush zone. Test speed 1.7 m s^{-1}. Segment removed for micrographic examination.

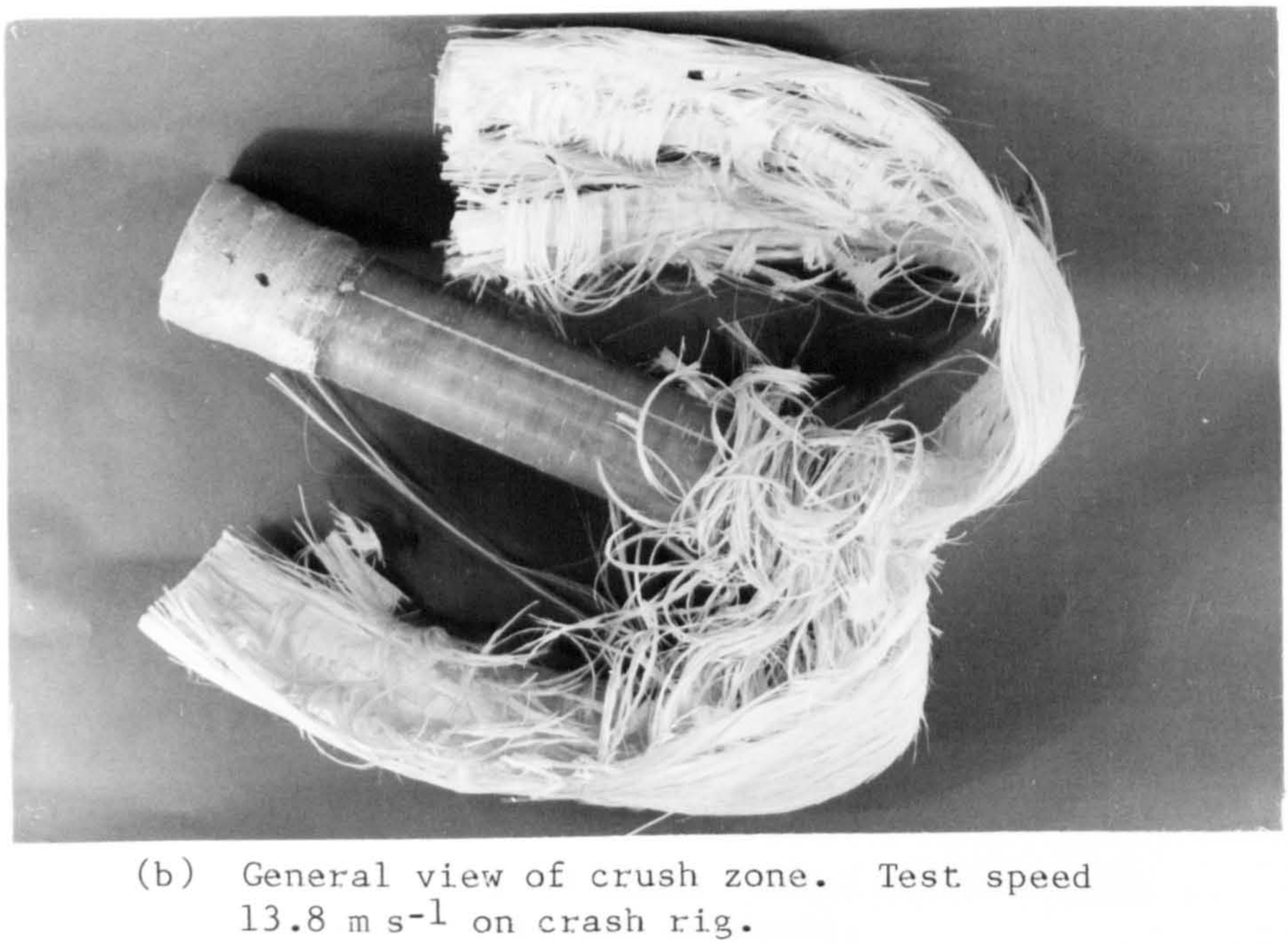

(b) General view of crush zone. Test speed 13.8 m s^{-1} on crash rig.

Fig.5.6. Crushed polyester 0°/90° tubes at various speeds as indicated.

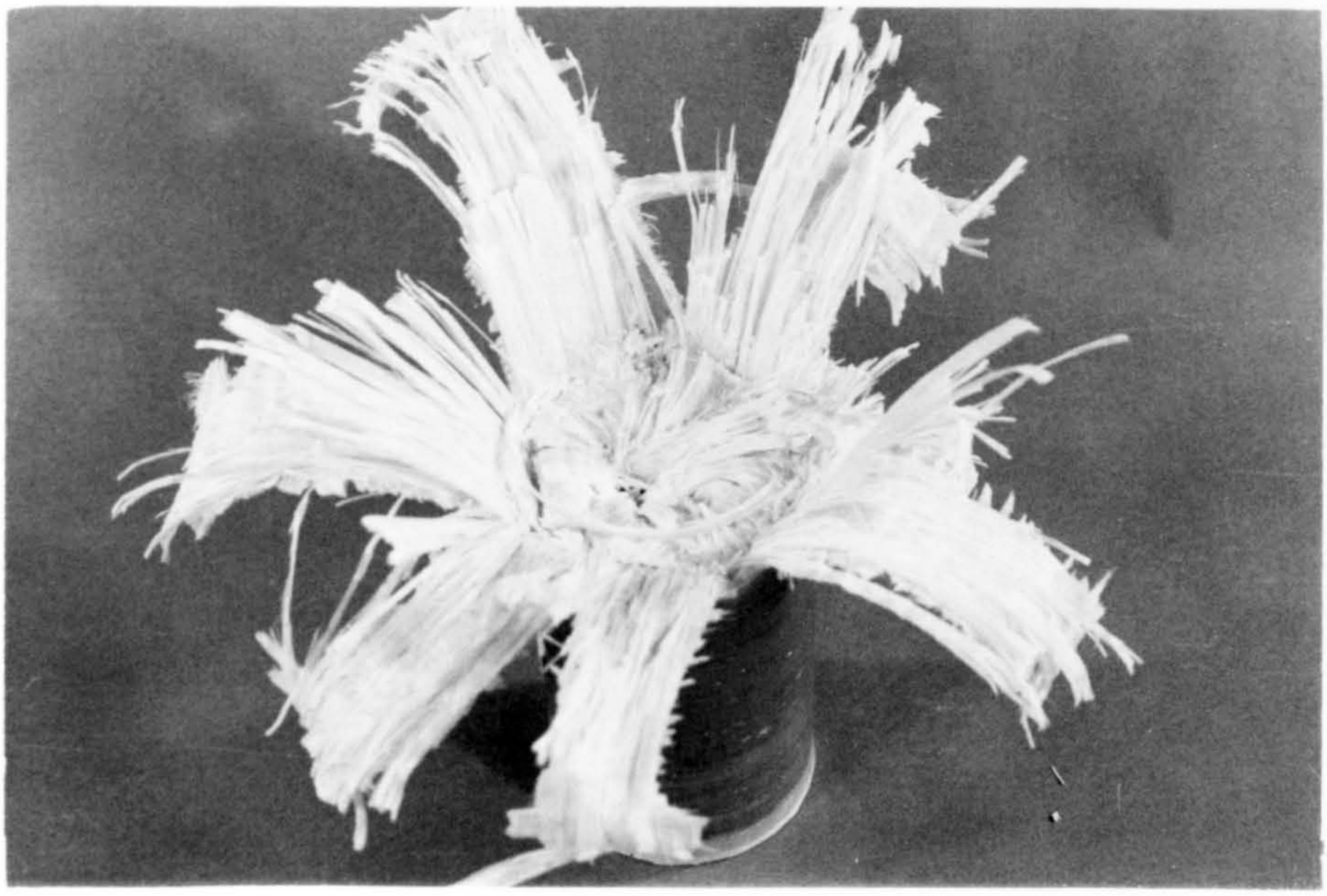

(a) General view of crush zone.

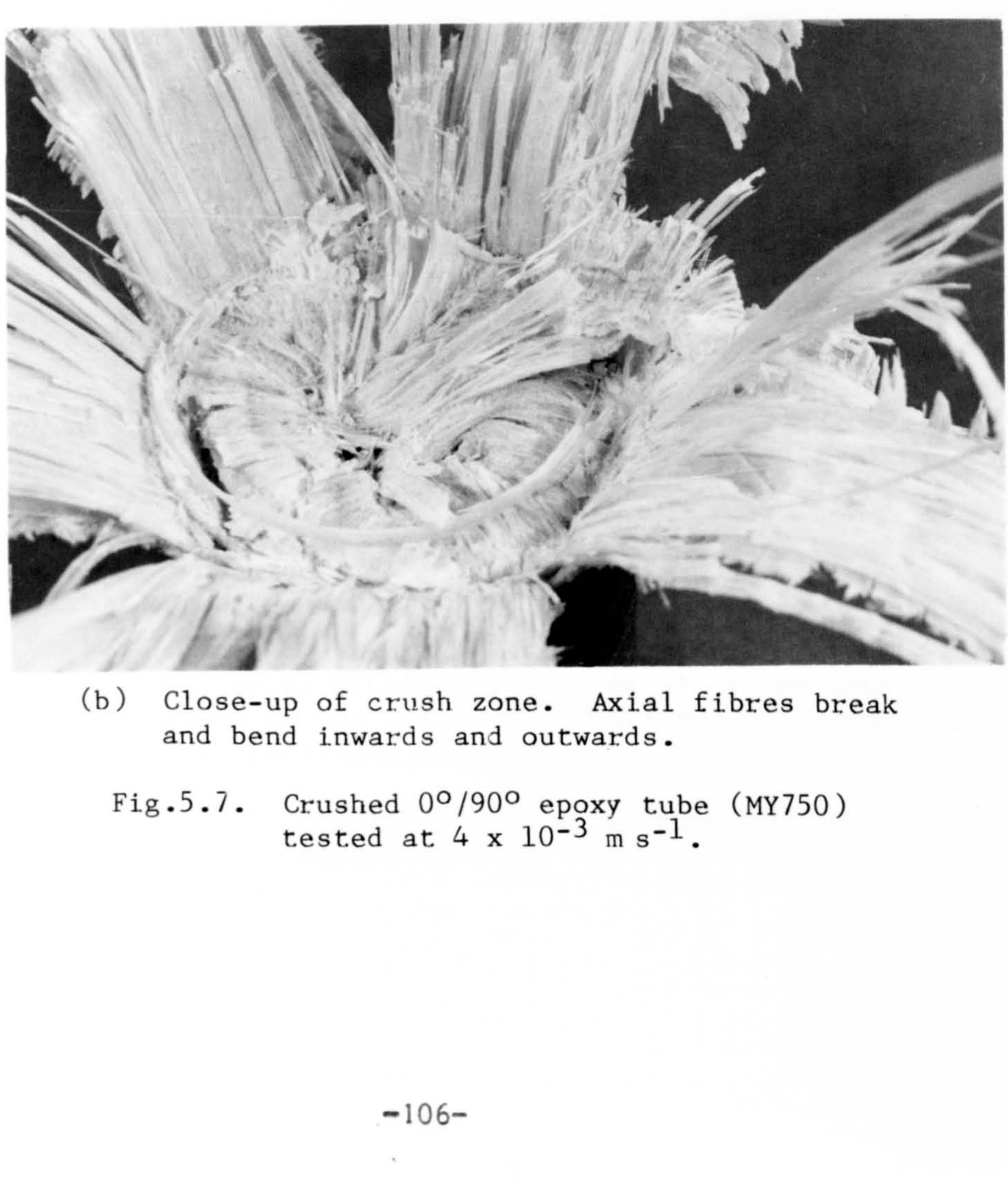

(b) Close-up of crush zone. Axial fibres break and bend inwards and outwards.

Fig.5.7. Crushed 0°/90° epoxy tube (MY750) tested at 4×10^{-3} m s^{-1}.

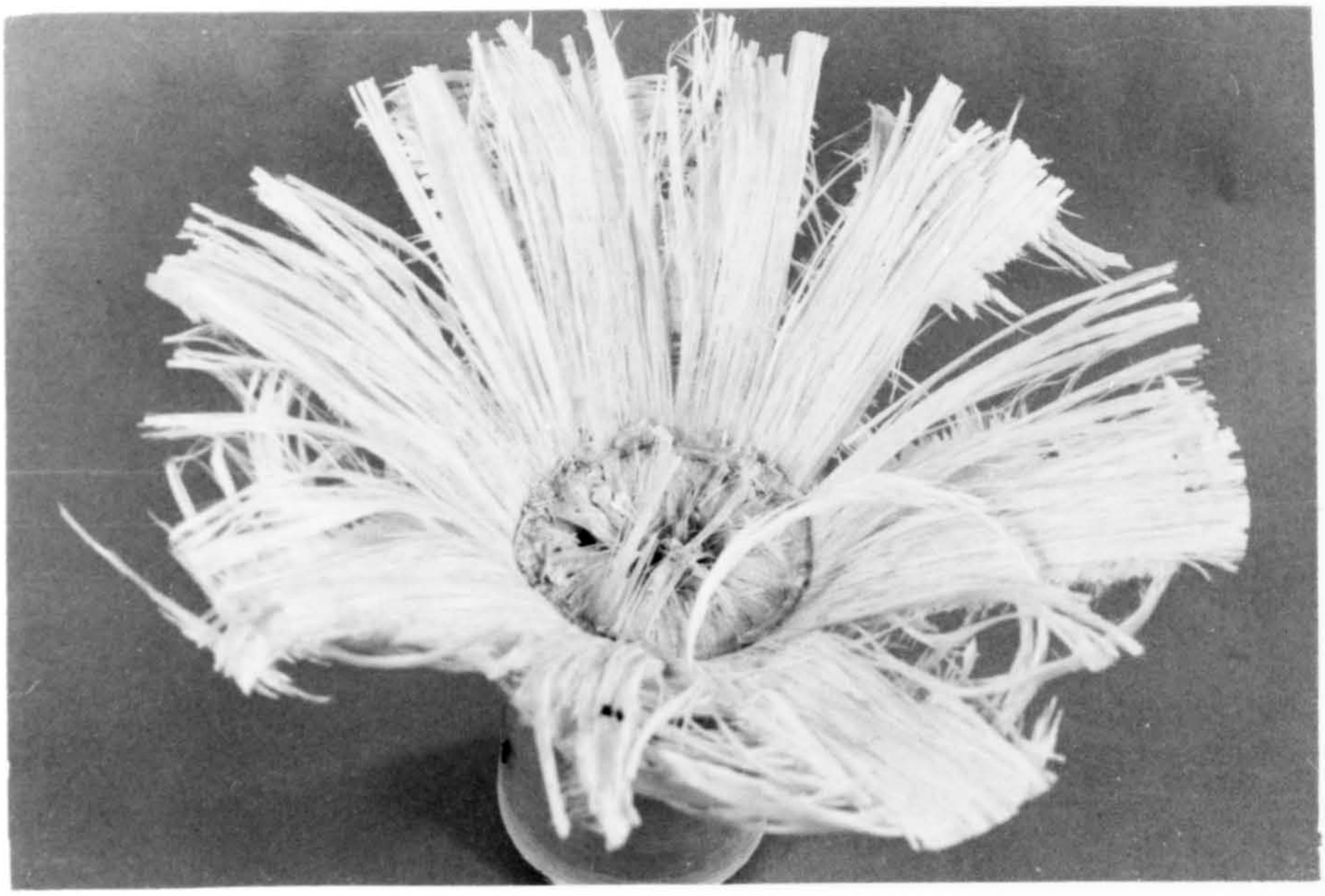

(a) General view of crush zone.

(b) Close-up of crush zone. Axial fibres bend inwards and outwards. Outer axial fibres are generally unbroken.

Fig.5.8. Crushed $0^{o}/90^{o}$ epoxy tube (MY750) tested at 4 m s^{-1}.

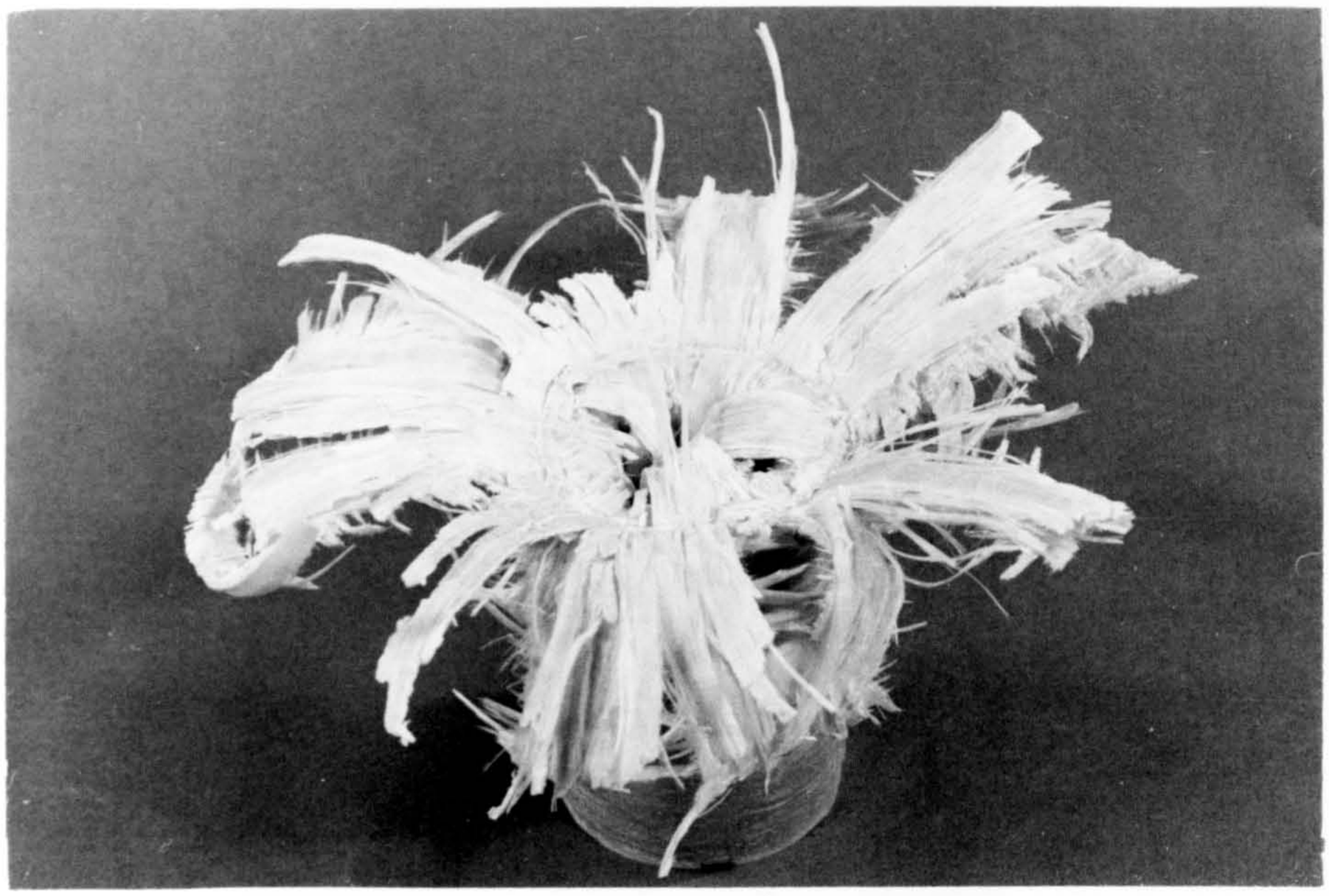

(a) General view of crush zone. Test speed 0.4×10^{-3} m s^{-1}.

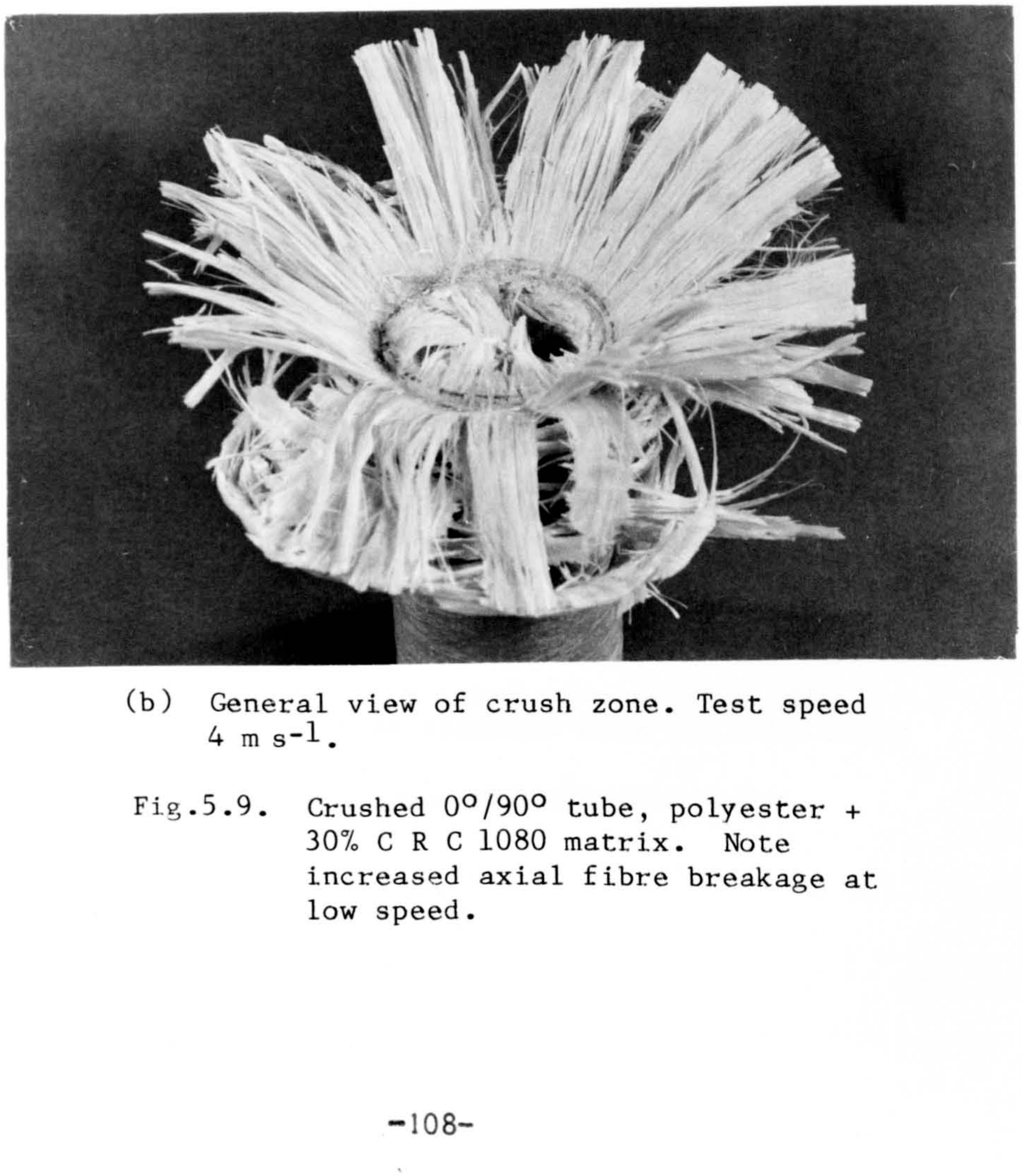

(b) General view of crush zone. Test speed 4 m s^{-1}.

Fig.5.9. Crushed $0^{o}/90^{o}$ tube, polyester + 30% C R C 1080 matrix. Note increased axial fibre breakage at low speed.

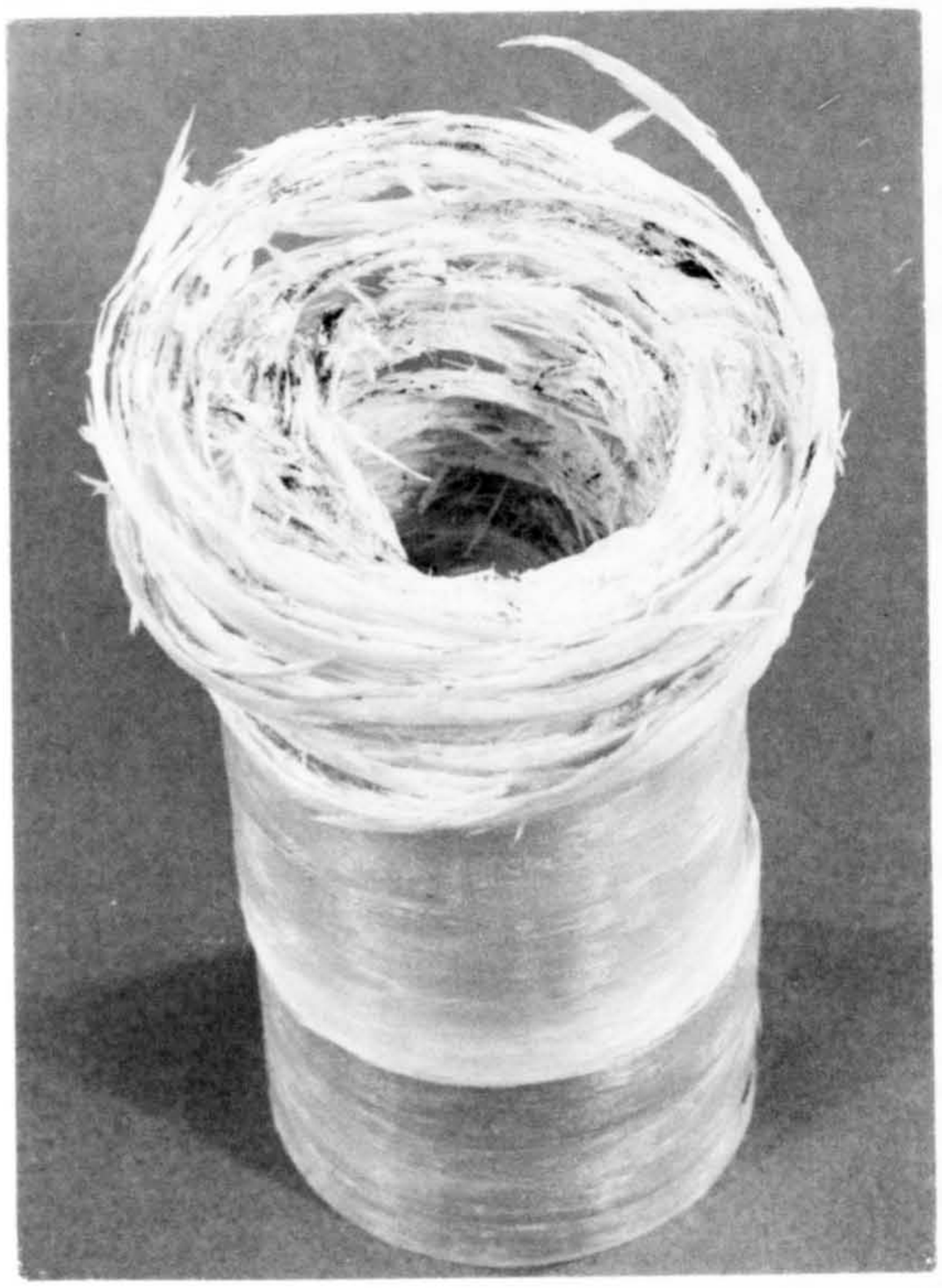

(a) General view of crush zone.

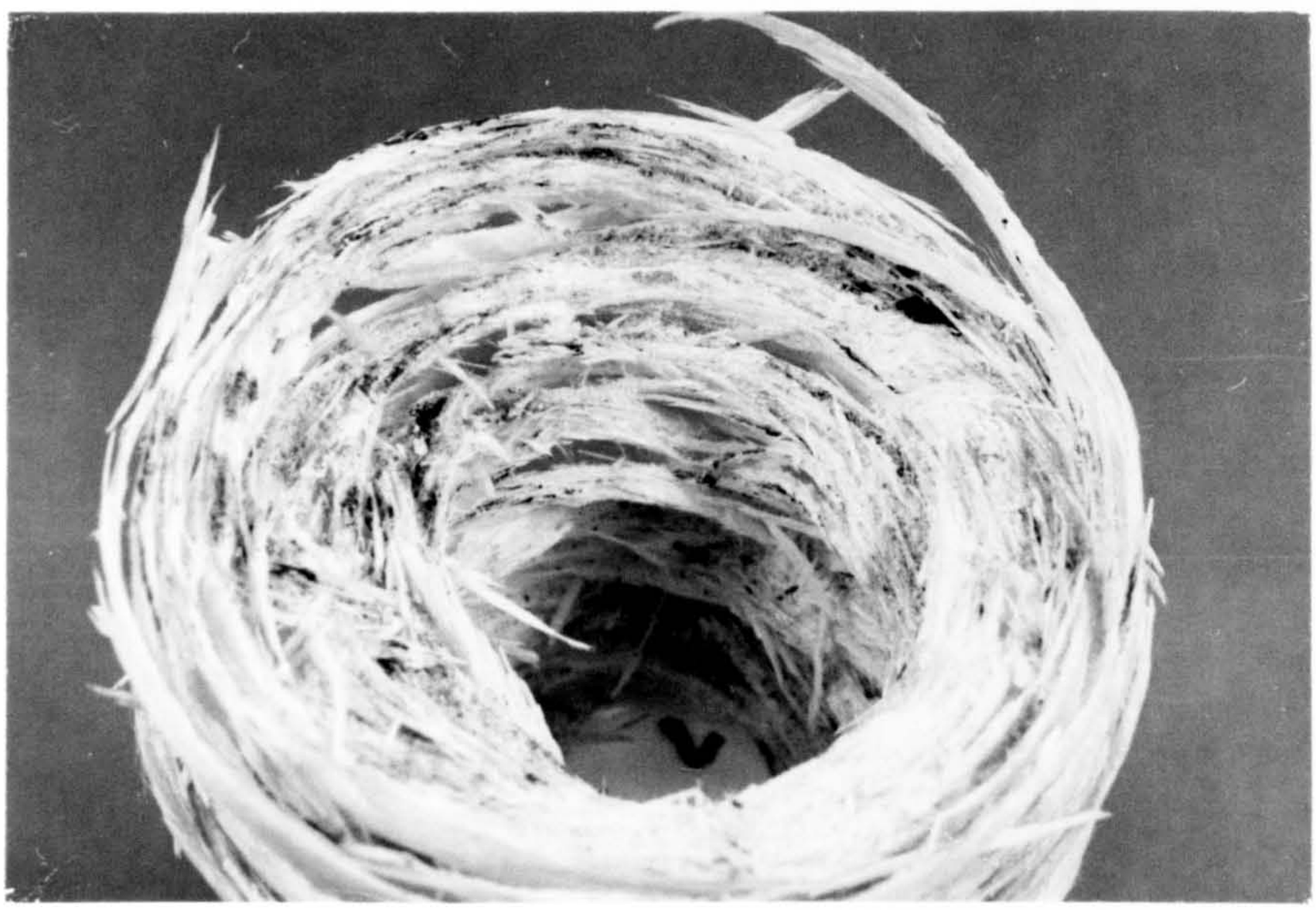

(b) Close-up of crush zone showing long fibre tows detached from the tube wall.

Fig.5.10. Crushed hoop-wound tube.

became detached from the tube wall as progressive crushing occurred. The outer hoop windings fractured in a tensile manner and then separated from the tube wall by shear, passing down the outside of the uncrushed tube. These fibres tows fractured into various lengths which varied from two to three times the tube circumference to short lengths of less than 1 cm. The long detached hoop windings are shown in Fig. 5.10(b).

As the outer hoops were fractured and compressed down the outside of the tube, the inner hoops were crushed inwards and downwards into the cavity of the tube. Because of the necessary reduction in circumference, a complex crushing process occurred involving bending, fracture and interpenetration. The short lengths of fractured fibre bundles can be observed in the inner region of the tube wall in Fig. 5.10(b).

The mechanism of failure of 85^{o} and 75^{o} angle-wound tubes was similar to that for hoop-wound tubes. During crushing, long fibre bundle tows became detached from the tube wall. These passed downwards either inside or outside the uncrushed tube wall. The width of the fibre bundles in 75^{o} angle tubes (Fig. 5.12) was greater than in the hoop-wound tubes. This was partly a result of the lay-up sequence which led to the formation of cross-overs of the fibre tows during tube manufacture. These cross-over regions tended to hold the fibre bundles together so that plates of material, rather than long thin bundles, became detached from the tube wall.

Similar effects were observed in 65^{o} angle tubes, with laminar plates, instead of long fibre tows, becoming detached from the tube wall (Fig. 5.13). The crushing process was progressive. The inner laminae were bent inwards and downwards into the tube cavity, with the outer laminae bending outwards then downwards. Both crushing processes involved fracture, mainly into plates of laminae, but

(a) General view of crush zone.

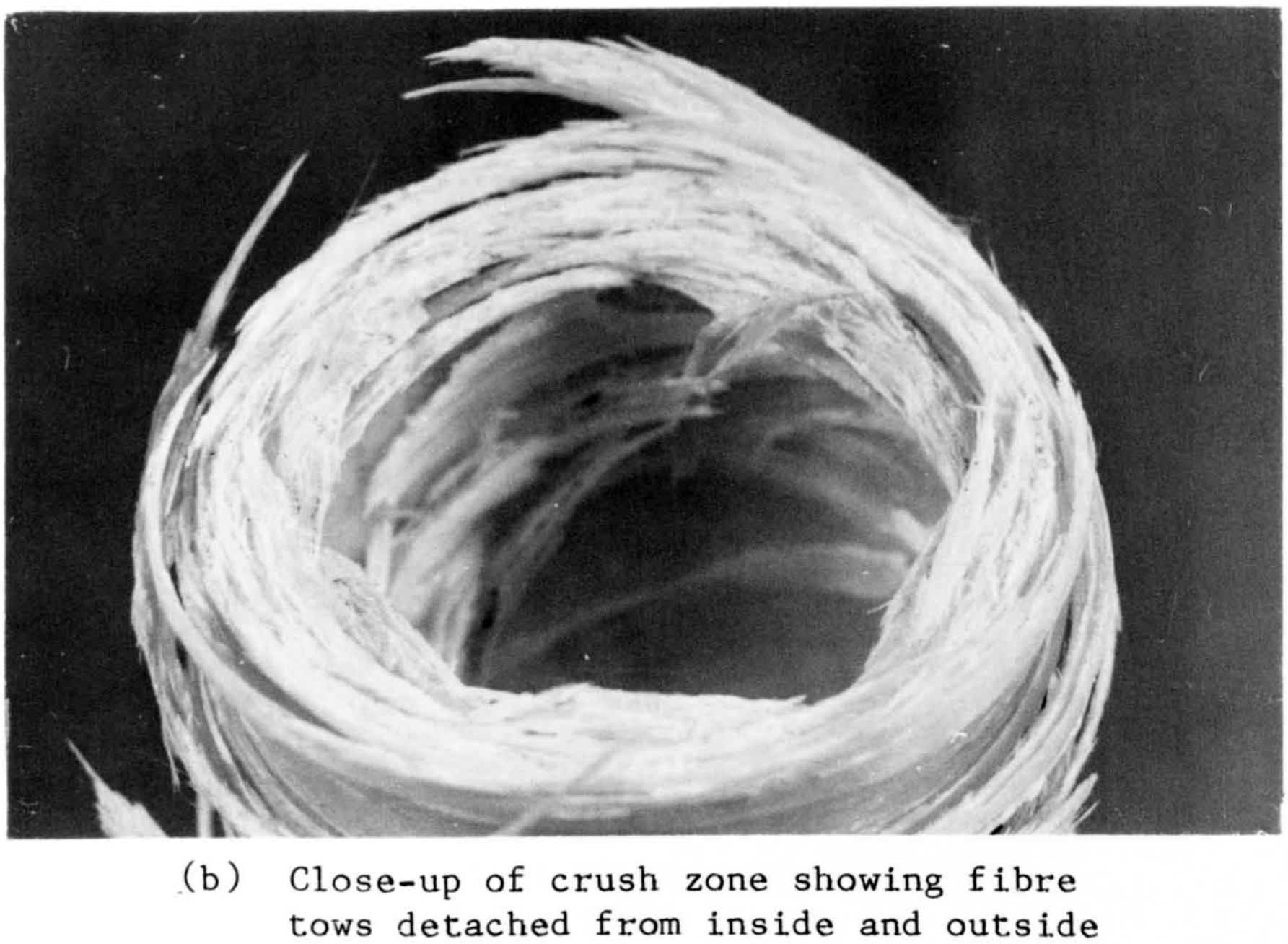

(b) Close-up of crush zone showing fibre tows detached from inside and outside of the tube wall.

Fig.5.11. Crushed 85° angle-wound tube.

(a) General view of crush zone.

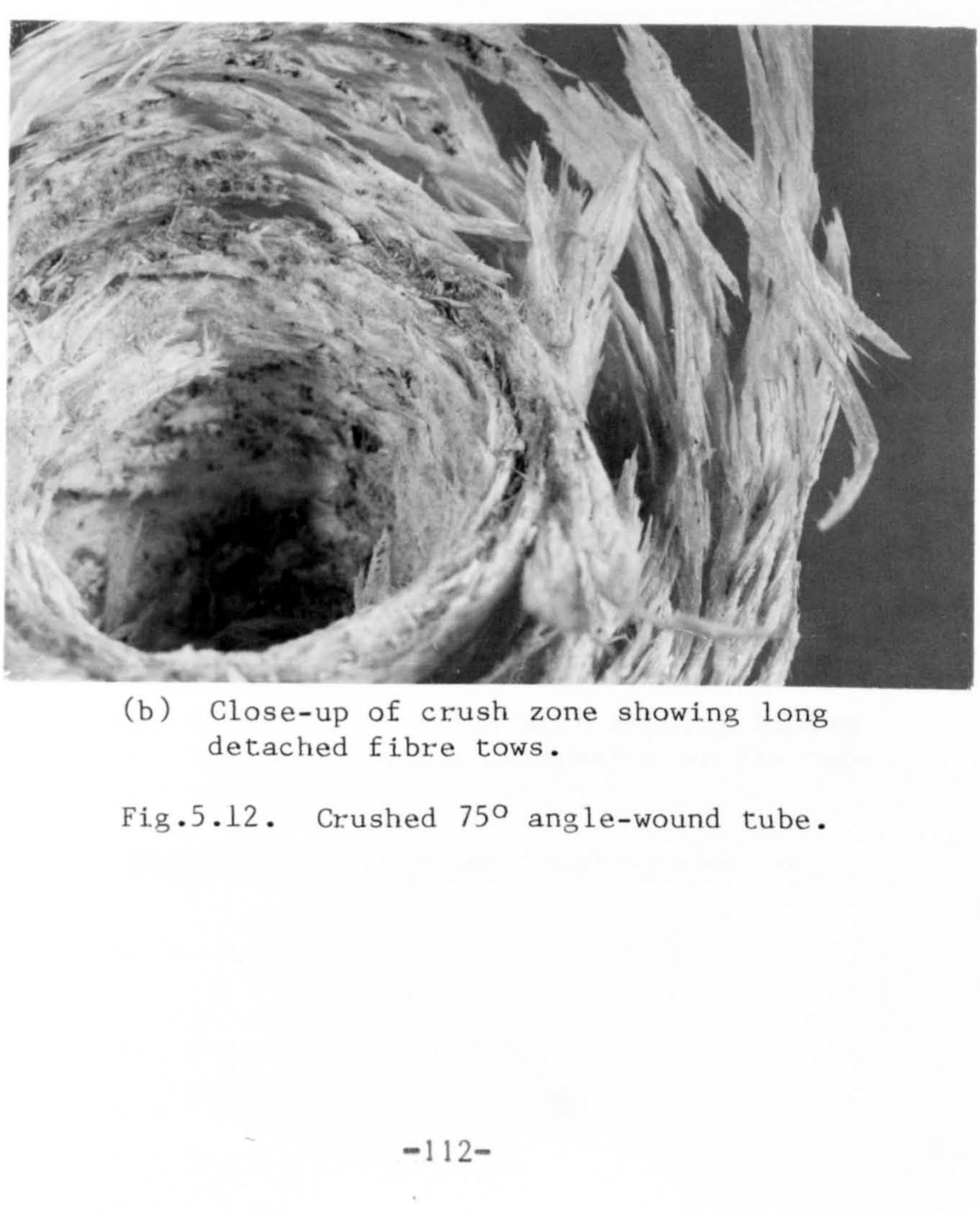

(b) Close-up of crush zone showing long detached fibre tows.

Fig.5.12. Crushed 75° angle-wound tube.

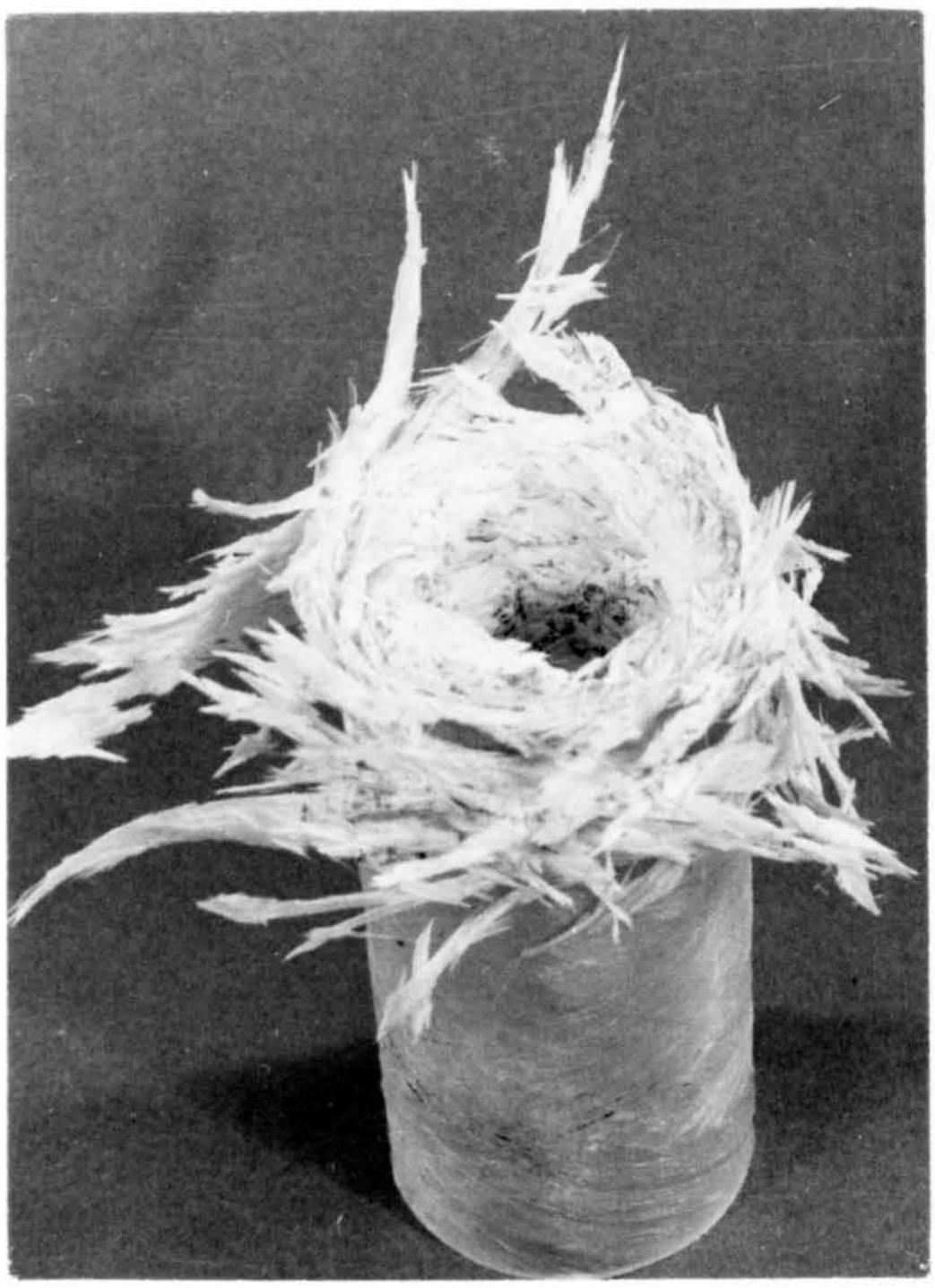

(a) General view of crush zone.

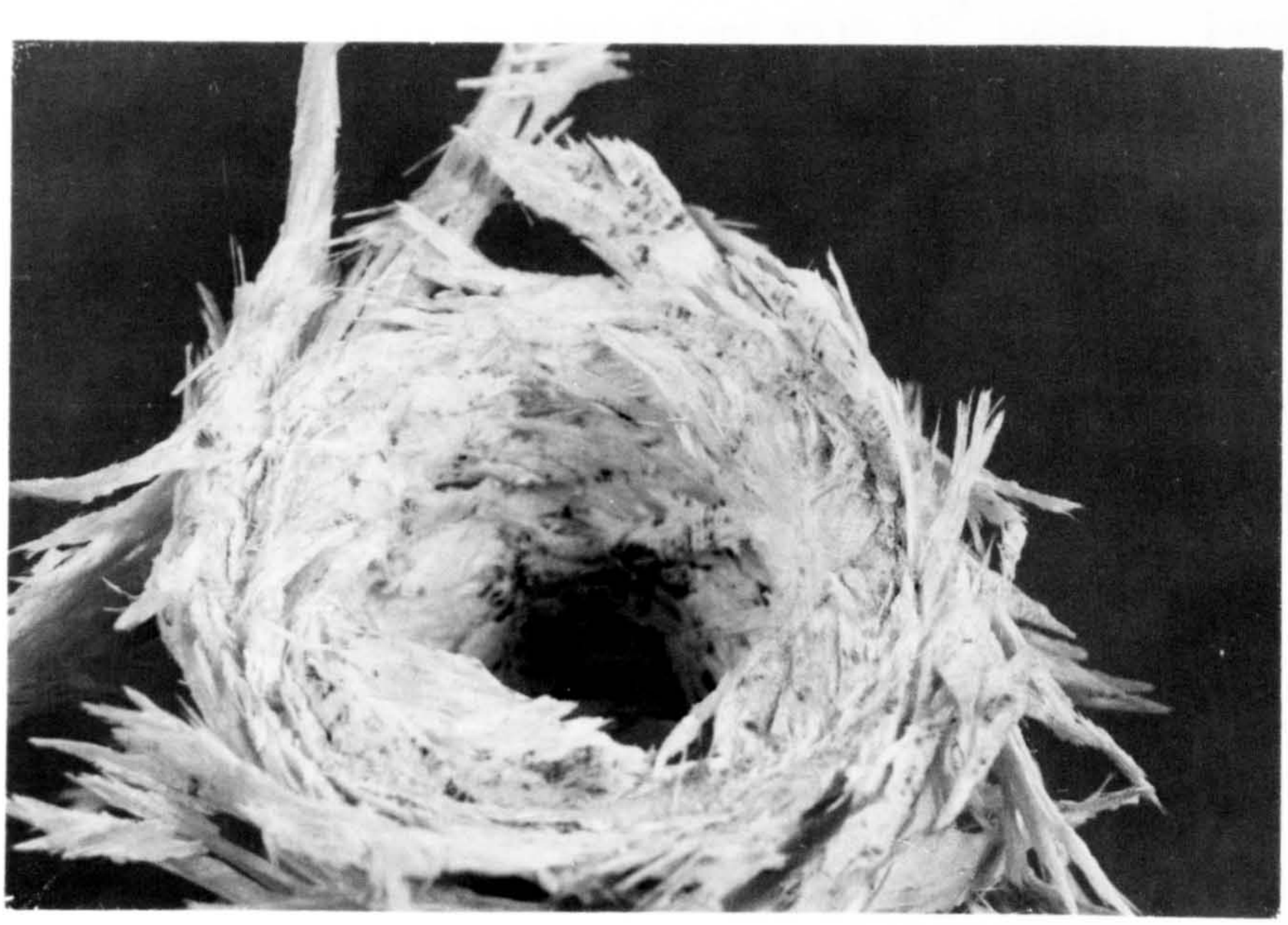

(b) Close-up of crush zone showing lamina plates becoming detached from the tube wall.

Fig.5.13. Crushed 65° angle-wound tube.

occasionally forming long thin fibre bundles.

Figs. 5.14 and 5.15 show the typical appearance of the crush zone in 55^{o} and 45^{o} angle-wound tubes. Progressive failure occurred with large plates of laminae being detached from the tube wall as crushing took place. These plates were bent inwards and outwards. Fig. 5.14(a) is confusing as most of the tube wall appears to have been bent inwards. Observation of the specimen indicated that the outer lamina divided from the inner laminae, became bent outwards, then fractured at a point adjacent to the tube wall. This resulted in complete separation from the uncrushed tube wall and gave the misleading appearance. This fracture was thought to be most likely to occur at a cross-over point owing to the complex interweaving of the fibres.

45^{o} angle tubes (Fig. 5.15) were observed to undergo a crushing process similar to that found with 55^{o} tubes. Large plates of broken laminae became detached from the tube wall as inward and outward bending occurred during progressive crushing.

The crush zone of a 35^{o} angle-wound tube is shown in Fig. 5.16. Progressive failure occurred from the bevelled end. A mixture of large plates and fibre bundles from the outer laminae bent away from the tube wall prior to complete detachment. The inner laminae were bent inwards and downwards into the tube void, fracturing into large plates of material which then fractured again (bending into) the tube cavity.

Tubes manufactured with two layers of axial fibres and a limited veil-cloth layer on the inner and outer wall followed a completely different crushing mechanism (Fig. 5.17). After a limited amount of crush at the bevel end, long cracks grew rapidly down the

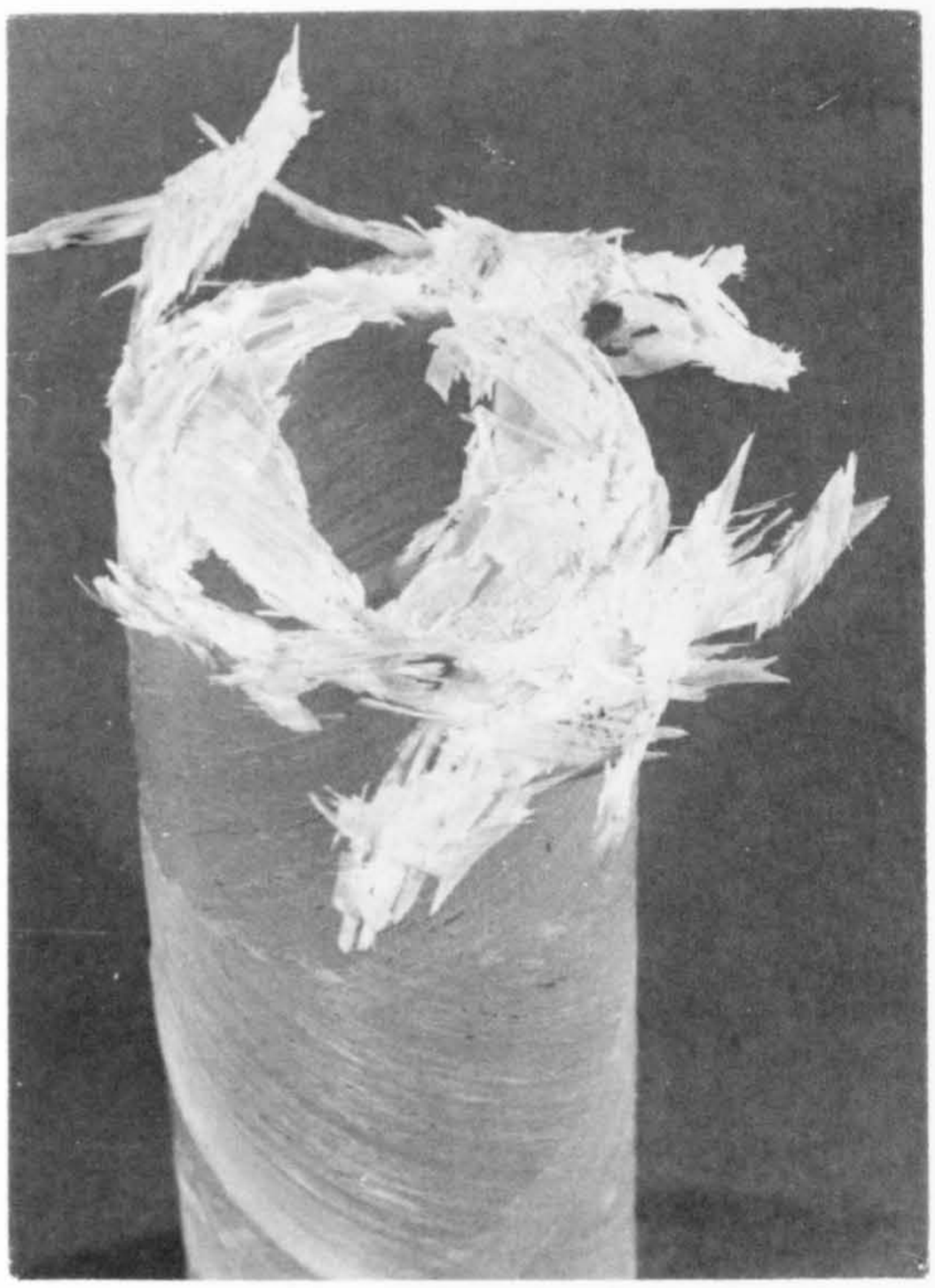

(a) General view of crush zone.

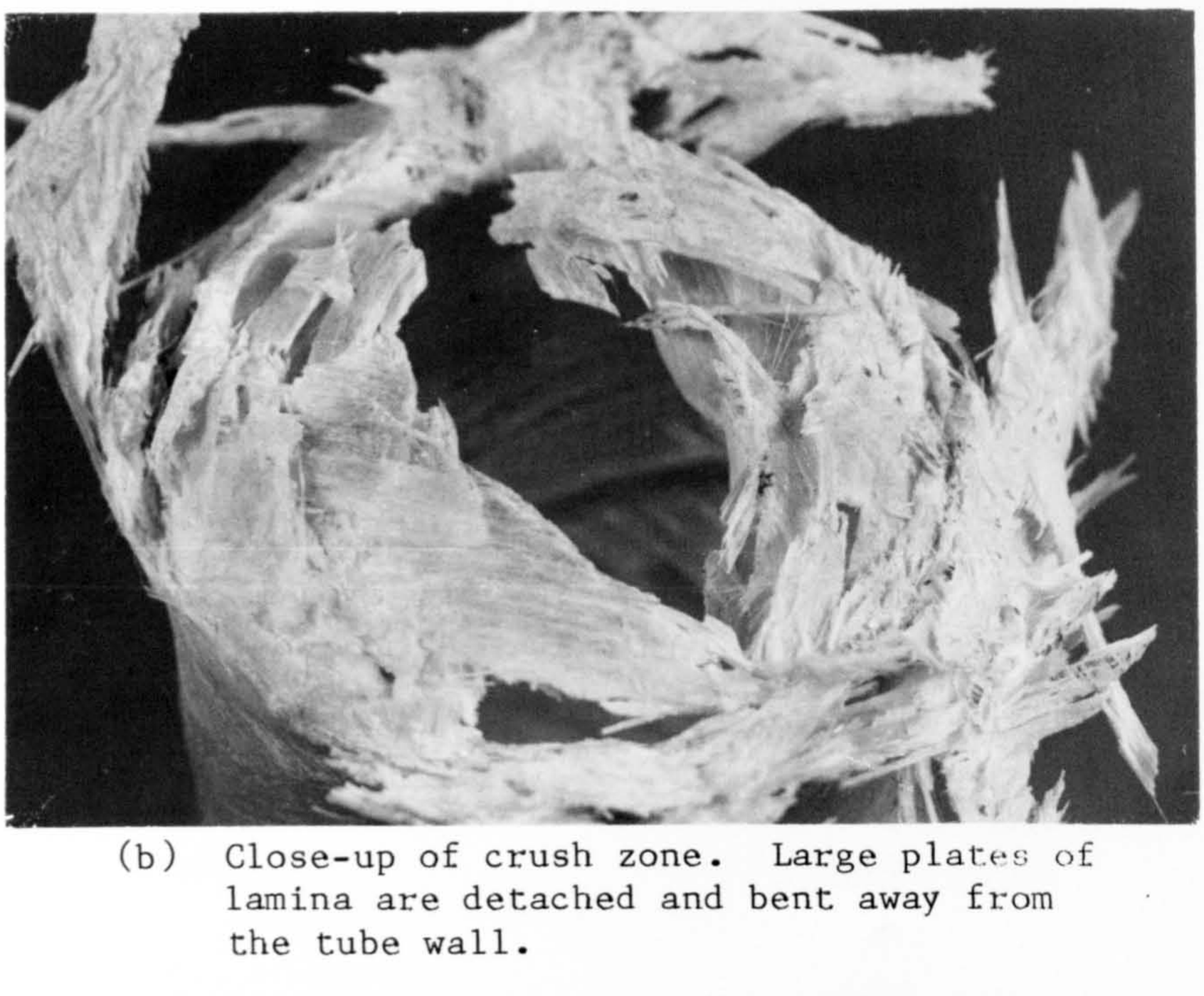

(b) Close-up of crush zone. Large plates of lamina are detached and bent away from the tube wall.

Fig.5.14. Crushed 55° angle-wound tube.

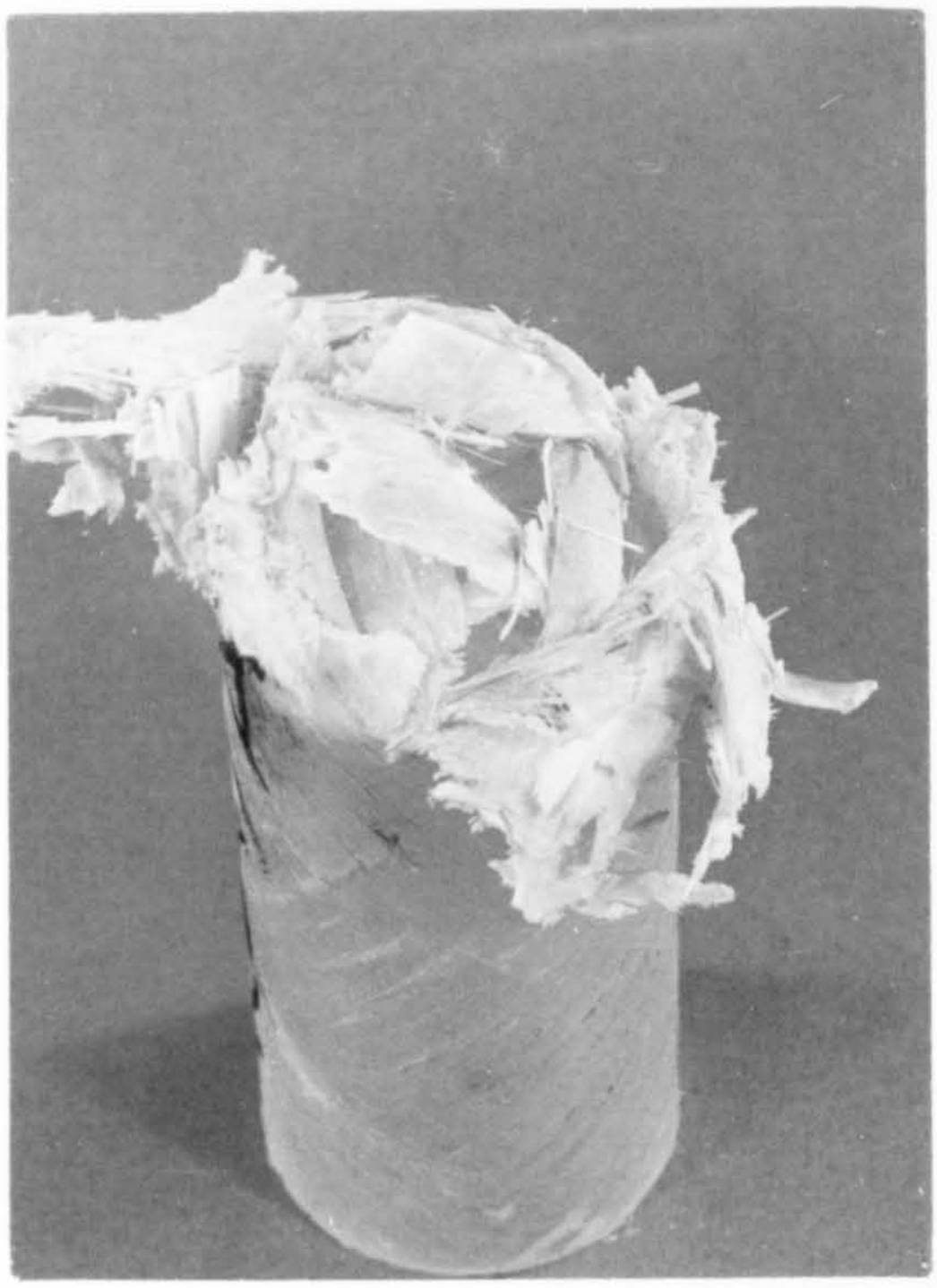

(a) General view of crush zone.

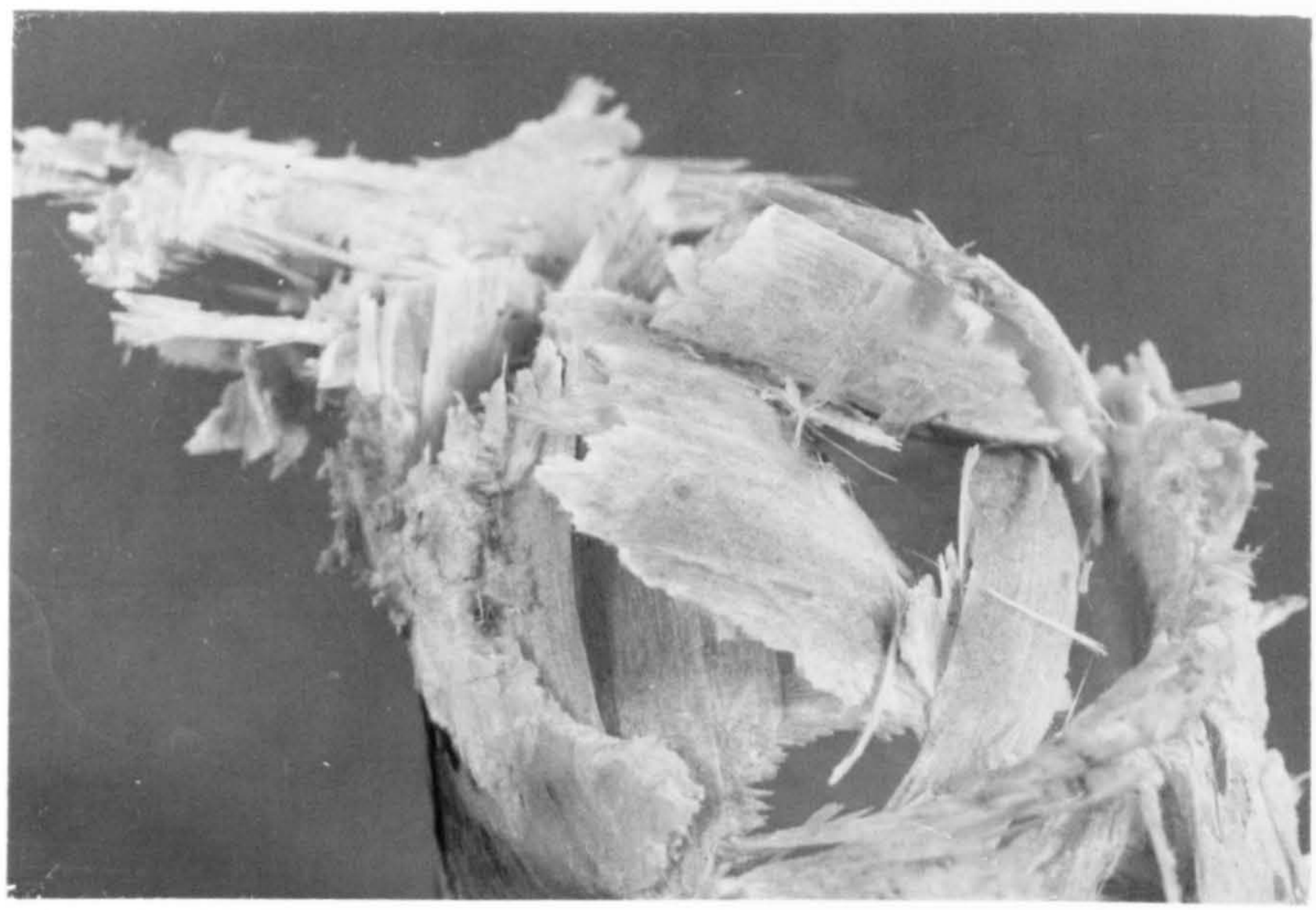

(b) Close-up of crush zone showing large detached lamina plates.

Fig.5.15. Crushed 45° angle-wound tube.

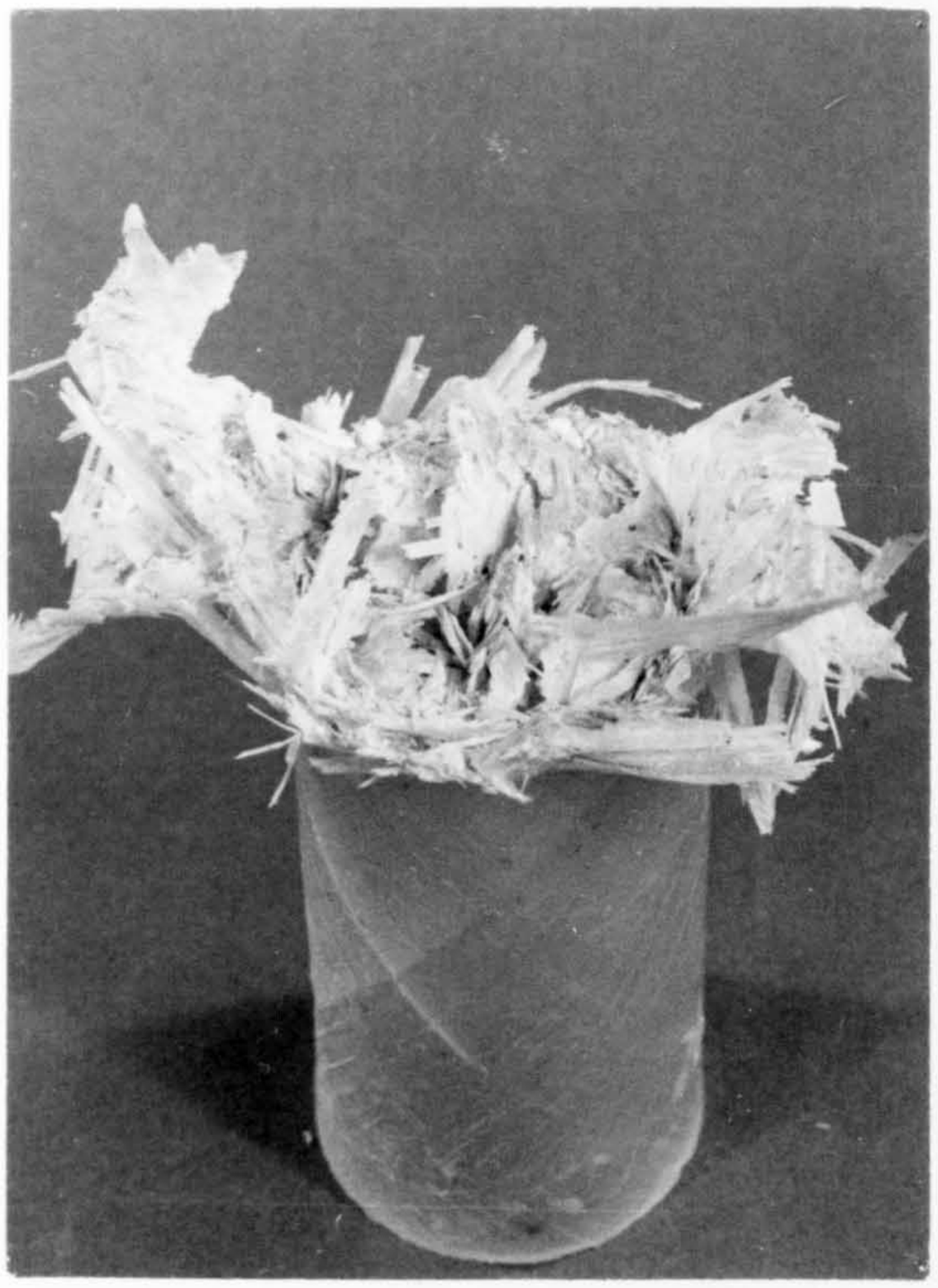

(a) General view of crush zone.

(b) Close-up of crush zone. Lamina plates bend inwards and outwards.

Fig.5.16. Crushed 35° angle-wound tube.

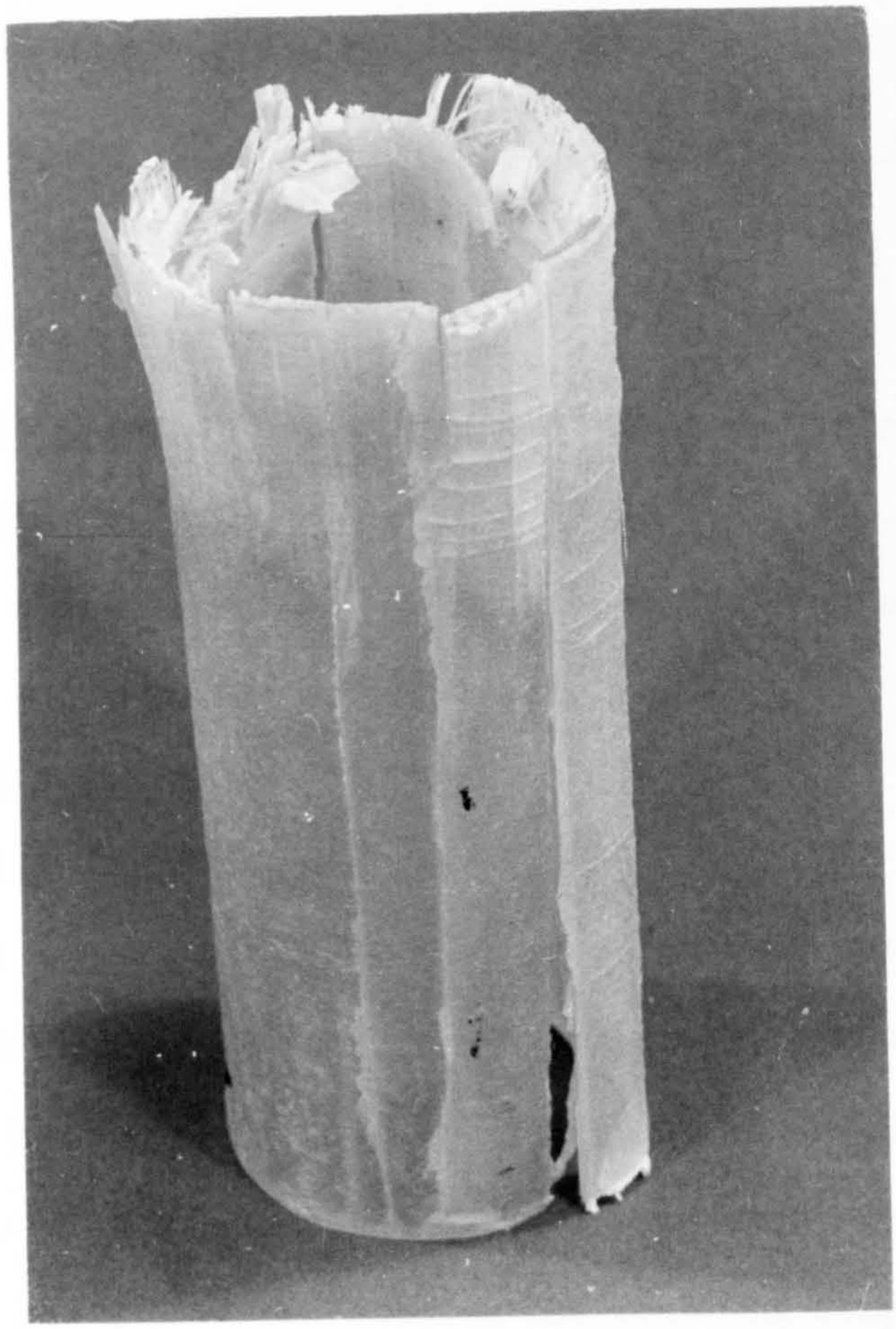

Fig. 5.17. Axially wound tube crush mechanism.Note long axial cracks.

tube wall. These separated the axial tubes into long thin struts which bent outwards. The test was halted before the bending forces caused the axial fibres to fracture or the ends to slide over the loading platens. The circumferential cracks visible in Fig. 5.17 were caused by the tensile stresses set up in surface layers during the bending process.

5.4 Photomicrography of sequential crushing of $0^{o}/90^{o}$ polyester tubes

5.4.1 Introduction

The progress of crushing was studied in a series of $0^{o}/90^{o}$ polyester (Crystic 272) tubes tested at 4×10^{-3} m s^{-1}. Each specimen was crushed by a predetermined amount between 2 and 8 mm, and then sections taken and examined as previously described.

5.4.2 Photomicrographs of crushed specimens

5.4.2.1 2 mm crush

After 2 mm crush (Fig. 5.18) only part of the bevel end region had been crushed. The four laminae forming the tube wall were separated by resin-rich layers. This is shown by the lighter regions in Fig. 5.18. The thick dark line adjacent to the inside wall is due to the separation between the mounting compound and the specimen.

The initial crushing involved the compression of the inner hoop lamina normal to the fibre direction. The hoop windings became separated from the tube wall and moved inwards. This occurred when the hoop windings on the inside buckled circumferentially and cracked away from the inner axial lamina. At this stage, much of the work done is in bending the hoop lamina inwards, thus causing wide cracks which show as dark areas in the photomicrograph. A small

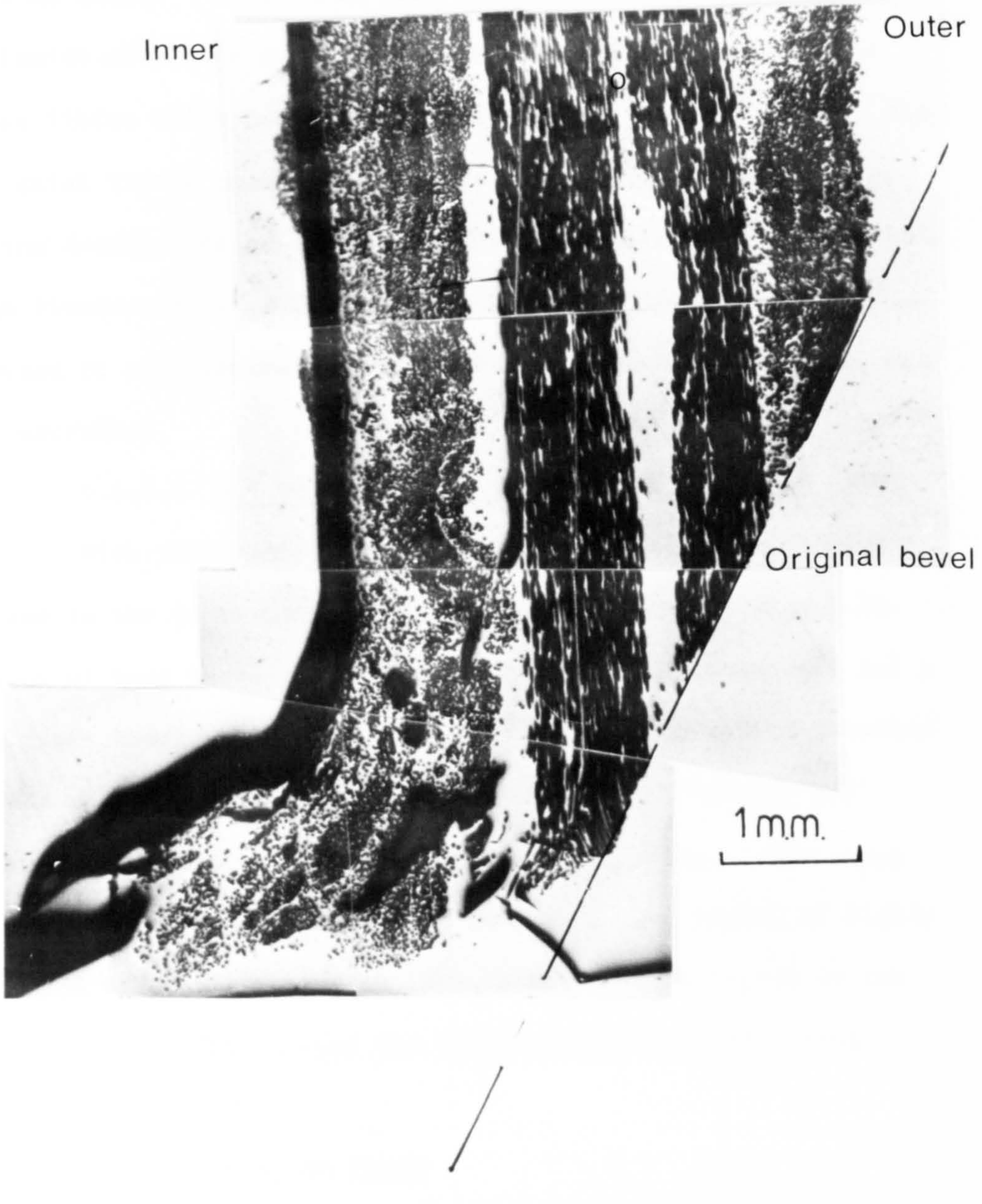

Fig. 5.18. Photomicrograph of a section through the wall of a 0/90 tube after 2.0 mm crush.

amount of bending of the axial fibres also took place, increasing with the crush distance.

5.4.2.2 3.4 mm crush

Fig. 5.19 shows a photomicrograph of a specimen subjected to 3.4 mm crush. Large void-like cracks occurred in the outer hoop lamina with some separation from the tube wall. A bundle of hoop fibres which had completely separated is shown at X. The inner axial lamina commenced fracture by bending and compressive buckling accompanied by kinking. This is similar to that reported in the literature (21, 22, 23) for a unidirectional composite subjected to compressive loading. Part of the bevelled edge, was still uncrushed.

5.4.2.3 4.8 mm crush

With this amount of crush, a large amount of cracking occurred in the inner hoop lamina. This is shown in Fig. 5.20. Sections of hoop bundles became separated from the tube wall and a large fibre bundle, marked X in Fig. 5.20 is shown almost detached from the wall. The axial lamina started to bend inwards and outwards with local regions of compressive buckling. The outer hoops were still intact because of the bevel. A region of highly fragmented material started to form in the central region of the specimen wall. This marked the beginning of the bundle wedge noted in Section 5.3.

5.4.2.4 6.4 mm crush

On reaching 6.4 mm crush, (Fig. 5.21) the bevel was completely destroyed and all of the wall was involved in the crush. The inner hoops separated from the tube wall and the inner axial lamina were bent inwards as the constraining influence of the hoops was removed. A well-developed bundle wedge developed in the centre of the

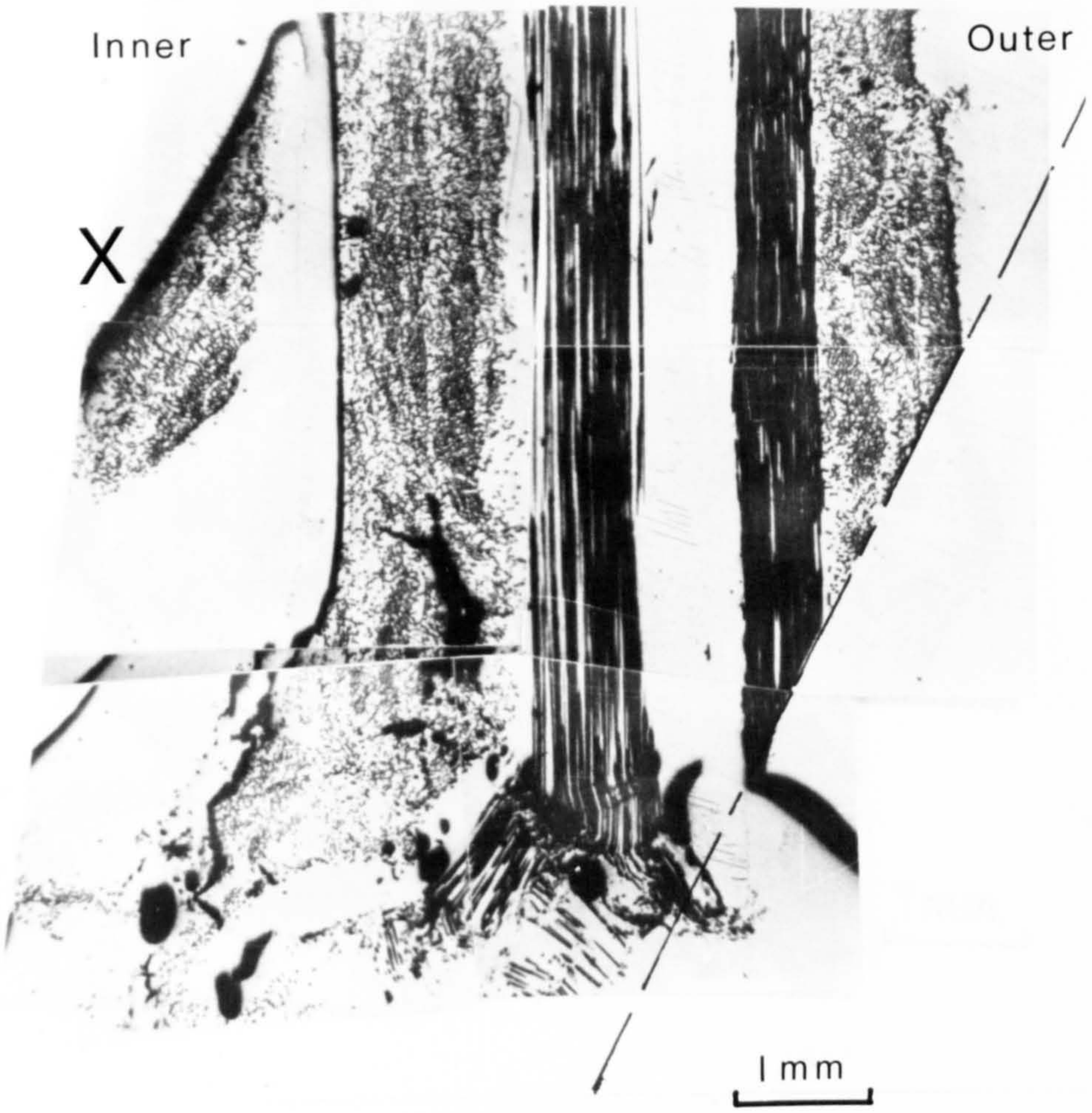

Fig. 5.19. Photomicrograph of a section through the wall of a 0/90 tube after 3.4 mm crush.

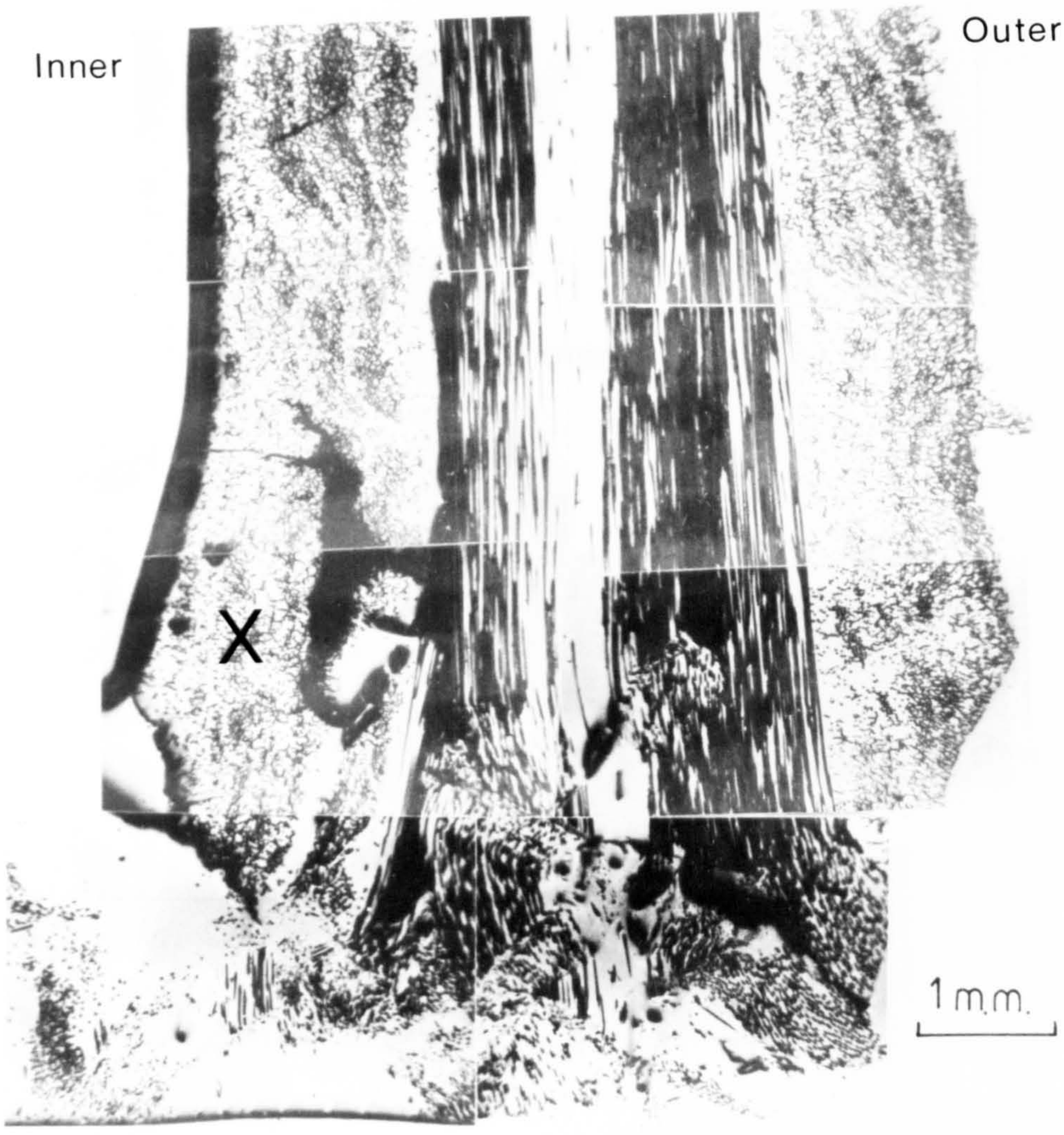

Fig. 5.20. Photomicrograph of a section through the wall of a 0/90 tube after 4.8 mm crush.

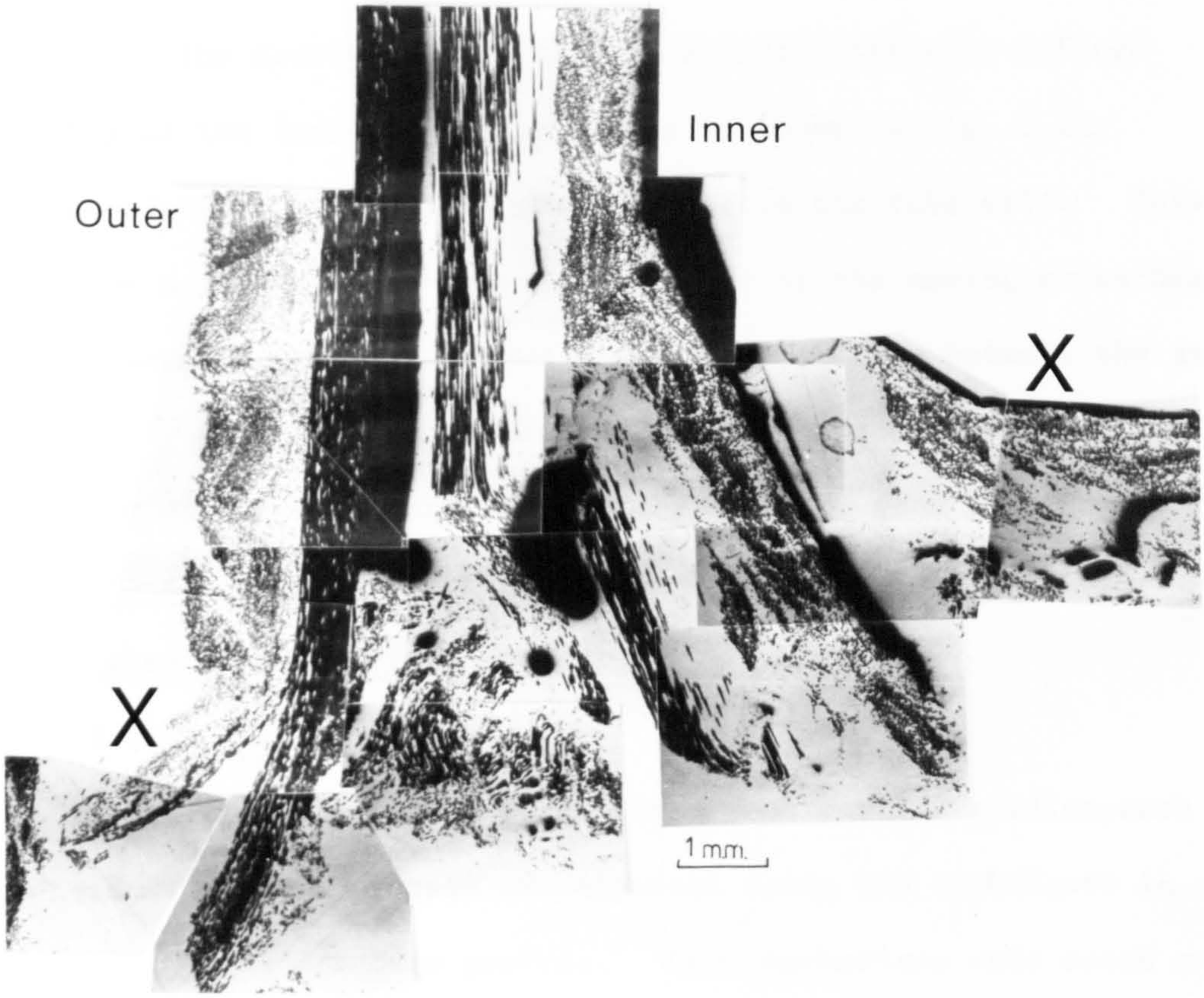

Fig. 5.21. Photomicrograph of a section through the wall of a 0/90 tube after 6.4 mm crush.

tube wall comprised of small particles of fractured resin and glass. Bundles of fibres from the inner and outer hoop laminae separated from the tube wall, marked X. The outer axial lamina was slightly bent outwards as the outer hoop restraint was gradually removed.

5.4.2.5 8.0 mm crush

The development of the crush front with well-defined bending of the inner and outer axials is shown in Fig. 5.22. An interlaminar centre line crack formed in the tube wall. This crack extended a considerable distance in front of the moving cross-head and in general proceeeded down the resin-rich area between the axial laminae. Intralaminar cracking in the inner and outer hoop laminae occurred as they fractured and become detached from the tube wall.

5.5 Scanning electron microscopic examination of individual fragments taken from the crush zone

5.5.1 Introduction

Using the knowledge obtained from earlier studies, each individual failure process was examined using SEM techniques in order to identify the fracture process. Nine mechanisms were noted and are listed below. These are cross-referenced with Fig. 5.23 by number.

1. Bending of the inner and outer axial laminae.
2. Splitting of the outer axial lamina due to increasing circumference.
3. Crushing and multiple fracture of the inner axial lamina due to reducing circumference and volume availability.
4. Cracking down the centre of the tube wall.
5. Tensile fracture of the outer hoop lamina due to increasing circumference.

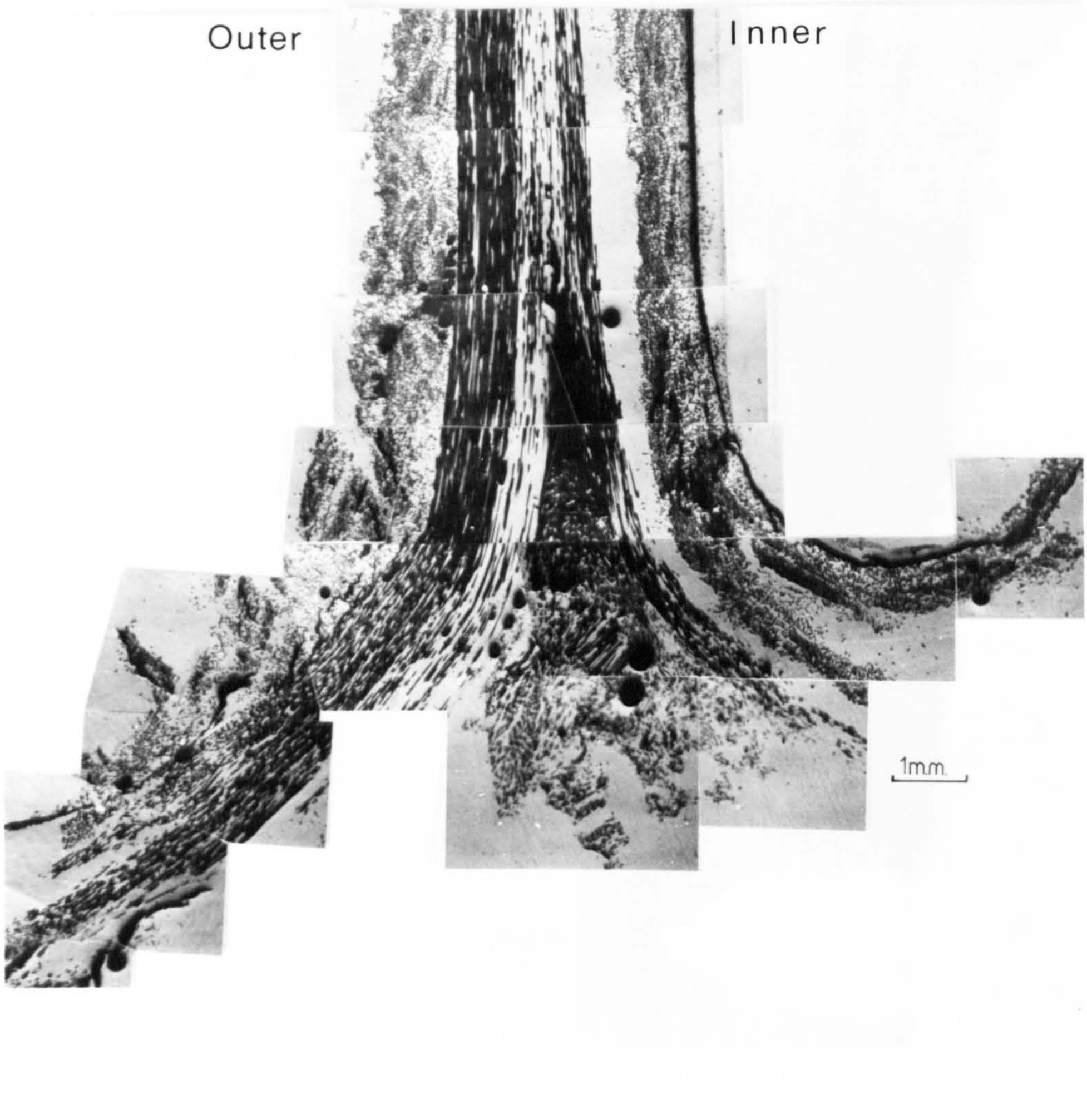

Fig. 5.22. Photomicrograph of a section through the wall of a 0/90 tube after 8.0 mm crush.

Fig. 5.23. Photomicrograph of a section through the wall of a crushed 0/90 tube indicating areas of individual failure mechanisms as described in the text.

6. Crushing and multiple fracture of the inner hoop lamina due to reduction in circumference and volume availability.
7. Fracture between the hoop and axial laminae as the axials expand outwards/inwards and downwards.
8. Cracking within the hoop laminae due to compressive loading.
9. Accumulation of debris in the centre of the tube wall (bundle wedge).

These mechanisms are discussed below.

5.5.2 Bending of the inner and outer axial laminae, region (1)

As bending occurred, the axial laminae split into progressively thinner layers. Typical fracture surfaces of these layers are shown in Figs. 5.24 to 5.26. The plane of view and general crack direction is shown schematically in Fig. 5.28.

In most cases the fibre surface was clean with little adhering resin, indicating that the crack grew along the fibre/resin interface. Occasionally, however, resin adhered to the fibres as shown in Fig. 5.24(b). Fig. 5.26(a) shows the impression of the glass-fibre surface in the resin with slight indentations which are probably a mirror image of the coating applied to the fibres. The resin in most instances showed a torn, flaky or blocky fracture surface. This was thought to be due to the tearing of resin between the fibres as the crack grew through the lamina in the general direction of the fibres. In some regions, the resin was highly torn, almost into thin flakes, which protruded between the debonded fibres; whilst in others the resin fracture was more blocky in nature, see,for example,Fig. 5.24(b). In other regions a tendency to a planar resin fracture was apparent (Fig. 5.25(b), left-hand side). These variations in the fracture surfaces indicated that the loading

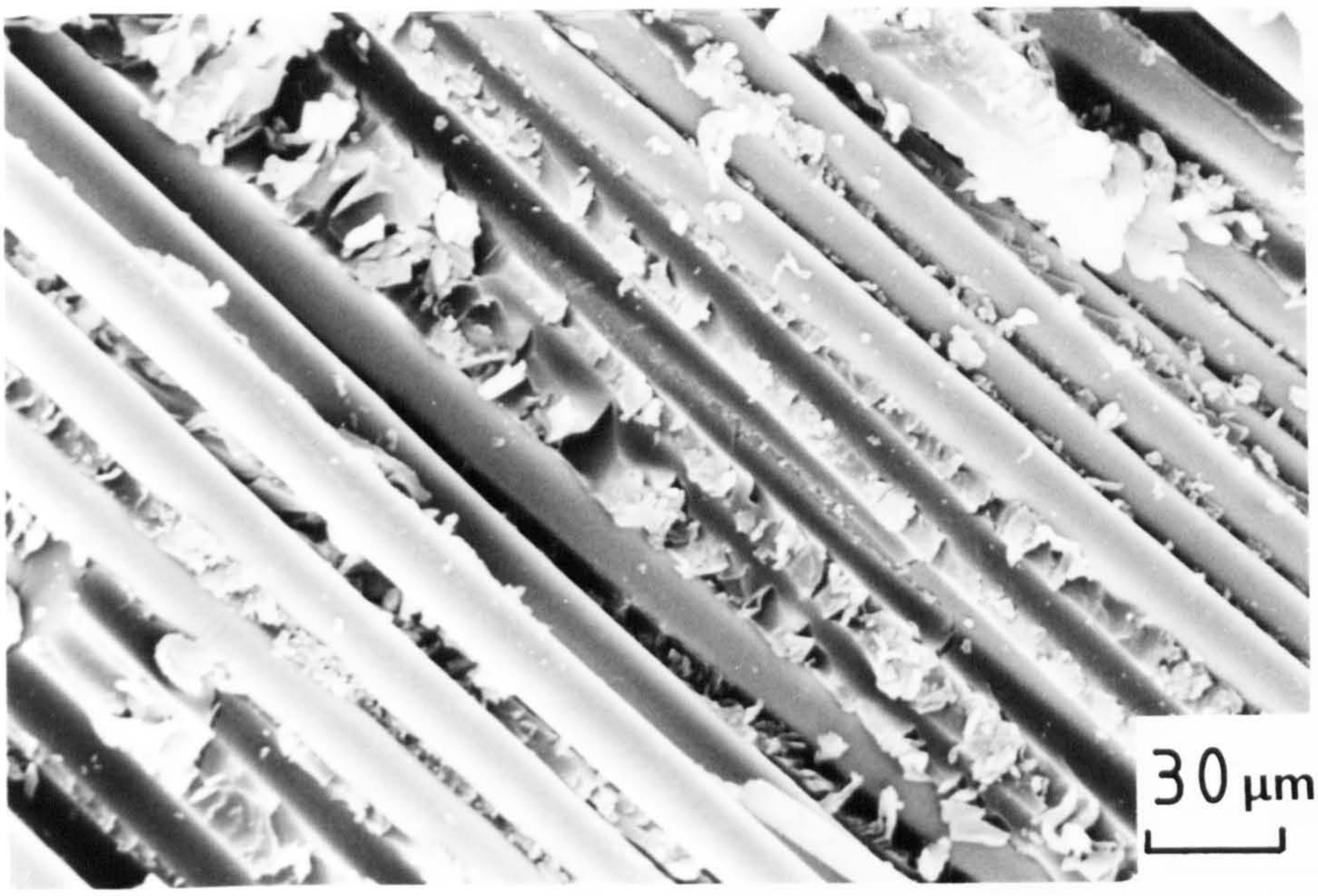

(a) General view showing rough resin fracture surface with clean fibres.

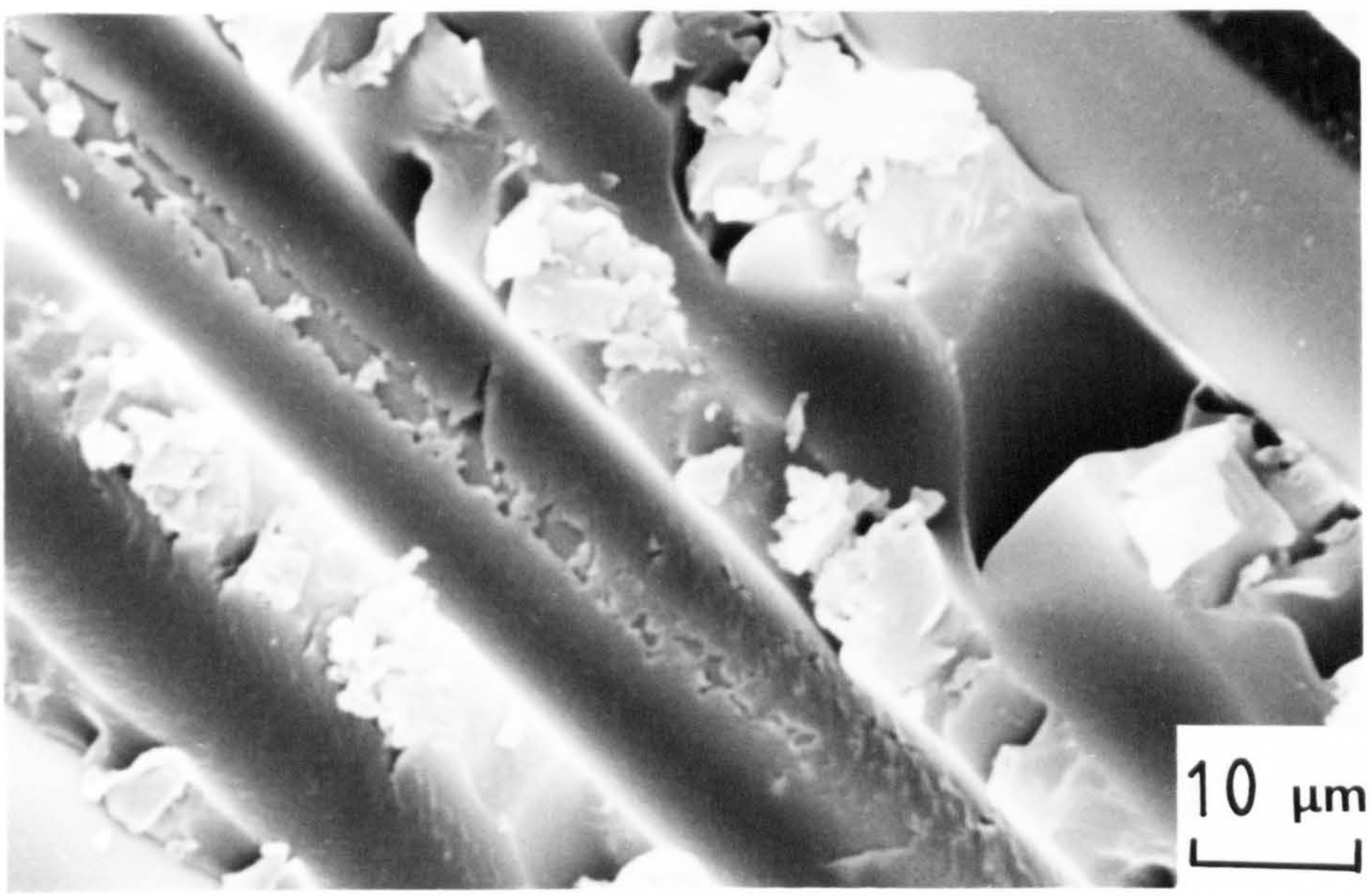

(b) Higher magnification showing highly torn blocky resin fracture.

Fig.5.24. SEM photomicrographs of fracture surface from a region of axial bending (Region 1). 0°/90° polyester tube tested at 4×10^{-3} m s^{-1}.

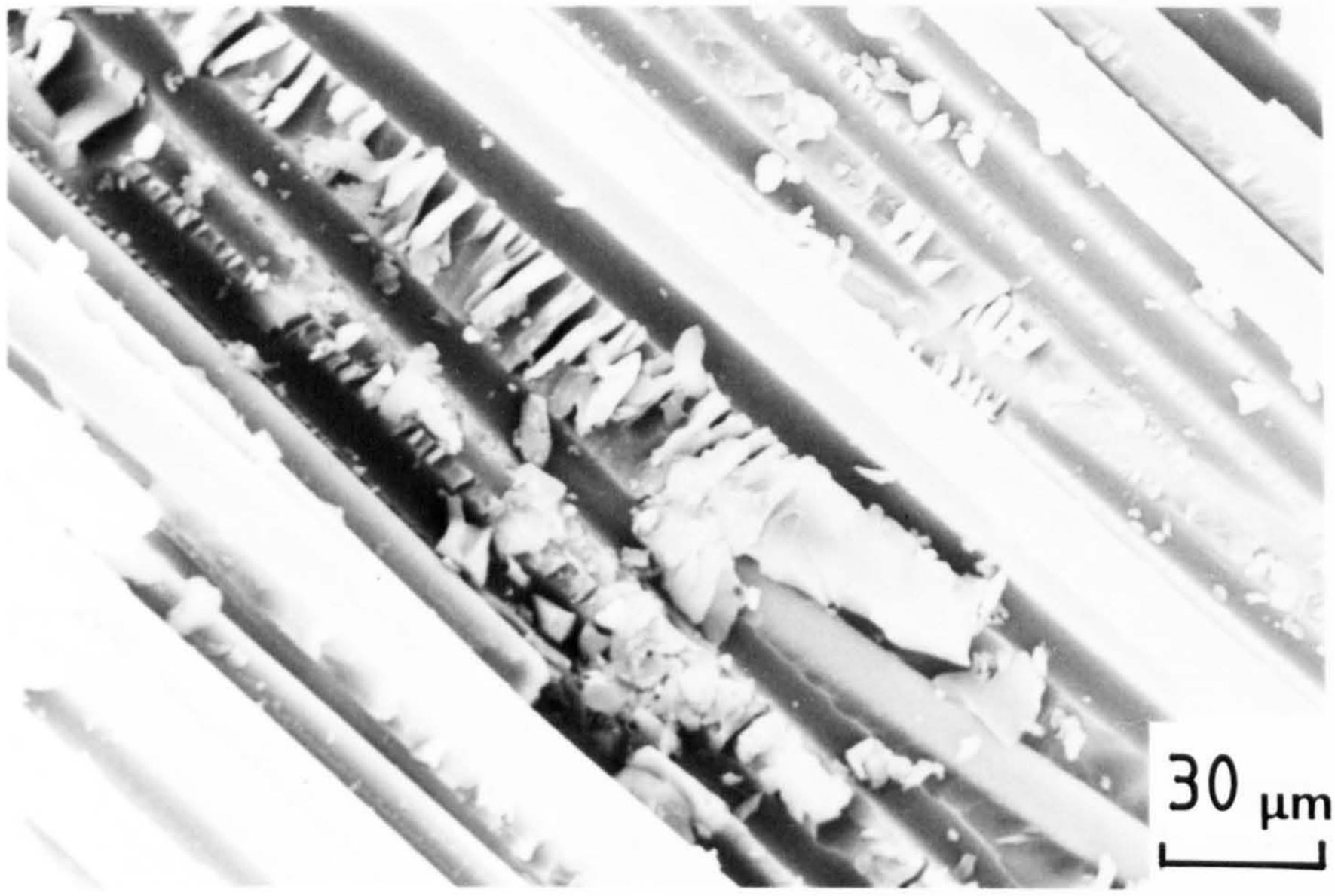

(a) General view of fracture surface.

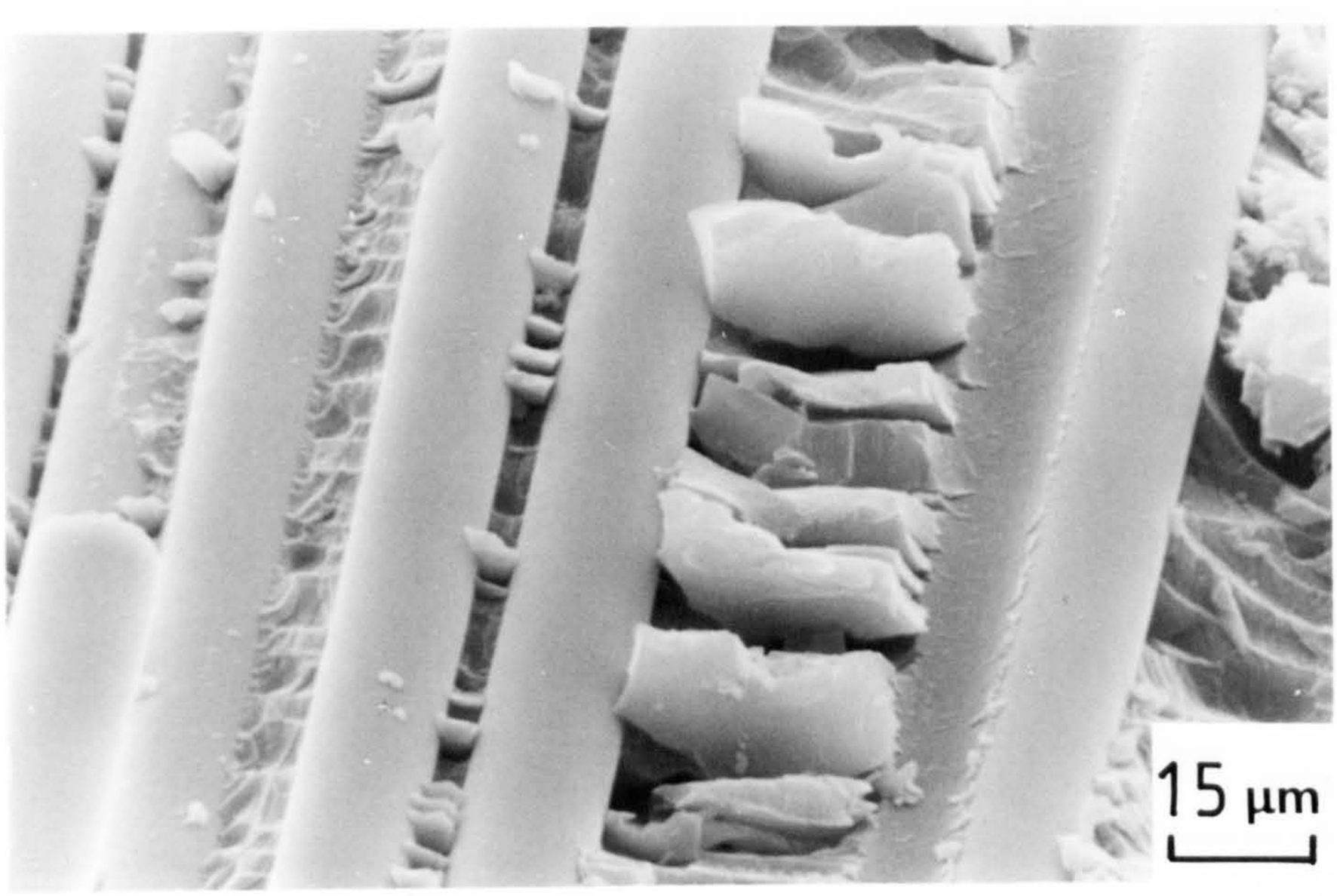

(b) Resin fracture varying from high torn to planar. Note appearance of clean fibres.

Fig.5.25. SEM photomicrographs of fracture surfaces from region of axial bending (Region 1). $0^{o}/90^{o}$ polyester tube tested at 4×10^{-3} m s^{-1}.

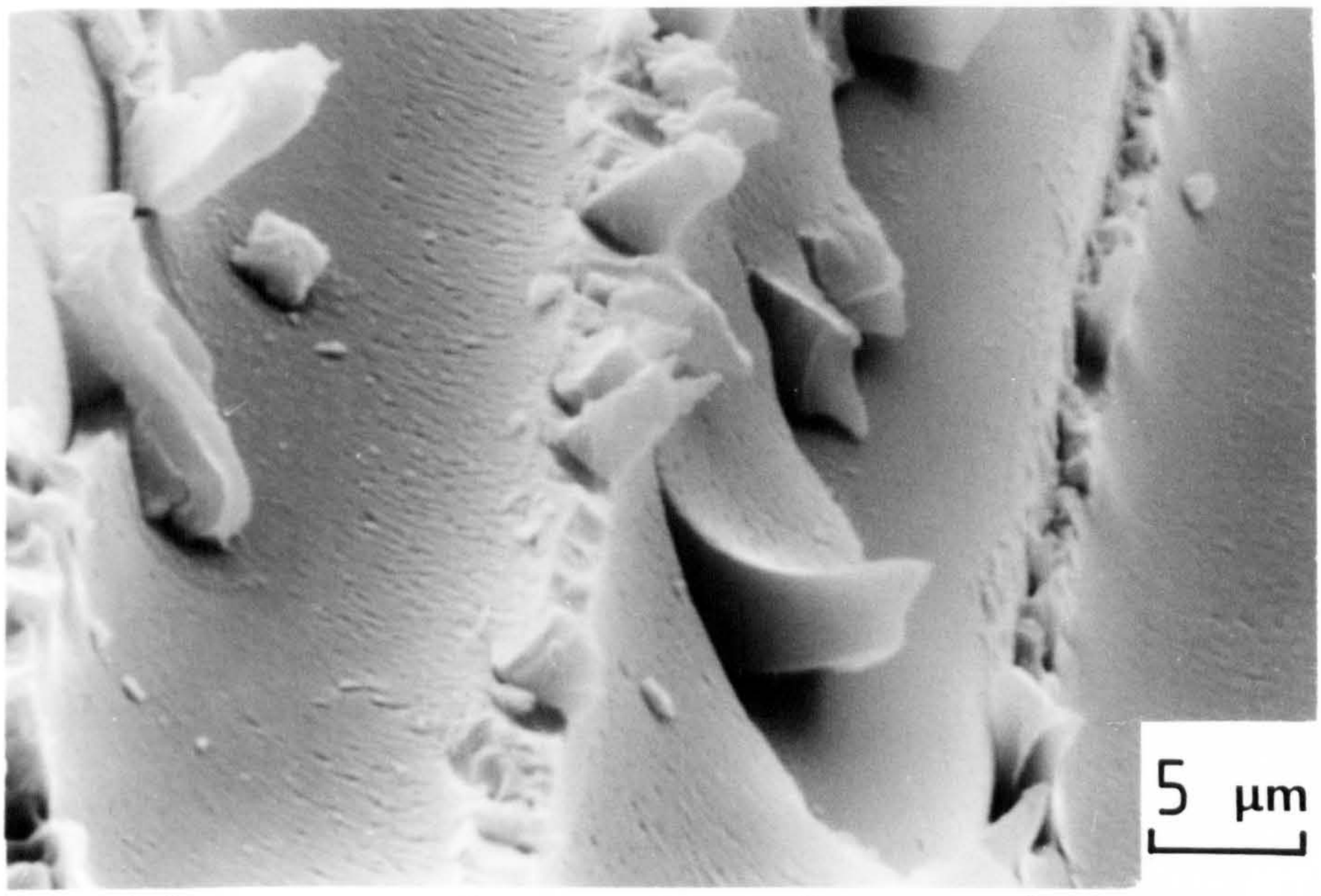

(a) High magnification view of torn resin surface and mirror image of resin-glass interface.

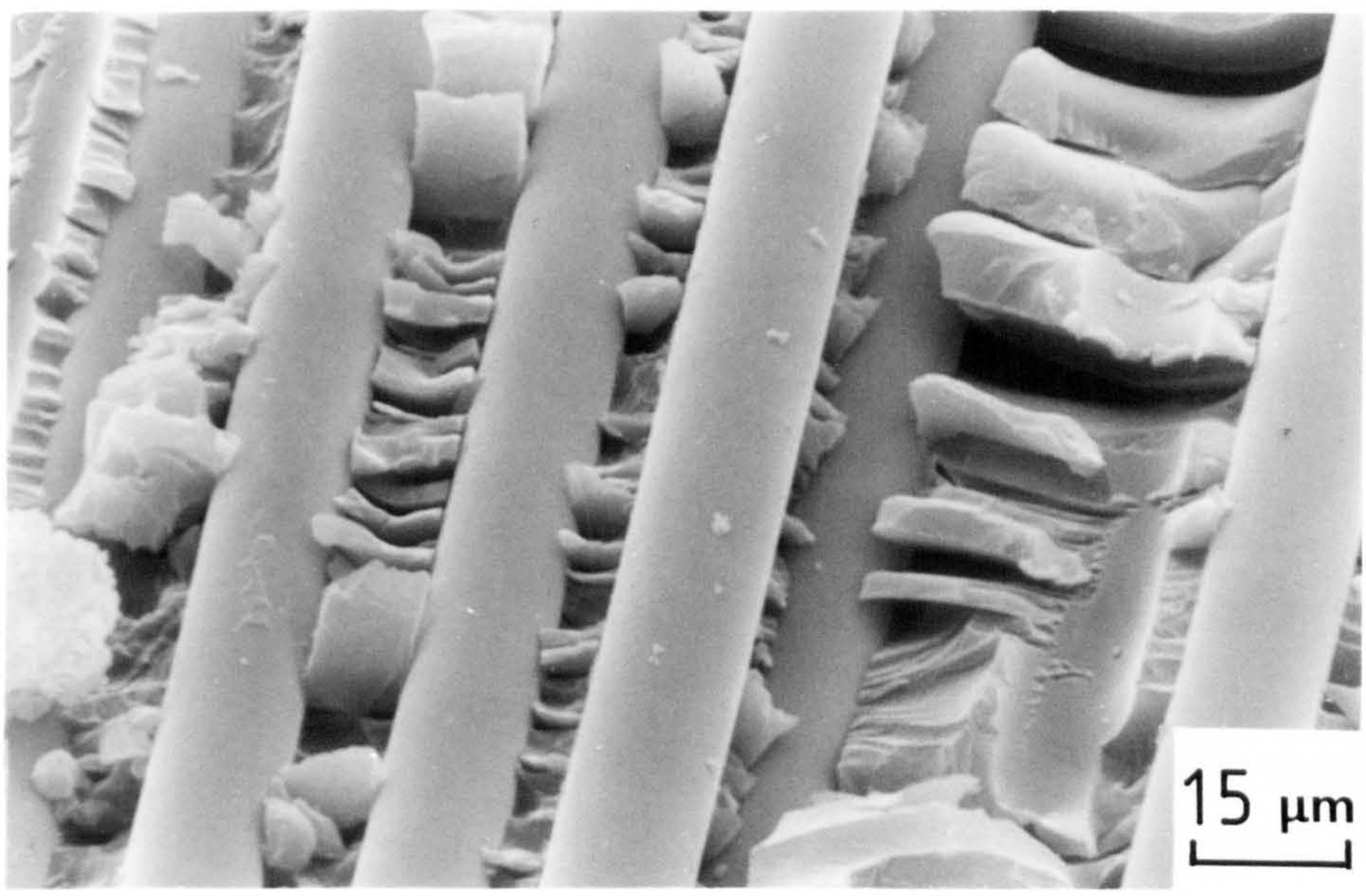

(b) Region showing clean fibres and torn, flaky resin fracture.

Fig.5.26. SEM photomicrographs of fracture surfaces from region of axial bending (Region 1). $0^{o}/90^{o}$ polyester tube tested at 4×10^{-3} m s^{-1}.

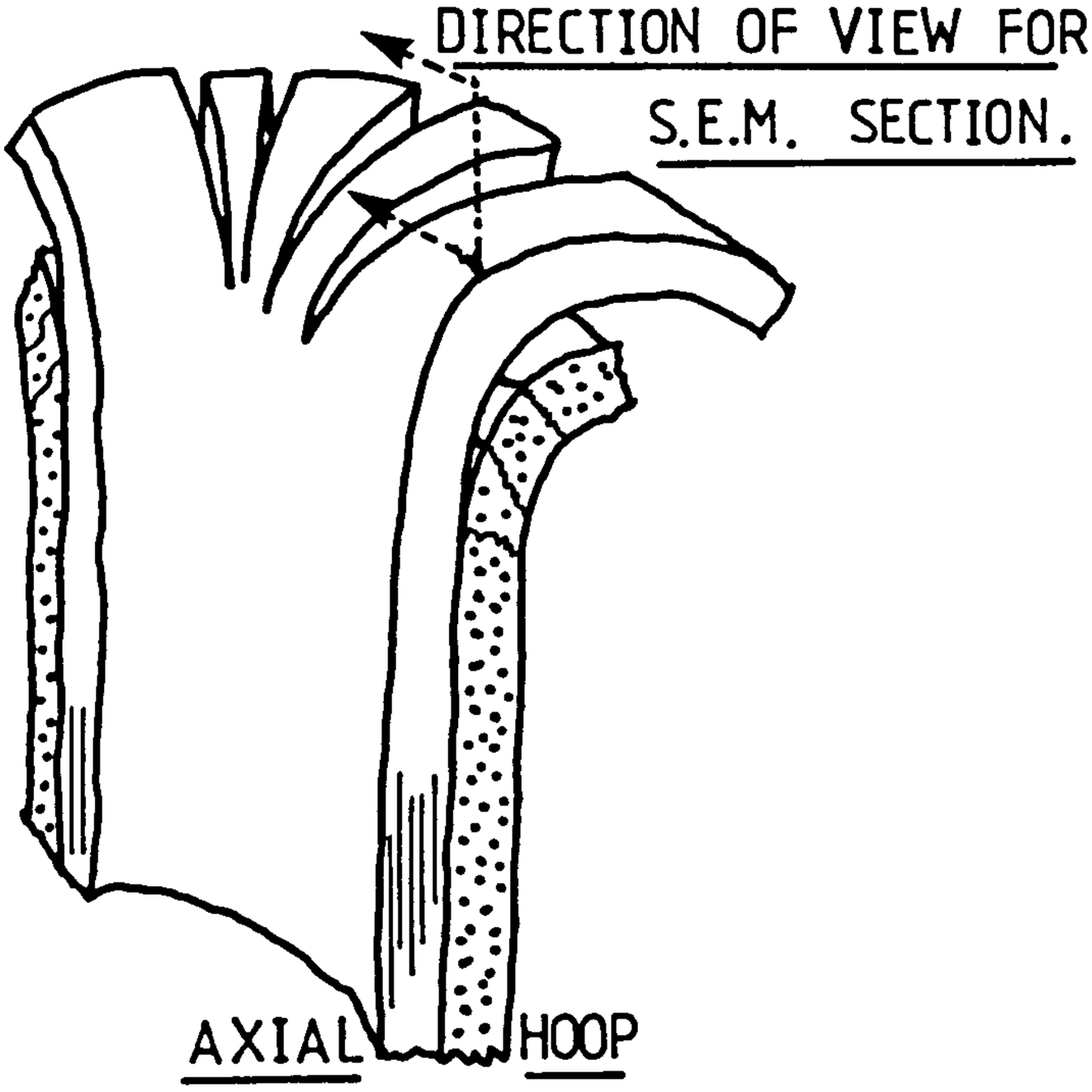

Fig. 5.27. Diagram of a segment from the crush zone of a 0/90 tube showing translaminar cracking in the axial laminae.

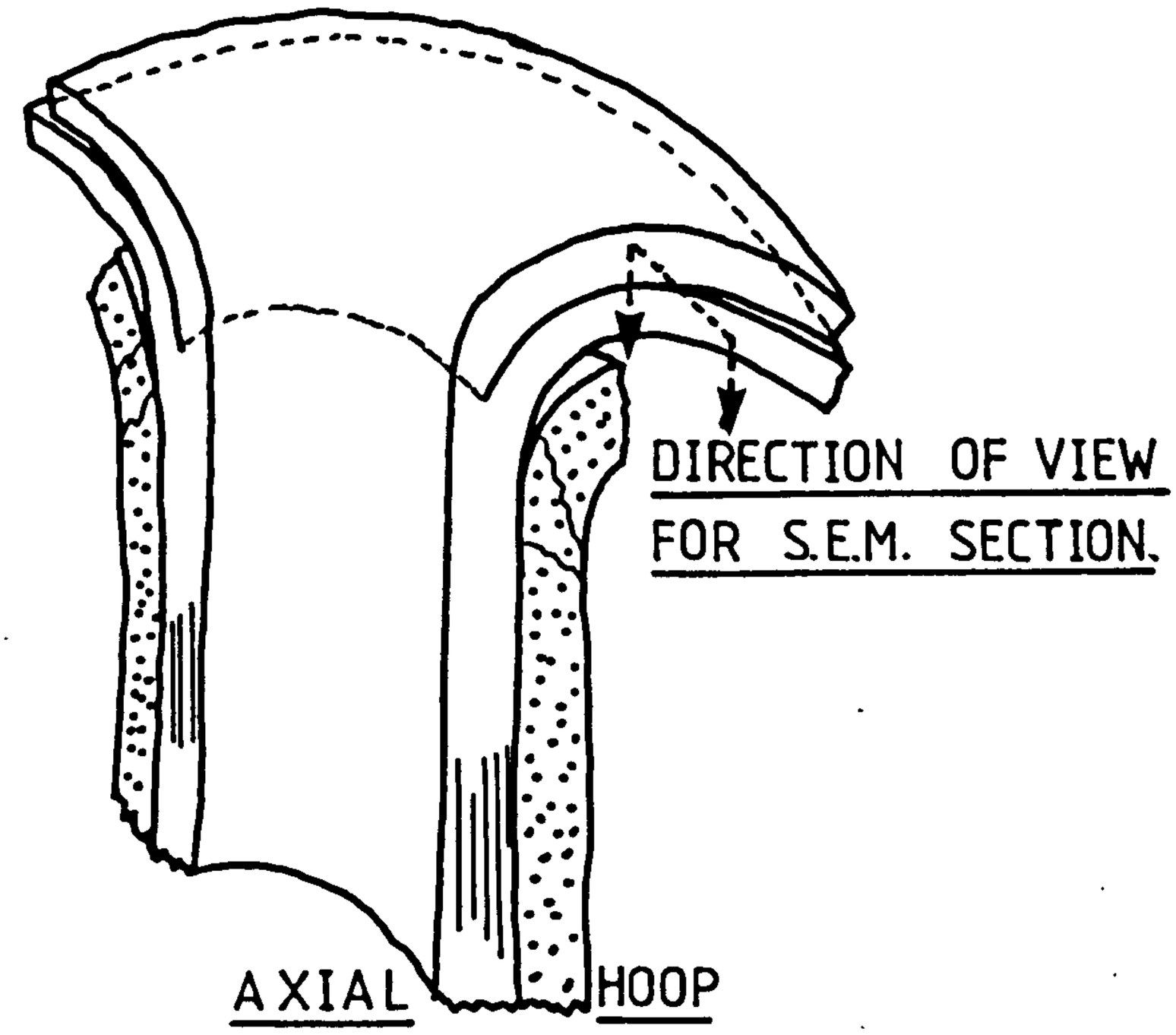

Fig. 5.28. Diagram of a segment from the crush zone of a 0/90 tube showing intralaminar shear cracking in the axial laminae.

situation varied across this region of the tube wall during crushing. Localised variations in glass volume fraction, resin-rich areas and voids in the laminae would complicate and alter the fracture mechanism.

A limited amount of localised fibre fracture occurred in the edges of the axial laminae. This fracture is shown in Fig. 5.29. A schematic diagram of the approximate region of fracture and field of view (Y-Y) is shown in Fig. 5.30. No evidence of fibre pull-out was apparent at this stage in the process which would indicate tensile fracture. However, some micro-buckling was observed and can be seen in Fig. 5.29(a). This could be due to compressive kinking occurring early in the crushing process. As further bending occurred, the initial crack due to kinking opened and caused complete fracture of the axial laminae. This failure mechanism has been described in Section 5.3.1 for tubes crushed at a speed of 4×10^{-3} m s^{-1}.

The axial laminae fractured in three crack directions. Firstly, translaminar cracking normal to the fibre direction, probably initiated by micro-buckling and fibre kinking, occurred with fibre fracture. Secondly, intralaminar cracking, which split the laminae into many thin layers also occurred but without fibre fracture. Finally, translaminar cracking parallel to the fibre direction occurred, without fibre fracture. The first two processes have been described above; the last process is described in Section 5.5.3. The general directions of these fracture mechanisms are shown schematically in Figs. 5.27 and 5.28. The last two processes divide the axial laminae into small flat segments.. These vary in shape and size, as shown by the sectional view

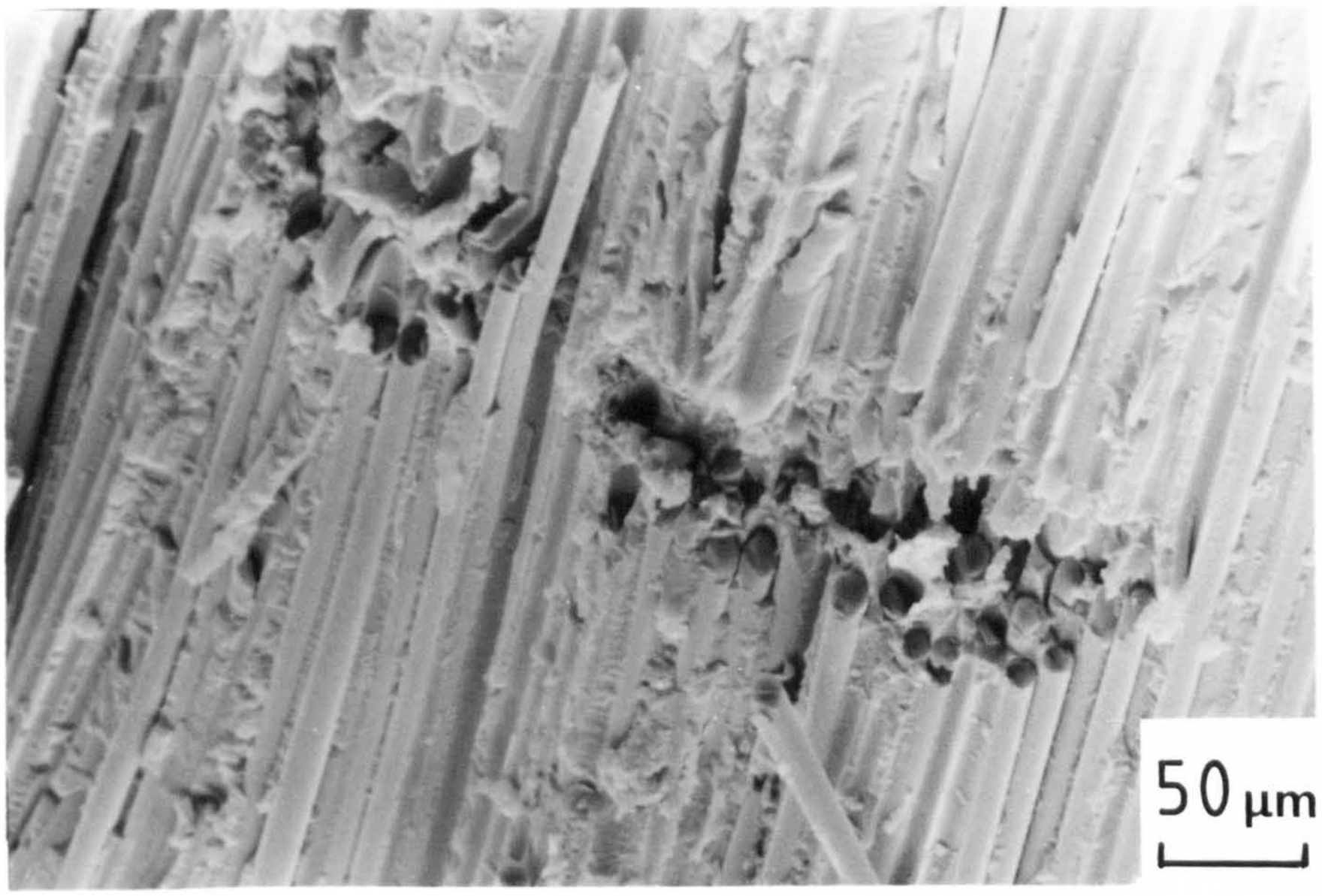

(a) General view. Note kinking mode of fracture and absence of fibre pull-out.

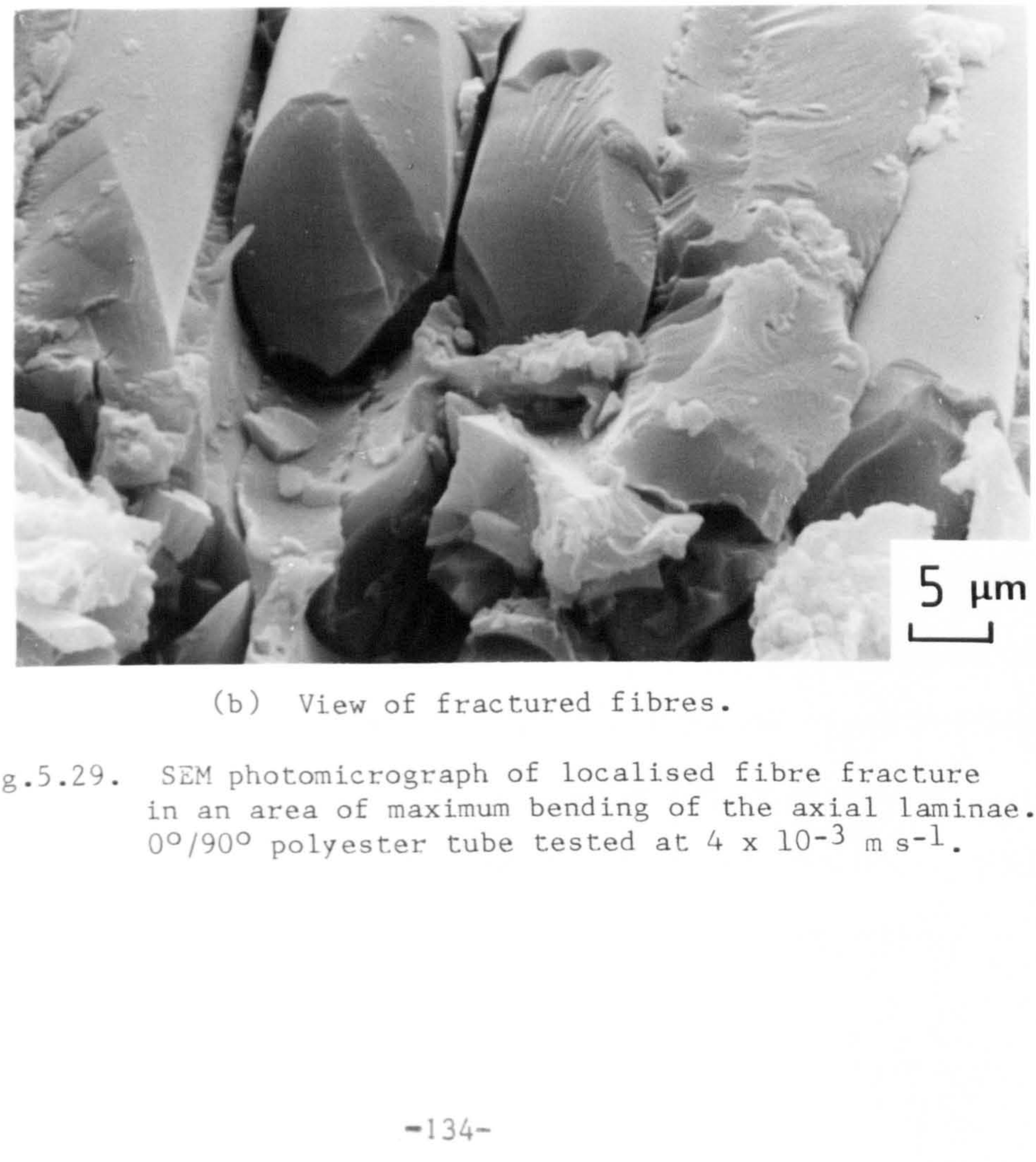

(b) View of fractured fibres.

Fig.5.29. SEM photomicrograph of localised fibre fracture in an area of maximum bending of the axial laminae. 0°/90° polyester tube tested at 4×10^{-3} m s^{-1}.

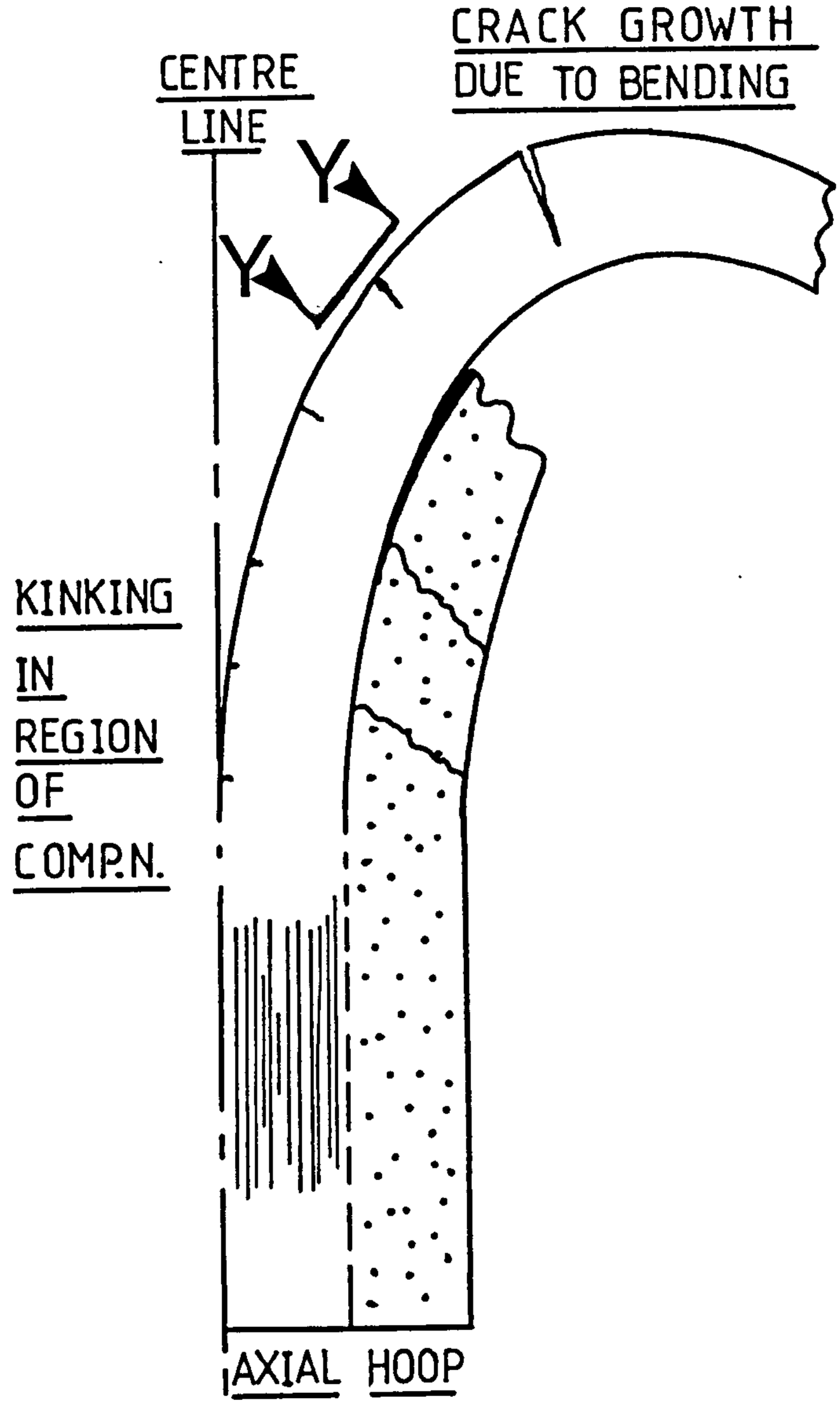

Fig. 5.30. Diagram of a section through the crush zone of a 0/90 tube showing the initiation and growth of cracks in the axial laminae.

in Fig. 5.31. Large numbers of separated segments can be seen, with the axial laminae divided by trans- and intralaminar cracks.

5.5.3 Splitting of the outer axial lamina region (2)

As briefly described in the previous section, the outer axial lamina split translaminarly, because of the increasing circumference of the deformed material during crushing. The fracture surface of these cracks is shown in Fig. 5.32. The direction and field for view for the SEM is shown in Fig. 5.27. The resin fracture was more planar than those observed from intralaminar cracking of axial laminae (region (1)). The surfaces of the fibres were clean with little adhering resin. The fracture surfaces were not similar to pure transverse tensile or shear as shown by Figs 5.1 to 5.3. The loading situation on the axial lamina indicated that the fracture mode should have been tensile in nature, but this is not supported by the micrograph in Fig. 5.32, which shows mixed fracture with both planar and shear modes. These observations are difficult to reconcile, but may be due to non-uniform loading during the crushing process.

5.5.4 Multiple fracture of the inner axial lamina, region (3)

Figs. 5.33 and 5.34 are photomicrographs of typical fracture surfaces in the inner axial region after inversion into the tube cavity. The viewing directions are shown schematically in Fig. 5.35. Fig. 5.33 was taken from a region shown in Fig. 5.35 by Y-Y immediately after inversion of the axials into the tube cavity. Fig. 5.34 shows a region during a later stage in the crush process; the direction of view is indicated by Z-Z in Fig. 5.35.
An increase in the amount of resin/glass debris was apparent. In some areas this almost obscurred the original fracture surface.

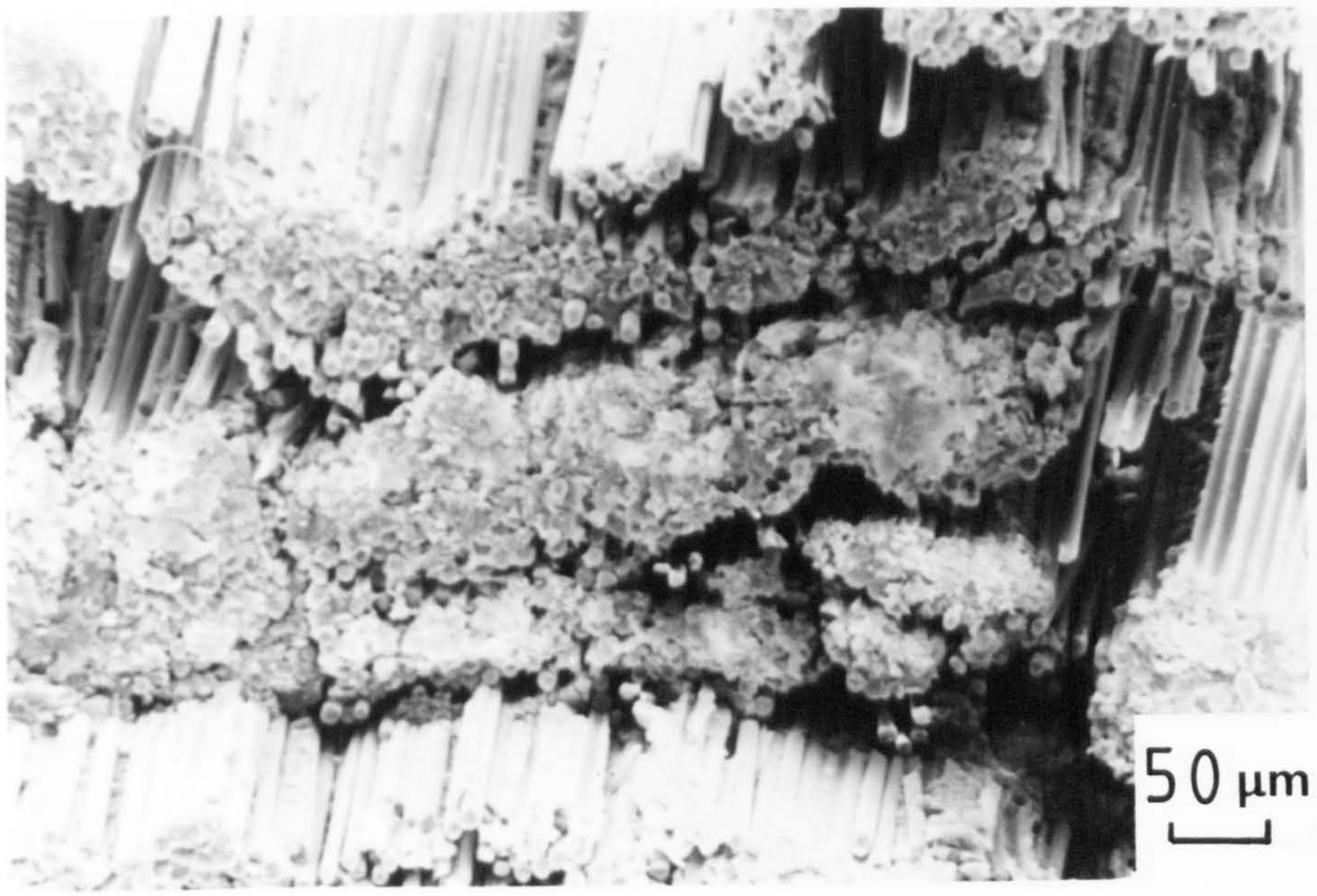

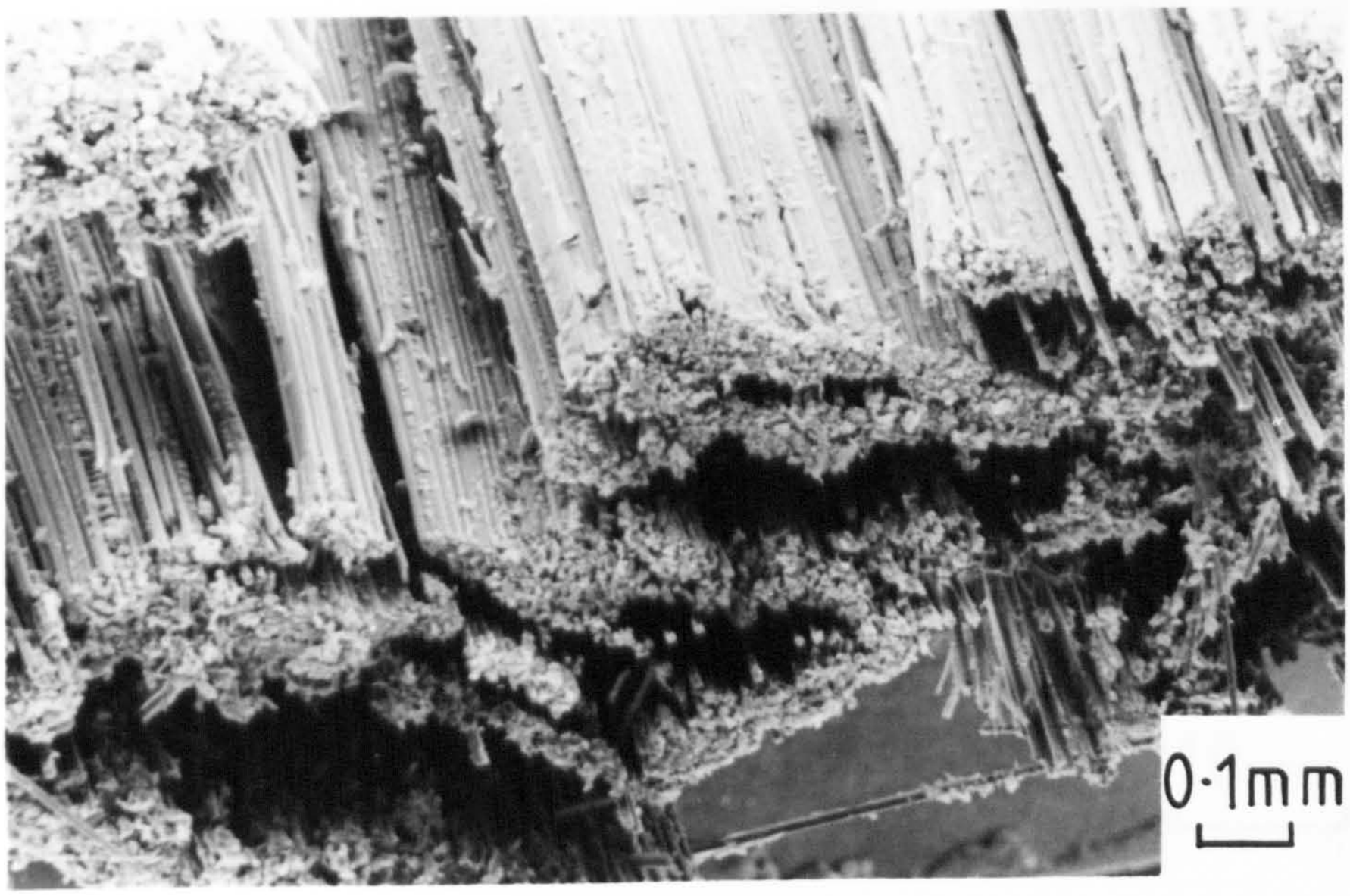

Fig.5.31. SEM photomicrographs showing the separation of the axial lamina into small bundles of fibres.0/90 polyester tube tested at $4x10^{-3} ms^{-1}$.

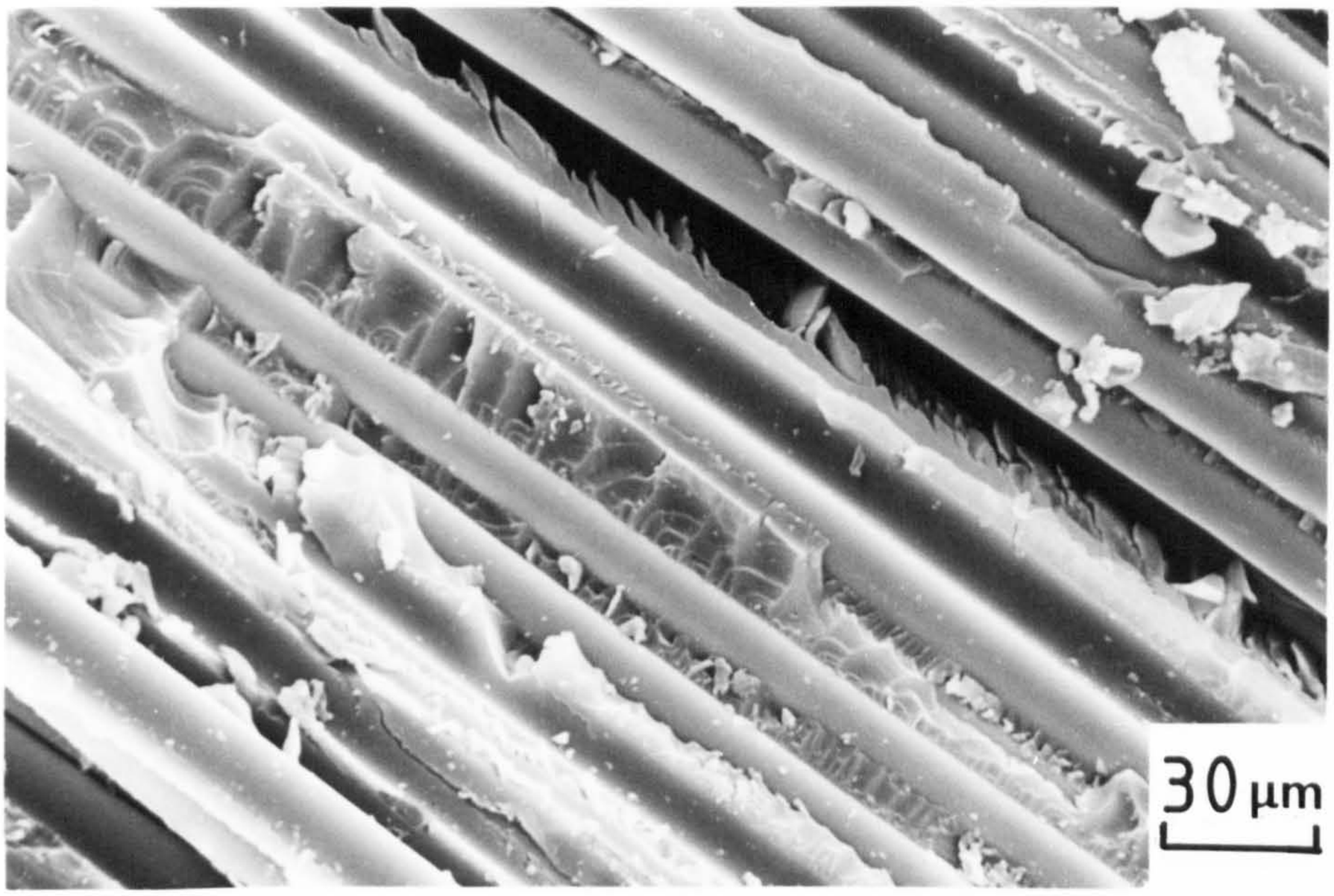

(a) General view showing resin fracture surface and clean fibres.

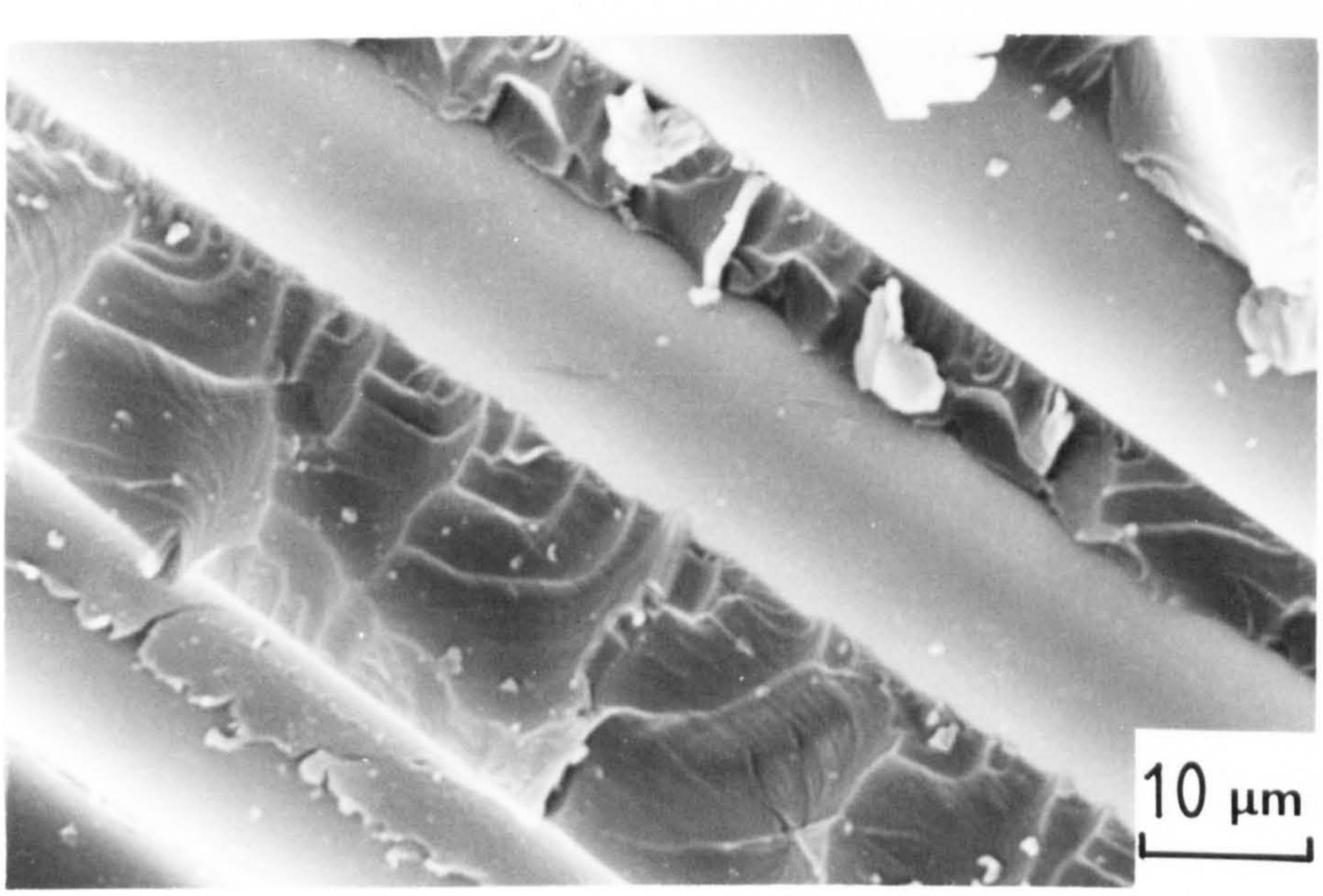

(b) Higher magnification of region of smooth resin fracture.

Fig.5.32. SEM photomicrographs of translaminar cracks in outer axial fibres (Region 2). 0°/90° polyester tube tested at 4×10^{-3} m s^{-1}.

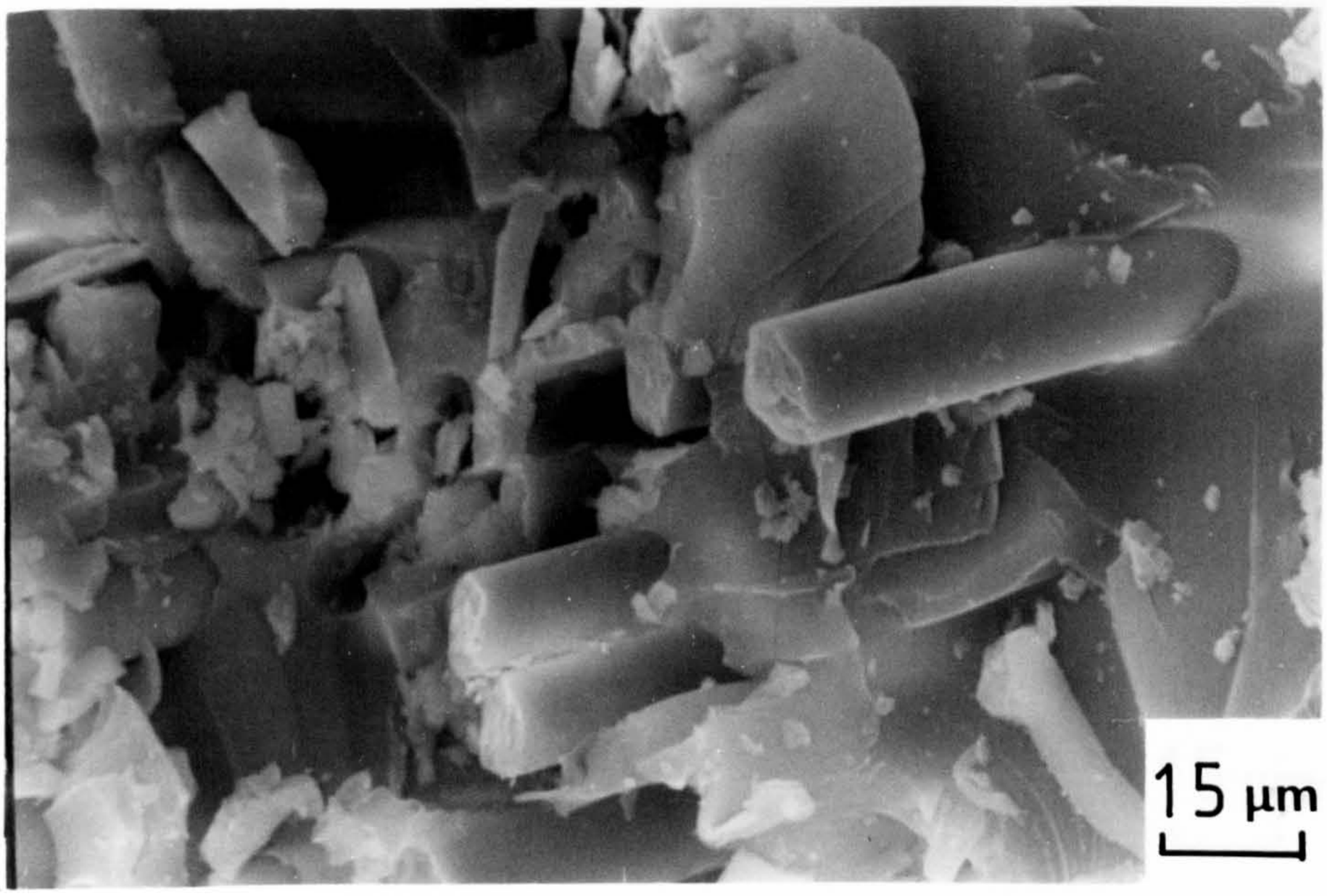

(a) View showing fibre fracture, pull-out and resin debris.

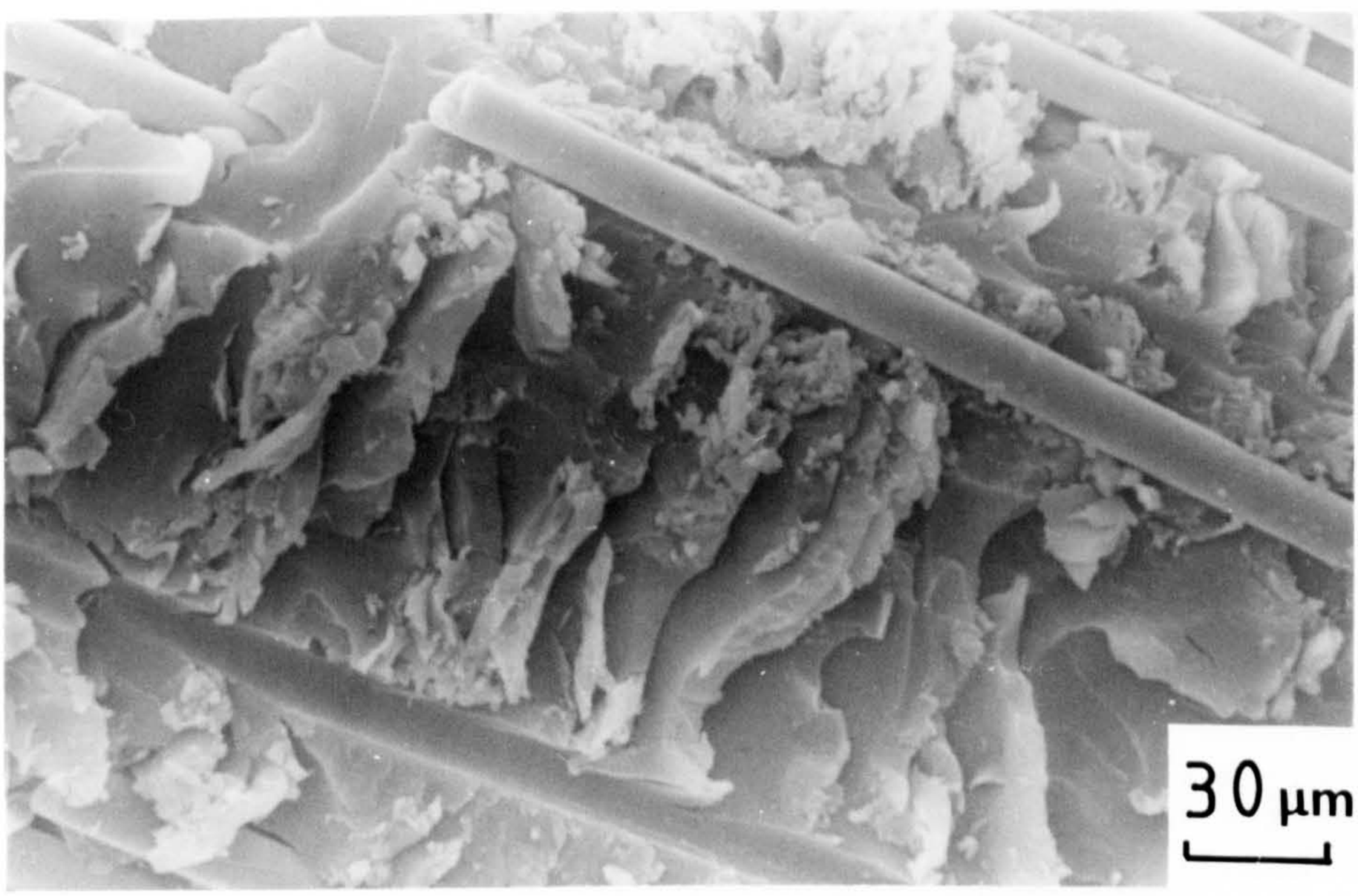

(b) View showing resin debris tending to obscure original fracture surface.

Fig.5.33. SEM photomicrographs of inner axial region after inversion into tube cavity. $0^{o}/90^{o}$ polyester tube tested at 4×10^{-3} m s^{-1}.

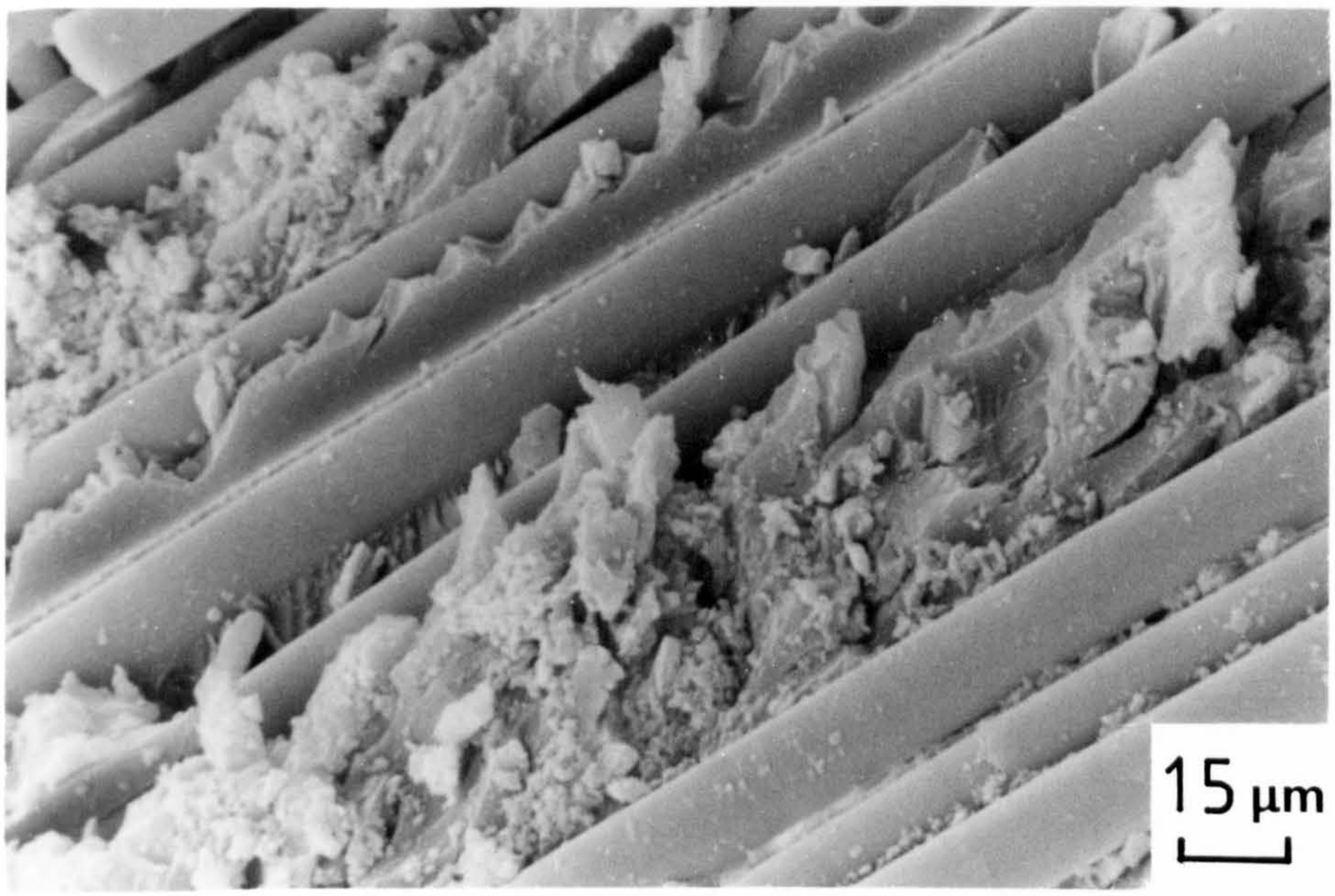

(a) View showing debris due to fracture processes.
Areas of original fracture surface still visible.

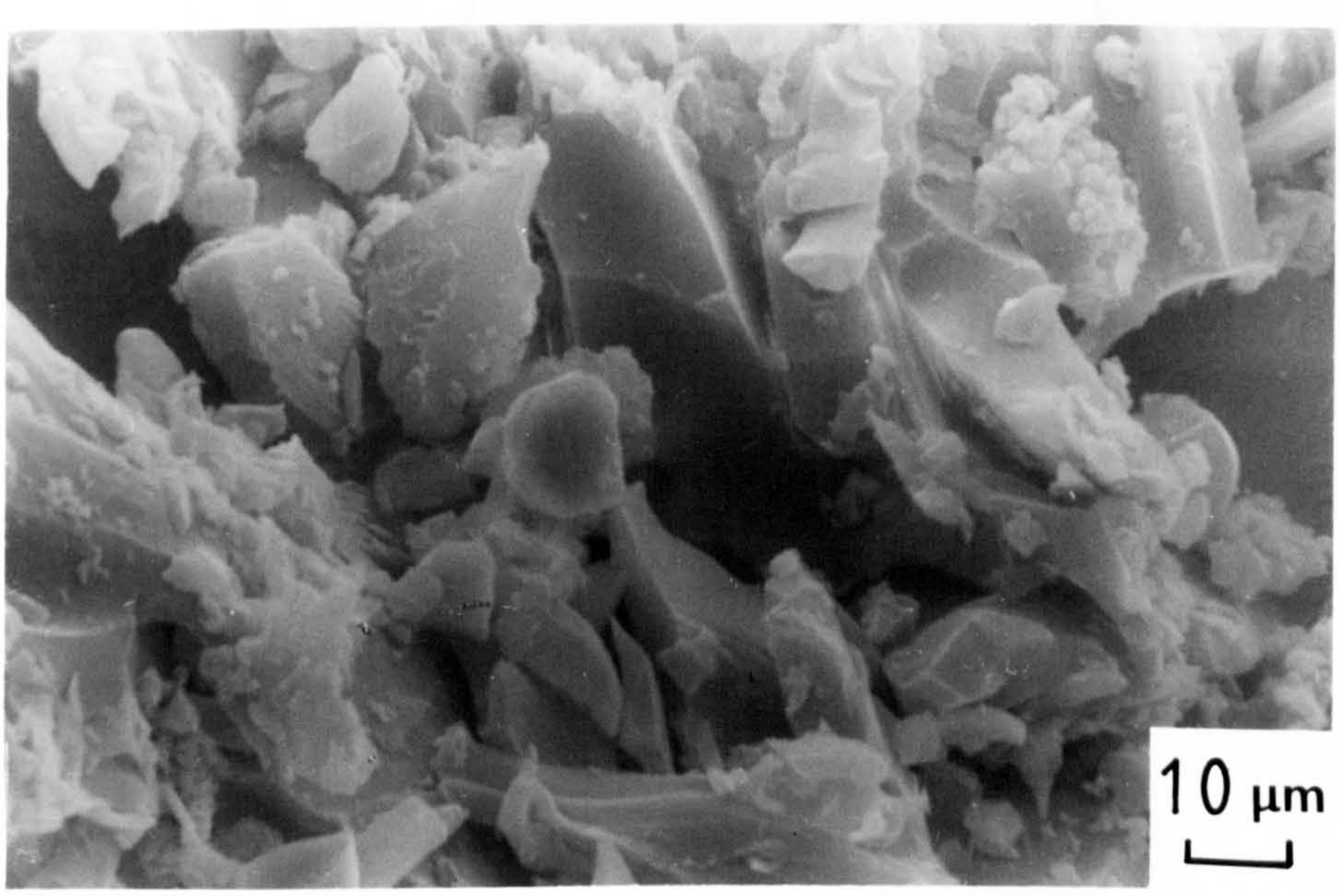

(b) Debris from fracture processes.

Fig.5.34. SEM photomicrograph of inner axial lamina after inversion into tube cavity (Region 3). $0^{o}/90^{o}$ tube tested at 4×10^{-3} m s^{-1}.

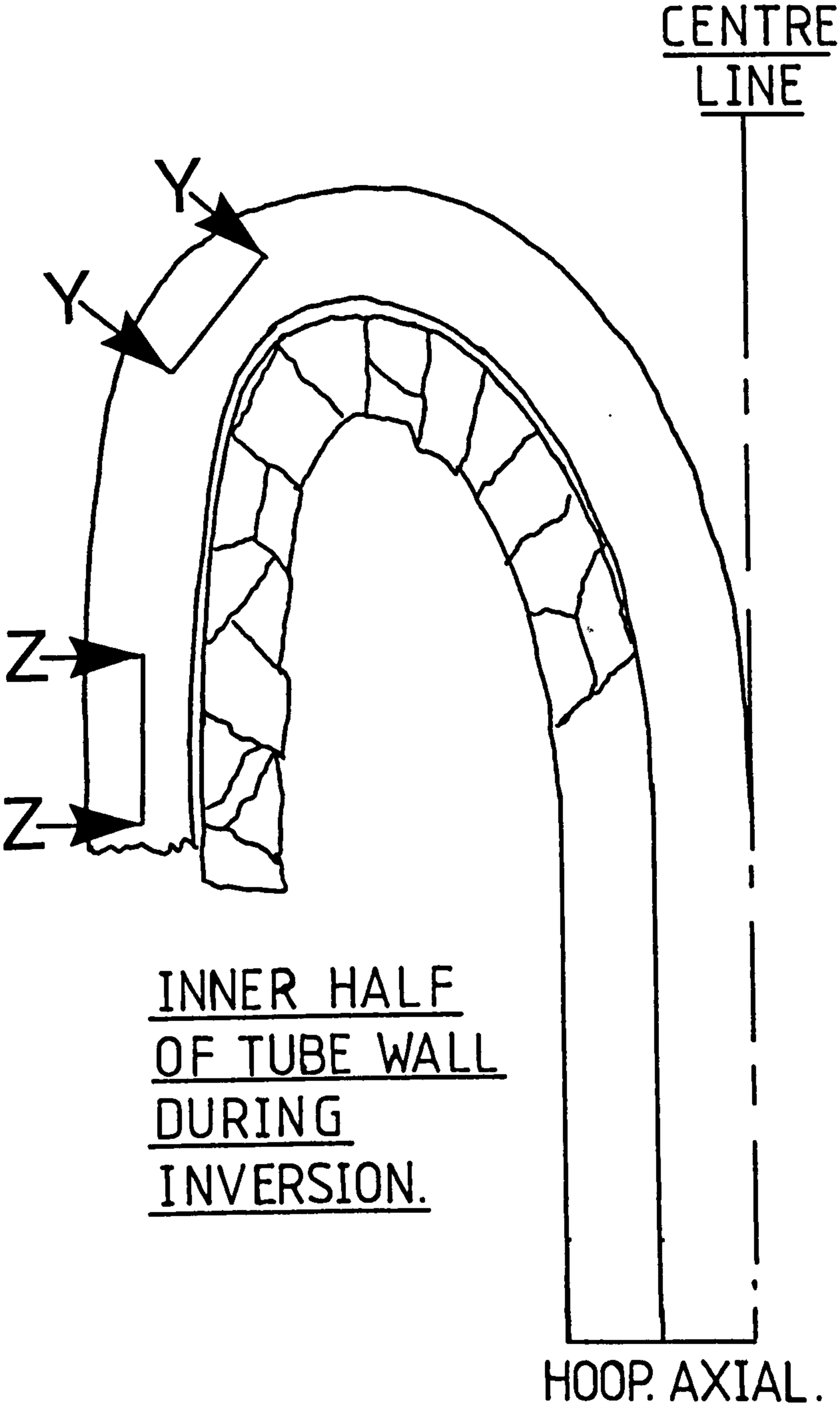

Fig. 5.35. Diagram of a section from the inner region of the crush zone of a 0/90 tube showing the direction and field of view for scanning electron microscopy.

Underneath the debris (Fig. 5.33 (b)) the fracture surface was similar to the surfaces described in section 5.5.2, with torn flaky resin and clean fibres indicating shear fracture. Fibre fracture occurred in many areas, a typical example of which is shown in Fig. 5.33 (a) This shows fibre pull-out indicative of tensile fracture.

Further crushing caused the axial lamina to become compressed into the tube cavity. This degraded the material into small particles of debris to such an extent that the original fracture surfaces were completely destroyed. This is shown in Fig. 5.34. This debris probably results from a complex process of fibre bundles bending, interpenetrating and sliding over each other because of the limited volume in the tube cavity.

5.5.5 Centre line cracking, region (4)

In all $0^{o}/90^{o}$ tubes studied, a crack formed in the central region of the tube wall. The crack grew ahead of the cross-head by 10 - 15 mm for polyester tubes crushed at 4×10^{-3} m s^{-1}. This dimension varied slightly around the tube wall but was constant during the crush. These measurements were made on sections taken from the crushed tube wall that were under load. They are discussed in section 5.6.

Fig. 5.36 shows the fracture surface of the crack. Both planar and tearing shear fracture occurred. The fibre surface was clean and free from any adhering resin. The resin surface between the fibres was covered with fine river-line markings which travelled from fibre to fibre. Similar markings also occurred on the fracture surface from short beam shear tests (Fig. 5.2). In this case, the markings tended to run parallel to the fibres, indicating a growth direction from fibre to fibre.

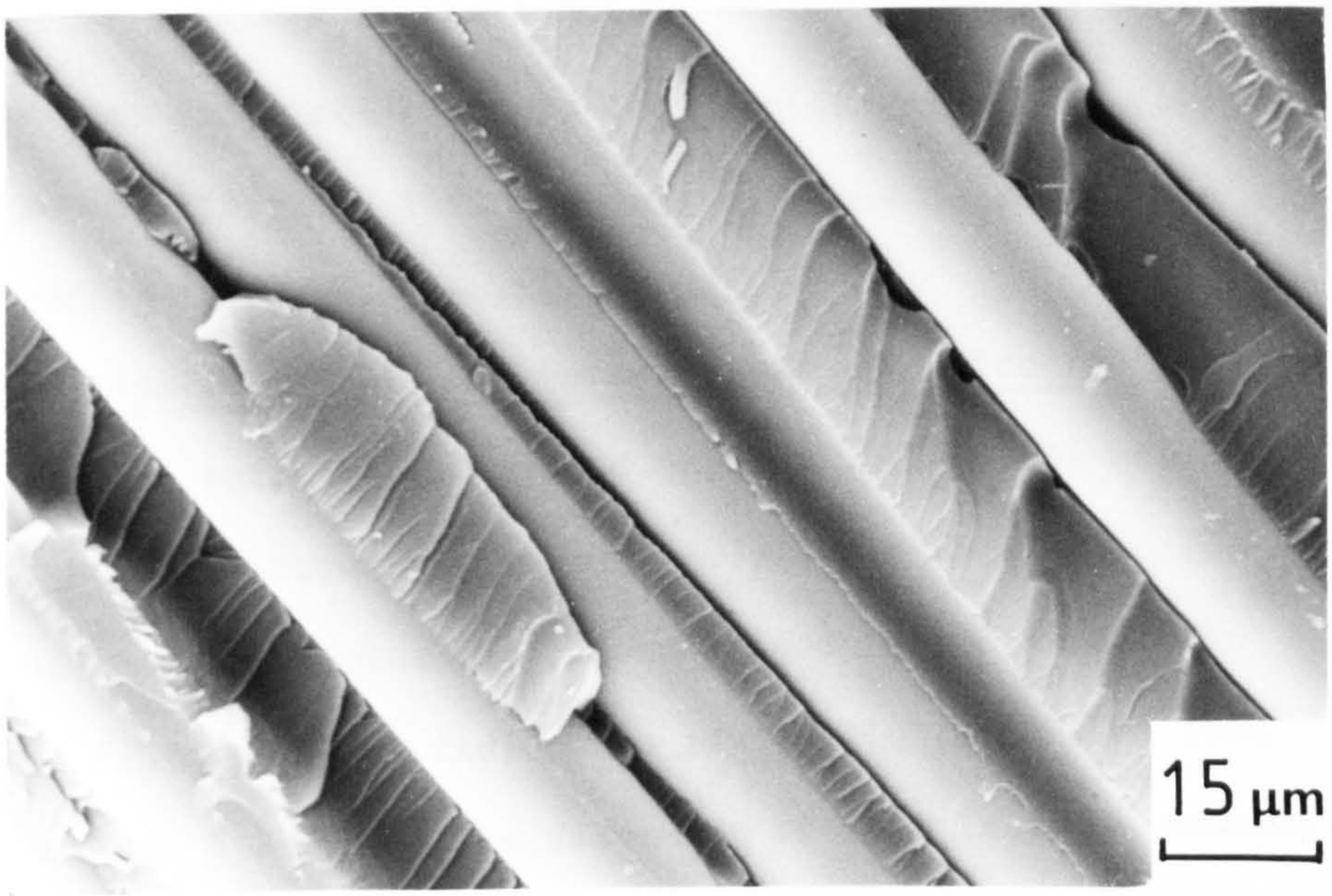

(a) View showing clean fibres and planar resin fracture with striations.

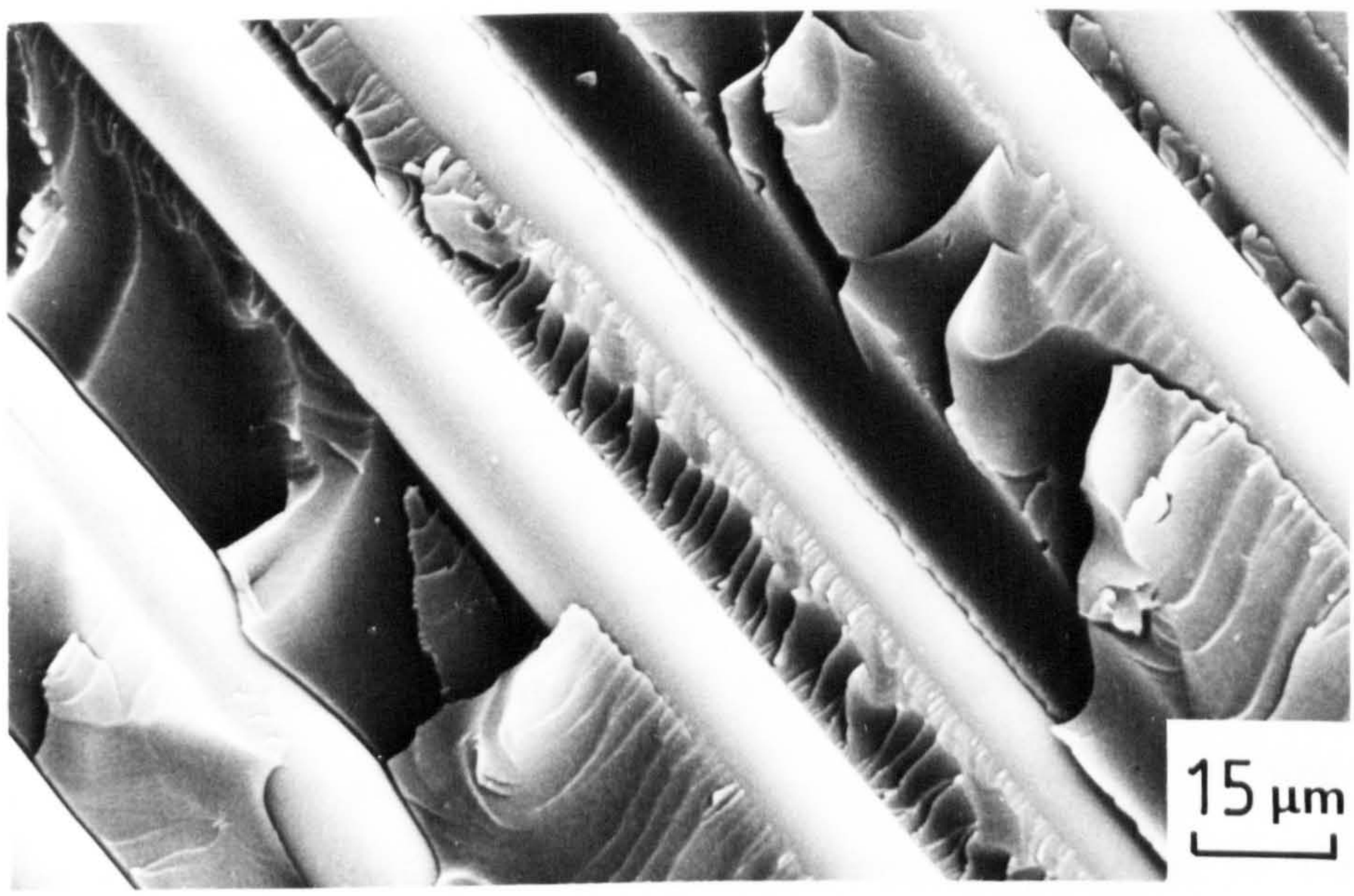

(b) View showing resin fracture surfaces with river-line markings.

Fig.5.36. SEM photomicrograph of fracture surface from centre-line crack (Region 4). 0°/90° polyester tube tested at 4×10^{-3} m s^{-1}.

The river-line markings on the fracture surface from the centre-line crack show that the crack front in this region grows in a direction parallel to the fibres. This dissimilarity may be due to the non-uniform loading during the crushing process.

5.5.6 Tensile failure of the outer hoops, region (5)

As the outer axials spread outwards, the hoops must expand and become, therefore, subject to tensile loading. The fracture of the hoop lamina was characterised by a planar resin surface and fibre pull-out indicative of tensile failure. This is shown in Fig. 5.37(b). The direction of view is shown schematically in Fig. 5.41 as Z-Z.

In areas near the fracture, cracks grew parallel to the fibres to give a fracture surface as shown in Fig. 5.37(a). This gave a tapering effect to the fracture surface, the fibre bundles reducing in size until total fracture took place. The cracks grew across the fibres, initiating tensile fracture, then changed direction, growing parallel to the fibres changing back to tensile failure until complete fracture occurred.

5.5.7 Multiple fracture of the inner hoops, region (6)

The fracture surface of the inner-hoop region after crush was covered by large amounts of debris. The fibres fractured into short lengths and the resin into small irregular particles. The fracture surfaces are shown in Fig. 5.38. The original fracture surface of the hoop windings was completely destroyed owing to the bending, interpenetration and frictional effects as fracture segments of the tube wall were crushed into the tube cavity.

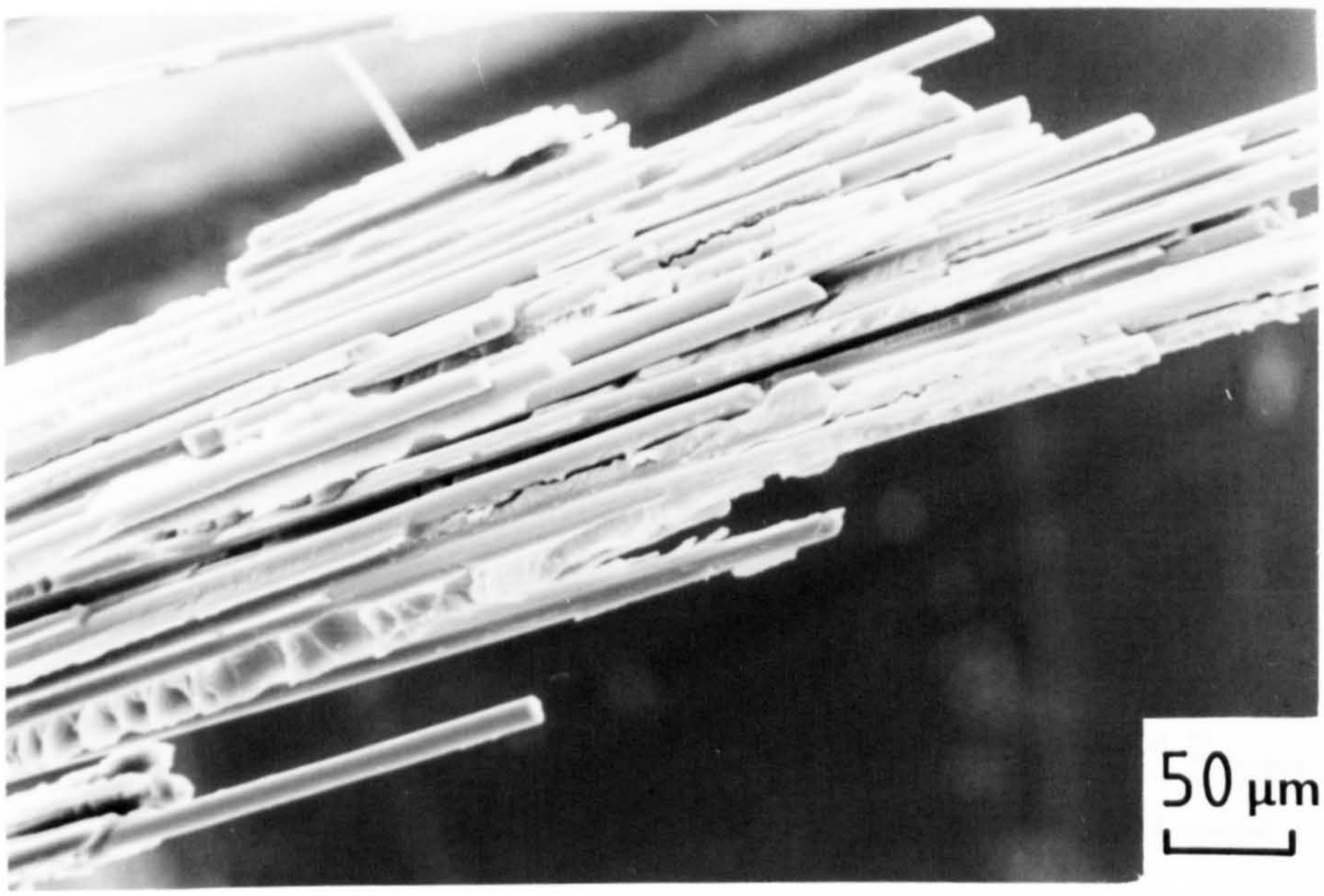

(a) View of fracture at the end of a hoop fibre bundle.

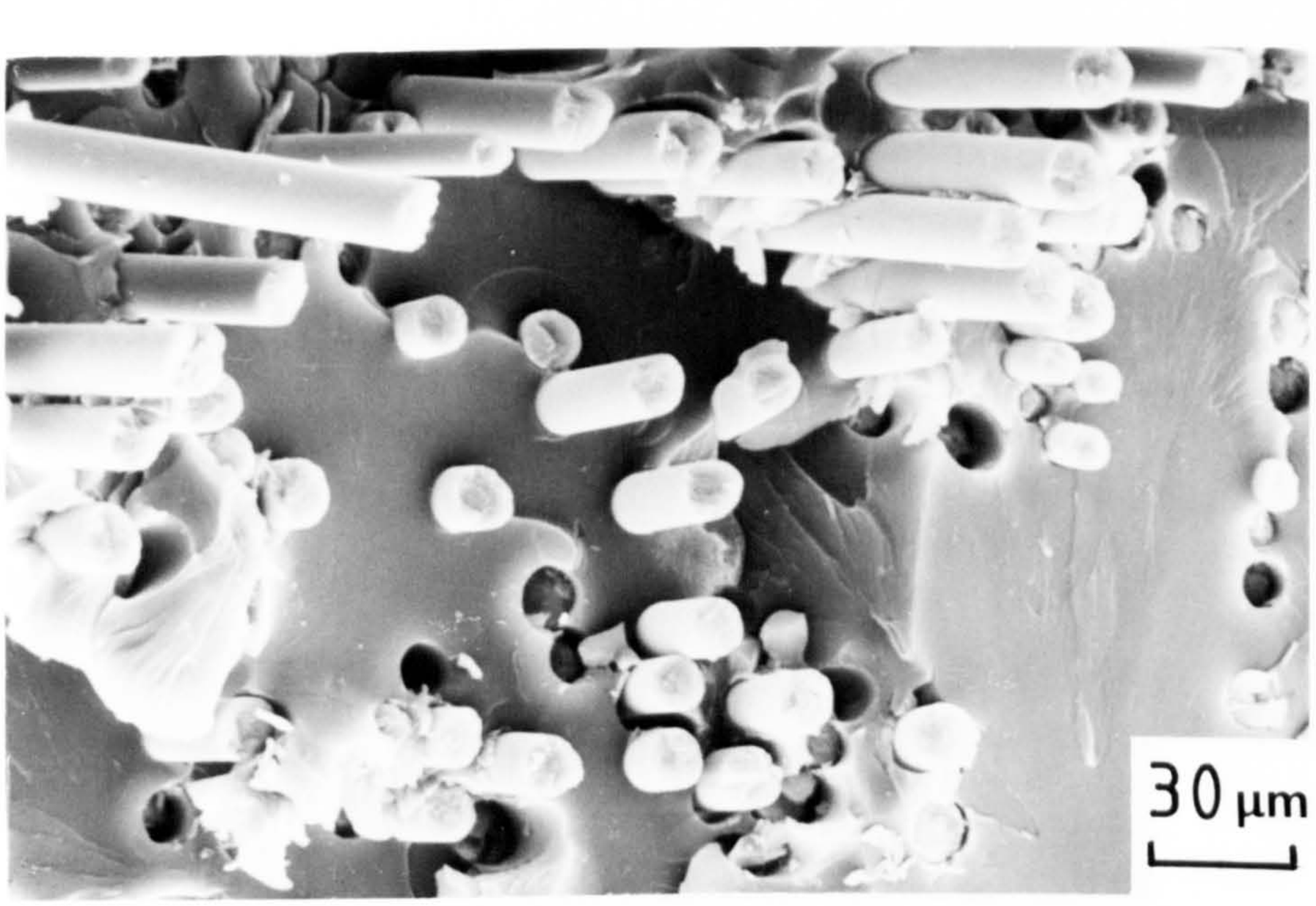

(b) View of fracture surface across a hoop fibre bundle showing fibre pull-out.

Fig.5.37. SEM photomicrograph of fracture surfaces from outer hoop lamina (Region 5). 0°/90° polyester tube tested at 4×10^{-3} m s^{-1}.

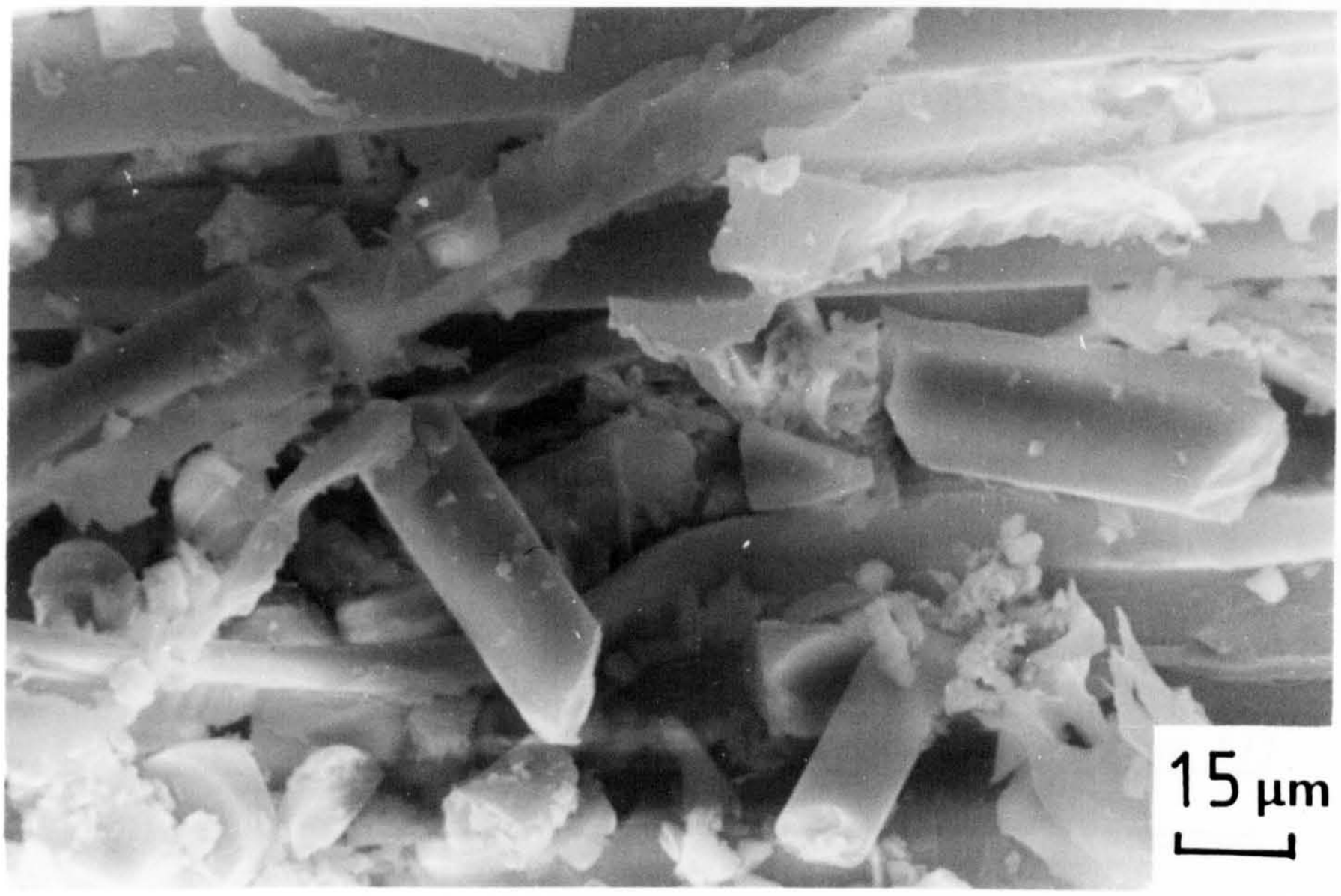

(a) View showing crush debris.

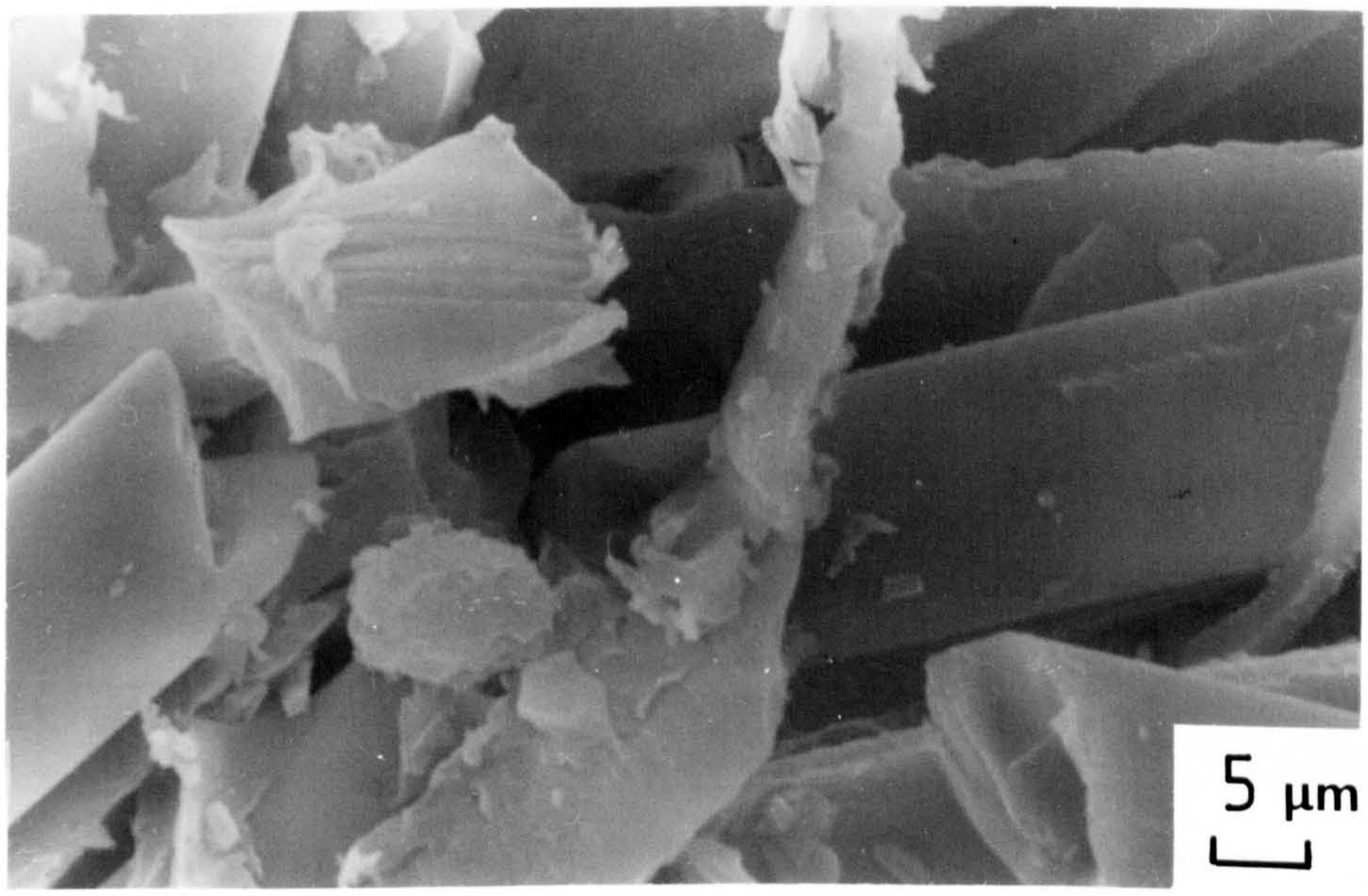

(b) View showing the constituents of the debris.

Fig.5.38. SEM photomicrographs of inner hoop lamina after secondary crushing (Region 6). $0^{o}/90^{o}$ polyester tube tested at 4×10^{-3} m s^{-1}.

A complete description of the fracture processes that take place in the centre of the tube is difficult. All of the crushed tube wall that inverted into the limited volume of the tube cavity was subjected to many different fracture mechanisms. These included frictional effects caused by fragmented segments of the tube wall sliding over each other and further fracture of the segments by many processes which reduced the size of the unbroken laminae until small particles of component materials were obtained.

5.5.8 Fracture between the hoop/axial laminae, region (7)

During crushing, the hoop laminations were separated from the axials. Photomicrographs of the fracture surfaces taken from the region between the outer hoops and axials are shown in Fig. 5.39. The direction of view is shown as X-X in Fig. 5.41. The cracks grew parallel to the plane of the axial fibres, but not always at the actual interface between the two laminae. The crack path was often a few fibres displaced from the interface. Fig. 5.39 shows a crack which has grown through the hoop windings, only occasionally propagating along the axial fibres. On a micro-scale, the resin and fibres showed a fracture surface similar to those previously described. The fibres were clean and free from adhering resin, whilst the matrix was characterised by a torn, blocky fracture surface indicative at shear fracture.

5.5.9 Cracking within the hoop laminae, region (8).

The hoop fibres underwent several different fracture mechanisms during the crush process. Tensile failure and hoop-to-axial interlaminar failure have been described. In addition to these mechanisms, bundles of hoop fibres, roughly corresponding to the dimensions of the original fibre tows, were compressed downwards and outwards from the tube wall, with cracking taking place

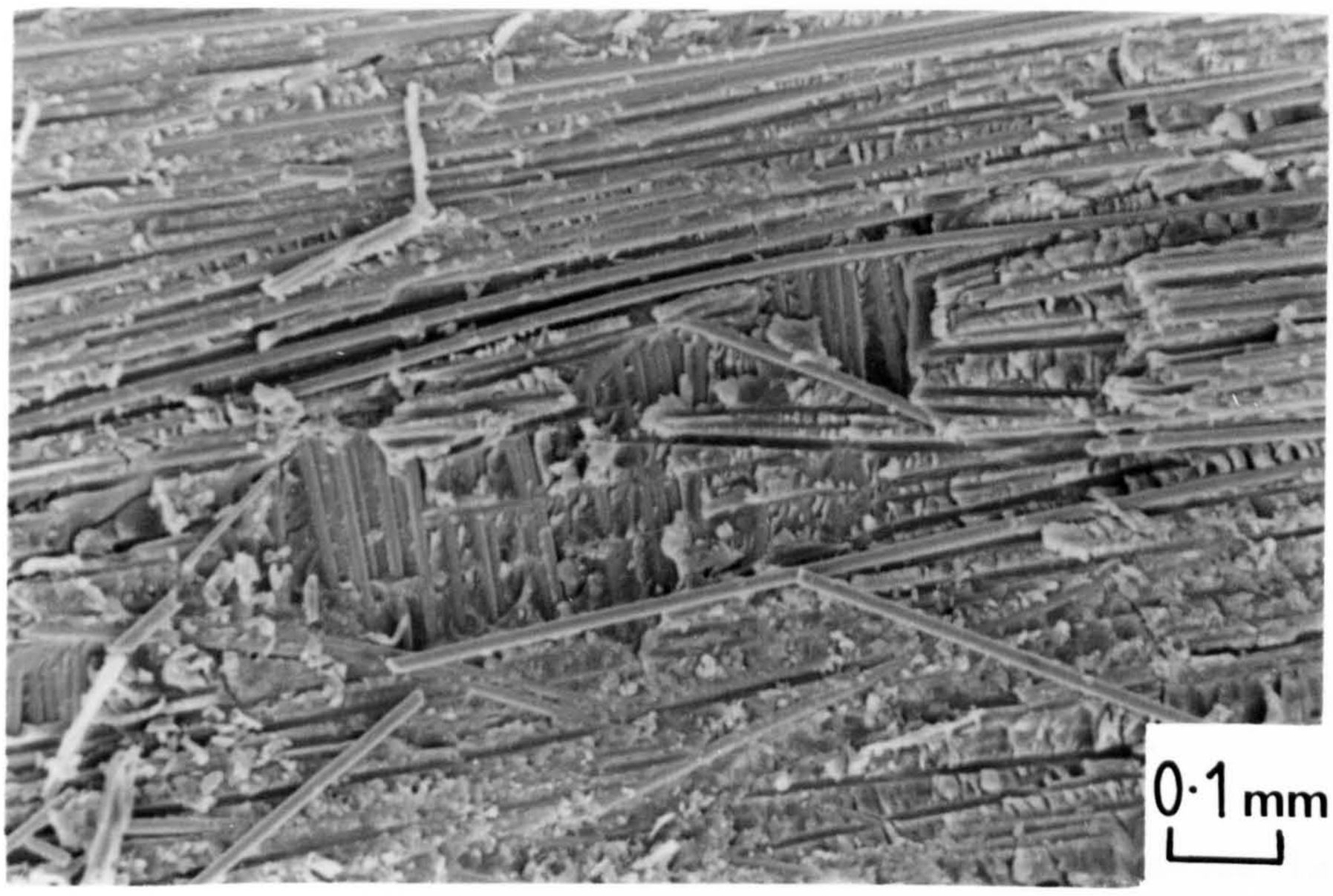

(a) General low magnification view.

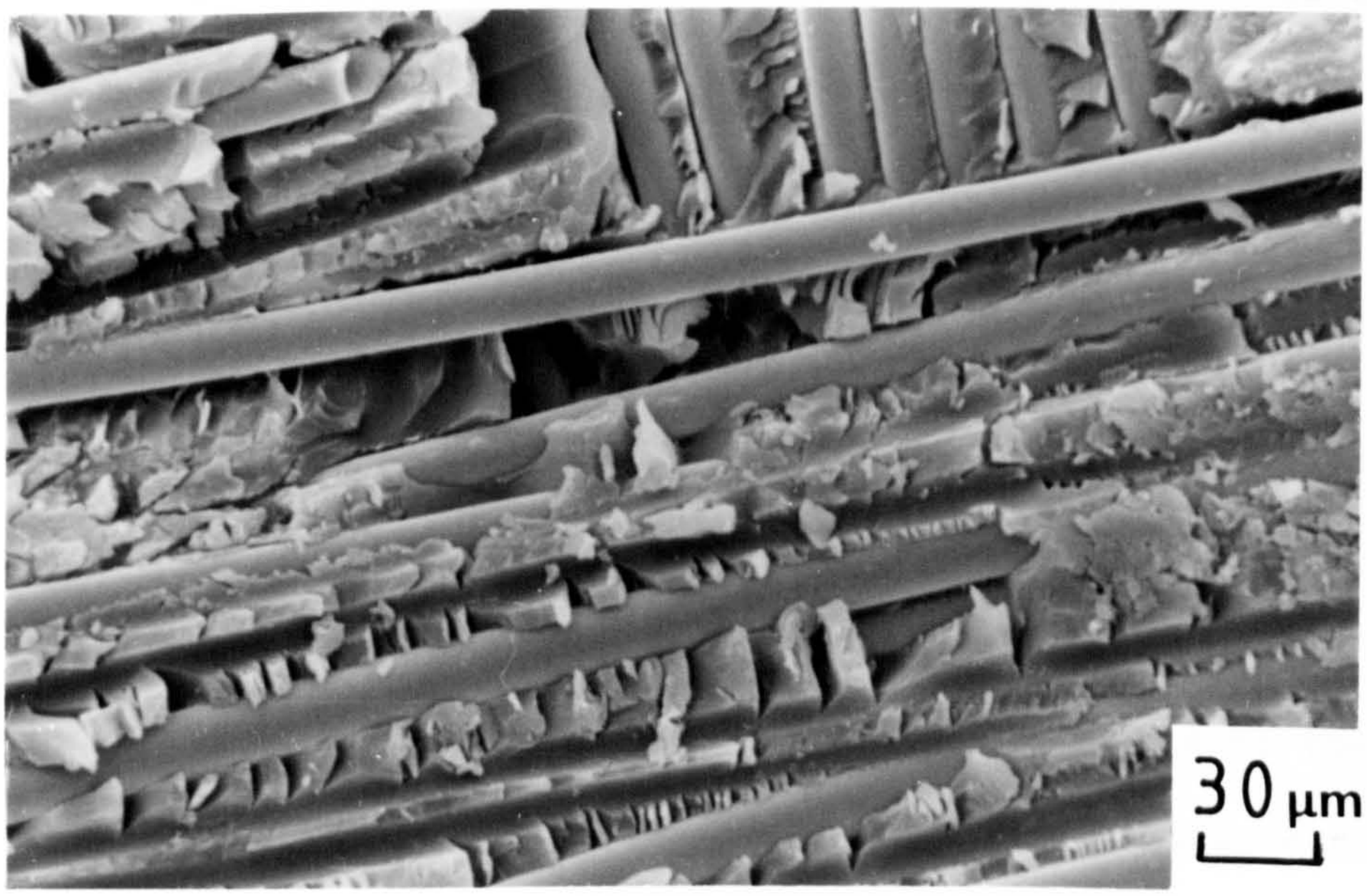

(b) View showing torn resin fracture surface and clean glass fibres.

Fig.5.39. SEM photomicrographs of interlaminar fracture surface between hoop and axial laminae (Region 7). $0^{o}/90^{o}$ polyester tube tested at 4×10^{-3} m s^{-1}.

at an angle to the tube axis. The fracture surface of these cracks is shown in Fig. 5.40. The direction of view is shown as Y-Y in Fig. 5.41. This was a planar resin fracture with faint striations and river-line markings, running between the fibres. The overall crack direction was perpendicular to the fibres and in the plane of the micrograph. The direction of the river-line markings would, however, indicate a crack direction parallel to the fibres.

5.5.10 Accumulation of debris in the centre of the tube wall, region (9)

During crush, a region of compressed debris collected in the area between the axial laminae. It consisted of small, irregularly shaped particles of resin and short lengths of broken fibres as shown in Fig. 5.42(b). This debris from the fracture processes became lightly compressed between the cross-head platen and the crushed axial laminae, forming a characteristic wedge shape as shown diagrammatically in Fig. 5.42(a). Once formed, this bundle wedge maintained its shape and size throughout the crush process.

The effect of this bundle wedge on the overall fracture process is difficult to assess. It could be a major factor in contributing to the opening of the centre line crack, by forcing the axial fibres apart. Alternatively, the region of the 'V' of the axial fibres could be only loosely filled with debris which contributes little to the overall crushing process. The actual case is probably between these two extremes.

5.6 Micrography of crushed sections of $0^{\circ}/90^{\circ}$ tubes under simulated load

Sections taken across the crush zone of $0^{\circ}/90^{\circ}$ tubes tested at 4×10^{-3} m s^{-1} were placed under load and examined. A typical photomicrograph is shown in Fig. 5.43. Only one half of the tube wall

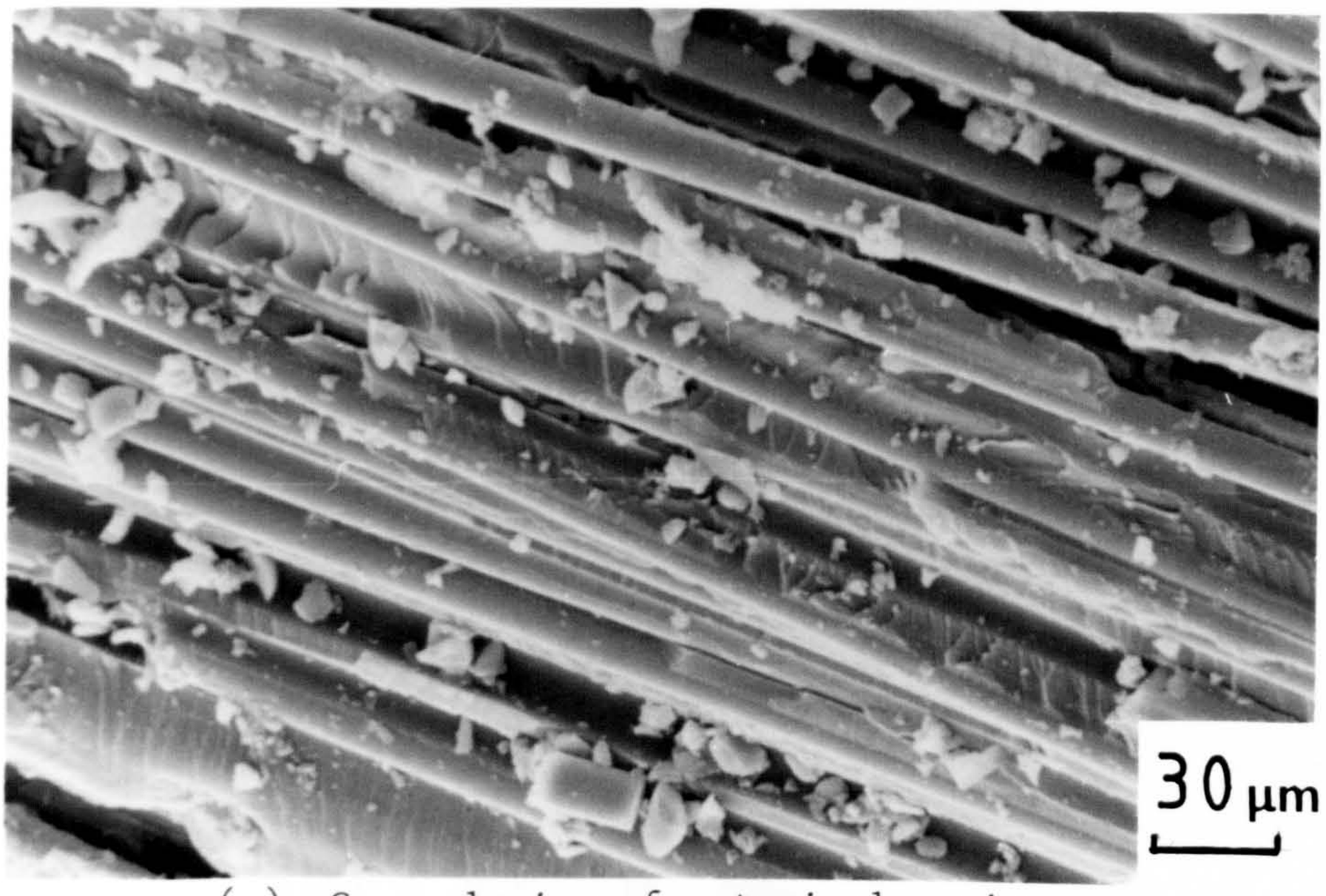

(a) General view of a typical region.

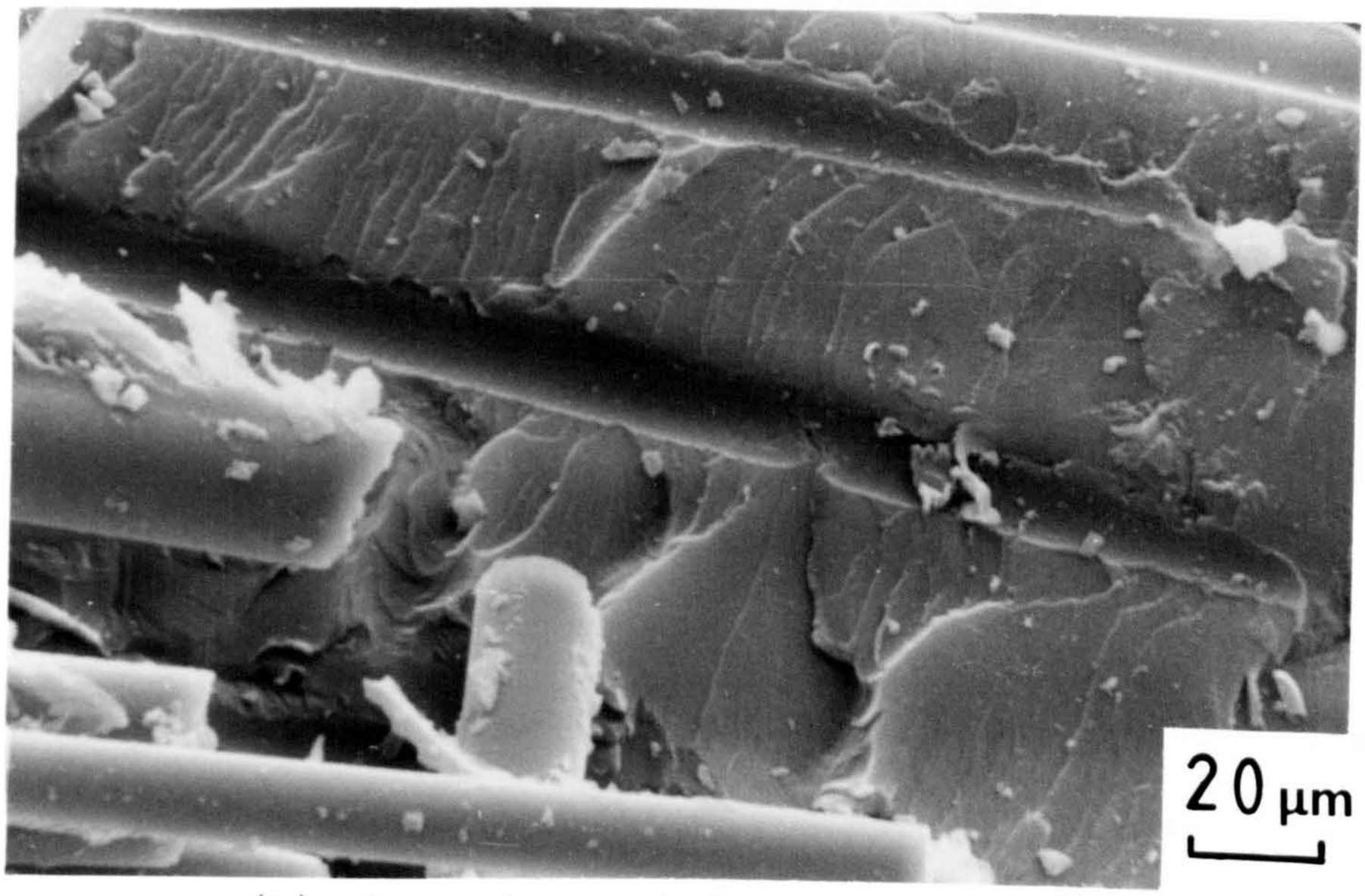

(b) View of smooth fracture surface with striations.

Fig.5.40. SEM photomicrograph of intralaminar fracture surface of hoop lamina (Region 8). $0^{o}/90^{o}$ polyester tube tested at 4×10^{-3} m s^{-1}.

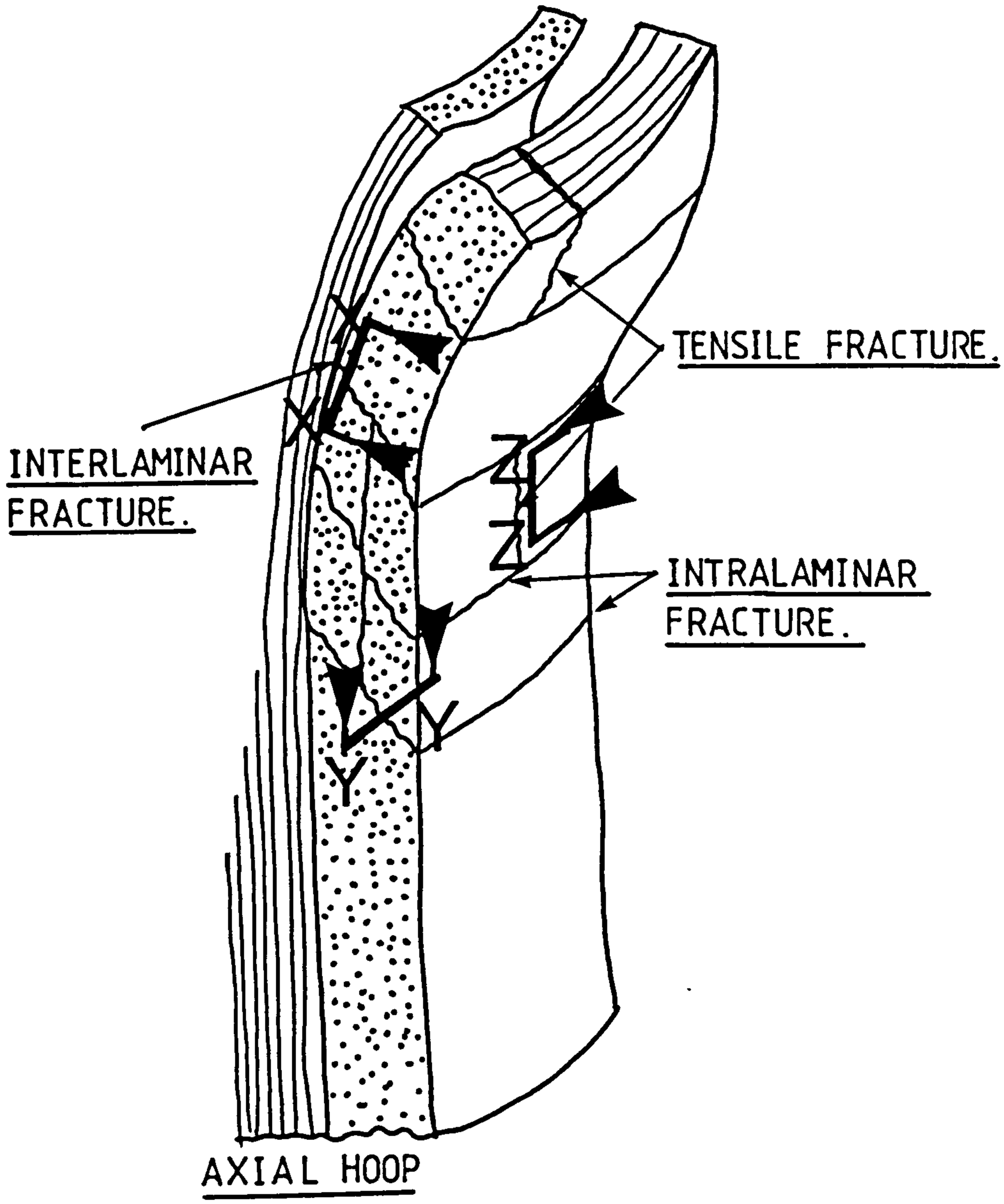

Fig. 5.41. Diagram of a segment from the crush zone of a 0/90 tube showing the three modes of fracture in the outer hoop lamina. The directions of view for scanning electron microscopy are indicated.

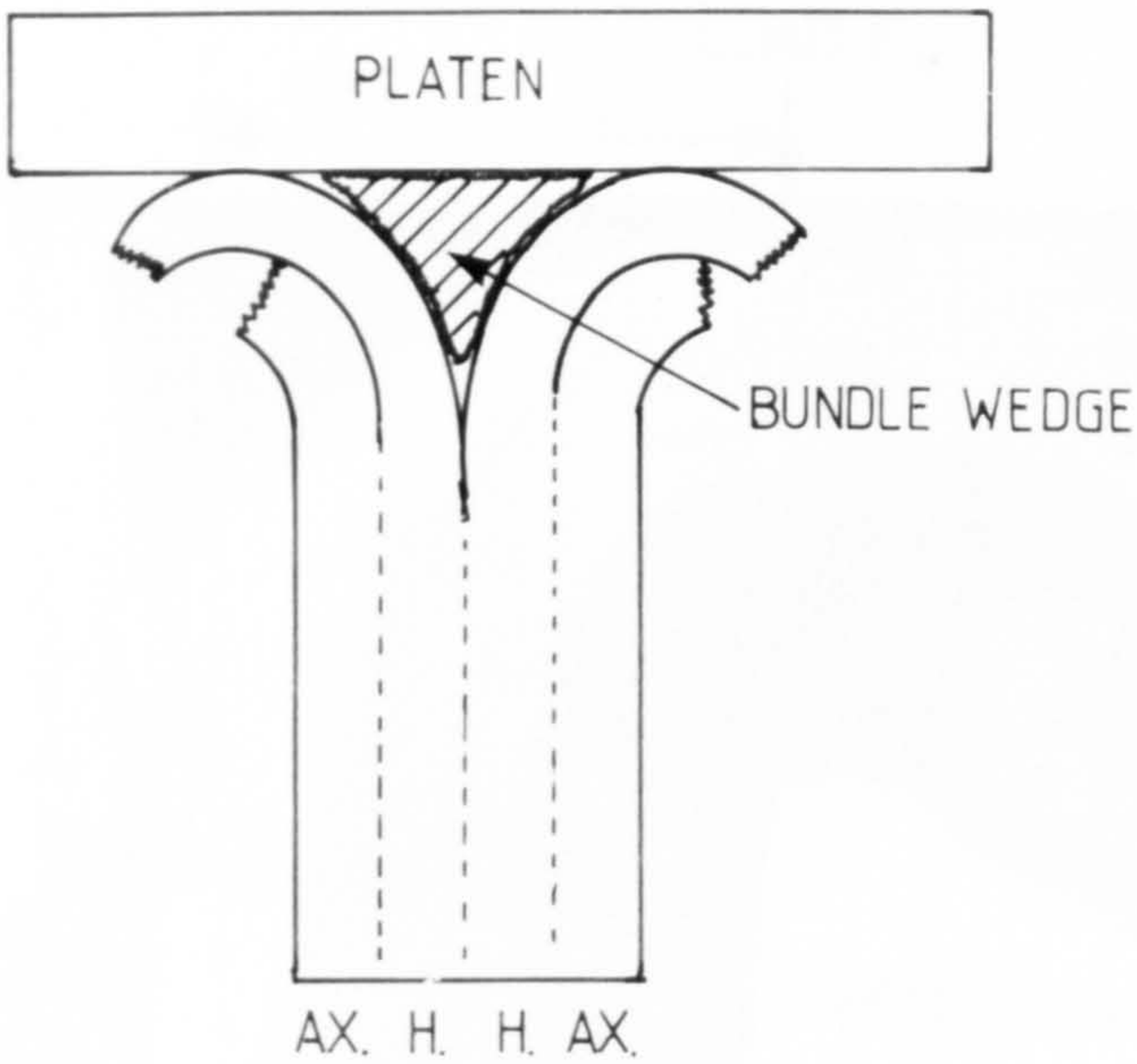

(a) Diagram of the shape and position of the bundle wedge.

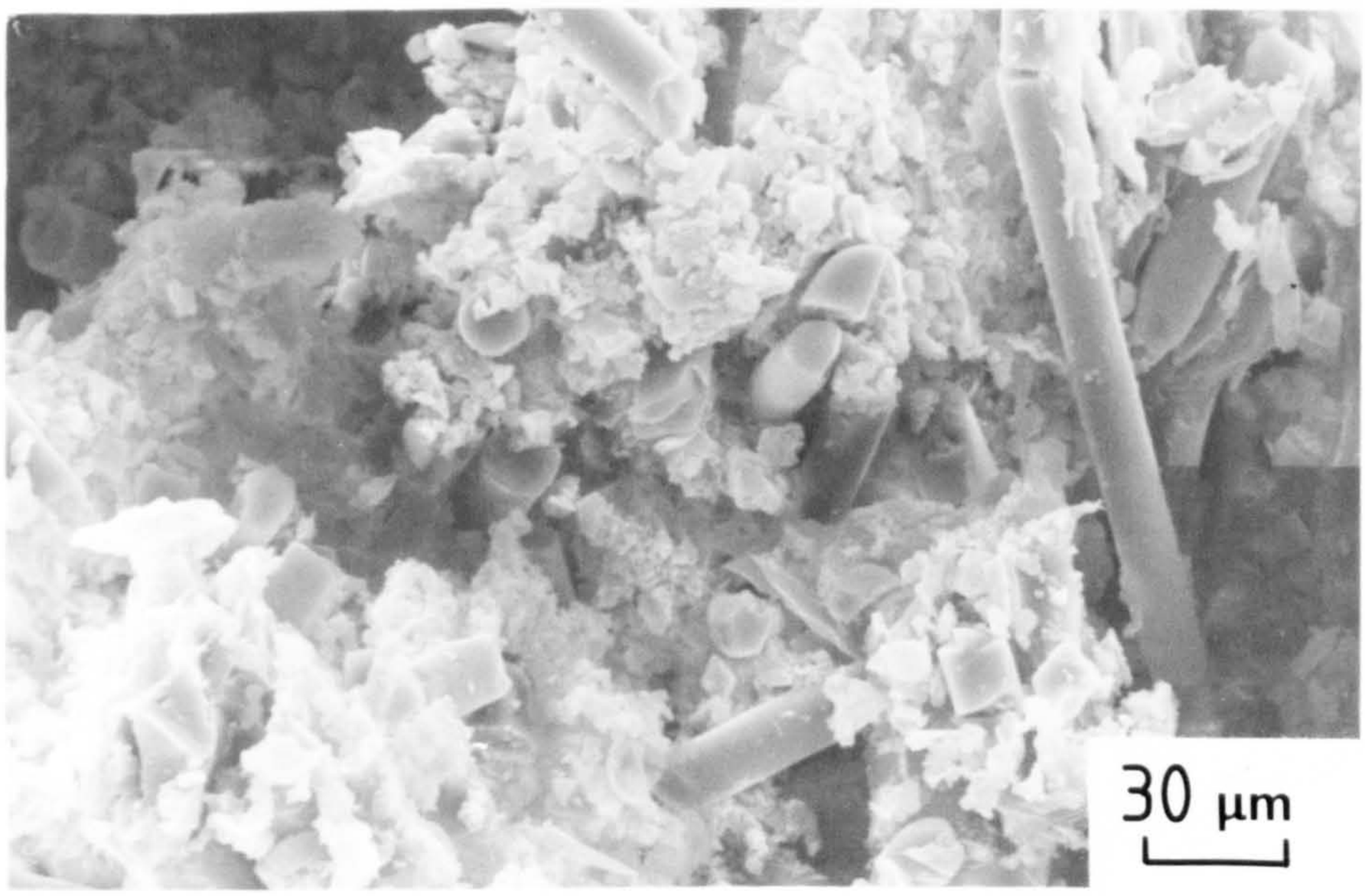

(b) SEM photomicrograph of debris in the bundle wedge.

Fig.5.42. Debris in the central region of a crushed 0/90 polyester tube tested at $4x10^{-3}ms^{-1}$ (region 9).

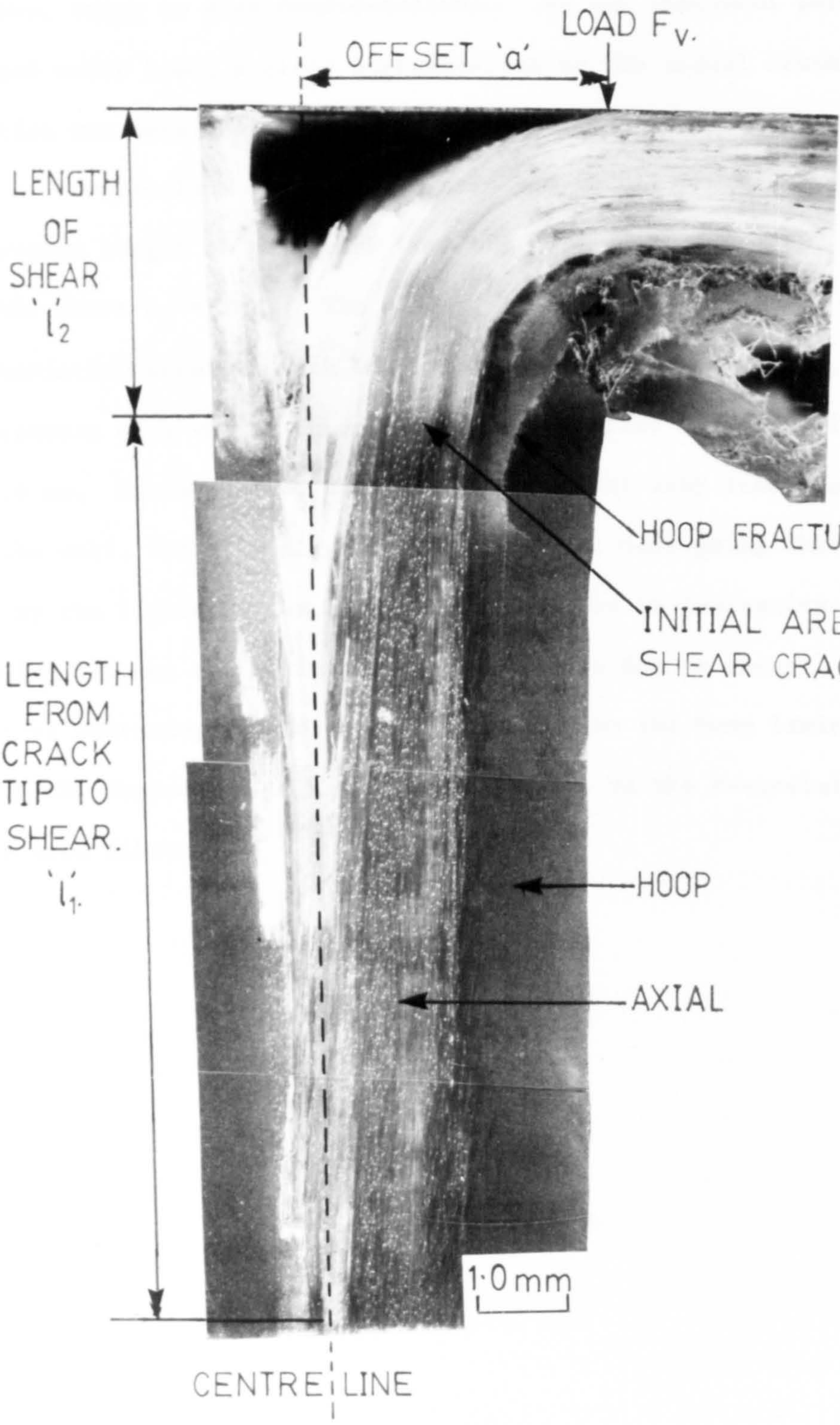

Fig.5.43. Photomicrograph of a crushed segment of a 0/90 polyester tube under load.Original test speed was $4x10^{-3}ms^{-1}$.
Notations referred to in text.

is shown, owing to size considerations. As the specimens were examined under load, a close approximation to the actual crushing situation was obtained.

Centre-line cracking was observed in all photomicrographs. The average length of the crack from tip to loading plate ($l_1 + l_2$), was 19.5 mm, where l_2 = 3mm. The offset, 'a,' was measured as 3.3 mm, although some variation occurred with both measurements. For example, six measurements of 'a' varied from 2.9 to 3.9 mm whilst 'l' varied from 9.4 to 11.6 mm. During crush, the axial fibres bent away from the centre of the tube wall, intially slightly then rapidly, undergoing whitening as shown by the lighter areas in Fig. 5.43. This is indicative of debonding between the resin and fibres and was due to shear. The initial region of whitening was adjacent to cracking in the hoop laminae, showing the dependence of axial shear bending on the restraint provided by the hoop fibres.

CHAPTER 6 - GENERAL DISCUSSION

6.1 Introduction

In this chapter the various facets of the work carried out are discussed and their interrelations considered. A qualitative analysis is presented for the failure mechanisms of $0^{o}/90^{o}$ tubes. The effects of winding angle, resin properties and test speed on the failure mechanism and energy absorption are discussed.

Each specific fracture process is examined and a quantitative analysis given from a fracture energy view point; the aim being to indicate the major energy absorbing processes and predict the total energy absorbed during the crushing process. Comparisons are made between the predicted and empirical results for energy absorption. Other possible sources of energy absorption are also investigated.

The factors affecting the load supported by the tube during crush are discussed with reference to loaded sections taken from the crush zone and a model proposed for further analysis. Finally brief suggestions are made concerning further work.

6.2 Qualitative analysis of the failure mechanisms of $0^{o}/90^{o}$ tubes

A preliminary proposal for the failure process for a $0^{o}/90^{o}$ tube can now be made. This is based on direct observation of crushed tubes and sequential photographs of the crushing process. The initial stages of crush show that compression caused cracking in the inner hoop laminae only, owing to the configuration of the bevelled end. This occurred at a comparatively low stress level as the failure stress of a composite in compression normal to the fibres is generally low. Large cracks occurred within the hoop lamina. These extended as segments of the lamina separated from the tube wall, leaving one side of the inner axial lamina without support. With increasing cross-head displacement, this lamina became loaded in compression and kinked

before bending inwards. Further displacement compressed the outer axial lamina which also initially buckled then bent outwards against the outer hoop lamina, causing it to fail in a similar manner to the inner hoop lamina. At this stage a wedge shaped void opened up in the centre of the tube wall which developed into a long crack down the centre of the tube between the axial laminae. Owing to the manufacturing methods, this central region tended to be resin rich and offered low resistance to crack propagation.

During bending, the axial laminae were subjected to a complicated fracture process, because of the changes in circumference that occurred. The outer axials split translaminarly to accommodate the increase in circumference, whilst the inner axials bend and interpenetrated during inversion into the centre of the tube. The axial laminae fractured intralaminarly into thin layers during bending, the plane of the cracks initially being parallel to the tube wall. This bending is analogous to a cantilever beam fixed at one end (the uncrushed tube wall) and bent by a load at the other end. Such an analogy would indicate the probability that intralaminar shear would be the most likely fracture mechanism in the axial fibres.

As the axials bent outwards or inwards and downwards, the hoop windings were subjected to a complex stress system. A circumferential tensile stress coupled with a longitudinal (relative to the tube axis) compressive stress separated the outer hoop lamina from the tube wall. The situation with regard to the inner hoop lamina is more complex. As the inner axial fibres bent, a compressive stress on the inner hoop lamina, in the direction of the fibres, resulted in buckling, separation from the tube wall, then crushing and interpenetration in the tube cavity.

The outer hoop lamina fractured into both long thin fibre tows and shorter plate-shaped segments. These were formed by intralaminar

cracking in the hoop lamina and interlaminar cracking between the hoop and axial laminae. Tensile fracture also occurred because of the expansion of the outer axial lamina. Shorter plate-shaped segments of hoop lamina which adhered to the axial lamina, corresponded in length to the spacing of the transverse cracks in the axial lamina. Failure into long fibre tows and short plate segments took place concurrently. The fracture processes of the hoop lamina tended to be complex owing to a non-uniform loading situation. This was further complicated in the region between the hoop and axial lamina by the different response of laminae orientated at right angles to each other. Further investigation of this aspect is outside the scope of this work.

A simple concept for the crushing mechanism to aid in the interpretation of other experimental phenomena can now be proposed. The axial laminae bend inwards and outwards away from the tube wall centre, down which passes a long crack. As the axials bend, the hoop lamina fail with a mixture of intralaminar and tensile cracking. As the hoops fail, support to the axial fibres is greatly reduced, thus allowing a greater degree of bending of the axials and elongation of the centre line crack. Consequently, increased stress isplaced on the hoop fibres further down the tube and the whole process is repeated.

This concept of crushing explains the serrated nature of the load-displacement traces. Each fracture of the hoop laminae results in an instantaneous reduction of the constraint placed on the axial laminae. This triggers further bending of the axial laminae with a corresponding reduction in the load carried by the tube. As the cross-head advances, the load increases until further hoop fractures occur, again reducing the axial constraint and load supporting capability. These individual processes occur many times around the

tube circumference. If several fracture processes occur simultaneously, the resultant drop in the load trace will be greater than with a single fracture process.

6.3 Effect of winding angle on the energy absorption

As indicated in Figure 4.14, the energy absorption of filament wound angle-ply tubes depended on the winding angle which also affected the crushing mechanisms and the shape of the load-displacement traces. Hoop, 85^{o} and 75^{o} angle-wound tubes failed mainly by hoop tensile fracture combined with a downwards motion of the crushed fibres. Angle-wound tubes with lower winding angles failed with plates or flat segments from the crushed tube wall bending inwards and outwards in a similar manner to the axials in $0^{o}/90^{o}$ tubes. The mechanism was complicated by secondary breakage of the fibre plates especially in the case of 35^{o} and 45^{o} angle-wound tubes.

The load-displacement traces varied from highly serrated for hoop-wound tubes to smooth and undulating for a 35^{o} angle tube, with little evidence of the sharp serrations observed with other tubes. Several energy absorbing mechanisms took place in the crushing process depending on the fibre angle to the applied load. With hoop (90^{o}), 85^{o} and 75^{o} angle-wound tubes, the individual fibre tows were subjected to a compressive load, approximately perpendicular to the fibre direction, which caused the tows to shear downwards and either outwards for the outer lamina or inwards for the inner lamina. After separation from the tube wall, the outer fibre tows expanded to pass over the uncrushed wall and failed in a tensile manner. The inner fibre tows contracted to pass inwards into the tube cavity then bent and buckled to accommodate the reduction in circumference.

As the winding angle is reduced, the hoop strength of the tube also reduces. This is because of the relationship between the

strength of a unidirectional composite and the direction of applied stress with respect to fibre orientation (26). As the hoop strength is reduced, the compressive strength of the tube increases. Shear through the laminate becomes more difficult with the result that flat segments of the tube wall bend outwards and inwards away from a centre line crack. Owing to the angle-ply construction of helically-wound tubes, the length of the lamina segments, in a direction parallel to the tube axis, is greatest with low angle windings. This is because of the cross-over effects of the glass tows. The long lamina segments have a lower bending stiffness when compared to the shorter segment obtained with 55^{o} and 65^{o} angle-wound tubes. This accounts for some of the variation in energy absorbed with angle.

Reference to the load-displacement traces for the lower angle tubes indicates a much smoother trace than with high-angle tubes. The smooth trace, found particularly with 35^{o} and 45^{o} angle tubes, was due to a crushing mechanism involving large segments from the tube wall being subjected to a controlled bending process with little fracture occurring. This resulted in a smooth undulating trace with few sharp serrations.

Tubes constructed only with axial reinforcement failed with a unique mechanism. Because of the lack of reinforcement in the hoop direction, the tensile failure strength in this direction was very low. During crush, longitudinal cracks formed at a low load. These cracks divided the tube wall into long thin beams approximately one centimetre in width. These beams were subjected to simple bending, sustaining a low crush load. This indicates the importance of the hoop restraint in the crushing process.

The differences in the energy absorbing values with winding angle are thus due to the variation in the crushing mechanisms. These

change from hoop-tensile fracture, through mixed bending and hoop-tensile fracture, to bending of small lamina plates of high stiffness and finally to bending of larger lamina plates of reduced stiffness. Tubes with only axial reinforcement crush non-progressively with longitudinal cracking down the fibres owing to the lack of hoop restraint.

6.4 Effect of resin properties on the energy absorption of tubes

Polyester resin, Crystic 272, was used for most of the tube manufacture. This was modified by CRC 1080 and flexibilised by Crystic 586. An addition of 10% of CRC 1080 improved the energy absorption properties by just under 20%. The addition of up to 40% Crystic 586 had little effect on the energy values. At test speeds of 4×10^{-3} m s^{-1}, the energy absorption of tubes made with epoxy MY 750 was 30% less than those made with Crystic 272, but at test speeds of 4 m s^{-1}, the energy absorption of tubes made with either resin was comparable. Flexibilisation of MY 750 by CY 208 increased the energy absorbed values at all test speeds by about 10 J g^{-1}.

During resin modification a trade-off in properties normally occurs. For example, improvements in the fracture toughness of the resin reduce the tensile modulus and heat distortion temperature. This has been shown by Crosbie and Phillips (107) with CRC 1080. If, as seems possible, the energy absorbing mechanisms of crushed tubes depend on resin properties such as fracture toughness, modulus and tensile strength, then an improvement in one property will be counteracted by the effects of a reduction in the other properties. Data in Table 20 show that the addition of 10% CRC 1080 to Crystic 272 causes a 400% improvement in the fracture toughness, 28% improvement in the tensile strength with only 10% reduction in the modulus. Flexibilising Crystic 272 with up to 40% Crystic 586 increased bulk resin toughness

by just under 300% but reduced modulus and tensile strength by 27% and 10% respectively. Above the 10% addition level of CRC 1080, the strength and modulus of the bulk resin is greatly reduced even though the toughness is still increasing.

These results of bulk resin properties are reflected in the energy absorption of crushed tubes. Flexibilisation by up to 40% Crystic 586 has little effect on crush properties. Modification by 10% CRC 1080 increases the energy absorption of tubes by 20%. This suggests that optimum resin properties, with respect to energy absorption of tubes during crushing, are obtained by using Crystic 272 modified with 10% CRC 1080.

An anomalous situation is shown by the results from tubes made with resin modified by CRC 1080. As described above, improvements in energy absorbed were obtained at test speeds of 4×10^{-3} m s^{-1}. This effect was not obtained at test speeds of 4 m s^{-1}. The reasons for this anomaly are not understood.

The load-displacement traces for tubes made with modified and flexibilised polyester resins were similar to the untreated resin, showing increased serrations at the higher test speed of 4 m s^{-1}. The traces were slightly smoother than for untreated resin at higher addition levels, but this effect was only marginal. Epoxy tubes also gave similar load-displacement traces to those of polyester tubes. The crushing mechanism was also similar.

The fracture toughness of epoxy MY 750 was found to be slightly higher than that of Crystic 272 at speeds of 4×10^{-3} m s^{-1}. The modulus and tensile strength, however, were lower. Modification of MY 750 by CY 208 reduced the modulus but increased both fracture toughness and tensile strength. Comparisons between energy absorption of epoxy and polyester tubes are difficult. At slow speeds of 4×10^{-3} m s^{-1},

polyester tubes gave higher energy absorbing values. This is attributed to the combined effects of resin modulus, fracture toughness and tensile strength on the crushing mechanism. Other factors may be important, such as the bonding between fibre and resin for polyester being dissimilar to that for epoxy. The glass used was manufactured with a silane coating compatible with polyester, but also, however, suitable for epoxies.

Modification and flexibilisation of a single resin can minimise variables thus making comparisons easier. The resin properties discussed earlier could all be envisaged as being important in the energy absorption process. For example, the high resin modulus would increase the load required to cause bending of the axials. An increase in the stiffness of the hoop fibres, due to increased resin modulus, would improve the restraint and support to the axial fibres. An increase in the tensile strength would cause all resin fracture processes to occur at a higher value, thus requiring more energy. An increase in the resin toughness would cause all fracture processes within the resin to absorb more energy. This would also have the effect of reducing the crack length in the centre of the tube wall, which may be important in controlling the ease of bending of the axial fibres.

6.5 The effects of test speed on energy absorption

The energy absorption of $0^{o}/90^{o}$ tubes varies with test speed. Tubes made with polyester matrices including both flexibilised and modified resins, showed a reduction in energy absorbed as cross-head speed increased. Tubes made with epoxy and modified epoxy matrices showed the reverse effect, i.e. energy absorption increasing with speed.

The load-displacement traces show that as test speed increased, the shape and magnitude of the serrations also increased. As discussed in the literature survey, the modulus of composite materials

tends to increase slightly with strain rate. The range of speeds used in the literature were, in general, much larger than those used in this work, but increasing modulus could be a contributing factor to this phenomenon. Thornton (46) noted an identical effect on load-displacement traces of graphite, glass,epoxy and polyester tubes, but gave no explanation.

Variations occurred in the appearance of tubes crushed at different speeds. This was particularly noticeable with $0^{o}/90^{o}$ tubes as shown in Figures 5.4 to 5.9. Fracture of the axial laminae involving fibre breakage occurred during crushing at speeds of 4×10^{-3} m s^{-1}. This gave a jagged appearance to the crushed tube. By comparison, at 4 m s^{-1}, the bending process was smoother with little axial fibre fracture. If this is a relevant factor, then glass and resin fracture is an additional energy absorbing mechanism at lower speeds. This does not, however, explain why more fibre breakage takes place at the lower speeds. One possible explanation may be that it is caused by the friction between the axial laminae and the cross-head platen. The effects of friction on the energy absorption of crushed tubes are discussed below in Section 6.6.8. During crushing at 4×10^{-3} m s^{-1}, individual fractured segments of axial laminae can be restrained by frictional forces so that relative motion between the cross-head platen and the segments of axial laminae ceases temporarily. As the coefficient of friction for the static case is always higher than for the dynamic case, a higher force on the segments is then required to commence movement of the laminae relative to the platen. This force may be sufficient to cause fracture of the axial fibres. Crushing at speeds of 4 m s^{-1} would cause the axial laminae segments to move across the platen at a much faster speed without the possibility of static frictional forces occurring. Hence, the maximum load sustained by

individual segments of the axial laminae would tend to be less and may not be sufficient to cause fibre fracture.

A further factor relating test speed to the fracture of the axial laminae may be the effect of friction on the bend radius of the axial laminae. As discussed in section 5.5.2, compressive kinking in the tube wall initiates cracking in the axial laminae during bending. Friction between the segments of axial laminae and the platen may be higher during slow speed crushing. This would result in a reduced bend radius of the axial laminae and a greater degree of fracture. At higher test speeds, friction forces would be lower giving a larger radius of bending of the axial fibres thus reducing the fracture of the fibres.

Further experimental work is required to determine which, if either, of these hypotheses is correct.

A speed effect was also observed with load-displacement curves from the crush of $0^{o}/90^{o}$ tubes. Speeds of 4 m s^{-1} gave a load trace with much larger serrations than that obtained for speeds of 4×10^{-3} m s^{-1}. One possible explanation may involve the different rates of increase of the strain energy in the uncrushed portion of the tube. During slow crushing, the strain energy increases until failure occurs at the top of tube. The strain energy is reduced as a slight relaxation takes place in the uncrushed tube. The failure is of a more controlled nature, ceasing as soon as the strain energy falls to below a certain value. With higher test speeds, the strain energy increases rapidly, possibly to a value much higher than that required to initiate fracture. This results in an "excess" of strain energy in the uncrushed tube which propagates the cracks for a greater distance before the strain energy required to promote more fracture is exhausted. This hypothesis would account for the greater serrations in the load-displacement

traces, as longer cracks would temporarily reduce the load supported by the tube by a greater amount than would shorter crack lengths.

A speed effect was exhibited by the fracture toughness of the bulk resin. Resin properties are important in controlling the energy absorbed during crush, because of the many resin controlled fracture mechanisms that take place. Epoxy resins become tougher as test speed is increased with an approximately linear relationship with the log of test speed. In contrast, polyester resins show little variation of fracture toughness with test speed. This phenomenon may explain the different response, with respect to the energy absorption, of crushed tubes with polyester matrices to that of tubes with epoxy matrices. Epoxy tubes displayed similar crushing mechanisms to polyester matrix tubes, with increased fracture of the axial laminae occurring at speeds of 4×10^{-3} m s^{-1}. A significant increase in resin fracture toughness could outweigh the effects of decreasing axial laminae fracture.

The very high speed (13.8 m s^{-1}) tests have been excluded from this discussion. A completely different measurement system using accelerometers instead of load cells was used. The tubes were much longer and the cross-head displacement was not constant throughout the crush. The load traces showed serrations of a very large magnitude. The initial part of the curve was thought to be confused by a certain amount of ringing within the framework due to the impact nature of the test and the response of the instrumentation.

6.6 Description and quantitative analysis of energy absorbing mechanisms of polyester $0^{o}/90^{o}$ tubes crushed at 4×10^{-3} m s^{-1}

6.6.1 Introduction

In this section, the energy absorbed during each of the crushing mechanisms is determined. A model polyester $0^{o}/90^{o}$ tube is used with dimensions taken from several similar tubes. A value of

energy absorbed is derived for each separate mechanism based on the fracture mode and corresponding value of fracture energy obtained from the literature or experimental work. These individual values of energy are then compared in order to identify the critical areas within the crush process and to test the concept of failure against experimental results. The mechanisms as observed with SEM techniques are also briefly discussed.

6.6.2 Basic parameters of energy absorption calculations

The following parameters have been used throughout the calculations given below. They are based on measurements of $0^{o}/90^{o}$ polyester tubes. The fracture energy values are taken from the literature and are for a unidirectional composite of Pilkingtons Equerove 23/47 glass in Crystic 272 resin. The volume fraction was similar to that of the tubes. The values used are as follows:

Tube internal diameter	$\simeq$ 49.97 mm
Axial lamina thickness	$\simeq$ 1.05 mm
Hoop lamina thickness	$\simeq$ 0.83 mm
Total wall thickness	$\simeq$ 3.78 mm
Weight per unit length	$\simeq 11.4 \times 10^{2}$ g m^{-1}
Fracture toughness values for cracks parallel to the fibres:	
(a) Opening mode (G_{IC})	$\simeq$ 120 J m^{-2}
(b) Forward shear (G_{IIC})	$\simeq$ 3230 J m^{-2}
(c) Parallel shear (G_{IIIC})	$\simeq$ 2500 J m^{-2}
Opening mode, G_{IC} cracks perpendicular to fibres	$\simeq 1 \times 10^{5}$ J m^{-2}
Opening mode, G_{IC}, bulk polyester resin	$\simeq$ 100 J m^{-2}

6.6.3 Crack opening in the centre of the tube wall

During crushing, a single crack propagates through the resin-rich region between the axial laminae. As these laminae are

forced apart, the applied stress at the crack tip would be such as to promote fracture by transverse tension. The fracture surfaces, as shown by the photomicrographs in Figure 5.36, indicate, however, that shear takes place. This may be due to a non-uniform loading situation in the tube wall. As the crack grows, the fibres are cleanly debonded from the resin; no resin is left adhering to the fibres. The resin matrix is torn and sheared into large blocks between the fibres. The striations on the resin fracture surface seen in Figure 5.36(a), spread from fibre to fibre. These may be caused by a stick-slip mechanism as the crack grows through the central region. In other areas, the resin fracture surface tended to be planar without any shearing and tearing. A fracture energy value of 1500 J m^{-2} is chosen as a compromise between tensile opening (G_{IC}) and forward shear mode (G_{IIC}). For a unit length of crushed tube, the area of the centre line crack is given by πD, where D is the diameter of the centre line of the tube wall. The energy absorbed per unit weight is given by

$$\text{Energy absorbed} = \frac{\pi D}{W} \times G.$$

W is the weight per unit length and G the fracture toughness appropriate to the mechanism. When values are substituted into this equation, the energy absorbed is 0.22 J g^{-1}. This is a small energy value when compared to the energy absorption results obtained empirically. However, this is to be expected from a single crack passing through a resin-rich area with little fibre fracture.

6.6.4 Fracture in the axial region

The photomicrographs in Figures 5.24 to 5.26 show fracture surfaces similar to those obtained from short beam shear tests (Figure 5.2). In certain instances, a similar fracture morphology to 10^{o} off-axis fracture was observed. This supports the view that the

main fracture process is one of shear. The fibres are clean and free from adhering resin. The resin fracture surface is highly torn and fractured into flakes and rough blocks as the crack propagates through the lamina in the same direction as the fibres. The debonding of the fibres is so precise that an imprint suggestive of the surface coating on the fibres can be observed at the high magnification levels shown by the photomicrograph in Figure 5.26(a). Figure 5.31, a photomicrograph taken perpendicularly to the crushed axial lamina, shows the large amount of cracking that occurs. The axial lamina is split into layers, each of a few fibres. It is difficult to estimate the number of cracks that occur in the crushed lamina. From the micrographs, five fibres is a good estimate of the bundle thickness. For a volume fraction of 0.50 and fibre diameter of 0.015 mm, the separation between the fibres is 0.0038 mm. This assumes square packing and gives a fibre plate thickness of 0.094 mm. Hence for a lamina thickness of 1.05 mm the number of cracks is approximately 11. Taking the fracture toughness as 3230 J m^{-2}, the energy absorbed per unit weight for both inner and outer axial laminae during bending in shear mode is 10.5 J g^{-1}. This value does not take into account the tensile failure which was observed in several instances (Figure 5.29). The contribution of the tensile failure to the energy absorbed is assessed at the end of this section.

Translaminar cracking, as shown in Figure 5.27, occurs in the outer axial lamina owing to the expansion of the lamina as crushing takes place. Photomicrographs shown in Figure 5.32 indicate the fracture mechanism to be a mixture of shear, characterised by a torn resin surface, and a smoother planar type of resin fracture. Little evidence of fibre fracture was observed. The fibres were clean and free from adhering resin. Due to the mixed mode of fracture, a fracture energy

of 1500 J m^{-2} is used to determine the energy absorbed. The fibre bundle width is estimated from Figure 5.31 as an average of 20 fibres, giving a 0.376 mm wide bundle. Using these values for a lamina 1.05 mm thick, the specific energy absorbed is <u>0.62 J g^{-1}</u>.

The fracture mechanisms and energy absorption of the inner axial lamina are more difficult to assess. Additional crushing and bending takes place as the axial lamina inverts into the centre of the tube. The reduction in circumference as this occurs results in shear fracture as seen in Figures 5.33(b) and 5.34(a). This fracture mechanism is partially obscured by debris from other fracture processes. Owing to the complex processes which occur as further fracture takes place, an estimate of the energy absorbed has to be made. This is because the fracture processes are very complex involving crushing, interpenetration, frictional sliding and bending. Using calculations on the outer axial laminae, therefore, an estimated value of <u>1.24 J g^{-1}</u> is proposed.

In a previous section (5.5.2), the tensile fracture of the axial fibres was discussed. This was initiated by compressive kinking of the axial fibres (Figures 5.29 and 5.30). These tensile cracks occurred every 2-3 cms in a short arc of the crushed axial lamina. In other regions of the axial lamina, this type of fracture did not occur; the fibres bending but not fracturing. This phenomenon is shown in Figure 5.4. For the purposes of calculation, a crack is taken as occurring every 2 cms, for 50% of the tube circumference. A value of 1×10^5 J m^{-2} is taken for the fracture toughness of the material during this type of fracture. This would be slightly high as the initial stages of crack growth are not tensile in nature. Calculations give an energy absorption for thus process as <u>0.78 J g^{-1}</u>.

6.6.5 Fracture mechanisms in the outer hoop lamina

Several fracture mechanisms occur in the outer hoop lamina during crush. These are tensile fracture (Figure 5.37), interlaminar fracture between the hoop and axial laminae (Figure 5.39), and intralaminar fracture of hoops (Figure 5.40).

Tensile fracture occurs as the hoop lamina expand owing to the forces applied by the outer axial lamina when bending outwards. The photomicrograph in Figure 5.37(b) shows a typical tensile fracture from a glass-polyester composite. Fibre pull-out can also be seen in Figure 5.37(b). The mechanism is not purely tensile, as, towards the end of the hoop fracture, the crack tends to grow partially parallel instead of perpendicular to the fibres. This can be seen in Figure 5.37(a).

Interlaminar fracture between the hoops and axial laminae does not take place at the interface between the two laminae, but is displaced by a few fibres. The fracture mechanism is one of shear, characterised by clean fibres without adhering resin and a torn blocky resin fracture surface. This is shown in Figure 5.39(b). Coincident with this fracture process is intralaminar shear of the hoop lamina. This is caused by the transverse compressive load on the hoop lamina owing to the axial lamina bending outwards and downwards. The fracture surface is planar with light striations on the resin. The crack direction, perpendicular to the fibres, does not coincide with the striations between the fibres. These indicate a crack direction parallel to the fibres. No explanation can be given for this anomaly.

Calculation of energy absorbed values for each mechanism is straightforward. Tensile fracture of the outer hoops, as observed from crushed tubes, occurs approximately ten times in the tube circumference.

The appropriate fracture toughness value for this process is 1×10^5 J m^{-2}. This data gives an energy absorption value of 0.72 J g^{-1}. This value is low as the area of fracture is small. Similarly, the fracture energy for interlaminar shear of the hoops can be calculated as 0.49 J g^{-1}. The fracture toughness value used in this case was 3230 J m^{-2} as the fracture process was mainly shear. Intralaminar fracture of the hoops is more difficult to quantify as the fracture mechanism is not easily identifiable. An estimate of 1500 J m^{-2} is used in the calculation of energy absorbed. It is also difficult to accurately estimate the number of cracks in the hoop lamina during unit length of crush. A single crack every millimetre at 45^{o} to the tube wall was used as the basis for the calculation. This gave an energy absorption value of 0.29 J g^{-1}.

6.6.6 Fracture mechanisms in the inner hoop lamina

Major differences occur between the fracture of the inner and outer hoop laminae. The inner hoops are compressed by the inner axial lamina bending inwards. In order to accommodate the reduction in circumference, the hoop lamina bend and fracture. Interpenetration of the fractured segments occurs because of the limited volume available in the tube. These mechanisms are complex, involving many load and fracture situations. The complete study of these mechanisms is outside the scope of this work. The amount of fracture caused by bending is estimated as double that of the outer hoop lamina. Thus the energy absorbed was estimated as 1.4 J g^{-1}.

The inter-and intralaminar fracture mechanisms of the inner hoop lamina are similar to those of the outer hoop lamina. Energy absorbing values of 0.49 J g^{-1} and 0.29 J g^{-1} were obtained.

6.6.7 Micro-fracture processes

The remaining fracture mechanism for discussion produces large amounts of small particles of resin and glass during the crushing process. With the SEM studies, this effect can be seen in the bundle wedge, Figure 5.42; the inner axials, Figures 5.33 and 5.34, and in the inner hoops, Figure 5.38. An analysis of the size, shape and amount of the particles would be required in order to provide an accurate estimate of the absorbed energy. This has not been possible. The influence on the measurements of overall energy absorbed, however, can be assessed by a semi-theoretical calculation.

Consider a cube of glass-resin composite with a glass volume fraction of 0.5. The density will be 1.9 g cc^{-1}, if this cube has an edge dimension of 1 mm and is subsequently crushed into cuboid particles each with a side dimension of one μm, the result is 10^9 cubes with a total surface area of 6×10^3 mm^2. If the surface energy is taken as 100 J m^{-2}, the total energy involved with this fracture is 0.6 joules. This takes place in an original one millimetre square cube with a weight of 1.9×10^{-3} grams. The energy absorption per unit weight is 315.8 J g^{-1}. In a similar manner, if the crush debris from a tube consists of 10 μm cubes, then the required energy is reduced to 31.6 J g^{-1}.

The above calculations illustrate the effect of a crushing process which produces a large volume of small particles. Observations of the relevant photomicrographs indicate that the particles have an irregular shape and size, but generally the size is in the order of ten to fifteen μm. The proportion of tube material crushed to this particle size is difficult to determine, an estimate being 10% which gives a value of approximately <u>3.1 J g^{-1}</u> for energy absorption in micro-fracture processes.

6.6.8 Assessment of energy absorption calculations

Summation of the fracture processes previously described should give the value of the energy absorbed per unit weight of crushed tube. These values are summarised below:

Centre line cracking between axials	0.22 J g^{-1}
Interlaminar shear cracking during bending of the axial	10.50 J g^{-1}
Translaminar cracking of the outer axials	0.62 J g^{-1}
Fracture of the inner axials	1.24 J g^{-1}
Tensile cracking (limited) of the inner and outer axials	0.78 J g^{-1}
Outer hoops tensile fracture	0.72 J g^{-1}
Interlaminar hoop fracture (outer)	0.49 J g^{-1}
Intralaminar hoop fracture (outer)	0.29 J g^{-1}
Inner hoop bending/interpenetration/fracture	1.40 J g^{-1}
Interlaminar hoop fracture (inner)	0.49 J g^{-1}
Intralaminar hoop fracture (inner)	0.29 J g^{-1}
Microfracture processes (estimated)	3.10 J g^{-1}
Total energy absorbed	20.14 J g^{-1}

This is low when compared to experimentally obtained values of 70 J g^{-1}. Several probable errors are immediately obvious. Energy is absorbed in several areas not studied. These include friction between the tube and the cross-head platen; friction within the crush zone between fractured segments of the tube; acoustic emission and increase in temperature. The higher speed tests (4 m s^{-1}) were all characterised by an increase in the temperature of the crushed region. This was attributed to friction effects between the crushed zone and the cross-head platen.

During crushing acoustic emission occurs, which was attributed to the fracture of the hoop fibres. The energy required to

produce noise is negligible hence this would only account for a small amount of the energy deficit.

The loss of energy from the system as strain energy in segments of crushed tube is another possible source of error. The crushing process in a tube is uncontrollable in nature with fracture processes occurring almost at random. In a "classic" tensile test, with controlled crack growth, the strain energy in the test specimen is considered to be totally absorbed in the production of the fracture crack. This ignores or minimises energy that is lost to the system by for example, acoustic emission, heat and friction. With a "classic" compression test the same principles apply. Providing no energy is lost from the system, the strain energy in the specimen is converted into fracture.

However, in crushing a tubular specimen, energy is lost from the system. Fragments contain more strain energy than that required to initiate and propagate the single crack which separates the fragment from the tube wall. The strain energy is related to volume whilst the fracture energy measurements are related to area. This implies that the technique of summing individual fracture energy measurements may only be valid for a simple specimen shape, particularly when energy losses can be minimised or quantified.

It is possible to estimate the loss of energy from the crushed tube as strain energy in material. If a section of the hoop lamina is considered, this can be taken as becoming separated from the tube wall with a single tensile fracture. The failure stress is denoted by σ and the failure strain by ϵ. The cross-sectional area is given by $b \times d$ and the tube circumference is D. The weight of this hoop section is given by:

$$\text{Section weight} = b\ d\ \pi\ D\rho$$

where ρ is the density.

The strain energy required to cause tensile failure is given by;

$$SE = \tfrac{1}{2}\ \sigma\ bd\ \varepsilon\ \pi\ D$$

Hence, if the contribution of energy to crack propagation is ignored, then the strain energy per unit weight is given by:

$$\text{Specific SE} = \tfrac{1}{2}\ \frac{\sigma\ \varepsilon}{\rho}$$

Taking the tensile failure stress of unidirectional glass polyester as 700 MPa, failure strain as 2% and density as 1.8 g cm^{-3}, then the strain energy per unit weight is 3.9 J g^{-1}.

This value is small when compared to the discrepancy between empirical and calculated energy absorption values, but comparable to that obtained with other energy absorbing mechanisms. The example using the tensile fracture of a hoop lamina gives a higher value of strain energy when compared to other failure mechanisms, such as shear, owing to the differences in failure stress of the various fracture mechanisms. This indicates that the loss of strain energy from the system as fragments of crushed material cannot account for all the discrepancy between values.

The remaining energy absorbing process to be considered is that of frictional effects. During the crush of a $0^{o}/90^{o}$ tube, the axial laminae bend and pass across the surface of the cross-head platen. They then either invert into the tube cavity or progressively move away from the tube. During this process, frictional forces act on these fractured laminae, with the direction of the frictional force opposing the motion of the axial lamina relative to the cross-head platen. This is shown diagrammatically in Figure 6.1.

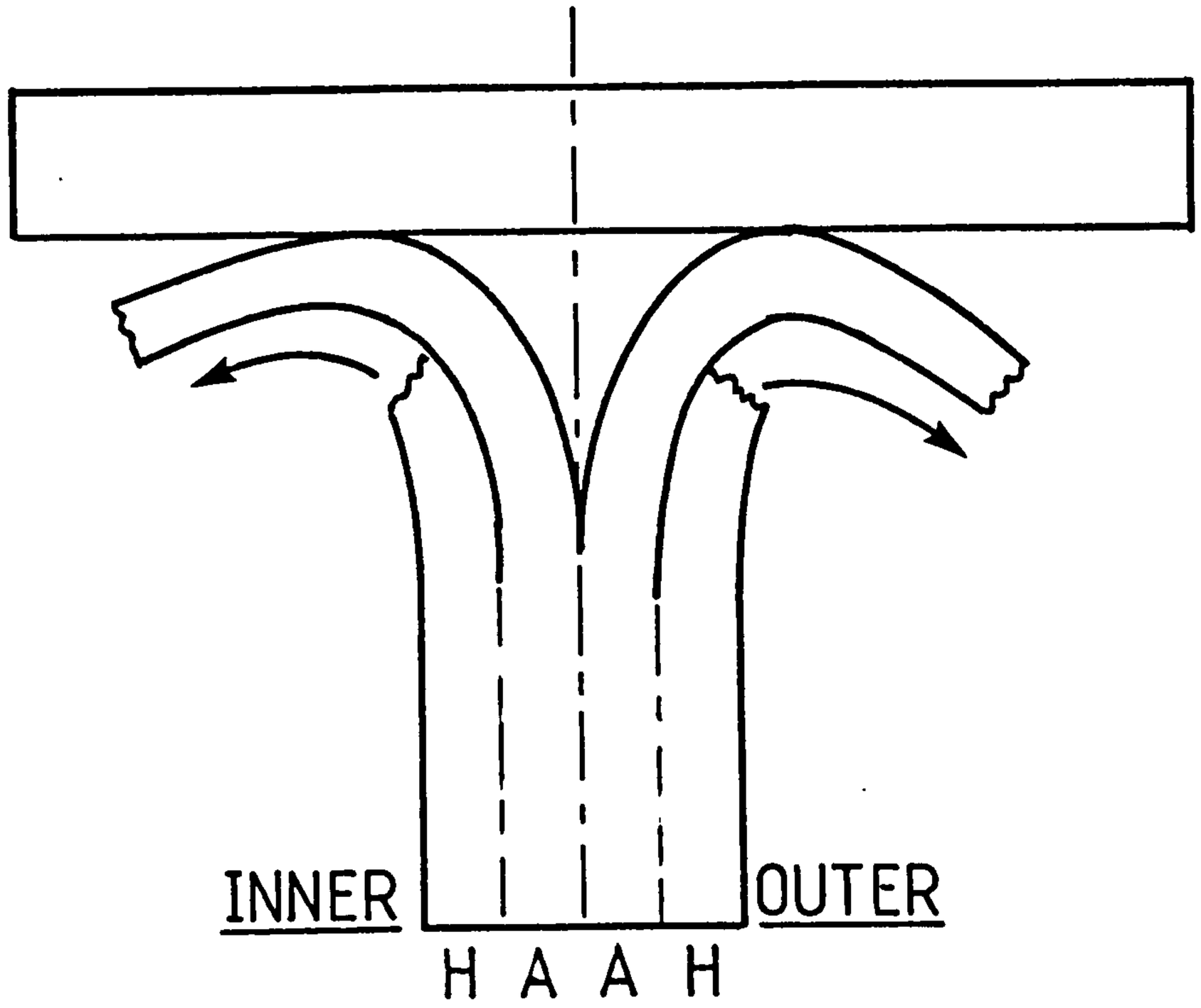

(a) Motion of axial laminae relative to cross-head platen.

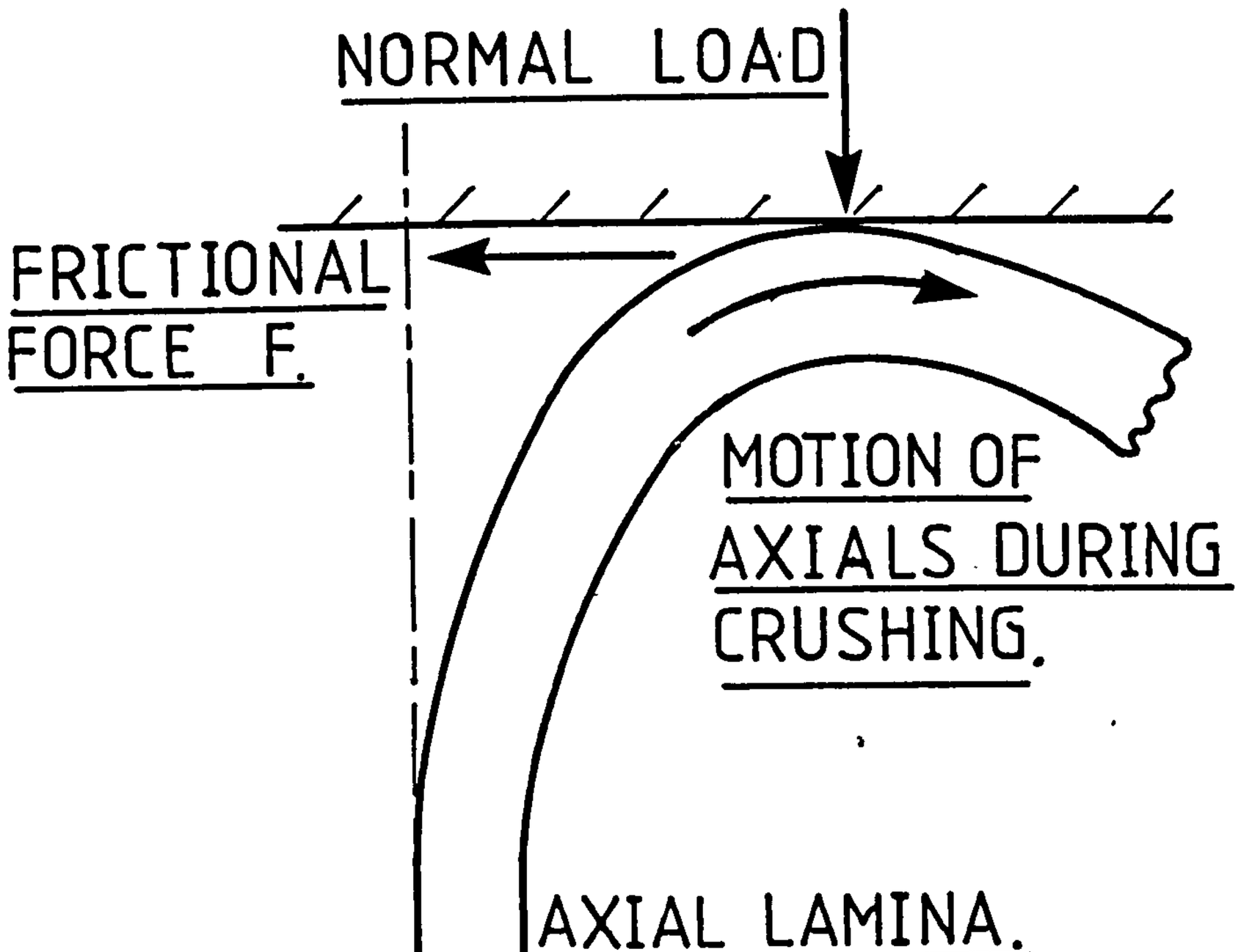

(b) Action of frictional forces on an axial lamina.

Fig. 6.1. Diagram of the frictional forces on the axial laminae during crushing a 0/90 tube.

Frictional effects between any two materials are governed by several simple principles, (108). These are:

(a) The frictional force between sliding surfaces is proportional to the normal force between the surfaces.

(b) The frictional force is independent of the apparent area of contact between the two surfaces.

(c) The frictional force is independent of the velocity of sliding.

(d) The frictional force depends on the nature of the surfaces.

All these princples are only true within certain limitations. The force required to inititate sliding is always higher than that required to maintain sliding. These two cases are called static and dynamic friction. The proportionality between the applied and normal load is termed the coefficient of friction and is designated by μ. Thus one can write, with certain reservations:

$$F = \mu P$$

where F is the frictional force and P the applied normal load to the two sliding surfaces. The determination of the coefficient of friction for a crushed $0^{o}/90^{o}$ tube required a simple additional experiment to those described in Chapter 3.

A $0^{o}/90^{o}$ polyester tube, crushed at 4×10^{-3} m s^{-1} was placed on a flat steel plate similar to the cross-head platens of the test machines. The weighed tube was arranged with the crush zone in contact with the plate. Weights were placed on the uncrushed end. An increasing horizontal force was then applied to the tube using a string and pulley system. The weight at which movement commenced was noted for each load applied normal to the tube. The results are shown graphically in Figure 6.2. These give a coefficient of friction of 0.41.

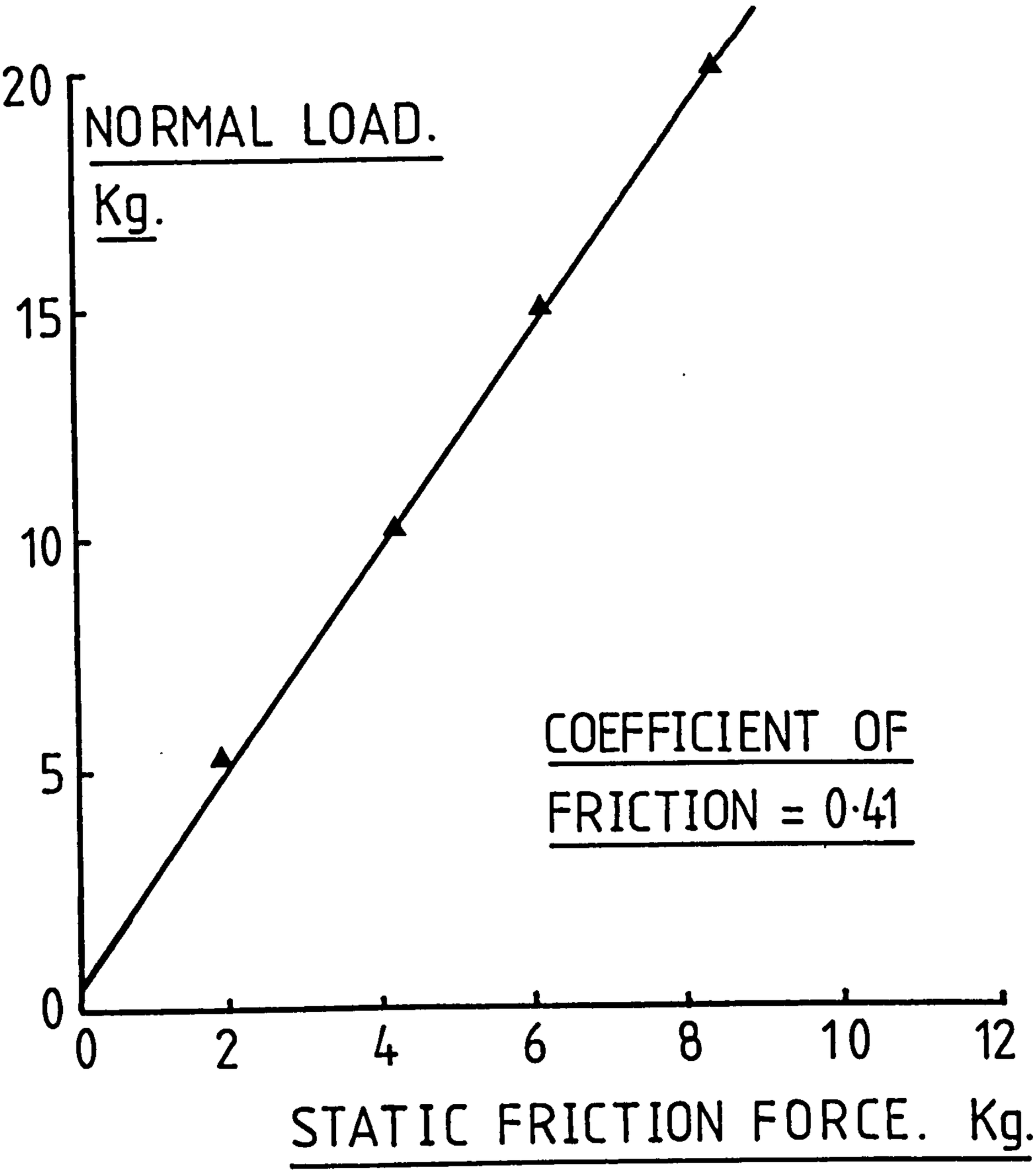

Fig. 6.2. Graph determining the coefficient of friction between a crushed 0/90 tube and a steel plate. Gradient of graph is 0.41.

Thus for a tube crushing at an average load of 70 KN, the frictional force is given by $F = \mu P$ or 28.7 KN. As this force is exerted against the motion of the fibres during crush, the energy absorbed is a product of the force multiplied by the crush distance. This can be converted into specific energy by dividing by the weight per unit length; in this case 11.4×10^2 g m^{-1}. This calculation shows the specific energy absorbed due to friction to be 25.2 J g^{-1}.

It can be seen, therefore, that friction plays a significant part in the crushing process. Furthermore, when this amount of energy is added to that of the specific energy mechanisms, the increase in calculated energy is much closer to the empirical values obtained.

Friction within the crush zone has not been considered as this would be very difficult to assess. For example, once shear has occurred in the axial laminae, the resultant thin layers must move relative to each other. Frictional forces must occur, absorbing energy. The same argument applies for other mechanisms where fractured segments of lamina slide over each other. This has been mentioned previously as occurring in the centre of the tube with fractured segments of hoop and axial laminae interpenetrating and sliding over each other.

The advantage in analysing the specific fracture mechanisms is that those mechanisms which contribute most to the overall process can be identified. These are the shear that takes place in the axial laminae during bending; the crushing, interpenetration and bending that takes place inside the tube cavity and the multitude of minor fracture processes that result in small particles of resin and glass. It must be emphasised that these values of energy for all the processes are only approximations. Fracture energy measurements derived from controlled experiments are not entirely applicable to the crushing

process. Additionally, in certain cases, estimates of the crack surface area had to be made due to the complex fracture processes occurring.

6.7 The factors affecting the crush load of polyester $0^{o}/90^{o}$ tubes

The load continuously supported by a tube during progressive crushing is a major factor in the determination of the energy absorbed. The factors controlling this load have been assessed by detailed examination of sections of the tube wall, which were placed under a load and examined by low power micrography. The load used was equivalent to that occurring during crushing. A typical photomicrograph of such a section in shown in Figure 5.43.

As previously noted, bending of the axial fibres occurs during crushing. In the loaded sections examined, this bending can be divided into two types. Initially the hoop and axial laminates each side of the centre crack line bend away from the tube wall. This bending is elastic in manner, and only occurs by a small amount. The length of the axial/hoop laminate during this part of the bending process is approximately 10.5 mm. This is indicated as '1' in Figure 5.43. During bending, the outer axial/hoop laminate moves outwards and downwards by an amount sufficient to cause failure in the hoop lamina. A similar process occurs with the inner axial/hoop laminate but with compressive failure of the hoop lamina. This process of hoop failure can be seen in Figure 5.43 by the white line in the hoop region, indicating that fracture has occurred. Thus the restraining force of the hoop lamina on the axial lamina is significantly reduced. The axial lamina then bend with intralaminar shear occurring, shown in Figure 5.43 by a light region in the axial lamina indicating that debonding has taken place. This is the second type of bending in the

axial region which now consists of many thin layers, which all bend through 90^{o} with a small radius of curvature. The crushing load on the tube is supported by the axial laminae which are displaced from the centre line of the tube wall by an offset 'a' of approximately 3.3 mm. This load acts perpendicularly to the fibre direction at the contact area and provides the bending moment for the axial/hoop laminate during the elastic part of the bending process.

The stiffness of the axial/hoop laminate is important as this controls the displacement of the laminate from the centre line of the tube wall during the initial stages of the bending process. The intralaminar shear stress is also important as this affects the ultimate fracture of the axial lamina into the thin layers which can easily bend through 90^{o}. This has been reported in published work (46) which found that interlaminar cracking was the main mechanism of failure during the crush of $0^{o}/90^{o}$ tubes constructed from many thin layers of carbon tape or cloth with epoxy resin.

As seen in the photomicrograph, the axial/hoop laminae behave in a similar manner to a beam fixed at one end with an applied load at the other end. If this is so, then it would be possible to describe and quantify the bending of a laminate using applied mechanics principles applicable to a cantilever beam. These give the relationship between the intralaminar shear stress 'τ' and the load 'F' applied to the end of a cantilever beam as:

$$\tau = \frac{3F}{2bd} ,$$

where 'b' is the breadth and 'd' the depth of the beam (109). This approach shows that the shear stress is a maximum on the neutral axis of the beam, which for a rectangular section is the centre plane.

Providing the intralaminar shear stress of the material of the cantilever beam is known, then the load required to cause fracture can be predicted. If the load that just causes shear in the axial lamina of the tube during bending is related to the applied crushing load through the bending moment and offset 'a', then the total crushing load can be predicted.

Sources of error in this proposed model are due to the constraints imposed by using applied mechanics principles. For example, beam deflections are always considered to be small and elastic in nature; point loads are applied exactly at right angles to the beam axis and beams of narrow rectangular cross-sections are used with the depth much greater than the width. Correction factors can be applied to allow for these errors. These do, however, give very complicated equations. It is also difficult to accurately relate the bending moment on the lamina due to the crush load and offset, $F_v \times a$ in Figure 5.43, with the bending moment in the lamina where shear commences. This must be done as, in order to utilise the general relationship between load and shear stress, the load on the lamina beam during shear is assumed to act perpendicularly to the beam axis.

The elastic bending of the axial/hoop laminate may also predict the crush load, using the criterion of hoop laminae fracture. As the axial/hoop laminate bend either inwards or outwards, the hoop laminae are loaded in compression or tension. These hoop laminae then fail at a strain governed by the material. This can be related to the degree of displacement of the laminate from the centre line of the tube wall. The deflection 'y' of a cantilever beam is given by applied mechanics (109) as;

$$y = \frac{FL^3}{3EI} ,$$

where 'F' is the load perpendicular to the beam, 'L' the length, 'E' the tensile modulus and 'I' the second moment of area. If the tensile strain at failure for the outer hoop lamina is known, together with the modulus of the axial/hoop laminate, then the load applied to the composite cantilever beam to cause hoop failure can be predicted. By using this equation and relating the bending moment on the laminate to the moment of the crush load and offset, the total crushing load on the tube can be determined.

As an example, if the tensile strain at failure for the outer hoop lamina is taken as 2%, then the calculated deflection of the axial/hoop laminate at which fracture of the hoop lamina would occur is 0.45 mm. This compares favourably to empirical measurements of 0.6 mm taken from loaded specimens.

Similar problems to those discussed earlier in this section may also occur in relating the predicted bending load on the elastic part of the beam to the bending moment of the crushing load and offset. It would appear, however, that several material properties are predicted as being important in the crushing mechanisms of $0^{o}/90^{o}$ tubes. The intralaminar shear stress is critical in determining the crushing load. This is a restatement of an earlier conclusion drawn from different experimental work. This material parameter controls the load at which shear commences during the bending of the axial laminae. Thus a high value for interlaminar shear stress corresponds to a high value for the bending load before fracture occurs. The tensile modulus is also shown to be important in the control of the displacement of the axial/hoop laminate. A stiff laminate bends less for a given applied load, hence the stress and resultant strain in the hoop laminae are minimised. The restraint provided by the hoop laminae on the axial laminae is thus increased resulting in a higher crush load.

The models discussed above show a route whereby an approach using applied mechanics may be used to predict the crush load. However, in order to obtain accurate results, the relationships between the applied crush load and the bending load on the laminae must be quantified and correction factors used to allow for departures from the ideal case of a cantilever beam.

6.8 Critique of present work and suggestions for further research

Several areas for further work have already been indicated in previous chapters. As with most research programmes, questions are raised by the results of experimental work. Some of these have yet to be answered.

Prediction of crush load using the approach derived from mechanics of materials may provide the means of relating easily determined material properties to crush load and energy absorption. Some assumptions in the model, because of constraints in this approach, require quantifying. These include the relationship between the direction of the applied load and the assumption that the load is always applied perpendicularly to the beam at all times. Once an accurate model is produced, then this can be tested by the use of various reinforcements such as glass, carbon and kevlar, combined with polyester and epoxy matrices. The main properties of interest would be the modulus and the intralaminar shear stress.

From the limited results comparing the effects of matrix properties on the energy absorption of crushed tubes, it would appear that resin fracture toughness, modulus and tensile strength are all important. The interrelationships between each of these three properties and energy absorption have not been fully quantified. A programme involving several chemically similar resins with different

physical properties, tested in bulk form to give modulus, fracture toughness, etc. and as matrices in $0^{o}/90^{o}$ tubes to give energy absorption, would indicate the relative importance of each property.

The influence of the strain energy and stiffness of the uncrushed tube on the shape of the load-displacement trace has not yet been investigated. As the crush progresses, the size and shape of the crush zone remains constant, the uncrushed tube becomes shorter and the stiffness increases. Hence, the slope of the serrations on the load-displacement trace should also increase. An investigation into this facet of crushing would involve either crushing tubes identical in all respects except for original length or crushing a long tube to complete disintegration. In either case, the load trace would require careful monitoring.

As the amount of crushed tube decreases, the available strain energy is correspondingly reduced. This could reduce the total height of the serrations, as the driving force to promote the fracture processes is being progressively reduced. As demonstrated, however, the amount of energy required for each fracture mechanism is small, so this effect may not be easily observable.

The effect of test speed on the energy absorbed of $0^{o}/90^{o}$ tubes is different for tubes with epoxy or polyester matrices. The reduction in the amount of fracture in the axial laminae as test speed increases is one area where less energy is absorbed during crushing. Work on specific fracture mechanisms shows, however, that only small amounts of energy can be attributed to this fracture mechanism. Epoxy resin tubes also exhibit a reduction in axial fracture as speed increases, but show an increase in energy absorption. This is attributed to the increasing fracture toughness of epoxy resin with

test speed. This phenomenon does not occur with polyester resin which exhibits a fracture toughness independent of speed. A complete explanation of these effects requires further work. Scanning electron microscopy may indicate some of the speed effects with respect to crush mechanisms. Resin fracture toughness at a test speed of 4 m s^{-1} must also be determined.

Several topics within this thesis have only been briefly examined. A cursory study of the failure mechanisms of angle-wound tubes has been presented. Greater understanding of the crush mechanisms would require experimental work similar to the scanning electron and optical microscopy carried out on $0^{o}/90^{o}$ tubes.

The energy absorbed due to friction between the axial laminae and cross-head platen has been estimated. These frictional forces, however, may affect the bending mechanisms. For example, a high frictional force will tend to decrease the bend radius of the axial laminae, which would have the same effect as increasing the stiffness of the laminae during bonding.

As described earlier, the surface of the crushed axial laminae is smoother at a test speed of 4 m s^{-1} than at 4×10^{-3} m s^{-1}. This indicates that the frictional forces between the cross-head platen and a tube crushed at 4 m s^{-1} may be less than with a tube crushed at 4×10^{-3} m s^{-1}. As the coefficient of friction between two surfaces depends on the surface roughness, this inference requires further investigation.

Internal friction, i.e. the friction between crushed segments of the tube, has not been considered as an energy absorbing mechanism. Obviously friction must occur, especially during the inversion of the laminae into the centre of the tube. The measurement of these effects in terms of energy absorption, however, does not appear to be feasible.

The reproducibility of results give some cause for concern. With inherently brittle composite materials like glass and resin, some scatter is inevitable. The manually controlled manufacture of $0^{o}/90^{o}$ tubes requires conversion to automatically controlled winding. This would improve consistency between specimens. The effect of manufacturing techniques on scatter can be assessed by comparison between energy absorption results of angle-wound tubes made under machine control, (Figure 4.2) and $0^{o}/90^{o}$ tubes made partially under machine control and partially manually, (Figure 4.14). The scatter of results is less with angle-wound tubes. Batch to batch variations in resins and glass also occurred, thus increasing the possibility of scatter.

A possible solution to reduce the effects of scatter on the mean empirical values is to increase the number of specimens tested for a given set of conditions. The time factor, however, is a major constraint in increasing the number of test results in order to reduce the effects of scatter on the mean values. Any improvement in this value has to be balanced against the limitations of time and resources.

The reproducibility of results for standard $0^{o}/90^{o}$ tubes is estimated as being within the range $\pm$ 4 J g^{-1} for specimens taken from the same original tube, whilst specimens taken from different tubes exhibit a slightly larger scatter.

CHAPTER 7 - CONCLUSIONS

The crushing mechanisms of filament-wound tubes tested in axial compression have been studied at cross-head speeds from 0.33×10^{-3} to 13.8 m s^{-1}. Values of specific energy absorbed have been presented for tubes with various fibre orientations and matrices. All tubes were pre-triggered by a bevel cut into the tube wall. Crushing was, with one exception, progressive from the triggered end. The crush mechanisms were examined by optical and scanning electron microscopy.

The crushing mechanisms were found to be complex with many different fracture processes occurring simultaneously. For a polyester $0^{o}/90^{o}$ tube tested at 4×10^{-3} m s^{-1}, these were as follows:

(a) Centre-line cracking between the axial laminae.

(b) Elastic bending of the axial laminae inwards and outwards, placing a load on the restraining hoop laminae. This load was tensile in the outer and compressive in the inner hoop laminae.

(c) Fracture of the outer hoop lamina with tensile, interlaminar and intralaminar cracking. The inner hoop lamina failed with inter- and intralaminar shear. Fracturing of the inner hoop lamina was also caused by bending owing to the reduction in circumference of the inner regions of the wall during crushing.

(d) With the hoop restraint removed, the axial laminae bent through 90^{o}, fracturing by intralaminar shear into many thin layers.

(e) Translaminar splitting of the outer axial lamina owing to an increasing circumference. This occurred with little

fibre fracture.

(f) Limited cracking, normal to the fibre direction, in the axial laminae. This occurred with fibre fracture and was initiated by a kinking mechanism in the tube wall which progressed through the laminae during the bending process.

(g) Inversion of the inner axial lamina into the centre of the tube. This was accompanied by interpenetration and further fracture of the crushed lamina segments.

(h) Further, bending, fracture and interpenetration of the inner hoop lamina inside the tube cavity, because of the limited volume available.

(i) Formation of debris consisting of small particles of glass and resin, by the fracture processes. Some of this accumulated in the V-shaped area between the axial fibres, forming a wedge of material.

The general shape of the load-displacement traces during crushing was independent of fibre orientation, resin properties and test speed. These traces were all serrated about a constant average load. The magnitude and shape of these serrations were found to depend on the test speed for $0^{o}/90^{o}$ tubes, and on fibre orientation for helically wound tubes.

The energy absorption of polyester $0^{o}/90^{o}$ tubes decreased with increasing test speed. The reverse occurred with epoxy $0^{o}/90^{o}$ tubes. No firm conclusions can be drawn as to the causes of the different rate sensitivities of polyester and epoxy tubes. The rate sensitivity of the mechanism of fracture of the axial laminae, and also of the fracture toughness of the bulk resins, were thought to be contributory factors. The fracture toughness of epoxy (MY 750) resin

increased with test speeds from 0.5 x 10^{-3} m s^{-1} up to 1 m s^{-1}; however with polyester (Crystic 272) resin there was little variation with speed.

Modification of Crystic 272 polyester resin with 10% by volume of CRC 1080 gave an improvement of 20% in the energy absorption of tubes at a test speed of 4 x 10^{-3} m s^{-1}. This improvement did not occur with tubes tested at 4 m s^{-1}. Flexibilisation of Crystic 272 by Crystic 586 at levels up to 40% by volume had little effect on the energy absorption of tubes. Above 40% by volume the energy absorption was reduced. This was true for all test speeds. Flexibilisation of epoxy (MY 750) by 50% by volume of CY 208 increased the energy absorption at all test speeds. The bulk resin properties of fracture toughness, tensile modulus and tensile strength were important factors in the energy absorption of crushed tubes. However, no firm conclusion can be made as to which property was the most important.

Energy absorption in helically wound tubes was sensitive to the winding angle. This was due to the dependence of the crush mechanism on the winding angle. These mechanisms varied considerably from tensile fracture of hoop laminae to bending and fracture of laminae plates of varying sizes and stiffnesses. Tubes with axially orientated fibres crushed non-progressively with longitudinal cracking down the fibres. The energy absorption was low.

The individual mechanisms of fracture of polyester $0^{o}/90^{o}$ tubes were assessed on the basis of the energy required to cause each specific mechanism. The total calculated energy for all the fracture processes was low compared to empirical values. Friction between the axial laminae and the cross-head platen absorbed significant amounts of energy during the crush process, which was comparable to the total energy absorbed by the fracture mechanisms. Comparisons of

individual fracture processes indicated that intralaminar shear in the axial laminae was the major energy-absorbing process; however, many estimates were made in the calculations.

Studies of loaded sections from the crush zone supported the initial concepts of crushing. These indicated that the intralaminar shear strength and the tensile modulus were important material properties during crushing. This is in agreement with published literature (46).

Filament-wound composite tubes tested in axial compression possess the ability to absorb large amounts of energy with a controlled progressive crushing mechanism. On a specific basis, the energy absorption can be comparable to, or may exceed, that of mild steel.

As a final comment, even though composite materials can surpass convential materials, many factors have to be considered before their utilisation in automotive structures. Among these, the most important is the non-technical requirement of ease of manufacture and cost.

REFERENCES

1. Griffith, A.A., Phil. Trans. R. Soc., A221, (1922), 163.

2. Ainsworth, L., Composites, 8, (1977), 14.

3. Rosato, D.V. and Grove, C.S., "Filament winding. Its development, manufacture, applications and design." Wiley and Sons, New York, (1964).

4. Oleesky, S.S. and Moram, J.G., "Handbook of reinforced plastics." Reinhold, New York, (1964).

5. Jube, G., 20th Ann. Conf. Reinforced Plastics/Composites Inste., SPI, (1965), Sect. 16B, 1.

6. Harwood, J.J., Robertson, R.E. and Beardmore, P., "New developments and applications in composites." Conf. Proc. AIME, (1978), 299.

7. Charlesworth, D., Mat. in Engng., 2, (1981), 149.

8. Coppa, A.P., NASA TN-D1510, (1962).

9. Redwood, R.G., J. R. Aeronaut. Soc., 68, (1964), 418.

10. Hull, D. et al, "Resin profile.", Univ. Liverpool, Dept. Metallurgy and Material Science, (1979).

11. Kirk, J.N., Munro, M. and Beaumont, P.W.R., J. Mat. Sci., 13, (1978), 2197.

12. Beaumont, P.W.R. and Harris, B., J. Mat. Sci., 7, (1972), 1265.

13. Marston, T.U., Atkins, A.G. and Felbeck, D.K., J.Mat. Sci., 9, (1974), 447.

14. Kelly, A., Proc. R. Soc. London, Ser.A. 319, (1970), 95.

15. Piggott, M.R., J. Mat. Sci., 5, (1970), 669.

16. Outwater, J.O. and Murphy, M.C. 25th Ann. Conf. Reinforced Plastics/Composites Inste., SPI, (1969), Sect. 11C.,

17. Rosen, B.W., "Mechanics of composite strengthening in fibre composite materials." ASM, (1965), 37.

18. Timoshenko, S., "Theory of elastic stability." McGraw-Hill, New York, (1936).

19. Lager, J.R. and June, R.R., J. Composite Mat., 3, (1969), 48.

20. Kulkarni, S.V., Rice, J.S. and Rosen, B.W., Composites, 6, (1975), 217.

21. Piggott, M.R. and Harris, B., J. Mat. Sci., 15, (1980), 2523.

22. Ewins, P.D. and Ham, A.C., TR 73057, RAE, (1973).

23. Hancox, N., J. Mat. Sci., 10, (1975), 234.

24. Argon,A.S., Fracture of composites. Treatise of material science and technology, VI, Academic Press, New York, (1972).

25. Chaplin,C.R. J. Mat. Sci., 12, (1979), 347.

26. Hull, D.,"An introduction to composite materials.", Cambridge Univ. Press. Cambridge, (1981).

27. Greszczuk, L.B., AGARD Conf. Proc., (1974), Paper 12.

28. Gatward, C.H., Private communication.

29. Phillips, D.C. and Wells, G.M., J. Mat. Sci. Letters, 1, (1982), 321.

30. Marom, G. and White, E.F.T., J. Mat. Sci., 7, (1972), 1299.

31. Scott, J.M. and Phillips, D.C. J. Mat. Sci., 10, (1975), 551.

32. Corten, H.T., "Modern composite materials." Eds. Broutman, L.J. and Krock, R.H., Chap. 2, Addison-Wesley, London, (1967).

33. Fried, N. 20th Ann. Conf. Reinforced Plastics/Composites Inste., SPI, (1965), Sect. 1C..

34. Adams, D.F. and Doner, D.R., J. Composite Mat. 1, (1967), 4.

35. Bader, M.G., Bailey, J.E. and Bell, I., J. Phys. D. Appl. Phys., 6, (1973), 572.

36. Markham, M.F. and Dawson, D., Composites, 6, (1975), 173.

37. Dharan, C.K.H., J. Mat. Sci., 13, (1978), 1243.

38. Johnson, W. and Reid, S.R., Appl. Mech. Rev. 31, (1978), 277.

39. Alexandra, J.M., Q. J. Mech. Appl. Math., XIII, Pt. 1, 10 (1960), 10.

40. Pugsley, Sir A. and Macaulay, M., Q. J. Mech. Appl. Math., XIII, Pt. 1, 10, (1960), 1.

41. Thornton, P.H. and Magee, C.L., J. Eng. Mater. Tech.,Trans. ASME, Ser. H, 99, (1977), 114.

42. Soden,P.D., Al Hassani, S.T.S. and Johnson, W., "Mechanical properties at high strain rates." Inste. Phys. Conf. (1974), 327.

43. Magee, C.L. and Thornton, P.H., SAE 780434 (1978).

44. Hull, D. "Progress in science and engineering of composites." Proc. ICCM, No. IV, Tokyo, (1982), 861.

45. Jahnle, H.A., "Feasibility study of plastic automotive structure." DOT, HS 801771, (1975).

46. Thornton, P.H., J. Composite Mat., 13, (1979), 247.

47. Gordon, J.E., "Structures." Penguin Books, Harmondsworth, (1978), 285 - 290.

48. Kirsch, P.A. and Jahnle, H.A., SAE 810233, (1981).

49. Kelly, A., "Strong solids." Clarendon Press, Oxford, (1973).

50. Young, R.J., "Developments in polymer fracture, 1." Ed.. Andrew, E.H., Applied Science, Barking, (1979).

51. Paris, P.C. and Sih, G.C., ASTM STP 381, (1964).

52. Liebowitz, H. (Ed.),"Fracture" Vol. VIII, Chap. 9., Carter, H., "Fracture mechanics of composites." Academic Press, New York, (1972).

53. Irwin, G.R., "Encyclopedia of physics." Vol. VI, Springer, Berlin, (1959).

54. Irwin, G.R., TAM Report 213, Univ. Illinois, (1962).

55. Smith, G., Green, A.K. and Bowyer, W.H., Ann. Conf. Stress Analysis Group, Inste. Phys., Sheffield, (1976), 271.

56. William, J.G., Adv. Polym. Sci., 27, (1978), 69.

57. Phillips, D.C. and Scott, J.M., J. Mat. Sci., 9, (1974), 1202.

58. Yamini, S. and Young, R.J., J. Mat. Sci., 14, (1979), 1609.

59. Selby, K. and Miller, L.E., J. Mat. Sci., 10, (1975), 12.

60. Phillips, D.C. Scott, J.M. and Jones, M.J., J. Mat. Sci., 13, (1978), 311.

61. Meeks, A.C., Polymer, 15, (1974), 675.

62. Mostovoy, S. and Ripling, E.J., J. Appl. Polym. Sci., 10, (1966), 1351.

63. Mostovoy, S. and Ripling, E.J., J. Appl. Polym. Sci., 15, (1971), 641.

64. Christianson, A. and Shorthall, J.B., J. Mat. Sci., 11, (1976), 1113.

65. Griffith, R. and Holloway, D.G., J. Mat. Sci., 5 (1970), 302.

66. Leevers, P.S., J. Mat. Sci., 17, (1982), 2469.

67. Andrews, E.H. and Stevenson, A., J. Mat. Sci., 13, (1978), 1680.

68. Yamini, S. and Young, R.J., J. Mat. Sci., 15, (1980), 1814 (Part 1). and 1823 (Part 2).

69. Bascom, W.D., Cottington, R.L., Jones, R.L. and Peyser, P., J. Appl. Polym. Sci., 19, (1975), 2545.

70. Bascom, W.D., Ting, R.Y., Moulton, R.J., Riew, C.K. and Siebert, A.R., J. Mat. Sci., 16, (1981), 2657.

71. Tattersall, H.G. and Tappin, J. J. Mat. Sci., I, (1966), 296.

72. Beaumont, P.W.R. and Phillips, D.C. J. Mat. Sci., 7, (1972), 682.

73. Ting, R.Y. and Cottington, R.L., J. Appl. Polym. Sci., 25, (1980), 1815.

74. Owen, M.J. and Rose, R.G., J. Phys. D. Appl. Phys., 6, (1973), 42.

75. Wu, E.M. and Reuter, R.C., TAM Report 275, Univ. Illinois, (1965).

76. McKinney, J.M., J. Composite Mat., 6, (1972), 164.

77. Phillips, D.C. and Tetelman, A.S., Composites, 3, Sept., (1972), 216.

78. Harris, B., Morley, C. and Phillips, D.C., J. Mat. Sci., 10, (1975), 2050.

79. Murphy, N., Private communication. Univ. Liverpool.

80. Hertzberg, R.W., "Deformation and fracture mechanics of engineering materials." Wiley and Sons, New York, (1976), 35 - 37.

81. Armenakas, A.E. and Sciammarella, C.A., Exp. Mech. 13, Oct. (1973), 433.

82. Cameron, N.M., TAM Report 274, Univ. Illinois, (1965).

83. Otto, W.H., Owens Corning Fiberglass Corp., AD 228851, Contract No. NOas. 58-841-e.

84. Morrison, A.R. et al, Owens Corning Fiberglass Corp., ASD TDR 62747, (1972).

85. Frickett, P.J. et al, Owens Corning Fiberglass Corp., TR 60-24, (1960).

86. Johnson, A.F., "Engineering design properties of GRP." British Plastics Federation, London, (1979).

87. Harding, J. and Parry, T., Contract No. AT 2057058 NCRE, Dept. Eng. Sci., Univ. Oxford, (1975).

88. Harding, J., "The effect of dynamic loading on the mechanical properties of GRP." Dept. Eng. Sci., Univ. Oxford.

89. Amijima, S. and Fujii, T., Proc. 3rd Int. Conf. on Composite Materials, August (1980), 399.

90. Daniel, I.M., LaBedz, R.H. and Liber, T., Exp. Mech. 21 (1981), 71.

91. Daniel, I.M. and Liber, T., IITRI Report D607-IV for NASA CR 135087, Oct. (1973).

92. Rotem, A. and Lifshitz, J.M., 26th Ann. Conf. Reinforced Plastics/Composites Inste., SPI, (1971), Sect. 10G.

93. Broutman, L.J. and Mallick, P.K., 30th Ann. Conf. Reinforced Plastics/Composites Inste., SPI, (1975), Sect. 9C.

94. Barker, A.J. and Beeby, M.E., 29th Ann. Conf. Reinforced Plastics/Composites Inste., SPI, (1974), Sect. 21B.

95. Chou, S.C., Robertson, K.D. and Rainey, J.H., Exp. Mech. 13, (1973), 422.

96. Technical information. FIS 1050, Fiberglass plc., (1977).

97. Technical information. Crystic 272, Scott Bader Ltd.

98. Technical information. Araldite MY 750, Hardener HY 917, Accelerator DY 070, Instruction sheet C36b, Ciba - Geigy, (1977).

99. "Polyester handbook." Scott Bader, Ltd., (1981).

100. "Araldite CY 208." Sheet No. C54d, Ciba - Geigy, July, (1972).

101. Legg, M.J., "The effect of resin flexibility on the properties of glass filament wound pipes." PhD Thesis, Univ. Liverpool, (1980).

102. Jones, M.L.C., "Failure mechanisms in filament wound composites." PhD Thesis, Univ. Liverpool, (1981).

103. Gatward, C.H., PhD Thesis, Univ. Liverpool. To be published.

104. ASTM D2344, (1965).

105. ASTM D2584, (1967).

106. Hull, D., Phys. Technol., 14, (1983), 99.

107. Crosbie, G.A. and Phillips, M.G., 37th Ann. Conf. Reinforced Plastics/Composite Inste., SPI, (1982), Sect. 8C.

108. Hannah, J. and Hillier, M.J., "Applied mechanics." Pitman, London, (1971).

109. Case, J. and Chilver, A.H. "Strength of materials." Edward Arnold Ltd., London, (1959).